# UNIVERSITY OF GENOA
## POLYTECHNIC SCHOOL

**DIME - Department of Mechanical, Energy, Management and Transportation Engineering**


PhD in Engineering of Machines and Systems for Energy, the Environment and Transport
Curriculum Engineering of Machines and Systems for Energy, the Environment and Propulsion

**PhD Thesis**
XXXVIII Course

# Hydrogen Integration in Gas and Steam Turbine Combined Cycles for Maritime Applications: Design and Performance Assessment of Hybrid LNG/$LH_2$ Fuel Systems


**Supervisor:**
Prof. Alberto Traverso

**Co-supervisor:**
Dr. Alessandro Dotto

**Candidate:**
Matteo Passalacqua



May 2026

# UNIVERSITÀ DEGLI STUDI DI GENOVA
## SCUOLA POLITECNICA

**DIME - Dipartimento di Ingegneria Meccanica, Energetica, Gestionale e dei Trasporti**


Dottorato di Ricerca in Ingegneria delle Macchine e dei Sistemi per l'Energia, l'Ambiente e i Trasporti
Curriculum Ingegneria delle Macchine e dei Sistemi per l'Energia e la Propulsione

**Tesi di Dottorato**
XXXVIII Ciclo

# Integrazione di Idrogeno in Cicli Combinati Turbina a Gas e Vapore per Applicazioni Navali: Progettazione e Valutazione delle Prestazioni di Sistemi Ibridi LNG/$LH_2$


**Supervisore:**
Chiar.$^{\text{mo}}$ Prof. Alberto Traverso

**Correlatore:**
Dott. Alessandro Dotto

**Candidato:**
Ing. Matteo Passalacqua


Maggio 2026

# Content

# Abstract

The global energy transition towards low-carbon technologies has prompted significant efforts into high-efficiency, low-emission propulsion systems capable of operating with alternative low- or zero-carbon fuels while complying with the stringent regulations imposed by policymakers. In this context, the uptake of hydrogen-based propulsion systems is regarded as a promising route towards the decarbonisation of passenger shipping. Nevertheless, the use of hydrogen alone on board as an energy carrier poses complex challenges in terms of technology, storage, operations and safety. Particularly, due to its physical characteristics, significant quantities of energy cannot be stored for the typical mission profiles of a cruise ship; this is true even when its densest form, i.e. liquefied hydrogen ($LH_2$), is utilised. Therefore, in order to exploit hydrogen power onboard in a manner that is both effective and sustainable, it is recommended that a hybrid hydrogen-natural gas fuel system be conceived. This system would then be able to feed gas turbine generators in combined cycle (CCGT) configuration.

In the first part of this dissertation, commercial data were used to build weight and volume functions of low-emission alternative propulsion system, and such functions have been employed to conduct an assessment of different alternative technologies to determine the actual suitability of liquid hydrogen onboard large ships from both logistic (weight and volume occupancy) and environmental perspectives.

In the second part, the system design and thermodynamic performance analysis of a hybrid hydrogen–natural gas ($H_2$–NG) fuel handling and delivery system for a CCGT power plant is presented, with a specific focus on maritime applications, and particular emphasis on cruise ship propulsion and onboard power generation. The complete design, component sizing, and performance simulation of the hybrid combined cycle were developed using AVEVA Pro/II thermodynamic modeling tool to assess steady-state energy balances for efficient shipboard integration. A novel concept of hydrogen heat exchanger, namely a pressurizing heat exchanger (PHEX), is also presented as possible innovation from standard design to improve energy consumption, and its

integration in the fuel system is assessed. Moreover, the preliminary control logic to convey fuel at the proper conditions to the generators is also proposed, considering the aim of potentially feed them with any combination of $H_2$ and NG, as well as with the fuels taken individually as it is currently done in dual fuel (DF) engines. Moreover, basic safety considerations are made and potential outcomes of a failure in the fuel system are evaluated. In the design process, starting from the vast knowledge and technological efforts on LNG for the maritime as a drop-in solution, the main differences with $LH_2$ are assessed, and the extent to which its good practices are applicable to $LH_2$ are considered, in order to give a comprehensive overview of large scale hydrogen uptake readiness.

Finally, granted the availability of hydrogen onboard of ships and/or in the harbour and island context, the thesis also analysed two auxiliary systems connected to the hydrogen transportation economy: (i) small size power generation on board, using low temperature fuel cell solutions, aiming at the potential application of $LH_2$ to small size ships or boats, and (ii) the possibility of integrating fresh water production basing on high temperature reversible fuel cells.

# Sommario

La transizione energetica globale verso l'uso di tecnologie a basse emissioni di carbonio ha stimolato notevoli sforzi nello sviluppo di sistemi di propulsione ad alta efficienza e a basse emissioni, capaci di operare con combustibili alternativi a basso o nullo contenuto di carbonio, nel rispetto delle sempre più stringenti normative imposte dai diversi attori politici. In questo contesto, l'adozione di sistemi di propulsione basati sull'idrogeno è considerata una delle prospettive più promettenti per la decarbonizzazione del trasporto passeggeri marittimo. Tuttavia, l'impiego dell'idrogeno come unico vettore energetico a bordo presenta rilevanti sfide tecnologiche, operative e di sicurezza. A causa delle sue caratteristiche fisiche, infatti, non è possibile immagazzinare quantità di energia sufficienti per i tipici profili operativi di una nave da crociera, nemmeno utilizzando la sua forma energeticamente più densa, ossia quella liquefatta ($LH_2$). Pertanto, al fine di sfruttarlo a bordo in modo sostenibile, si propone la concezione di un sistema di alimentazione ibrido idrogeno–gas naturale per l'alimentazione di turbine a gas operanti in ciclo combinato (CCGT), caratterizzate da una maggiore flessibilità in termini di combustibili rispetto ai motori a combustione interna alternativi.

Nella prima parte della tesi sono stati utilizzati dati commerciali per costruire funzioni di peso e volume relative a sistemi di propulsione alternativi a basse emissioni. Tali funzioni sono state impiegate per confrontare diverse tecnologie e valutare la reale idoneità dell'idrogeno liquido a bordo di grandi navi sia dal punto di vista logistico (peso e volume) sia da quello ambientale.

Nella seconda parte viene presentata la progettazione del sistema e l'analisi delle prestazioni termodinamiche di un sistema ibrido di gestione e alimentazione di miscele idrogeno–gas naturale ($H_2$–NG) destinato a un impianto a ciclo combinato, con particolare riferimento alle applicazioni marittime e con specifica attenzione alla propulsione di navi da crociera e alla generazione di energia di bordo. La progettazione completa, il dimensionamento dei componenti e la simulazione delle prestazioni del ciclo combinato sono stati sviluppati mediante il software di modellazione termodinamica AVEVA Pro/II,

per valutare i bilanci di massa ed energia in condizioni stazionarie e garantire la corretta integrazione a bordo nave. Viene inoltre presentato un nuovo concetto di scambiatore di calore per idrogeno liquido, denominato “pressurizing heat exchanger” (PHEX), come possibile innovazione rispetto alle configurazioni standard finalizzata al miglioramento dei consumi energetici. Date le inerenti caratteristiche di funzionamento, tale sistema innovativo è stato simulato dinamicamente, verificandone le prestazioni.

Inoltre, viene proposta una logica preliminare di controllo volta a garantire l’alimentazione dei generatori nelle condizioni operative appropriate, considerando la possibilità di alimentarli con qualsiasi combinazione di idrogeno e gas naturale, nonché con ciascun combustibile singolarmente, come avviene attualmente nei motori dual-fuel (DF) marini. Sono state inoltre sviluppate considerazioni preliminari di sicurezza e sono stati valutati i possibili rischi all’interno del sistema di alimentazione del combustibile. Nella progettazione sono state inoltre analizzate le principali differenze tra gas naturale liquefatto (LNG) e idrogeno liquido, valutando in quale misura le pratiche consolidate nell’impiego dell’LNG nel settore marittimo possano essere adattate all’$LH_2$, in modo da fornire una visione complessiva della maturità tecnologica per l’adozione dell’idrogeno su larga scala.

Infine, assumendo la disponibilità di idrogeno a bordo o in ambito portuale e insulare, vengono analizzati due sistemi ausiliari connessi all’idrogeno: la generazione di potenza di piccola taglia mediante celle a combustibile PEM a bassa temperatura, potenzialmente applicabili a imbarcazioni di dimensioni ridotte, e l’integrazione della produzione di acqua potabile tramite celle a combustibile reversibili ad ossidi solidi (rSOC).

# Acknowledgements

I would like to thank Prof. Alberto Traverso for his continuous mentorship and insightful recommendations during all these years. I would also like to thank Prof. Alessandro Sorce for a brief but truly enriching collaboration.

I would also thank Fincantieri DSCM, and especially Dr. Alessandro Dotto for the collaboration, the continuous support and guidance towards the completion of this interesting and truly innovative project.

A heartfelt thank you goes to Federico, my supervisor during my period at NTNU, and to all NTNU people. Also, thank to you and to Dr. Monica Canepa for having accepted to revise this thesis. Your contribution is really unvaluable.

Finally, thank you to everybody outside university: Asia, my friends, and my parents, who have supported me, and everybody else that has ever had to bear me.

Activities described in this thesis have been developed within Fincantieri project "Wave 2 the Future" (W2F) funded by the European Union – NextGenerationEU. W2F project is part of IPCEI Hy2Tech.

# Nomenclature

**Acronyms**

| | |
|---|---|
| AC | Aftercooler |
| BLEVE | Boiling Liquid Expansion Vapor Explosion |
| BOG | Boil-off Gas |
| BOR | Boil-off Rate |
| BESS | Battery Electric Storage System |
| BSFC | Brake Specific Fuel Consumption |
| CAPEX | Capital Expense |
| CCC | Committee on Carriage and Cargo |
| CCGT | Combined Cycle Gas Turbine |
| CCS | Carbon Capture and Storage |
| $CH_2$ | Compressed Gaseous Hydrogen |
| CI | Compression Ignited |
| COGES | Combined Gas, Electric and Steam |
| DBTT | Ductile to Brittle Transition Temperature |
| DF | Dual Fuel |
| ECA | Emission Controlled Areas |
| EMSA | European Maritime Safety Agency |
| EoS | Equation of State |
| ESS | Energy Storage System |
| GHG | Greenhouse Gas |
| GFRP | Glass Fiber Reinforced Polymer |
| GT | Gas Turbine |
| HEX | Heat Exchanger |
| HFL | Higher Flammability Limit |
| HTF | Heat Transfer Fluid |
| HVO | Hydrotreated Vegetable Oil |
| ICE | Internal Combustion Engine |
| IMO | International Maritime Organisation |
| LCOE | Levelised Cost of Electricity |

| | |
|---|---|
| LCOW | Levelised Cost of Water |
| LFL | Lower Flammability Limit |
| LNG | Liquefied Natural Gas |
| $LH_2$ | Liquefied Hydrogen |
| LHV | Lower Heating Value |
| MDO | Marine Diesel Oil |
| MEDO | Multi-Energy Dispatch Optimizer |
| MFR | Massflow Rate |
| MGO | Marine Gasoline Oil |
| MH | Metal Hydrides |
| MILP | Mixed Integer-Linear Programming |
| MLI | Multi-Layer Insulation |
| MSF | Multi-Stage Flash Desalination |
| O&M | Operation and Maintenance |
| OCCS | Onboard Carbon Capture and Storage |
| OD | Off-Design |
| ORC | Organic Rankine Cycle |
| P&ID | Piping and Instrumentation Diagram |
| PCM | Phase Change Material |
| PEMFC | Polymeric Exchange Membrane Fuel Cell |
| PFD | Process Flow Diagram |
| PHEX | Pressurizing Heat Exchanger |
| PG | Power Generator |
| PPP | Pressure Peaking Phenomenon |
| PV | Photovoltaic Panels |
| Ro-PAX | Roll on/off & Passengers |
| RES | Renewable Energy Sources |
| RO | Reverse Osmosis Desalination |
| RPT | Rapid Phase Transition |
| rSOC | Reversible Solid Oxide Cell |
| SEC | Specific Energy Consumption |
| SCI | Specific Carbon Intensity |
| SI | Spark Ignition |

| | |
|---|---|
| SOFC | Solid Oxide Fuel Cell |
| SOFI | Spray-on Foam Insulation |
| SOLAS | Safety of Life at Sea |
| TES | Thermal Energy Storage |
| TtW | Tank-to-Wake |
| USD | US Dollars |
| VCS | Vapor Cooled Shield |
| WtT | Well-to-Tank |
| WtW | Well-to-Wake |
| WHR | Waste Heat Recovery |

**Subscripts**

| | |
|---|---|
| BL | Baseline |
| des | Design condition |
| el | Electric |
| filling | Filling time |
| fuel | Relative to fuel |
| min | Minimum |
| mix | Related to mixing or mixture |
| max | Maximum |
| pc | Per Capita |
| RO, pay | Fraction of RO powered by un-curtailed RES |
| tank | Relative to tank |
| th | Thermal |
| v | Vapour pressure |

# List of figures

# 1 Introduction

## 1.1 Background

Since the industrial revolution, the world energy demand, and therefore fossil fuels consumption, have increased progressively. Though, only in the 1980s a concern regarding climate-altering emissions has arisen on global scale. After Kyoto Protocol was adopted in 1997 and went into force in 2005, criticism was made as that only developed countries were asked to take actions. Then, the Paris Agreement in 2015 updated the measures with the aim of containing the global temperature rise within 2°C compared to pre-industrial levels, and making efforts to keep it below 1.5°C. It was already clear that urgent and consistent actions should have been taken immediately at global level in order to tackle this issue. However, these actions have been seemingly insufficient: after a slight rebound due to COVID-19 pandemic, reports from relevant institutions depict a scenario where 1.5°C temperature rise is already reached as of 2024 [1]. Besides, the total amount of greenhouse gases (GHG) has reached the alarming level of 38.1 Gt $CO_2$ at the end of 2024 [1]. The sectors that give the largest contribution are, in order of magnitude, energy production in both forms of power and heat, industrial processes, and transports, with shares of around 41%, 23% and 22%, respectively [1].

Regarding power and heat production, while renewable sources penetration has sky-rocketed in the last decade, electrification of heating systems is still lagging behind due to the large demands and the significant influence of hard-to-abate sectors. These include mainly heavy industrial processes with high thermal energy demand (e.g. glass, steel and concrete production, chemicals and petrochemicals synthesis, oil and gas refinery) and long-haul heavy transport (shipping, aviation, and long-haul trucking). Shipping is considered within the category of hard to abate sectors due to the strong reliance on energy-dense fossil fuels, the massive scale of influence, and the lack of a single viable alternative to conventional energy sources [2], despite accounting quantitatively only for short of 3% total GHG emission and around 14% of the GHG emission within the transport sector (Figure 1).

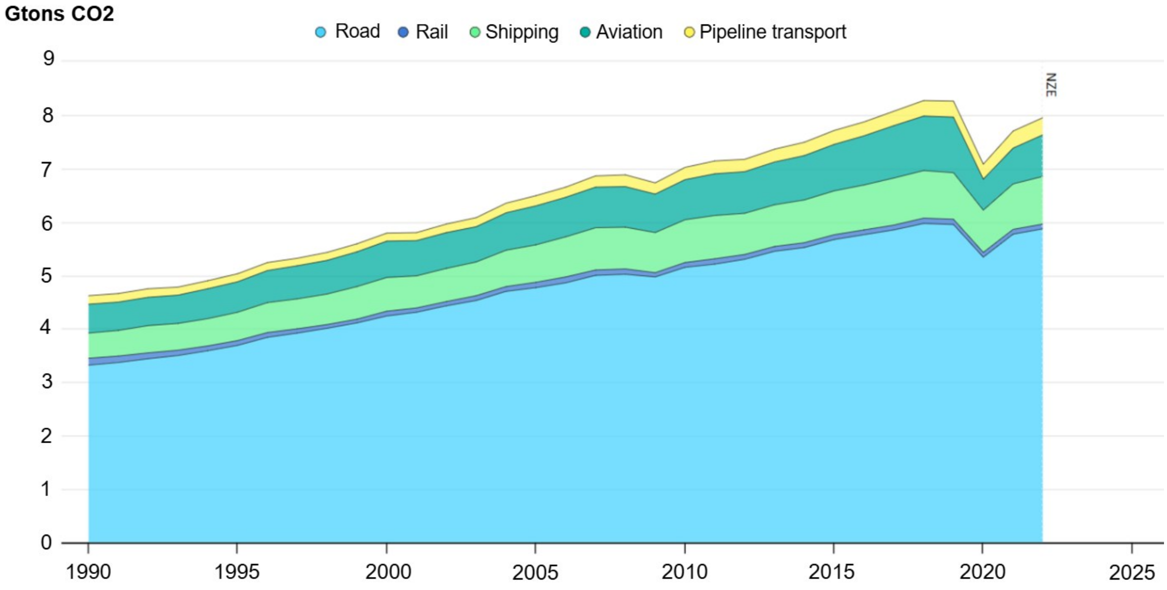


*Figure 1 – Share of GHG emission due to transport. Adapted from [1]*

Especially, sea transport presents several differences compared to road or rail transport. Firstly, sea transport must rely on energy dense storage and conversion system able to guarantee sufficient range and to comply with Safe Return to Port requirements posed by the Safety of Life at Sea (SOLAS) convention, adopted by the IMO in 1974 [3]. Therefore, electrification is absolutely more complicated than it is for land-based vehicles. Moreover, the worldwide scale of shipping deployment and the size of ships themselves means that, during port visits, an additional greenhouse gas (GHG) amount is emitted into areas already densely populated, the equivalent of that produced by a small city.

In the scope of the "Fit for 55" package [4], proposed by the European Union to reduce at least 55% the greenhouse gas emissions by 2030, shipping and seagoing transport in general is affected by both the EU Emission Trading System (EU-ETS) [5] and the FuelEU Maritime [6].

The first is a real carbon market based on a system of cap-and-trade of emission allowances for energy-intensive industries and the power generation sector, and all vessels more than 5000 Gross Tonnes dead weight are included since 2024. Basically, shipowners may purchase a certain number of carbon quotes that allow a determined total GHG emission of their entire fleet. The cap-and-trade configuration ensures that emission allowances become more and more costly, possibly pushing towards investments in new, zero-emission solutions rather than expenditure in more carbon allowances.

The second was adopted in 2023 and contains a set of measures designed to progressively reduce the average specific emission of vessel fleets by establishing, among others, a series of increasingly lower limits on their Well-to-Wake (WtW) carbon intensity. In case of non-compliance, shipowners are subject to a penalty proportional to the excess over the target GHG index, which is currently 91 $kg_{CO2}/MJ$ and is expected to decrease by 6% in 2030. Besides, FuelEU also imposes shore-to-ship power supply (also known as "cold ironing") to be available by 2030 at European ports.

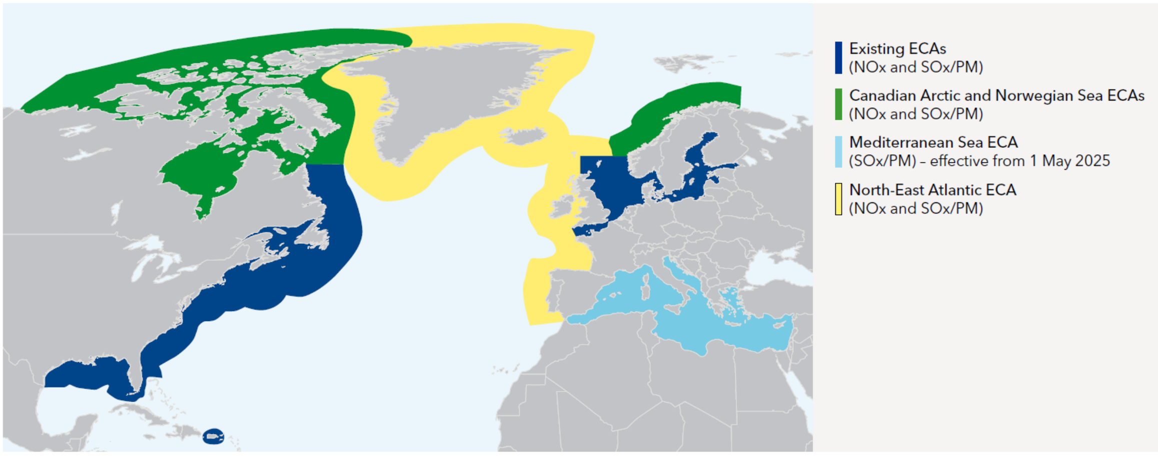


*Figure 2 – ECAs according to MARPOL Annex VI. Enforced from March 2026*

However, greenhouse gases are not the only ones to be appointed by regulations in terms of pollutant reduction. In fact, being more than 98% of the vessels fuelled by maritime Diesel oil (MDO) or maritime gasoline oil (MGO) [7], nitrous oxides ($NO_x$) and sulphur oxides ($SO_x$) are also appointed regulators. The IMO has designated Emission Controlled Areas (ECAs), where limits on $NO_x$ and $SO_x$ emissions are set by IMO Tier III.

By these premises, it is also to be pointed out that although overall ship efficiency can be improved by cheaper drop-in solutions such as onboard waste heat recovery, powertrain hybridisation with batteries, improvement to hull hydrodynamics, and logistic measures, the ambitions of IMO in terms of complete net-zero by 2050 cannot disregard the use of alternative fuels [7]. Therefore, in the long term an effort is anyhow required to develop ready and cost-effective solutions for alternative fuels utilisation onboard vessels.

## 1.2 Alternative fuels for maritime propulsion

As said, climate change and evolving economic interests are leading many countries towards energy policies more focused on an energy transition. As international shipping faces tightening regulatory frameworks and heightened scrutiny from policymakers and industry stakeholders, conventional fossil-based propulsion is becoming misaligned with long-term sustainability objectives. Emerging fuels such as methanol, ammonia, hydrogen, and advanced biofuels such as bio-methane, bio-ethanol or Hydrotreated Vegetable Oil (HVO) offer promising pathways to mitigate harmful emissions. The share of vessels that are equipped with alternative fuel power systems is still very low, as shown in Figure 3. This includes ships of various sizes, but the trend is promising, showing an increase of around 25% for vessels currently being built as compared to those in operation [7]. Moreover, more than 50% of current alternative fuelled ships are equipped with LNG powertrains, and this share is expected to become larger for ordered ships. This is certainly an improvement compared to the current state, but illustrates that there still exists a diffused reluctance of the shipping industry to adopt new yet unexplored solutions that would facilitate effective decarbonisation of maritime transport.

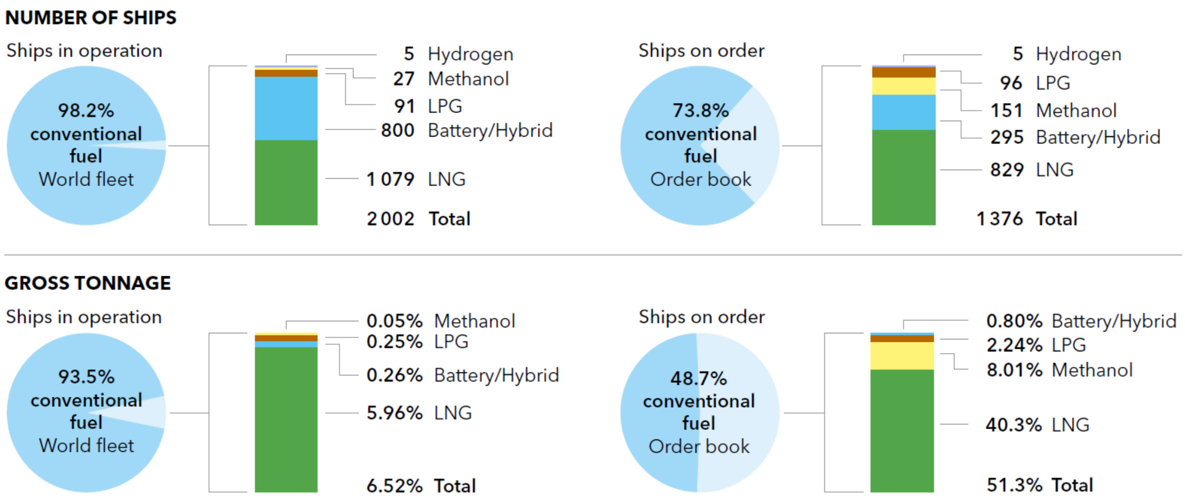


*Figure 3 – Alternative fuel uptake as of mid-2023 [7]*

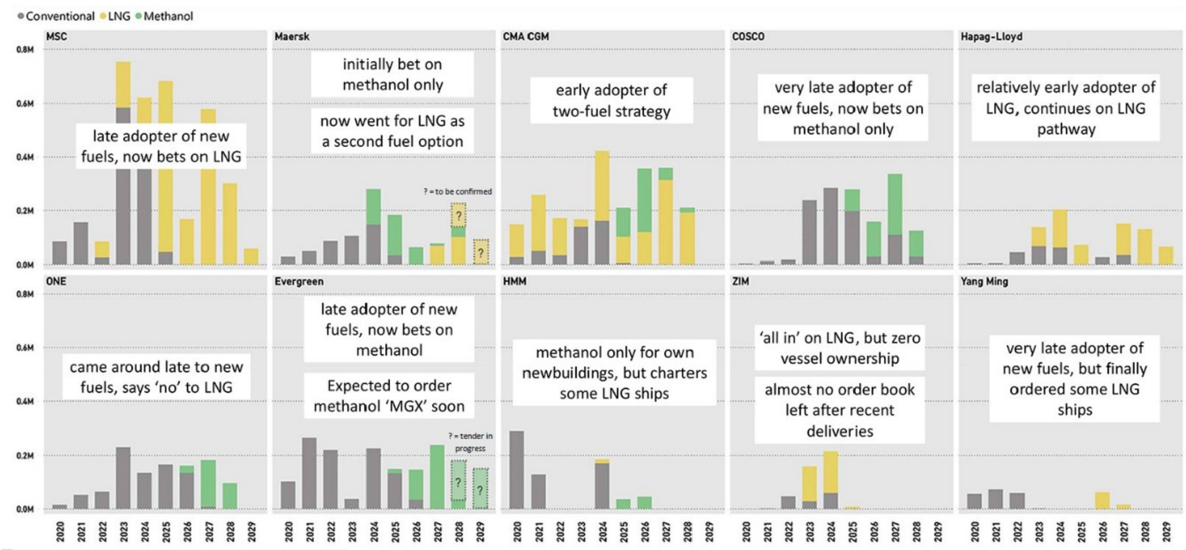


*Figure 4 – Forecast scenarios for different cargo shipping companies*

The underlying issue has many folds. On the one hand sits the unmatched energy density of conventional MGO and MDO, which is the highest on volumetric basis and among the highest on mass basis as shown in Figure 5.

However, it is important to note that the fuel amount stored on board is typically calculated on a volumetric basis, while consumption is generally measured on a mass basis. This is particularly true for fuels that are fed to the prime mover in gaseous form, where density changes considerably with feed pressure, ranging from 3-5 barg for fuel cells, 10-15 barg for reciprocating engines and up to 40-50 barg for gas turbines. Consequently, a discrepancy may emerge between the stored energy and the consumed energy. The discrepancy is more pronounced for those alternative fuels that are gaseous at ambient and supply conditions but are typically stored in liquefied form (LNG, $LH_2$, ammonia) to increase density. This aspect becomes particularly evident in the case of hydrogen, where the tiny density completely overshadows the fact that it is the molecule with the highest LHV of all.

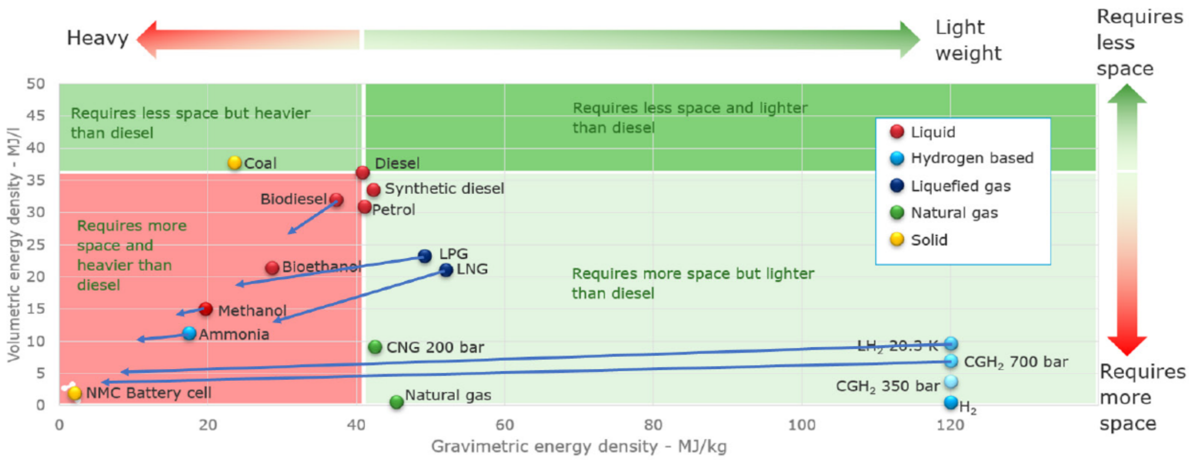


*Figure 5 – Overview of energy densities for different alternative energy carriers comparing gravimetric and volumetric performance [8]*

A quantitative comparison of the most relevant properties of alternative fuels, including volumetric and gravimetric energy content, is reported in Table 1. LNG appears to be the readiest solution, with higher LHV as compared to MDO and volumetric density only 62% as high as the one of conventional fuel but has to deal with cryogenic storage and challenges associated. The low density of hydrogen, even in liquefied form, is a significant obstacle. From an economic standpoint, ammonia is likely to prove more advantageous, despite requiring 0.78 kWh/kg for its synthesis only (i.e., in addition to hydrogen and nitrogen production) [9]. Finally, methanol is hindered by toxicity, common to ammonia, and lower LHV as compared to conventional marine fuels. A summary of the current readiness and the main challenges associated with the most prominent alternative fuels is reported within Table 2.

*Table 1 – Relevant properties of the main alternative fuels*

| | MDO | MGO | LNG | MeOH | $NH_3$ | $LH_2$ |
|---|---|---|---|---|---|---|
| **Storage density [kg/m³]** | 848 | 855 | 470 (avg.) | 790 | 682 | 71 |
| **LHV [MJ/kg]** | 44 | 45.9 | 49 (avg.) | 20 | 18.8 | 120 |
| **Vol. Energy Density [MJ/m³]** | 35.7 | 36.6 | 21.8 (avg.) | 15.6 | 12.8 | 10 |
| **LFL - HFL [%vol]** | 1.8-8.2 | | 4-15 | 6.7-36 | 15-28 | 4-75 |
| **Converters (with TRL >5)** | ICE, GT | ICE,GT | ICE, FC, GT | ICE, FC | ICE, FC | ICE, FC, GT |

*Table 2 – Readiness and associated challenges for conventional and alternative fuels*

| | MDO | MGO | LNG | MeOH | $NH_3$ | $LH_2$ |
|---|---|---|---|---|---|---|
| **Carbon neutral** | ✗ | ✗ | ✗ | ✗ | ✓ | ✓ |
| **Storage convenience** | ✓ | ✓ | ✗ | ✓ | ~ | ✗ |
| **Energy density** | ✓ | ✓ | ✓ | ✗ | ✗ | ✗ |
| **Flammability/ explosion** | ✓ | ✓ | ✓ | ~ | ✓ | ✓ |
| **Non-toxic** | ✓ | ✓ | ✓ | ✗ | ✗ | ✓ |
| **Ready to use** | ✓ | ✓ | ✓ | ✓ | ✗ | ✗ |

### 1.2.1 LNG

Liquefied natural gas (LNG) has gained traction as a leading drop-in solution for reducing greenhouse gas emissions in the maritime sector, largely because it offers immediate, scalable improvements without requiring a full overhaul of existing vessel designs. Its combustion produces significantly lower $CO_2$, $NO_x$, and particulate emissions compared with conventional marine fuels, helping ship operators meet tightening international regulations. LNG is also supported by a stable and rapidly expanding global market, also due to recent geopolitical implications, and ultimately a growing operational experience in the maritime sector, making it a practical transitional fuel while the industry advances toward long-term zero-carbon alternatives [10]. Besides, its bio-derived counterpart, i.e. biomethane, has also gained more and more attention in transportation thanks to its reduced carbon footprint as compared to fossil natural gas [11]. However, when liquefied, bio-LNG has to account for both cost of liquefaction and production.

From a technical perspective, LNG has to deal with boil-off gas (BOG), whose rate of evaporation (boil-off rate, BOR) is estimated to be in the order of 0.1% of the stored mass per day of dormancy [12,13]. Reliquefaction of evaporated LNG is often considered impractical for several reasons: firstly, its non negligible energy input requirement [12,14,15] does not justify the volume encumbrance of the system, and secondly its utilisation as a fuel source for the prime movers or onboard generators is significantly more operationally practical. Moreover, in view of the fact that this is a necessity for utilisation in engines, the option of pre-compressing the BOG in order to reduce the footprint of the reliquefaction system was also evaluated. The outcome of this investigation is that reliquefaction load is reduced by a mere 1.5% between the cases with BOG at 2 bar and at 15 bar [16]. Besides, as opposed to hydrogen, simply a moderate storage pressurisation can increase the temperature of the two-phase fuel by several dozens of Celsius degrees [17,18], further improving the storage performance.

### 1.2.2 Hydrogen

Hydrogen is gaining attention as a clean marine energy carrier thanks to its potential for truly zero-carbon Tank-to-Wake operation. It offers exceptionally high specific energy, enabling efficient use in fuel cells to achieve higher conversion efficiency and zero $NO_x$ production. Substantial modifications to the fuel supply lines are a prerequisite for installing a hydrogen-ready internal combustion engine (ICE) for propulsion, and market-ready solutions are only suitable for low power applications [19]. By contrast, given their inherent fuel flexibility, there is evidence demonstrating that turbine engines are much more hydrogen-ready than reciprocating engines. This is also confirmed by several companies showcasing total or partial hydrogen readiness as a main feature of their products [20,21].

Despite it has been observed that demonstration vessels have traditionally employed pressurised gaseous or metal hydride hydrogen storage systems, liquefied cryogenic storage ($LH_2$) emerges as the most suitable storage option [22]. This is also confirmed by comparative analyses conducted on different vessel types, such as small leisure vessels with installed power around 1 MW [23] or cruise ships at berth, considering 7 MW of hotel load [24].

However, storage and onboard handling remain not completely solved technical hurdles, especially for long voyages. Where liquid storage is concerned, the main challenge still to be tackled is undoubtedly BOG handling. Compared to LNG, the evaporated BOG is more relevant in terms of percentage of stored fuel mass, in particular around an order of magnitude higher [18,25]. This drives the energy intensity of reliquefaction of evaporated $LH_2$ to the same ten-fold ratio with respect to LNG, sitting at around 12-15 $kWh/kg_{H2}$ for large scale liquefaction plants with dozens of tonnes of $LH_2$ yield per day, and may be even higher for small onboard systems.

Hydrogen BOR is more affected by storage conditions than LNG or ammonia, but increase in storage pressure (and temperature, as a consequence) has a negligible impact on the BOR and requires significant technological improvement [26]. Currently, typical BOR values for large $LH_2$ tankers are evaluated to be between 2% and 3% per day of storage [26,27]. Besides, the energy efficiency of the storage system expressed as ratio between the usable and the stored mass decreases as much as 3% without BOG recovery [27].

To strengthen how crucial the quantitative influence of BOG is, it was evaluated that in an unrealistic zero boil-off scenario, $LH_2$ would surpass ammonia from a whole supply chain perspective [28]. Furthermore, the disposal of $LH_2$ BOG is such a wasteful process that it has been determined that $LH_2$ tankers would benefit significantly from full BOG reliquefaction with conventional or DF propulsion systems, as opposed to BOG utilisation as fuel both in a steam power cycles and a polymer electrolyte membrane fuel cell (PEMFC) [29]. This is partially applied on the only existing $LH_2$ carrier built to date, where propulsion system is conventional but reliquefaction is not employed due to extreme complexity [30].

To these premises, hydrogen reliquefaction is all the more impractical to be performed onboard vessels and hydrogen BOG is conveniently used as direct fuel for the ship's prime movers.

### 1.2.3 Ammonia

Ammonia has higher energy density compared with other carbon-free fuels, and the ability to store it in liquid form under moderate conditions should make it suitable for long-distance shipping [31]. Ammonia is often seen as a natural competitor of hydrogen, as this is one of its constituent elements. However, hydrogen is surpassed from both energy and economic standpoints. In fact, granted that gaseous hydrogen is available at a specific energy consumption (SEC) in the order of 35-48 $kWh/kg_{H2}$ [32], ammonia synthesis is less energy intensive as compared to hydrogen liquefaction: even considering 100% conversion efficiency, the minimum theoretical SEC values are 0.8 kWh/kg and 3.1-3-7 kWh/kg, respectively [9,33]. Besides, ortho to para conversion makes $H_2$ liquefaction SEC closer to 4 kWh/kg [33]. Ammonia remains energetically advantageous also if used as hydrogen carrier, that is, hydrogen is extracted back through cracking and used as fuel. This process requires averagely 6.4 $kWh/kg_{H2}$ [28]. Moreover, ammonia contains a greater quantity of hydrogen mass than hydrogen itself, with a weight percentage of 17.7%. Consequently, when considering liquefied storage, ammonia contains 116 kg of hydrogen, in comparison to 71 kg of hydrogen per $m^3$ of $LH_2$.

*Table 3 - Comparison of value chain energy consumption of liquefied $NH_3$ vs $LH_2$. Values are expressed in $kWh/kg_{product}$.*

| | **Production** | **Synthesis** | **Liquefaction (w/ p-o conversion)** | **Cracking** |
|---|---|---|---|---|
| **$H_2$** | 35-48 | - | 3.1-3.7 (4) | - |
| **$NH_3$** | 35-48 | 0.8 | 0.72 | 6.4 |

As engine and fuel-handling technologies mature, ammonia is increasingly viewed as a strong candidate for deep-sea decarbonisation [34]. The main technological challenges are associated with the slow combustion kinetics, an increased nitrous oxides emissions, and ammonia slip. While the first can be tackled with partial cracking or utilisation in blends with methane [35], the others require tailored post-treatment devices such as selective catalytic reducers (SCR) and ammonia afterburners. In fact, ammonia is toxic and the concentration limit on human exposure is set in the range 25-50 ppm, depending on local legislation [34]. Despite this, there are some examples of market-ready 4-stroke DF ammonia engines for small power application [36], while 2-stroke compression-ignited (CI) ammonia combustion is currently under final research [37].

It can be then concluded that ammonia can function as a versatile hydrogen carrier in addition to its role as a fuel. Indeed, when employed in the first mode, it exhibits a substantially higher overall transport efficiency.

### 1.2.4 Methanol

Methanol is considered one of the readiest alternative to conventional fuels alongside LNG because it strikes a balance between cleaner combustion, manageable storage requirements, and partial compatibility with existing vessel designs. Carbon emission is lower as compared to methane or MDO/MGO because its specific carbon content is lower (38% vs 75% for $CH_4$), but also LHV is more than 50% lower (Table 1), hence the advantage is lost by requiring twice as much liquid fuel as methane. Methanol delivers lower $NO_x$, $SO_x$, and particulate output than traditional marine fuels. Nonetheless, methanol diffusion as a fuel is still not widespread because it cannot count on an established market and value chain as it is the case for natural gas.

There is only a limited number of DF methanol-powered ships in operation, mostly ferries and notably one large cruise ship, the *Disney Adventure* [38].

It can be used in modified diesel engines with comparatively modest retrofitting, and its liquid state at ambient conditions simplifies bunkering and handling relative to other alternative fuels. With multiple large-scale methanol-capable vessels already in operation, it is becoming one of the most immediately deployable options for greener shipping.

### 1.2.5 Other "drop-in" alternative fuels

In addition to the well-known fuels already mentioned, the maritime sector is exploring the use of other alternative fuels with the aim of reducing greenhouse gas emissions. Examples of this include HVO, LPG and ethane. Whilst the first is essentially interchangeable with maritime diesel, the others are primarily employed in gas carriers, where the payload contributes partially to the energy source for propulsion eliminating the need for a separate fuel conditioning and supply system. By contrast, since they are equipped with 2-stroke CI engines, liquefied gas carriers require a pilot injection of diesel fuel to ensure stable combustion.

#### *1.2.5.1 Hydrotreated Vegetable Oil (HVO)*

Hydrotreated Vegetable Oil (HVO) is a synthetic diesel obtained from the hydrotreatment of vegetable oil or waste fats with hydrogen. It is chemically very similar to fossil diesel but has almost no sulfur, aromatics, or oxygen, and a much higher cetane number. In the maritime sector, HVO is marketed as a “drop-in” fuel that can replace conventional diesel in existing marine diesel engines, either as a pure fuel (HVO100) or blended with fossil diesel [39]. HVO presents lower density and higher LHV as compared to conventional diesel, resulting in a trade-off between reduced engine power and lower brake specific fuel consumption (BSFC) [40]. Moreover, in automotive reciprocating engines a general reduction in particulate emission has been observed, while $NO_X$ levels do not decrease significantly unless injection is retarded to a point where emissions of particulate matter are compromised. [40]. However, when engine parameters are optimised for HVO or other bio-derived fuels, there seem to be a reduction in $NO_X$ up to 20% [41].

As regards gas turbines, there is unexpectedly vast experience with HVO, especially on aero engines. $NO_X$ emissions show a decrease in a wide range of operating speeds as well as in specific fuel consumption [42], while particulate emissions are reduced up to 96% [42]. Besides, there are a number of maritime engines manufacturers that have expressed interest in pursuing HVO as one of the readiest alternatives.

#### *1.2.5.2 Liquefied Petroleum Gas (LPG)*

Liquefied Petroleum Gas (LPG) is arguably the least innovative of all alternatives to Diesel fuel, having initially been identified as a by-product of oil distillation. It contains a mixture of light hydrocarbons, usually propane, butane and light olefins, so it is stored onboard in compressed gaseous or liquefied form.

LPG has higher gravimetric energy density than MDO and MGO, therefore it can be readily integrated into existing hulls, though only minor modifications may be required to ensure adequate gaseous supply. As compared to another drop-in solution as HVO, LPG has higher lower heating value (46.1 MJ/kg vs 44 MJ/kg, [43]) and reduces $NO_X$ while cutting to zero sulphur oxides. In particular, information on $NO_X$ emissions are not widely available but are estimated to be around 2.3-2.5 kg per $m^3$ of LPG [44]. However, as it is primarily fossil-derived except for areas with large quantities of available bio-feedstock [45], it cannot be considered to be zero-carbon. Despite this, LPG is also a by-product of HVO production by the extent of 5-10% of the total [45], hence the combined production of both fuels is actually helpful to reduce the overall WtW emission of greenhouse gases and climate-altering substances.

Given all these premises, to date this fuel founds applications almost exclusively on LPG carriers, retrofitted from HFO propulsion [46]. In the case of refrigerated transport, the technology is analogous to LNG, where the tanker is mainly fed by the boiled-off LPG and partly by the payload, thereby augmenting it by the necessary amount [47]. A pilot injection of Diesel fuel is anyhow needed in 2-stroke CI engines to ensure stable combustion.

#### *1.2.5.3 Ethane*

Ethane is the second lightest hydrocarbon, and its economic worth is much lower than that of LNG. It has emerged that certain sources of fossil natural gas are particularly ethane-rich (e.g. shale gas sources in the US), thus justifying the implementation of dedicated handling procedures [48]. As discussed for LPG, ethane is used as fuel only on ethane carriers, where the gas is usually stored in liquefied form in slightly pressurised conditions. Fuel systems are conceptually the same as LNG and LPG, and engines can run on multiple gases on top of ethane itself. It is of interest to note that the most recent ethane carriers are among the few vessels known to be equipped with a reliquefaction system, which in this case has been engineered purposely by Wartsila [49].

## 1.3 Energy recovery and other solutions for increased energy efficiency

Alternative fuels are not the one and only solution to maritime decarbonisation. However, it appears clear that to achieve a consistent carbon reduction, the target must be the carbon removal. Despite being consolidated that zero-emission is only achievable through zero-carbon fuels, several options for efficiency improvement are also taken form the maritime industry to mitigate the short term effect of GHG and to slowly drift towards a decarbonised sea transport. Such options are listed in Figure 6 alongside their estimated GHG reduction potential [7].

Still, yet at present most passenger ships make use of waste heat for cogeneration or air conditioning [50], while additional power generation in combined configurations with bottoming ORCs [51,52] or steam cycles [53] is still under exploration with only a few operating examples. Generally, ORC works better than steam for low temperature and part-load waste heat recovery, while classic steam Rankine systems give higher peak power from very hot and massive exhaust on large ships. In practice, ORC tends to suit retrofits, smaller, lower temperature engines, WHR from jacket water rather than exhausts, and variable load operation, whereas steam systems suit big main engines with high exhaust temperatures and stable long-voyage profiles. This is quantitatively explained in several works [54,55]. Modelled performance of a WHR from a marine engine favour ORCs over steam cycles thanks to a lower increase in engine BSFC, giving a comparable overall system efficiency (52% vs 51%) [54]. The result is attributable to the very poor efficiency of the steam cycle, which plummets down to typical ORC values.

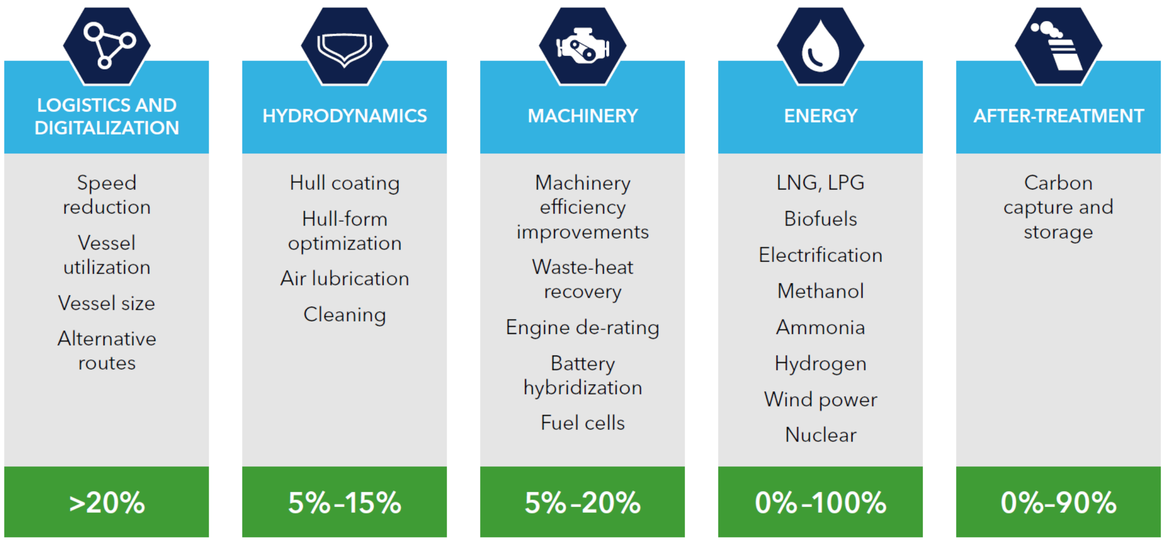


*Figure 6 – Solutions contributing to the decarbonisation of shipping sector [7]*

Regarding alternative fuels, LNG is considered to be a transitional fuel to maintain efficient and economical operation. Still, the presence of LNG onboard also offers possibilities for the exploitation of its cold energy as a thermal well for heat rejection of power cycles. This paradigm has been explored in the past for land-based power systems utilizing LNG [56], for energy recovery in natural gas liquefaction plants [57] or coupled to cryogenic carbon capture and storage (CCS) [58–60]. Regarding onboard applications, it is undoubtedly interesting to be explored as an enhancement of system-level efficiency [61].

Besides, LNG-driven onboard CCS (OCCS) has a potential also where onboard application are considered. This is evaluated onboard both passenger ships utilizing an intermediate ORC system to power the CCS plant [62], and LNG carriers in combination with a reliquefaction line [59]. General sustainability assessment is performed in [61], showing that only chemical absorption and cryogenic separation potentially require no additional energy input. Indeed, membrane and pressure swing adsorption would require an excessively low operating temperature and a cold duty at least six times higher than that provided by LNG owing to the relatively large amounts of low-condensable present in the separated $CO_2$ stream.

Nonetheless, integration of such a demanding system must respect LNG flow, engine load, and storage constraints, so practical designs usually must combine several processes such as solvent capture, LNG-driven $CO_2$ liquefaction, and waste-heat recovery into a tightly coupled energy system to be optimised as a whole without disrupting the main power supply to the ship electric grid.

## 1.4 Aim of present work

As described in the abstract, the aim of this work is to conduct an assessment and conceptual development of a hybrid LNG–$LH_2$ powertrain suitable for marine propulsion. The research begins in Chapter 2 with an evaluation of the technical, operational, and regulatory factors that influence the adoption of dual-cryogenic fuel systems on board modern vessels. Besides, in Chapter 3 a techno-economic assessment is performed for different alternative fuel solutions on three case studies, namely i) the sole hotel load of a large cruise ship, ii) the navigation load of a medium cruise ship and iii) the navigation load of a medium pax & car ferry. This analysis shows how hydrogen in general, and specifically liquefied hydrogen, performs as compared to the state-of-the-art and to other solutions.

Building on this assessment, Chapter 4 of the thesis develops a powertrain architecture that integrates LNG and liquid hydrogen in a complementary manner, balancing energy density, efficiency, and emissions performance. A central part of the work involves the selection and justification of key components, including storage tanks, fuel conditioning systems, and supply lines capable of handling varying compositions of LNG–hydrogen blends. Special attention is given to the complexities of cryogenic system integration, safety considerations, and the thermal management strategies required to ensure reliable operation under dynamic load profiles. The study also examines the operational flexibility afforded by the ability to run on a range of LNG–$LH_2$ blend ratios, exploring how such flexibility can support gradual decarbonisation, fuel availability constraints, and evolving emissions regulations. Ultimately, this thesis aims to deliver a structured design rationale and integration framework that can guide future development of hybrid cryogenic powertrains for cleaner marine propulsion.

Finally, two different examples of prospective hydrogen exploitation onboard are proposed: hydrogen utilization in fuel cells as Auxiliary power units (APUs) and combined hydrogen and freshwater production. In Chapter 5, the performance of the air supply system of an experimental turbocharged PEMFC emulator plant is evaluated. In Chapter 6, a techno-economic analysis of a combined hydrogen-freshwater production system based on renewable sources and a Reversible solid oxide cell (r-SOC) is performed, introducing the possible application of such system onboard large passenger ships, where the freshwater demand is critical and usually high.

# 2 Overview of cryogenic fuels handling and conditioning systems

A general state-of-the-art assessment for LNG and $LH_2$ hydrogen handling systems in the marine environment depicts a general two-fold situation. The following sections will present the technological and safety details of such an assessment, explaining the differences and future challenges to be addressed in order to gather experience with LNG and translate it as extensively as possible to $LH_2$.

It is known that extensive research effort is now put on hydrogen technologies. Reviews explore either the whole value chain level [22,27,28,33,63], production and liquefaction [33,64], storage [65–69], or utilisation [70,71]. Utilizing hydrogen onboard could be performed either in thermal engines (ICE, GT) or in both PEMFC and solid oxide fuel cell (SOFC). Fuel cells have been demonstrated to achieve the highest conversion efficiency [70], however, they are not easily scaled up to multi-MW sizes for application in cruise ships, cruise ferries and large Ro-Pax vessels. Furthermore, on the one hand gas turbines are generally considered more compatible with hydrogen use than reciprocating internal combustion engines, although requiring higher fuel pressure at the injector. Besides, when coupled to steam bottoming cycle in a CCGT configuration, higher efficiencies are obtained. On the other hand, upscale of large marine ICEs is lagging behind that of gas turbines, which are benefiting from increased interest from the power production market.

## 2.1 LNG technologies for maritime applications

LNG is a well-established technology in the marine sector from container ships and ferries of various sizes and configurations to cruise ships, having a high TRL and being the preferred alternative for short-term decarbonisation [72]. Although it is demanding in terms of components and materials for the handling system owing to the cryogenic temperatures, the wider and wider uptake fosters solidity of the market of related technologies. In fact, the liquefied natural gas feedstock market has demonstrated notable stability in recent times, a consequence of the recent geopolitical developments that have stimulated gas demand from Americas to Europe, thereby compensating for the diminished or extinguished gas supply from Eastern Europe [1,10]. Moreover, natural gas-running prime movers count on long time technological maturity, irrespective of the fuel source. Hence, LNG is a ready-to-go alternative for immediate uptake of mass-produced low emission power solutions [14].

LNG-powered ships make use of three types of tanks, according to IMO classification (IGC code, [73]):

- Type A, employing a prismatic design and a complete secondary barrier, non-pressurised.
- Type B, employing spherical (Moss type) or prismatic design and a partial secondary barrier, non-pressurised.
- Type C, cylindrical-shaped single-lobed or two-lobed, pressurised.

As depicted in Figure 7, the different designs are employed in very different circumstances.

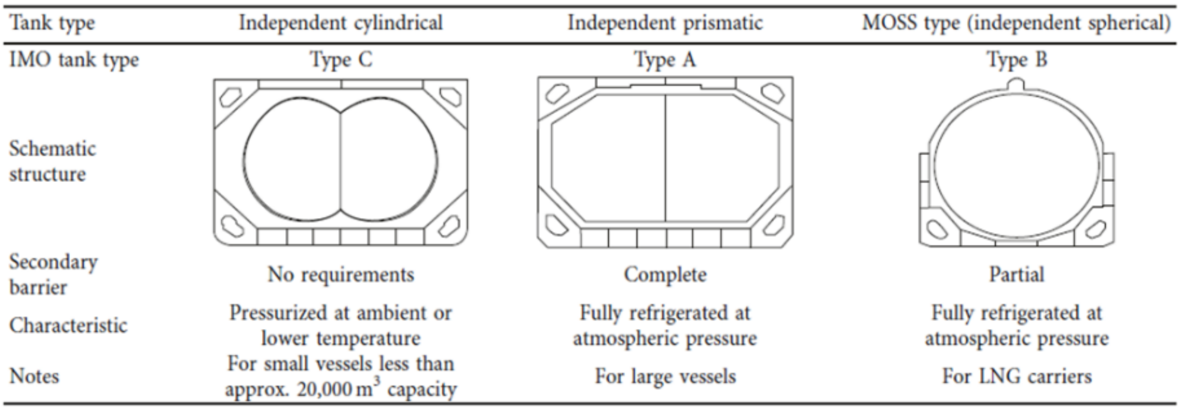

| Tank type | Independent cylindrical | Independent prismatic | MOSS type (independent spherical) |
|---|---|---|---|
| IMO tank type | Type C | Type A | Type B |
| Schematic structure | | | |
| Secondary barrier | No requirements | Complete | Partial |
| Characteristic | Pressurized at ambient or lower temperature | Fully refrigerated at atmospheric pressure | Fully refrigerated at atmospheric pressure |
| Notes | For small vessels less than approx. 20,000 $m^3$ capacity | For large vessels | For LNG carriers |

*Figure 7 – Outlook of tank types for LNG-fuelled ships [74]*

Type A and Type B are used for LPG and LNG tankers, where the liquefied gas constitutes the payload and the wet volume has to be maximised. The choice between them is mainly in design method and secondary barrier arrangement. A secondary barrier is constituted of a layer of opportune material that insulates the cryogenic containment from the frame hull structure. The fundamental requirement of this layer is that it must be impermeable to any liquid gas.

Type A tanks are concepted using classical ship-structural analysis methods, and recognised standards, but must have a complete secondary barrier capable of containing the entire cargo volume for a defined period and protecting the hull [75]. This means that, as far as toughness and resistance are proven, a wider set of materials is permitted. They are originally conceived for LPG, but knowledge is currently being transferred to LNG tankers. They exhibit 20-30% lower tank weight than comparable Type B [76]. Type B are designed through detailed stress/fatigue analysis with a fail-safe concept, and secondary barriers can accept leakages that are collected in a separate drip tray rather than containing the whole tank volume [75,76]. Therefore only fracture-tough metals, such as Ni stainless steels and aluminium alloys, are permitted [74]. In general terms, architectures of Type A are characterised by a focus on ease of construction and economic efficiency, while those classified as Type B demonstrate a preference for safety and reliability. In any case, both architectures are utilised as cargo tanks on gas carriers, and not as fuel tanks. Their main features are summarized in Table 4.

In contrast, Type C tanks are used as fuel tanks in which the liquefied gas serves exclusively as the propulsion fuel for the vessel. This technology is primarily applied in LNG-powered ships, such as passenger vessels, Ro-Pax ferries, and container ships. The IGC Code provides specific design requirements for Type C tanks, which constitute the standard applicable to LNG-powered passenger ships but is also envisioned for liquefied ammonia [77] and $LH_2$ [78], while a prescriptive regulation is awaited.

Regarding fuel handling systems, given the maturity of such fuel, several manufacturers have commercial products for LNG storage and handling. Wartsila ([79–81]) and Everllence SE (formerly “MAN Energy Solutions”, [37,82]) have the largest industrial experience in LNG fuel tanks, fuel supply system, and dual fuel engines for maritime propulsion. Figure 8 reports a real example of application of the LNGPac™ from Wartsila onboard a fast passenger ferry for regional navigation [83].

*Table 4 – Overview of key differences between IMO Type A and Type B tanks*

| Aspect | Type A | Type B |
|---|---|---|
| **Design basis** | Classical ship-structural rules | Refined analysis, fail-safe rationale |
| **Typical shape** | Prismatic | Spherical, rarely prismatic |
| **Secondary barrier** | Full, entire volume | Partial, leak collection only |
| **Pressure rating** | Non-pressurised | Non-/semi-pressurised |
| **Materials** | Broad set of steels/aluminium if toughness proven | Narrower set due to strict fatigue and fracture requirement |
| **Typical use** | Mainly LPG carriers, more rarely LNG carriers | LNG carriers |

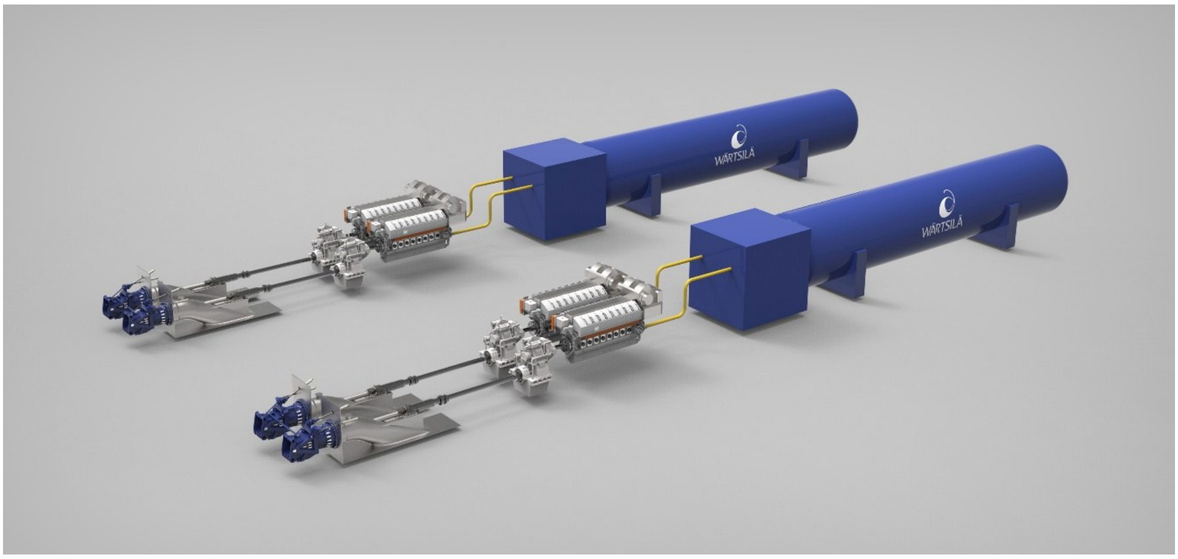


*Figure 8 – Example of application of LNGPac™ system on the Margarita Salas fast ferry catamaran [83].*

As a general consideration, two alternatives are possible for LNG (and cryogenic fuels in general): a conventional pump-driven system or a pump-free layout with a pressure buildup (PBU) unit. In the first case, the liquefied gas is drawn from a pump, usually submerged and insulated, and conveyed to the vaporizer via vacuum-insulated piping. In the second system, the cryogenic tank is pressurised via a pressure buildup system, which regulates the natural boil-off tendency via the thermal load from the PBU heat exchanger. The pump-driven system allows for higher delivery pressures and wider range of deliverable mass flows to the user but features a critical and expensive component like a cryogenic pump. In the case of LNG, the storage pressure is usually in the range of 0.4 to 1 barg, then insufficient to meet the engine pressure requirement. Therefore, virtually all LNG vessels currently in operation operate a pump driven system [18]. With regard to the selection of components, the preferred pump is of the cryogenic submerged type. In the field of heat exchangers, there is a distinction between shell-and-tube architectures and full plate or shell-and-plate heat exchangers (HEX) designs. However, the applicability of this paradigm is dictated by the operating parameters of each specific application, therefore it is difficult to be generalized.

## 2.2 $LH_2$ technologies for maritime applications

Although liquid hydrogen is widely recognised as a key enabler of deep decarbonisation, its technological readiness and industrial deployment remain significantly behind those of LNG. In fact, while liquefied natural gas counts on mature supply chains, standardised infrastructure, and extensive cross-sector adoption in maritime and heavy duty transport, $LH_2$ technologies are still constrained by unresolved challenges related mostly to handling, cost, and regulatory frameworks [18,22,72]. Meanwhile, research focuses on establishing the starting point criteria to extend cryogenic knowledge to liquefied hydrogen sector.

From a state of the art analysis, it appears that a two-tier situation unfolds with the two largest sectors interested in $LH_2$. On the one hand, the aviation industry puts consistent effort on $LH_2$ research with several projects, patents submitted and activities summarised in [84]. Such projects and research regard both component level e.g. cryogenic pumps [85], novel cycle architecture with integrated heat exchanger [86], and assessment at system level [87,88]. For instance, in [86] a detailed design of a recuperative-intercooling heat exchanger for aero engines is proposed. However, since by employing such a system hydrogen delivery temperature would strongly vary with engine load, authors in [88] evaluated a similar system coupled to a parallel hydrogen combustion, where the fuel is mixed to air bled from the engine and the off-gases are sent to a heat exchanger, allowing a better control of the cold hydrogen temperature at the expenses of an increase in fuel consumption.

Conversely, there appears to be a lesser degree of investment and development in the maritime sector with respect to $LH_2$ technology enhancement, despite reviews assess that it is the best solution for hydrogen storage in transportation [22]. Other research focuses on fuel storage system. Type C design concept is translatable to actual $LH_2$ applications through computation of thermal and mechanical stresses [89], also for the specific application of heavy duty trucks [68].

Despite the lack of technological readiness, there are examples of companies offering ready $LH_2$ fuel handling systems for ship propulsion (Everllence SE, [90]), while others are working on international projects to design a complete fuel storage and supply system [91,92]. In particular, Figure 9 illustrates the architecture of the "MAN Power Pack" system, comprising a containerised pressure-driven fuel supply system for PEMFCs powerplant that complies with the safety standards stipulated by the International Maritime Organisation (IMO). The system is pressure-driven, with a PBU maintaining a pressure level compatible with the fuel cell supply requirements.

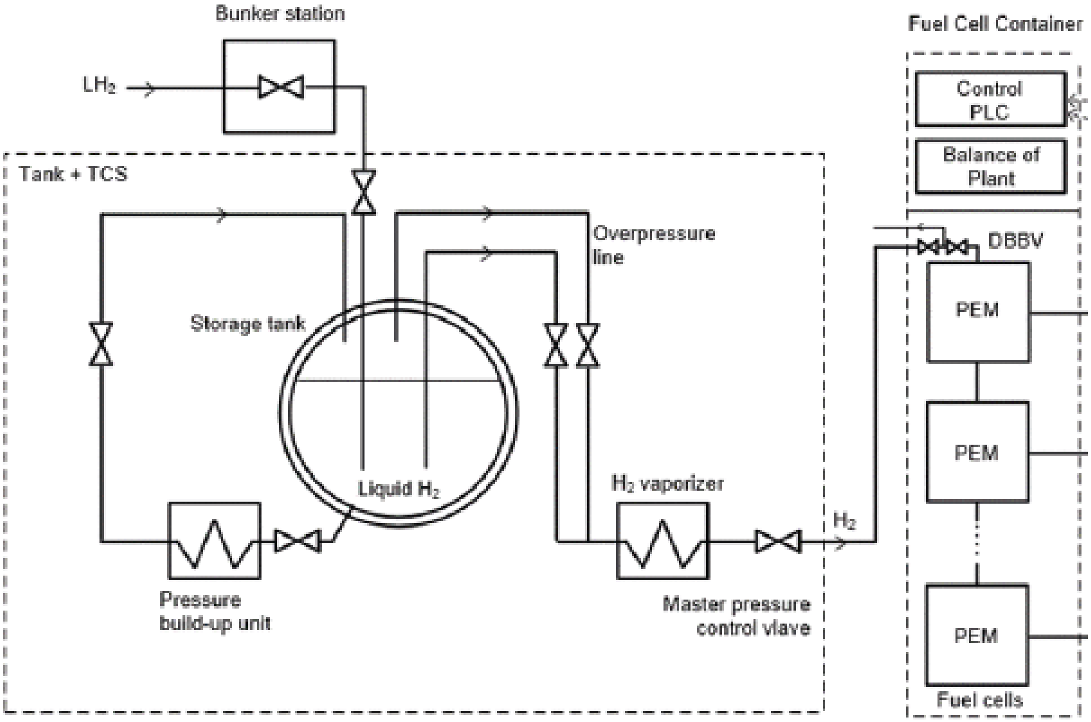


*Figure 9 – Overview of the complete LH2 Marine Power Pack [90]*

Currently, there is only one notable example of liquefied hydrogen powered vessel aside the demonstrative prototypes: *MF Hydra* is a Pax & car ferry cruising across southern Norwegian fjords propelled by a hybrid $LH_2$ PEMFC-diesel engines powerplant [93]. The dynamic modelling, control strategy and simulation of the optimal energy management schedule of a equivalent vessel is performed in [94] and [95], respectively. Ultimately, in the next future *Viking Lybra* will be the first medium cruise ship to be equipped with a hydrogen based power system [92], namely a 6 MW $LH_2$-PEMFC configuration possibly targeting zero-emission hotelling during port stays.

## 2.3 Materials for onboard cryogenic service

### 2.3.1 Properties of materials at cryogenic temperatures

Severe cryogenic conditions pose problems in selecting a material capable of withstanding mechanical stress within an acceptable range. In general, exceptionally low temperatures tend to make materials very brittle. In particular, as the Ductile to Brittle Transition Temperature (DBTT) is overcome, the ability of a material to withstand dynamic stresses (i.e., impacts or sudden changes in pressure) is highly reduced. Metallic materials usually have excellent fracture toughness in ambient conditions. However, only some of those retain acceptable figures in cryogenic conditions and are chosen for such sectors. In fact, at cryogenic temperatures, the material has improved mechanical resistance, but it is also more brittle [96,97]. This is a common trend for most steels, especially martensitic and ferritic, while for austenitic ones such as AISI 316 the deviation is less evident [96].

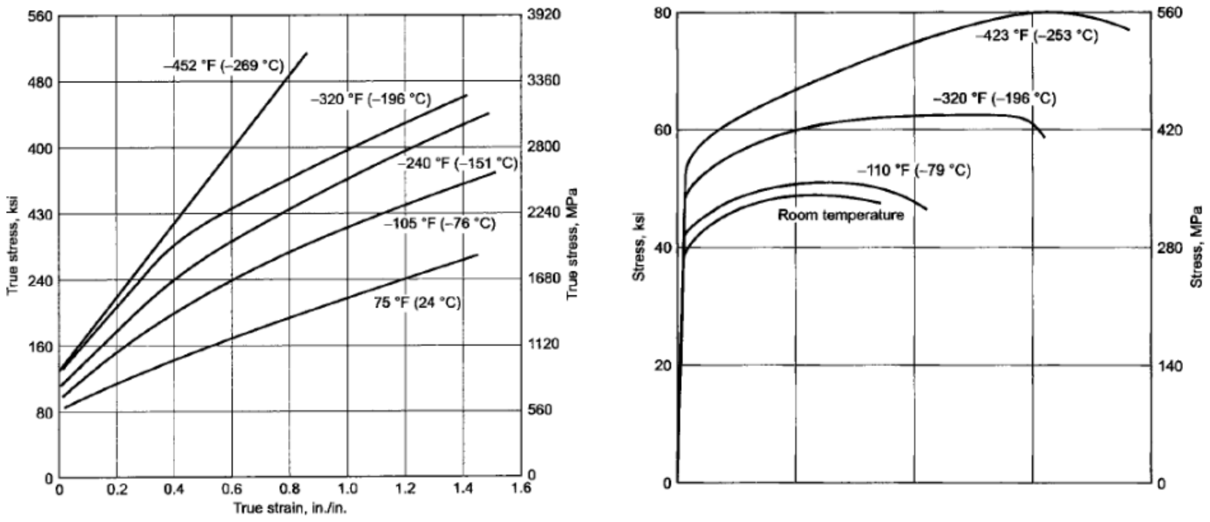


a) b)

*Figure 10 – Stress-strain diagram for a) AISI 316 and b) 6061-T6 aluminium alloy at various temperatures [97]*

Materials that show suitable properties at low temperatures generally also have lower thermal conductivity than other similar metal alloys. This is true for AISI 316 and Ti-6Al-4V but also holds for other metallic materials. Although not decisive, this is a clear advantage for cryogenic applications in terms of reduced heat flow to the liquefied gas [67].

Regarding marine field, the corrosive environment calls for specific characteristics of the material to be utilised. AISI 316 has adequate characteristics at cryogenic temperatures [67], as depicted in Figure 10a. The Korean Register quantifies that tensile strength is more than twice for AISI 316 and 316L at 20 K with respect to room temperature [98]. This is undoubtedly convenient, since such material has a wide range of established marine-related applications and its cost is still acceptable. To prove it adequate, on the Suiso Frontier $LH_2$ tanker both the inner vessel and the outer containment are realised utilizing austenitic stainless steel [99]. It is also known that nitrogen-enriched stainless steel alloys, commercially known as Nitronic®, offer considerable corrosion resistance and tensile strength thanks to their nitrogen-enhanced austenitic stability, both at very high temperatures and at cryogenic condition. Hence, these might be considered as alternative to more conventional materials when very harsh environment is present.

Composite materials have distinctive characteristics. At present, those materials are widely used for high pressure storage tanks and lightweight applications. In [100] authors report data for various unidirectional epoxy composites, showing that even at temperatures of few Kelvins not only they suffer almost no degradation in tensile strength, but they also perform better. As an example of real world application of composites, the Suiso Frontier employs glass fibre-reinforced plastic (GFRP) for the inner vessel saddles [99].

### 2.3.2 Hydrogen embrittlement

Hydrogen embrittlement refers to the mechanism involving hydrogen penetration into a solid material, starting from its surface, an event that can seriously reduce the ductility and load capability of susceptible materials. Hydrogen diffuses to the metal grain boundaries and forms voids, which are preferred nucleation sites for crack propagation under applied load. Metals, and materials with a lattice-like atomic structure in general, are among the most susceptible to hydrogen embrittlement.

According to NASA [101], hydrogen embrittlement can be classified into three categories:

- Hydrogen Environmental Embrittlement (HEE)
- Hydrogen Internal Embrittlement (IHE)
- Hydrogen Reaction Embrittlement (HRE)

Figure 11 clarifies the distinction among those categories based on competing factors [101]. Usually, this phenomenon is represented in terms of HEE index, namely a non-dimensional parameter which equals unity when HE has no influence and decreases as much as the material is affected.

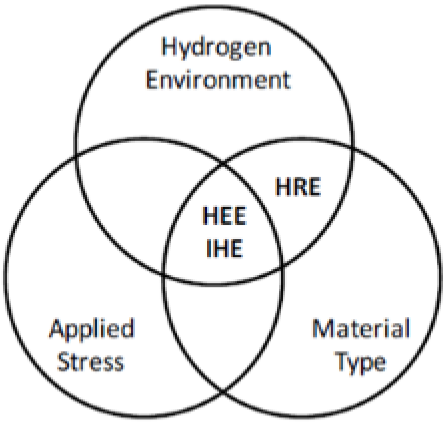


*Figure 11 – Classification of hydrogen embrittlement depending on mechanism [101]*

Hydrogen embrittlement is particularly enhanced under very high pressures, since the natural tendency of hydrogen to escape through the metallic lattice is enhanced by the pushing effect of the pressure and promotes HEE effects at the tip of a propagating crack. For materials exposed in aqueous environment, a degradation mechanism known as Stress Corrosion Cracking (SCC) may appear [101]. In this phenomenon, material at the crack tip is removed by a corrosive process caused by aqueous environment or contact with moisture, enhancing crack propagation and possible related failure. In fact, this process is typical of materials with low corrosion resistance, such as aluminium alloys, while steels and corrosion-resistant metals are less prone [101].

The effect of cryogenic temperatures on hydrogen embrittlement is still not completely clear. Rapid cooling of metal from higher than ambient to room temperature can result in IHE due to the reduced hydrogen solubility at ambient conditions [101]. This appears to be relevant for $LH_2$, e.g. during bunkering or tank refill; however, it is not clear whether cooling from ambient to cryogenic temperatures enhances HE. Furthermore, in stable cryogenic conditions the material is less prone to hydrogen penetration into the metal lattice due to the reduced hydrogen mobility [101]. The idea that hydrogen mobility is exceptionally low at cryogenic temperatures is shared among other authors [102].

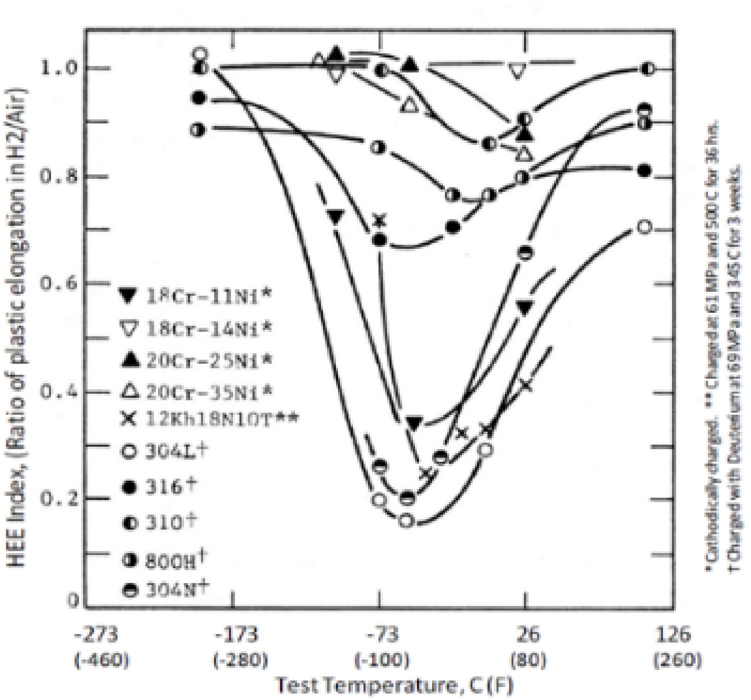


*Figure 12 - Effect of temperature on HEE index for selected steels [101]*

To better understand the effect and the severity of hydrogen embrittlement on certain materials, a Hydrogen Environmental Embrittlement Index (HEE index) has been defined in [101]. It assumes values from 0 to 1, where 0 corresponds to material worst affected and 1 refers to material unaffected. Therefore, to maximize the HE resistance, it is desirable to obtain values for the HEE index as close to unity as possible. NASA researchers [101] observed that HEE is most severe in the vicinity of room temperature or slightly lower. This can be explained as follows: at very low temperatures, diffusivity of hydrogen is too sluggish to fill a sufficiently high number of vacancies in the lattice, but at high temperatures, hydrogen mobility is enhanced, and trapping is diminished. For advanced metal alloys, the minimum of HEE index is moved towards higher temperatures. The aforementioned AISI 316 exhibits maximum decrease in HEE index by 30% at around -73°C, as highlighted in Figure 12.

Another interesting result, shown in Figure 13, is that a precise range of nickel content (13% - 33%) in the alloy exists for the material to be especially resistant to embrittlement. This is apparently valid for both superalloys and stainless steels [101].

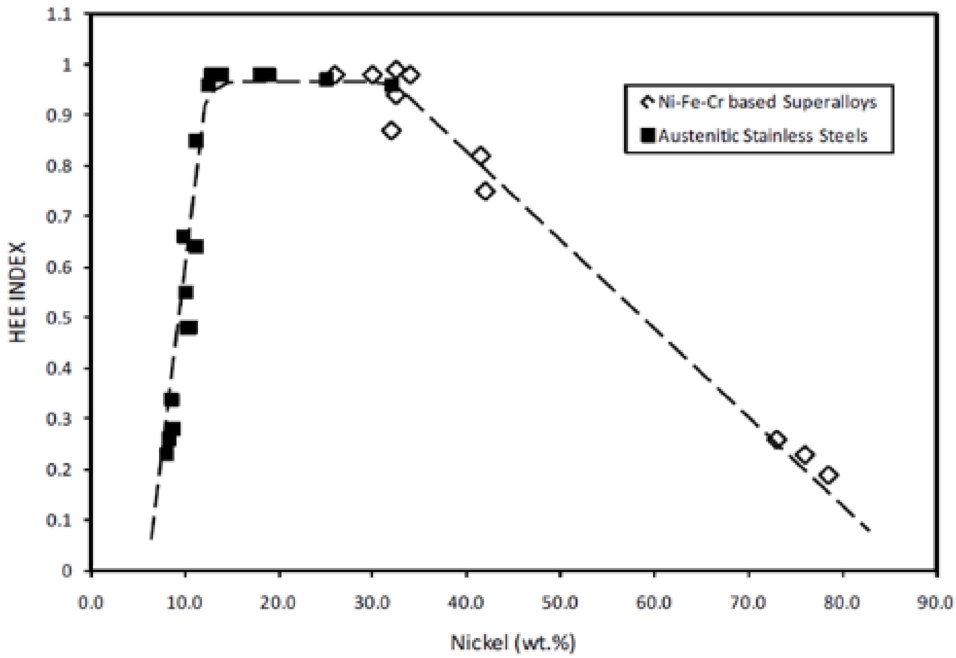


*Figure 13 – Effect of Ni content in alloy composition on HEE index*

The American Institute of Aeronautics and Astronautics (AIAA) has defined a ranking of metallic materials that best resist to hydrogen embrittlement [103]. These evidences are reported in Figure 14 and also include some composite materials and polymers. It is evident that most of the metals are resistant to hydrogen embrittlement, while only a couple of polymers sustain hydrogen rich environments.

| Material | Service GH$_2$ | LH$_2$ | SLH$_2$ | Remarks |
|---|---|---|---|---|
| Aluminum and its alloys | Yes | Yes | Yes | |
| Austenitic stainless steels with > 7% nickel (such as, 304, 304L, 308, 316, 321, 347) | Yes | Yes | Yes | Some make martensitic conversion if stressed above yield point at low temperature. |
| Carbon steels | Yes | No | No | Too brittle for cryogenic service. |
| Copper and its alloys (such as, brass, bronze, and copper-nickel) | Yes | Yes | Yes | |
| Gray, ductile, or cast iron | No | No | No | Not permitted for hydrogen service. |
| Low-allow steels | Yes | No | No | Too brittle for cryogenic service. |
| Nickel and its alloys (such as, Inconel® and Monel®) | No | Yes | Yes | Susceptible to hydrogen embrittlement |
| Nickel steels (such as, 2.25, 3.5, 5, and 9 % Ni) | No | No | No | Ductility lost at LH$_2$ and SLH$_2$ temperatures. |
| Titanium and its alloys | Yes | Yes | Yes | |
| Asbestos impregnated with Teflon® | Yes | Yes | Yes | Avoid use because of carcinogenic hazard. |
| Chloroprene rubber (Neoprene®) | Yes | No | No | Too brittle for cryogenic service. |
| Dacron® | Yes | No | No | Too brittle for cryogenic service. |
| Fluorocarbon rubber (Viton®) | Yes | No | No | Too brittle for cryogenic service. |
| Mylar® | Yes | No | No | Too brittle for cryogenic service. |
| Nitrile (Buna-N®) | Yes | No | No | Too brittle for cryogenic service. |
| Polyamides (Nylon®) | Yes | No | No | Too brittle for cryogenic service. |
| Polychlorotrifluorethylene (Kel-F®) | Yes | Yes | Yes | |
| Polytetrafluorethylene (Teflon®) | Yes | Yes | Yes | |

*Figure 14 – Summary of material compatibility for hydrogen and hydrogen cryogenic service [103]*

In conclusion, aluminum alloys and austenitic stainless steel appear to be sufficiently capable as fuel tank material for cryogenic hydrogen service. The choice between them depends on other parameters such as fatigue resistance, mechanical resistance, and thermal conductivity. With the focus on maritime uses, it is evident that resistance to corrosion is an additional requirement. This might suggest austenitic steels, in particular AISI 316 (or X5CrNiMo17-12-2 as per the European designation) or its low-carbon version (316L or X2CrNiMo17-12-2), which are both already well known to the maritime industry. Alternatively, titanium alloys and nickel alloys are equally suitable for use in cryogenic temperature but suffer from enhanced hydrogen embrittlement owing to the configuration of their crystal lattice and their cost is significantly higher.

### 2.3.3 Insulation of cryogenic tanks

Cryogenic tanks require high-performance insulation to prevent heat transfer toward the bulk liquid. Since the TRL of cryogenic tanks is increasing, research pushes towards better and better insulation techniques, as proven by a few European Projects investigating novel solutions for $LH_2$ tank insulation. As a general consideration, not every cryogenic tank today available has both active and passive insulation. Active insulation denotes a class of technological systems that are designed with the primary function of actively removing or creating conditions to minimise the heat ingress. These systems include refrigeration units, cryocoolers and reliquefiers, and they are the ones responsible for active heat extraction. Large cryogenic tanks typically employ a double-liner configuration, wherein a vacuum is generated to minimise thermal conductivity.. Since this is hardly sufficient to guarantee acceptable thermal flux, further passive insulation technologies are adopted. In this scope, some methods appear to be the most promising for future technological development [104].

Experimental values for the overall thermal conductivity of passive insulation technologies are found in [105] depending on vacuum pressure. Results were obtained using liquid nitrogen as a cryogen medium. Table 5 contains a summary of the possible insulation methods that are applicable to $LH_2$ tanks. Multi-layer insulation (MLI) is undoubtedly the readiest technology for cryogenic tank insulation, and also the most widespread [104]. MLI consists of dozens of very thin plastic films (such as Mylar or Kapton) coated with a metal like aluminum or silver to render them highly reflective. The layers are stacked with tiny spacer materials so that no surfaces touch, forming a blanket that is effective in vacuum environments. In the absence of both convection and most conduction in a vacuum, MLI becomes the primary method of controlling radiative heat transfer on spacecraft and cryogenic equipment. It also appears to be also the most suitable for maritime fuel tanks containing $LH_2$, considering their good performance, their relative simplicity, and technological readiness level. A typical arrangement of a MLI cross-section for spacecraft application is reported in Figure 15.

*Table 5 – Overview of the main insulation methods for liquefied gas tanks [18]*

| Insulation method | Comment |
|---|---|
| Multi-layer insulation (MLI) | Combines reflective layers and spacers to reduce heat transfer. Widely used and readily applicable for cryogenic tanks. |
| Spray-on Foam Insulation (SOFI) | Effective for LNG, but impractical for $LH_2$ marine use due to required thickness. |
| Vapor-cooled Shield (VCS) | Uses BOG to cool tank. Works well with MLI, especially in maritime systems. Performance is enhanced with para-ortho catalysis. |
| Glass microspheres (HGM) | Durable and vacuum-insensitive. Random packing reduces ideal performance. |
| Perlite powder | Lightweight, less durable. Used in the world's largest $LH_2$ spherical storage tank. |
| Aerogels | Very light but costly. Limited to research-scale cryogenic use, no known industrial applications |

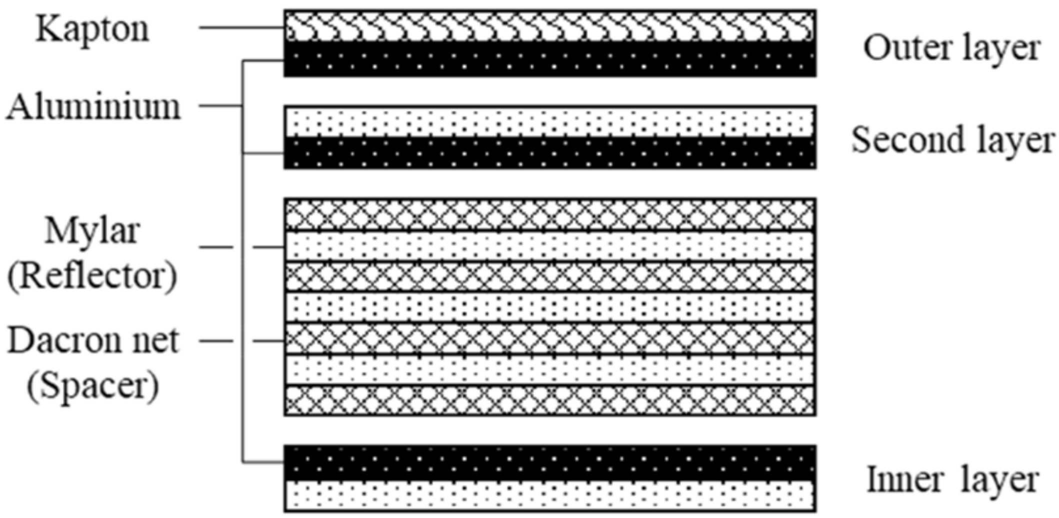


*Figure 15 – Schematic of typical MLI insulation for spacecraft application [69]*

Vapor-cooled shield (VCS) consists of a thermal shield from the environment created by allowing the cold BOG to flow around the tank. As the cold vapor absorbs heat while flowing through channels or tubes attached to the shield, the heat load reaching the inner tank is significantly reduced, cutting boil-off losses. In case of marine applications, and in general wherever BOG may be used for power generation, a VCS could be an interesting solution to simultaneously maintaining the bulk liquid at cold temperatures and exploiting the BOG for power production, possibly in combination with para-ortho conversion [106]. It is found that the optimal placement of VCS is at the midpoint of the MLI thickness, with an efficiency of approximately 60% observed in the case of $LH_2$, while for other cryogens such as nitrogen, oxygen and methane, the saving is no more than 27% [107].

Hollow glass microspheres insulation (HGM) has brittleness as their main challenge, although they do not usually fail due to vibration or thermal cycling [108]. Moreover, their performance is not affected by vacuum loss or vacuum pressure variations [104]. Theoretically, a face-centered cubic arrangement maximizes the insulation potential since the spheres have the least total contact area per unit volume and convection is virtually inhibited [108]. In practice, the sphere arrangement is random, with little chance to control their actual disposition, leading to a inherent sub-optimal condition.

Perlite powder is a granular material obtained from amorphous glass which is milled and graded to specific particle sizes and bulk densities. It is lighter but has a higher thermal conductivity than glass microspheres. It also has increased fragility and is less resistant to thermal cycles. Perlite powder has already some large size applications (tanks with more than $3m^3$ capacity) for liquid nitrogen [109] and very large $LH_2$ tanks.

Aerogels have very low density, but their thermal conductivity is somewhat higher than glass microspheres and perlite powder [104] and they are extremely expensive. Today, their application is limited to research scale cryogenic tanks [110].

## 2.4 Safety and regulatory framework

Cryo fuels utilisation as alternative marine fuel poses severe safety issues, especially with $LH_2$ as compared to LNG. The land-based storage, handling and utilisation of liquid hydrogen is subject to rigorous regulation by several prominent institutes (e.g. ISO, NASA). Nevertheless, no prescriptive rules or regulations have yet been established for novel applications such as hydrogen-fuelled vehicles, aircraft and vessels. It is evident that there is a considerable gap in knowledge regarding the precise regulations that are required for the future standardisation of hydrogen-powered ships.

As previously mentioned, LNG aspects are dealt with through an established set of rules and guidelines. Although it has more than a few similarities to LNG, liquefied hydrogen also presents numerous different and more challenging issues to deal with. Some researchers tried to summarize a comparison between LNG and $LH_2$ in terms of practical aspects, further assessing their main criticalities as reported in Table 6 [72]. Extensive research deals with hydrogen safety for mobile applications, highlighting the importance of setting comprehensive safety bases to help hydrogen uptake [111].

*Table 6 - Summary comparison between LNG and $LH_2$ in terms of practical feasibility. A "0" means that the property is similar for the two fuels. Adapted from [72].*

| Property | LNG vs $LH_2$ | Comment |
|---|---|---|
| Reactivity with materials | LNG | Hydrogen requires high grade materials |
| Heat capacity | $LH_2$ | $LH_2$ has greater heat capacity – advantage in liquefied storage |
| Heat flux from the surroundings | LNG | Consequence of lower storage temperature (provided equal insulation) |
| Flammability range in air | LNG | Flammable conditions are more easily formed with hydrogen leaks |
| Ignition energy | LNG | Hydrogen clouds are more easily ignited than NG clouds |
| Ignition temperature | 0 | NG has slightly higher ignition temperature |
| Liquid phase ΔT between 1 and 10 barg | LNG | Smaller range for $H_2$. Requires more efficient control of heat leakage |
| Laminar flame speed | LNG | Higher for hydrogen, i.e. higher risk of spreading fire |
| Dense phase behaviour of leakages | $LH_2$/0 | Both have density higher than air at near condensation temperature, but hydrogen tends to escape faster |

### 2.4.1 Current status of regulation for maritime hydrogen

In the scope of the marine sector, the International Maritime Organisation (IMO) has two sets of guidelines that are relevant to LNG and $LH_2$: the IGC-code and the IGF-code. The first is the standard that regulates the structure and the design of a ship carrying liquefied gases in bulk, while the second is the standard regulating ships propelled by low-flashpoint fuels, i.e., that have boiling point at sub-ambient temperatures (natural gas, hydrogen, and ammonia). However, hydrogen was not a subject of interest at the time these codes were issued and is therefore not specifically described in either of the two. Alongside, LNG as a fuel was covered in the IGF code. For these reasons, in 2016 the IMO issued the resolution MSC.420(97) - Interim Recommendations for the Carriage of Liquefied Hydrogen in Bulk [78] in order to lay the foundations for future rules and regulations in this area. In light of the increasing interest in hydrogen within the naval sector, and the necessity for timely standardisation, this document has undergone further revisions and has been updated by the subsequent MSC.565(108) in 2024 [112]. This document constitutes the most advanced and up-to-date set of recommendations regarding hydrogen onboard vessels, specifically addressed to it as a cargo but extendible to hydrogen fuel to some extent. Further amendments to IGC and IGF codes are expected to see the light by 2028 concerning the use of hydrogen as a fuel on board [113].

In the present context, project approval of hydrogen-powered vessels is contingent upon a risk-based evaluation process, whereby it is required to prove an equivalent level of safety compared to that of a conventionally fuelled ship [114]. This risk-based approval process is referred to as the Alternative Design (AD) approach, and it requires the fatality risk to be "as low as reasonably possible" (ALARP). Evidently, the process appears to be carried out on a case-by-case basis, and utilising it as a custom for hydrogen ships certification is rendered unfeasible by the substantial process involved (HAZID, HAZOP, explosion analysis, quantitative risk analysis, etc.), which is accompanied by a significant degree of non-standardisation. Nevertheless, the Alternative Design process is characterised by some flexibility in comparison to prescriptive rules. Consequently, to the extent that the requirements stipulated by the authority are met, designers are granted a certain degree of autonomy [114].

### 2.4.2 Hydrogen related hazard and mitigations

One of the aspects that surely do not bond LNG and $LH_2$ is surely safety. This is a fact which is largely agreed upon, and the main causes of unalignment are reported in Table 6. Quantitatively, the parameters affecting the safety of both fuels are summarised in Table 7.

*Table 7 – Thermophysical parameters of hydrogen and methane relevant to safety. Unless specified, all properties are expressed at ambient conditions.*

| Parameter | Hydrogen | Methane |
|---|---|---|
| LHV [MJ/kg] | 120 | 50 |
| Boiling point @ 1 atm [°C] | -253 | -162 |
| Critical point (p/T) [MPa/°C] | 1.3/-234 | 4.6/-83 |
| Flammability range [% vol] | 4-75 | 5-15 |
| Ignition energy in air [mJ] | 0.02 | 0.3 |
| Diffusion coefficient in air [cm/s] | 0.61 | 0.16 |
| Leidenfrost temperature [°C] | -240 | -113 |

Flammability is the most crucial aspect of hydrogen as compared to all other alternatives. It is classified it as highly flammable from the National Fire Protection Association (NFPA), and also extremely dangerous in liquefied form as per Figure 16, owing to the low flashpoint. Besides, the ignition energy is one order of magnitude lower than natural gas, meaning that static discharge, a spark or, under certain circumstances, the bare friction with pipes or external surfaces at high flow speeds or temperatures can be sufficient to generate ignition [111,115]. Besides, as discussed in section 2.3.2, it causes embrittlement of most metallic materials owing to its high diffusivity and small molecular size [116]. The flammability range strongly varies with respect to temperature and pressure: the available data almost always applies to ambient conditions or ambient temperatures. However, the following considerations might be drawn when dealing with cryogenic hydrogen:

- A decrease in pressure corresponds to an increase in lower flammability limit (LFL), a decrease in upper flammability limit (UFL) and an increase in minimum ignition energy. Hence, sub-atmospheric pressures are beneficial, but this effect is quantitatively negligible and irrelevant from a safety perspective [117].
- Higher temperatures increase the flammability range (lower LFL and higher UFL). The behaviour of $H_2$/air mixture at cryogenic temperatures

is still not clear, but the flammability range is expected to reduce: some authors concluded that at 100 K (-173 °C) the flammability range of hydrogen is narrower but again, not appreciably for safety concerns [118]. From this perspective, cryogenic storage does not represent an enhanced safety measure with respect to pressurised gaseous storage.

- The minimum ignition energy (MIE) appears to increase in case of hydrogen ignition in cryogenic conditions [119,120], thereby inherently augmenting the safety level of $H_2$ storage in liquefied form.

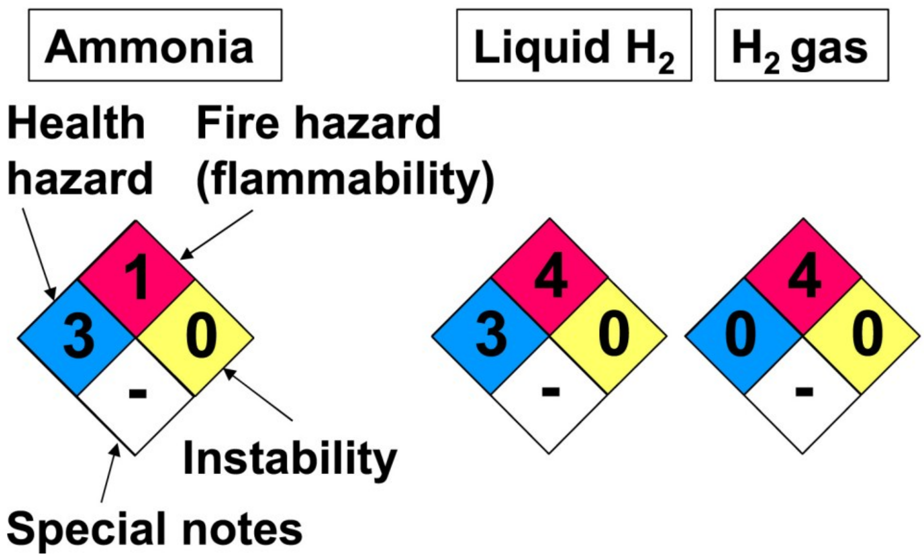


*Figure 16 - Fire diamonds of ammonia, liquid hydrogen and hydrogen gas [121]*

#### 2.4.2.1 Inerting of flammable and explosive atmospheres

Inerting is achieved by introducing inert gases such as nitrogen, helium, argon or carbon dioxide. Several works have explored the effectiveness of different inert gases, concluding that considering maximum explosion pressure and maximum rate of pressure rise as indicators, the effectiveness of inert gases on the inhibition of confined hydrogen explosions can be ranked as follows: $CO_2$, $N_2$, Ar and He [122,123]. In [103] also steam is assessed as inert, but it is straightforward to observe that this is not viable at cryogenic temperatures. Besides, no safety provision even suggests which inerting gas is the most appropriate for marine application, irrespective of the storage conditions.

Inerting of hazardous spaces with a traditional and largely available gas like $CO_2$ causes no issues if the hydrogen is in compressed form [103], but in case of $LH_2$ one should consider that those are solid at hydrogen boiling point. In event of leakages or cryogenic dispersion in the enclosure, this necessitates for a removal of the condensate, if not even defrosting. An alternative measure could be the exploitation of helium as inert: having the lowest boiling point, this substance is gaseous even at -253 °C. However, helium has ingent cost and the storage in large volumes may be anti-economical. Argon combines the two downsides of too high boiling point and excessive costs. Seemingly, the best choice remains nitrogen even for $LH_2$, provided that condensed $N_2$ be collected in insulated drip trays, evacuated from the room and disposed. It is also observed that nitrogen condensation or, worse, solidification can occur only in event of direct contact with liquefied hydrogen, remaining otherwise gaseous, though very cold. However, it should be assured that its evaporation does not represent a problem. It is to be noted that the same concern does not apply to LNG, since at its boiling temperature nitrogen is still in gaseous form, so it is completely adequate to purge natural gas rich enclosures.

Owing to the increased overall risk linked to hydrogen release event, some information was sought about a real case risk assessment. Some authors theoretically applied the IGF-Code's Alternative Design specifications for a short-sea high speed hydrogen ferry employing compressed $GH_2$ stored at 250 bar in Type IV cylinders [124]. In this work, they assessed the risk associated to the following items: storage tank, high pressure piping, low pressure piping, engine, and vent mast. They found that the estimated risk related to hydrogen system is very low, and much lower than the acceptable risk level related to hydrogen (two orders of magnitude).

### 2.4.3 Pre-normative research and associated risk events

The risk events associated with liquefied hydrogen system failure can generally be classified based on fire occurrence (ignited/unignited) or immediate/delayed combustion. Releases from an $LH_2$ tank could also be single phase or multi-phase. In the context of maritime operations, it should be pointed out that scenarios involving the release of liquid hydrogen within sub-deck enclosures are likely to be of minimal concern. This is confidently true because such an occurrence is to be avoided in the first place since the associated loss potential is very high and could possibly lead to an unacceptable risk level. Table 8 reports the main risk events that an $LH_2$ system can undergo. It appears that the most probable outcomes are either unignited releases, both in form of pool spill and two-phase jets, and ignited events, i.e., pool fire and jet fire. Boiling liquid expansion vapour explosion (BLEVE) is an event occurring whereby a vessel containing a pressurized liquid ruptures, therefore undergoing a rapid expansion with consistent liquid vaporization. Even though BLEVE does not necessarily involve a fire, the outcomes are usually evaluated under the assumption of complete burning of the whole tank content, which is overly conservative as demonstrated by experiments [125]. A Pressure peaking phenomenon (PPP) is the result of the release of a lighter gas into a vented volume containing denser gas, whereby the former displaces the latter creating a transient non-equilibrium pressure condition and occupying the whole volume [126]. It only occurs in enclosed spaces, and only if the $H_2$ leak is sufficiently large and the vent area sufficiently small [127].

*Table 8 - Overview on typical failure consequences of $LH_2$ systems, characteristics, and outcomes.*

| Failure consequence | Characteristics | Comment |
|---|---|---|
| Liquid pool release | Unignited | $LH_2$ spills form rapidly vaporizing pools with behavior dependent on surface type, lasting generally <5 s on solid ground. |
| Plume/jet release | Unignited | Large $LH_2$ releases can form dense vapor plumes near ground before buoyancy dominates due to convective heating from the ground and air mixing. Very likely occurrence. |
| Rapid phase transition (RPT) | Unignited, delayed | Occurs without combustion from sudden boiling due to vapor film collapse. Likely to occur in releases in water. |

| | | |
|---|---|---|
| Pool fire | Ignited, rapid or delayed | Initially conduction-dominated, then convection-dominated. Larger pools showing higher but possibly fragmented burn rates and risk of secondary explosion post-ignition. |
| Jet fire | Ignited, rapid | Ignited cryogenic jet releases generate high radiative heat flux. Usually originate from ignition of a plume release. Very likely to occur as escalation from a plume/jet release. |
| Deflagration/detonation | Ignited, delayed | Low initial temperatures reduce the likelihood of detonation by limiting the flame acceleration due to lower Zeldovich number. |
| BLEVE | Unignited, delayed | If ignited, may result in fires forming large fireballs whose diameter scales as $D \propto m^{0.45}$. Not as typical as a consequence because risk magnitude is usually overestimated. |
| Pressure peaking phenomenon (PPP) | Unignited or ignited | Occurs during ventilated indoor $LH_2$ releases, where vent size and enclosure volume influence pressure peak and delay. Release rate has a minor influence on pressure peaking. |

It is known that there exist a scarcity of data and general experience with hydrogen release, especially $LH_2$. Therefore, it is important to identify what are the most probable incidents or accidents, both in terms of causes and outcomes. In [115] were identified 287 occurrences and it was concluded that:

- Explosion occurs in 96% of $GH_2$ releases and about 50% of $LH_2$ releases.
- Hot surfaces constitute the ignition source in most cases (21% for $GH_2$ and 11% for $LH_2$).
- There were 199 injuries out of 201 $GH_2$ accidents and 10 injuries out of 86 $LH_2$ accidents.

The PRESHLY project identified 18 incidents related to $LH_2$ storage and containment systems during transportation and liquefaction/storage [115]. The causes and outcomes of such incidents are reported in Table 9.

Equipment failure included unexpected burst disk failure, loss of vacuum, or a loose flange connection. Of the five cases during transit, two were related to road traffic accidents and the other three concerned venting due to burst disk failure and/or loss of vacuum. Injury to personnel occurred in 3 (17%) cases, 2 of which were cold burns. Property or equipment damage occurred in 7 (39%) cases. It was noted that out of six major incidents involving storage vessels, three occurred during decommissioning/commissioning (warm-up/cool-down). There were several incidents where unexpected ignition upon venting occurred, resulting in fire or explosion. Injury occurred in 3 (8%) incidents and non-trivial damage in 23 (59%) cases.

*Table 9 – Overview of causes and outcomes of $LH_2$ failure events during transportation, liquefaction and storage. Adapted from [115]*

| Cause | Occurrences (transp./liquef. & storage) | Event | Occurrences (transp./liquef. & storage) |
|---|---|---|---|
| Design/construction failure or inadequate HAZID | 0/12 | No release | 2/5 |
| Equipment failure | 6/8 | Accumulation or dispersion | 12/14 |
| Incorrect operation or procedural inefficiency | 8/18 | Fire | 4/9 |
| Impact or road accident | 3/0 | Explosion | 1/13 |
| Natural cause | 1/5 | BLEVE | 0/1 |

### 2.4.4 Main open challenges for safe operation with $LH_2$

As previously mentioned, despite extensive effort it emerges that hydrogen ships still lack a single, globally harmonised regulatory and standards framework. Current rules are patchy, project-specific, and largely "interim," which cannot be translated into repeatable global rules and slow mainstream deployment worldwide. The IGF Code does not yet contain full prescriptive requirements for hydrogen as fuel, and safety management still relies heavily on LNG-oriented provisions that do not fully match hydrogen's properties. Interim IMO guidelines for hydrogen as fuel have been drafted at CCC11 [113], but they are not yet integrated as mandatory code text and only cover specific concepts [128]. International safety standards for hydrogen as a fuel (ship bunkering, hose and interface design, zoning, simultaneous operations) lag behind those for transporting hydrogen as a cargo, and standardisation of bunkering procedures is repeatedly cited as a key missing piece [128]. Finally, ports and coastal states lack harmonised rules for emergency response, exclusion zones, and coordination around hydrogen bunkering and incidents, leading to a patchwork of local restrictions that complicate international operation of hydrogen-fuelled vessels. In the absence of a comprehensive regulatory framework including all the aforementioned points, the standardisation of hydrogen-fuelled ship design remains unattainable at this stage. However, certain considerations regarding the most salient challenges to be addressed for the safe utilisation of hydrogen on board can be derived.

#### *2.4.4.1 Hydrogen tank and location of hydrogen pipeline*

At the current stage, the IMO recommendation for low flashpoint fuels is to have a open deck arrangement with fuel containment and piping system such as to prevent accumulation of hazardous mixtures in enclosed spaces onboard. When tanks are installed below deck or in enclosed spaces, they are only allowed subject to detailed risk assessment and strict ventilation, gas-detection, and fire-protection measures. Interim IMO hydrogen guidelines developed at CCC11 refer back to IGF Code section 10.3 for tank location, while adding hydrogen-specific requirements on hazardous zones around outlets and potential leak points. Therefore, sub-deck $LH_2$ storage is not prohibited, in fact it is virtually the only practically viable option for large passenger ships [114]. A typical placement complying with recommendations would be an independent Type C tanks placed either on open deck or in dedicated, well-ventilated fuel storage hold spaces with controlled access and defined hazardous areas, again respecting IGF setback distances from side and bottom

#### *2.4.4.2 Prevention of flammable clouds*

Rules on flammable cloud avoidance for hydrogen and other low-flashpoint fuels on ships are mostly goal-based: they require designs that prevent formation of dangerous gas clouds in the first place, and if clouds do form, limit their size, duration, and likelihood of ignition. Owing to the lack of uniformity, regulations rely heavily on ventilation design, hazardous-area zoning, and project-specific risk assessments.

The European Maritime Safety Agency (EMSA) has evaluated that existing IGF measures in terms of flammable clouds control, which are tailored for LNG, do not fully address hydrogen properties. For instance, the 30 air changes per hour (ACH) proposed by the Interim Guidelines seem too optimistic. Therefore, it is suggested to assume that an ignition source is always present and to mitigate the effects of ignition, which is assumed to occur in any case [129]. In general, there is currently no single global numerical standard (e.g., specific maximum flammable volume or exposure time) for hydrogen flammable clouds on ships; acceptance criteria are usually set through case-specific, formally documented risk assessments validated by flag and class [129].

#### *2.4.4.3 Inerting of enclosed spaces*

The use of nitrogen is straightforward for $GH_2$ storage and utilisation in enclosed spaces. However, in event of a $LH_2$ dispersion, nitrogen may condense and it should be collected in a drip tray. Alternatively, helium can be used as it guarantees a gaseous phase throughout all operating temperatures, but it is costly and cannot be produced onboard as nitrogen. EMSA has concluded that, since ventilation cannot be considered a dependable measure, inerting of hazardous zones might be employed. Nevertheless, there is the potential for complications to arise in relation to the prevention of access to the inerted zone, the possibility of bulk condensation of the inert due to loss of tank vacuum insulation, and the constant requirement for nitrogen availability [129].

#### *2.4.4.4 Safe venting*

Vent lines for hydrogen (including pressure relief lines and boil-off from cryogenic systems) should be routed to a safe location outside. Vent lines are also used to dispose of hydrogen purged from the system for maintenance. The vent should be designed to prevent moisture or ice from accumulating in the line, to be safely inerted, and should have a cross section large enough to accommodate the vented mass flow without choking occurrences [130]. In a study it was evaluated that a fuel cell enclosure of 3m x 3m x 2m requires around 1500 ACH to stay below a 1% hydrogen concentration in volume [130]. In fact, this is the value commonly evaluated in risk assessments and it is also the typical trigger threshold for hydrogen sensors. According to NASA/AIAA, flaring may be considered for hydrogen vent rates larger than 0.2 kg/s [131].

#### *2.4.4.5 Explosion and fire protection*

In light of what explained in section 2.4.4.2 and considering the very low ignition energy (Table 7), it is commonly accepted that any hydrogen leak will eventually ignite. General fire protection rules for hydrogen on ships build on the general IGF Code philosophy (limit releases, avoid flammable clouds, then control any fire) but add requirements and recommendations for non-sparking detection, suitable extinguishing media, and intensive cooling of tanks and equipment. Hydrogen-oriented documents require fixed hydrogen detection in all relevant spaces, linked to alarms and automatic emergency shutdown (ESD) of fuel supply, so any incipient leak and subsequent fire can be limited in size and duration [129]. The general recommendation is to treat hydrogen fires as expected outcomes in serious leak scenarios and designing fire-protection systems so that the ship can withstand credible hydrogen fire durations while maintaining critical safety functions [129].

# 3 Suitability analysis of $LH_2$ onboard integration

The uptake of alternative low-emission maritime fuels requires particular attention to several aspects regarding their solid integration onboard a passenger ship. Therefore, a thorough investigation including the volume, weight, emissions, cost, and environmental hazard of the various low- or zero-emission technologies is imperative, as it provides a precise indication of the complexity and expense associated with substituting conventional storage and power generation systems with alternative fuel-based ones. This analysis is performed by means of HELM, a MATLAB-based software that allows to compare different standard and innovative fuel-power generator combinations to assess the best option in terms of space occupancy, weight, and total cost (CAPEX, OPEX, and regulation penalties).

## 3.1 The HELM tool

The HELM (Helper for Energy Layouts in Maritime Applications) is a tool that compares the performance of traditional and innovative energy systems on board ships for concentrated and distributed generation applications. Its database was developed through an extensive analysis of available market solutions in terms of power generation devices (e.g. fuel cells and internal combustion engines), fuels (e.g. hydrogen, natural gas and MDO) and related storage technologies. A comprehensive array of maps has been derived from the database, correlating costs, volumes, weights, and emissions (the parameters on which the multi-criteria analysis is based) with the requisite installed power and operating hours, which are provided by the user as input. Another key parameter is environmental hazard, which is linked only to the chemical and physical characteristics of the fuel in question and its potential negative effects in the event of an outboard spill. Following the entry of the requisite data, the software assigns a score for each parameter evaluated, based on its value and in comparison with the minimum achieved by the most efficacious technology. This score is also influenced by relevance, i.e. a sort of weighting that gives greater importance to one parameter over another. These are defined, assuming different values for each parameter, through the required inputs with the exception of cost relevance alone. The scores for the various parameters are then added together to obtain a single total score for each technology under consideration, thus finalising the comparison process. The parameters underpinning the multicriteria analysis are divided into two macro-groups: technical and statistical parameters. Technical parameters are defined as characteristics that are constant throughout the duration of a mission and the operational lifetime of a vessel. These characteristics include volume, weight, and cost of the various technologies employed. In contrast, statistical parameters are employed to describe non-routine situations that are subject to randomness, such as environmental hazards. The distinction between the two groups is reflected in the maximum achievable scores: statistical parameters are penalised by a factor representing accident risk, whereas technical parameters are not subject to any score reduction.

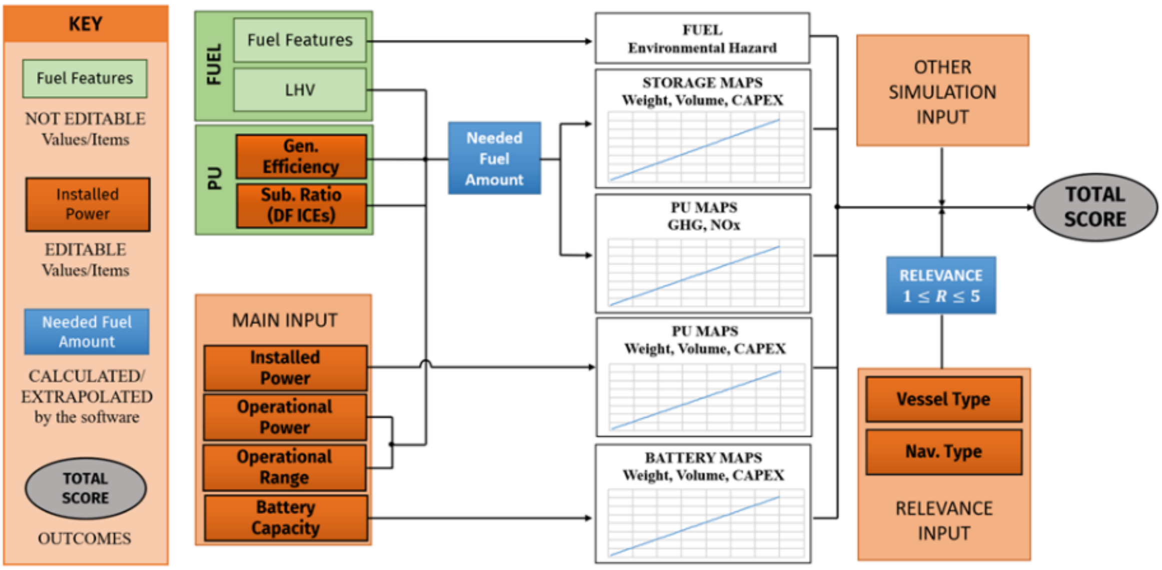


*Figure 17 – Simplified flow diagram of HELM tool.*

From Figure 17 one can understand the basics of the tool. Once defined the vessel type, its main inputs are selected. Then, based on operational range, installed power and operational power, the total fuel amount to be stored onboard and the volume required by each fuel tank or electricity storage are computed by means of maps. They contain correlations between a relevant parameter of the power generation unit (typically the PG rated power) and their volume or weight, while for fuel tanks or batteries the sizing parameter is the storable energy. The cost correlations are expressed in terms of capital expenditure (CAPEX) only; operational expenditure (OPEX) is computed as the net present value of 3.5% of the CAPEX for each technology, plus the fuel cost, plus the penalties deriving from the EU-ETS and FuelEU regulations. Further and more accurate details on the specifications of HELM are reported in [132].

## 3.2 Data collection and creation of correlations

To develop empirical correlations for maritime powertrain components and fuel/energy storage systems, data were collected from commercial datasheets of leading manufacturers, international reports, and peer-reviewed scientific literature. This file is divided into two main parts, the Power System and the Energy Storage sections. The former includes data for ICEs, gas turbines, fuel cells and ORCs, while the latter contains values for fuel storages, batteries, supercapacitors, TES and heat pumps. For each technology, a dedicated Excel sheet was created, including all relevant parameters of each device considered for this activity Based on these sources, scatter plots were generated for each technology using a dedicated Microsoft Excel repository. As described, these plots relate component ratings, such as rated power for engines and power generators (e.g., PEMFC and SOFC) or storage capacity for tanks and batteries, to key characteristics including size, weight, efficiency, and cost. Using the compiled datasets, polynomial fitting was performed through the embedded Microsoft Excel fitting tools. The resulting correlations enable the estimation of mass, occupied volume, and approximate cost of low- and zero-emission technologies intended for onboard installation.

A first-order polynomial was selected to fit the scatter plots associated with size and weight. This approach yielded coefficients of determination ($R^2$) equal to or greater than 0.9 for nearly all components, indicating a strong linear relationship. For efficiency trends, logarithmic fitting functions were adopted to better capture the underlying physical behavior, as efficiency typically approaches an asymptotic maximum with increasing power system size. Since efficiency is less strongly influenced by size than cost, weight, or volume, these correlations are inherently less accurate, generally exhibiting $R^2$ values of approximately 0.6-0.7.

As it was evident from the data collection, volume and weight data can be easily found on datasheets provided by the manufacturers, and plenty of those can be retrieved on their internet websites. On the other hand, cost data are never present on datasheets and anyhow hardly disclosed by manufacturers. Therefore, it relatively easy to collect a large amount of weight and size data to create custom correlations that better suit each specific technology, without having to rely on pre-existing literature correlations. This is impossible for cost functions due to the scarcity of cost data available, and it is necessary to rely on literature to understand the relationship between energy metrics and cost of many technologies. Therefore, a proper traditional literature survey has not been performed for size and weight correlations, considering that the topic is very specific and very little material is available aside of datasheets. On the other hand, specific cost data (i.e., USD/kW or USD/kWh) are widely available in literature, especially for non traditional power system and power generators (e.g. fuel cells and hydrogen tanks) because they are subject of current research [71,133]. This also means that total component costs have been subsequently calculated multiplying the specific cost by the regarding energy metric (i.e., power for PGs and energy for tanks and BESS). As a result, both cost scatter plots and cost maps frequently exhibit perfectly linear relationships, corresponding to an exact fitting and an $R^2$ value equal to 1.

The approach of employing data-sourced correlations is widely utilised for energy system subcomponents, such as compressors, pumps, motors, reactors, separators, heat exchangers etc. Moreover, many different cost functions for system components can be obtained from techno-economic analyses. In any case, once again these are cost functions and there is no reference to extensive quantities. However, as regards maritime power generation, only some authors have adopted the approach of creating “maps” of size, weight, and other relevant KPIs and have obtained correlations from them [23,134,135].

## 3.3 Correlations for power generators (PGs)

The complete set of correlation created is reported hereby in Table 10. Unless specified otherwise, volumes (V) are expressed in m$^3$, weights (W) in tonnes and costs (C) in USD. In accordance with the nomenclature commonly adopted in manufacturer datasheets, the term weight is used throughout this work to refer to the mass of each device.

*Table 10 – Volume, Weight, and Cost correlations regarding power generation systems (PGs).*

| **POWER GENERATION SYSTEM** | **Correlation** | | |
|---|---|---|---|
| | **Size (Volume) [m$^3$]** | **Weight[1] [tonnes or kg]** | **Cost [USD]** |
| ICE MDO (< 3MW) | $V = 0.0149 \cdot P_{rated}$ ($R^2 = 0.91$) | $W = 0.0107 \cdot P_{rated}$ ($R^2 = 0.92$) | $C = 262.5 \cdot P_{rated}$ |
| ICE MDO (3 - 7.5 MW) | | | $C = 258.9 \cdot P_{rated}$ |
| ICE MDO (> 7.5 MW) | | | $C = 318.2 \cdot P_{rated}$ |
| ICE DF LNG (< 4 MW) | $V = 0.0189 \cdot P_{rated}$ ($R^2 = 0.98$) | $W = 0.0129 \cdot P_{rated}$ ($R^2 = 0.98$) | $C = 457.7 \cdot P_{rated}$ |
| ICE DF LNG (4-8 MW) | | | $C = 289.1 \cdot P_{rated}$ |
| ICE DF LNG (> 8 MW) | | | $C = 369.3 \cdot P_{rated}$ |
| ICE DF MeOH | $V = 0.0152 \cdot P_{rated}$ ($R^2 = 0.95$) | $W = 0.0106 \cdot P_{rated}$ ($R^2 = 0.98$) | $C = 350 \cdot P_{rated}$ |
| ICE DF $NH_3$ | $V = 0.0201 \cdot P_{rated}$ ($R^2 = 0.98$) | $W = 0.0114 \cdot P_{rated}$ ($R^2 = 0.99$) | $C = 420 \cdot P_{rated}$ |
| ICE DF $H_2$ | $V = 0.0135 \cdot P_{rated}$ ($R^2 = 0.93$) | $W = 0.009 \cdot P_{rated}$ ($R^2 = 0.98$) | $C = 650 \cdot P_{rated}$ |

[1] In the case of PEMFCs, weight is reported in [kg] instead of [tonnes] as per datasheet due to their small sizes.

| | | | |
|---|---|---|---|
| Gas Turbines (GT) | $V = 0.0054 \cdot P_{rated}$ ($R^2 = 0.89$) | $W = 0.0018 \cdot P_{rated}$ ($R^2 = 0.82$) | $C = 1175 \cdot P_{rated}$ |
| 1PEMFC | $V = 0.0046 \cdot P_{rated}$ ($R^2 = 0.96$) | $W = 2.667 \cdot P_{rated}$ ($R^2 = 0.97$) | $C = 6000 \cdot P_{rated}$ |
| SOFC | $V = 0.1024 \cdot P_{rated}$ ($R^2 = 0.96$) | $W = 0.058 \cdot P_{rated}$ ($R^2 = 0.92$) | $C = 3000 \cdot P_{rated}$ |
| ORC | $V = 0.1711 \cdot P_{rated}$ ($R^2 = 0.85$) | $W = 0.049 \cdot P_{rated}$ ($R^2 = 0.91$) | $C = 4500 \cdot P_{rated}$ |

*Table 11 – Efficiency correlations for power generation systems (PGs).*

| **POWER GENERATION SYSTEM** | **Correlation** |
|---|---|
| | **Efficiency [-]** |
| MDO ICE | $\eta = 0.027 \cdot \ln(P_{rated}) + 0.226$ ($R^2 = 0.62$) |
| LNG ICE | $\eta = 0.0104 \cdot \ln(P_{rated}) + 0.423$ ($R^2 = 0.13$) |
| Gas Turbines (GT) | $\eta = 0.037 \cdot \ln(P_{rated}) - 0.005$ ($R^2 = 0.57$) |
| PEMFC | $\eta = 0.54$ ($R^2 = 0.017$) |
| ORC | $\eta = 0.024 \cdot \ln(P_{rated}) + 0.016$ ($R^2 = 0.26$) |

### 3.3.1 Internal combustion engines (ICE)

Internal combustion engines are the solid standard for maritime propulsion and electricity generation. Hence, a vast set of marine engines are available on the market, thus correlation of size and weight against rated power count on extensive data amount and can be easily derived by means of a linear regression with an excellent accuracy. Since datasheets of Diesel and LNG engines report a BSFC or BSEC, efficiencies are computed through assumptions of fuel LHV and operating hours. On the contrary, energy consumption of engines fuelled by alternative sources are not available. Figure 18 and Figure 19 report the scatter plot and the regarding correlation for weight of LNG ICEs and brake thermal efficiency of MDO ICEs, respectively.

The $R^2$ value for MDO ICEs is slightly lower than LNG engines, since data are available for a wider range of power produced, hence they are more scattered. Also, LNG efficiency correlation has an almost independent value with respect to rated power.

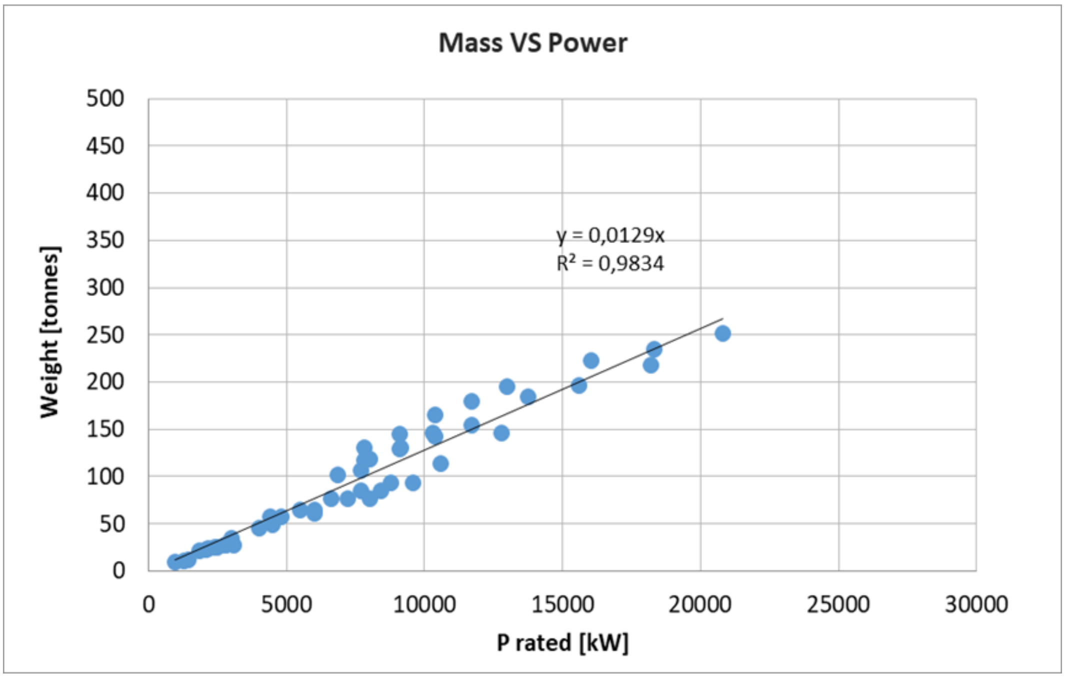


*Figure 18 – Weight map and correlation for LNG ICEs.*

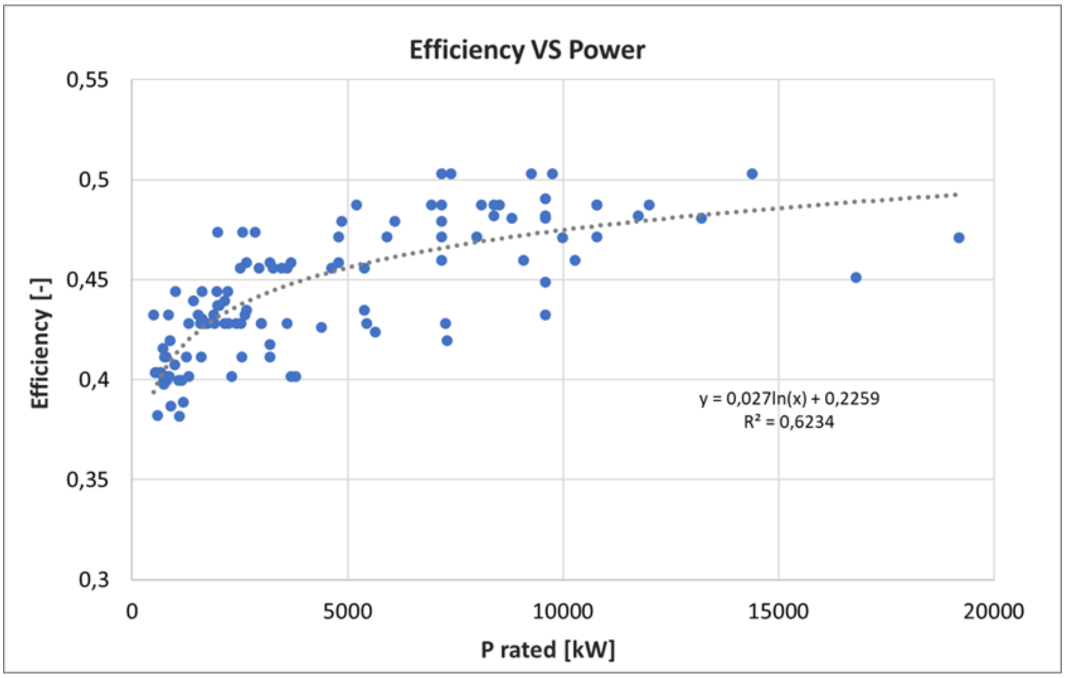


*Figure 19 – Efficiency map and correlation for MDO ICEs.*

### 3.3.2 Gas turbines (GT)

Gas turbines (GT) are not widely used for marine propulsion and power generation onboard, with the exception of some naval vessels or a few cruise ships, thus no source is available for such prime mover in terms of correlations. Data has been retrieved from commercial industrial and aero-derivative gas turbines, which are the ones more likely to be employed for power generation onboard vessels thanks to their flexibility of operation [136,137]. Besides, no information is available on different sizes, fuel consumption, heat rates or efficiencies of gas turbines fuelled by alternative fuels. In this case, the standard choice is clearly natural gas but most GTs, especially aeroderivatives, accept also liquid fuels. As example, the efficiency map of GT engines is reported in Figure 20.

Combined cycles (CCGT) suffer from the same consideration made for GTs or even worse, considered that only a little percentage of ships in the world employ CCGT.

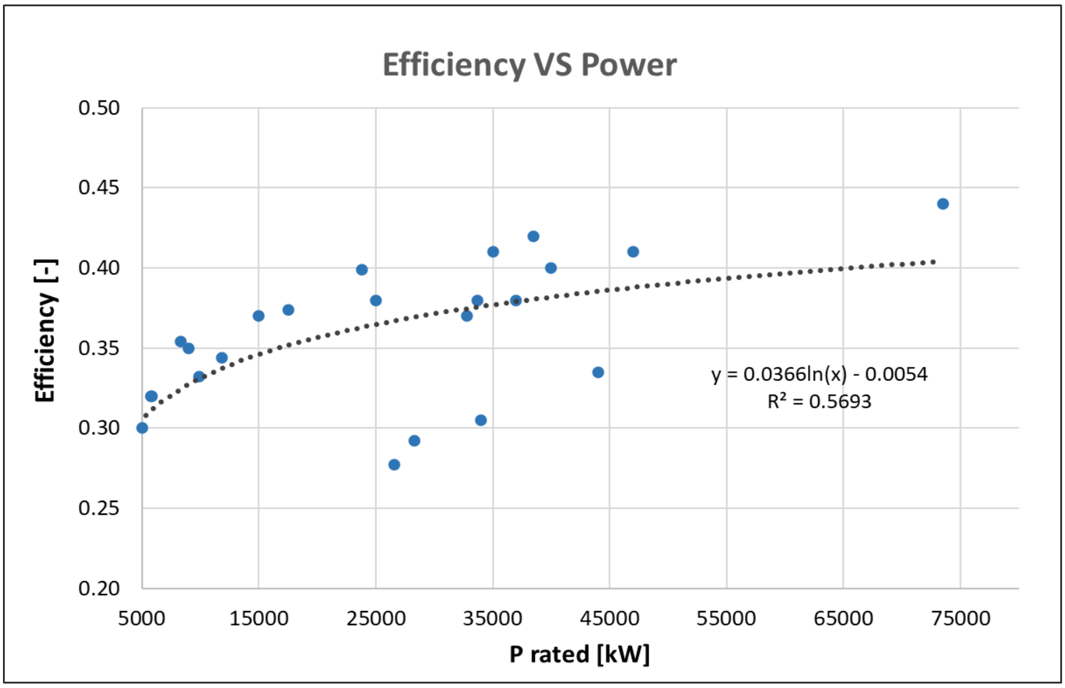


*Figure 20 – Efficiency map and correlation for industrial and aero GTs.*

As visible from Figure 20, the accuracy of the efficiency map in terms of $R^2$ is lower than its counterpart for reciprocating engines. This is

### 3.3.3 Fuel cells (FC)

Fuel cells are quite a peculiar power system. On the one hand, there is scarcity of market-ready systems, especially for maritime applications, and on the other the high attractiveness of such systems for decarbonised power production. As opposed to conventional ICEs and analogously to alternative-fuelled engines, values of energy consumption for fuel cells are not available, and only the maximum conversion efficiency is reported. It should be noted that this makes much of a difference, because in fuel cells the losses increase as the current density to the second power, hence maximum electric efficiency is not expressed at rated power as it is the case for thermal engines, but rather at quite low loads (usually 20-30%) [138,139]. Consequently, a fuel cell can either operate efficiently or at high power, but luckily the efficiency drop is often not too high.

### 3.3.4 Organic Rankine Cycle (ORC)

For ORCs, the same considerations of ICEs apply, except that the number of market available products is lower. Moreover, different thermodynamic cycles are possible, so even for the same rated power the system size and weight may be very different. However, an ORC is a power system composed by various sub-components, so its cost could be theoretically evaluated accounting for the sum of their costs. The ORC is a system which is well known for its low efficiencies, a problem that is mainly constrained by the low working temperatures at which it operates. The data dispersion reported in Figure 21 could be also attributed to the different maximum inlet temperature, which influences significantly the overall thermal efficiency.

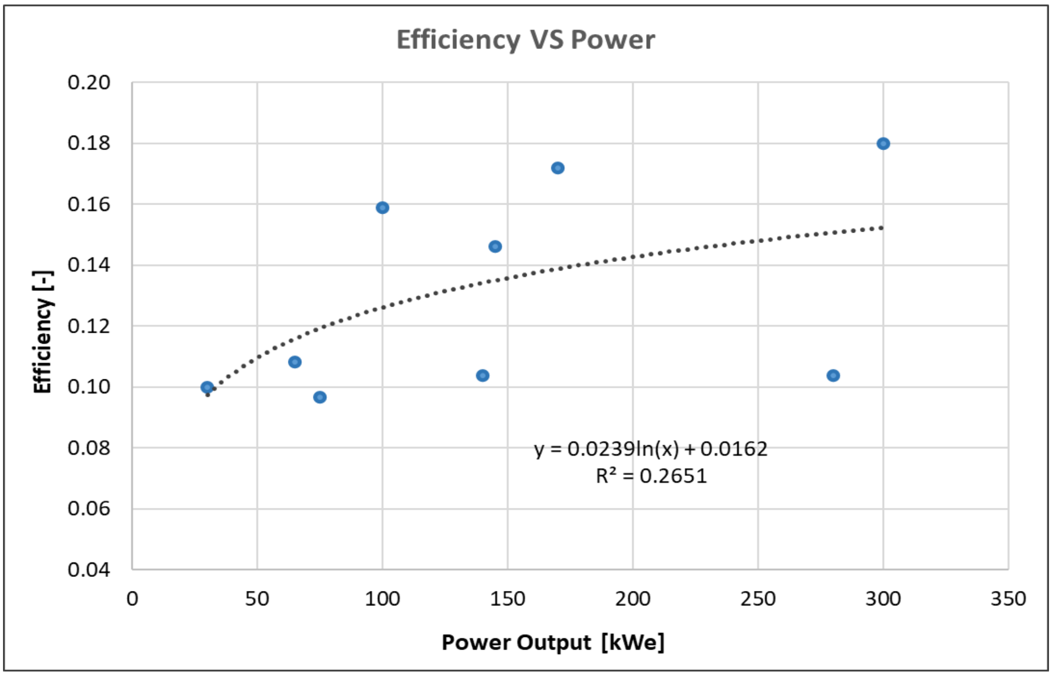


*Figure 21 – Efficiency map and correlation of ORC systems.*

## 3.4 Correlations for energy storage

### 3.4.1 Fuel tank storage

Fuel storage system correlations are reported hereby in Table 12. In this case, the independent variable is the rated capacity of the tank ($CAP_r$) expressed in litres for liquid fuels, and energy content ($EC_r$) expressed in kWh for gaseous compressed or liquefied fuels. A low $R^2$ value for MeOH weight correlation can be justified by a large variety of tanks available, which can be made with very different materials, i.e., polymer or steel, depending on their size. The lack of information about specific marinized products does not allow for a precise focus and makes this data sparsity even worse.

*Table 12 – Correlations for fuel storage systems.*

| **FUEL STORAGE SYSTEM** | **Correlation** | | |
|---|---|---|---|
| | **Size (Volume) [m³]** | **Weight [tonnes]** | **Cost [USD]** |
| LNG | $V = 0.0003 \cdot EC_r$ ($R^2 = 0.99$) | $W = 0.0001 \cdot EC_r$ ($R^2 = 0.98$) | $C = 3.06 \cdot EC_r$ |
| Methanol | $V = 0.0009 \cdot CAP_r + 14.5$ ($R^2 = 0.92$) | $W = 0.0005 \cdot CAP_r + 2.17$ ($R^2 = 0.76$) | $C = 2.407 \cdot CAP_r$ |
| Ammonia | $V = 0.0011 \cdot CAP_r$ ($R^2 = 0.98$) | $W = 0.0004 \cdot CAP_r$ ($R^2 = 0.98$) | $C = 1.347 \cdot CAP_r$ |
| Hydrogen ($CGH_2$), 350 bar | $V = 1.74 \cdot EC_r + 9.42$ ($R^2 = 0.99$) | $W = 0.329 \cdot EC_r + 22.2$ ($R^2 = 0.95$) | $C = 13.38 \cdot EC_r$ |
| Hydrogen ($CGH_2$),700 bar | $V = 0.48 \cdot EC_r + 7.88$ ($R^2 = 0.98$) | $W = 1.21 \cdot EC_r + 5.9$ ($R^2 = 0.97$) | $C = 10 \cdot EC_r$ |
| Hydrogen ($LH_2$) | $V = 0.69 \cdot EC_r + 150.2$ ($R^2 = 0.99$) | $W = 0.34 \cdot EC_r + 41.8$ ($R^2 = 0.99$) | $C = 10 \cdot EC_r$ |
| Hydrogen ($MH_2$) | $V = 0.00242 \cdot EC_r$ ($R^2 = 0.95$) | $W = 6.56 \cdot EC_r$ ($R^2 = 0.94$) | $C = 93.4 \cdot EC_r$ |

Regarding hydrogen storage, $CGH_2$ tanks structures differ considerably depending on the storage pressure. While 350 bar vessels are usually composed of a metal liner wrapped in composite fibre (type III), 700 bar cylinders are polymer wrapped in composite (type IV), thus much lighter since no metallic material is involved. Finally, $MH_2$ cost is obtained as average of values for several types of hydride powder with different adsorbent characteristics (e.g. AB, AB2 and AB5).

### 3.4.2 Energy storage (ESS)

Energy storage system correlations are reported hereby in Table 13. In this case, the independent variable is the rated energy capacity ($EC_r$) expressed in kWh. In this regard, only marinized Li-ion Nichel-metal Cobalt (NMC) batteries are considered as the state of the art of heavy duty BESS architecture, and TESs are only evaluated in their phase change material (PCM) configuration, that is the one that usually guarantees the highest energy density.

*Table 13 – Correlations for energy storage systems*

| **ENERGY STORAGE SYSTEM** | **Correlation** | | |
|---|---|---|---|
| | **Size (Volume) [m³]** | **Weight [tonnes]** | **Cost [USD]** |
| Batteries (BES) | $V = 4.7 \cdot EC_r$ ($R^2 = 0.89$) | $W = 6.77 \cdot EC_r$ ($R^2 = 0.93$) | $C = 150 \cdot EC_r$ |
| Thermal Energy Storage (TES) | $V = 0.0021 \cdot EC_r$ | $W = 1.679 \cdot EC_r$ | $C = 1000 \cdot EC_r$ |

## 3.5 Previous results of HELM

Examples of previous investigation performed using HELM tool, originally developed by TPG of University of Genoa, are reported in this section [134,140]. In particular, two instances will be presented. In the first work [24], four different vessels are taken into consideration: a leisure sail yacht, a small passenger ferry for medium duty island connection, a large cruise ship and a merchant container ship, characterised by strong differences in terms of installed power, operational power, mission profile, navigation areas and mission frequency. Table 14 contains the main characteristics of the case study vessels reported in this paragraph and in [24].

*Table 14 - Characteristics of the case studies reported in [24]*

| | **Sail yacht** | **Small Passenger ferry** | **Cruise ship** | **Container ship** |
|---|---|---|---|---|
| **Length [m]** | 20 | 55 | 325 | 260 |
| **Breadth [m]** | 5.3 | 10.8 | 42 | 32.3 |
| **Max. Power [kW]** | 30 | 600 | 61800 | 37000 |
| **Operational hours [h]** | 10 | 6 | 175 | 168 |
| **Navigation type** | Coastal | Inland | National | Deep Sea |

Results of the first work show that alternative fuels are penalised either on very small vessels (i.e., sail yacht) and very large vessels with long missions, mostly on open sea (i.e., containers). Inland ferries appear to have the largest benefit from hydrogen propulsion thanks to the environmental implications, up to the point that the combination $LH_2$ + PEMFC just outperforms ICE fuelled by conventional MDO. As regards large cruise ships, the best solutions depend on whether the entire navigation is considered or the hotel loads only. In the first case, the amount of fuel bunkered is the most crucial aspect, and ICE + LNG becomes the best solution. However, in the case of hotelling only, PEMFC + $H_2$ outstands as the most adequate from a comprehensive perspective of volume, weight, cost and environmental impact. This result highlights that there is a "sweet spot" combination of power installed, mission duration and mission type that actually poses hydrogen in a favourable position to replace conventional fuels. Such optimal place appears to be around 4-7 MW power requirement with no more than 5 hours of inland or national mission.

The second work includes a small Ro-Pax ferry for island connection and a large Ro-Ro ferry [23]. Table 15 highlights the main characteristics of the case study vessels reported in the second study [23] and for the first, only the hotel load was considered.

*Table 15 - Characteristics of the case studies reported in [23]*

| | **Pax & car ferry (1)** | **Large Ro-Pax ferry (2)** |
|---|---|---|
| **Length [m]** | 74 | 175 |
| **Breadth [m]** | 15 | 27 |
| **Max. Power [kW]** | 500 (hotel only) | 26200 |
| **Operational hours [h]** | 24/48/72 | 12 |
| **Navigation type** | National | National |

*Table 16 – Results for large Ro-Pax ferry*

| **Technology** | **Total volume [m3]** | **Total weight [tonnes]** | **Total cost [kUSD]** | **Eff. [%]** | **$CO_2$ emission [kg/h]** |
|---|---|---|---|---|---|
| ICE MDO | 791.6 | 437.9 | 625926.7 | 49.4 | 343.2 |
| ICE DF LNG | 1130.25 | 897.7 | 592208.6 | 50.7 | 194.6 |
| ICE DF MeOH | 882.46 | 487.7 | 751974 | 40 (est.) | 257.6 |
| ICE DF $NH_3$ | 1221.9 | 631.9 | 861641.9 | 40 (est.) | 0 |
| PEMFC $CGH_2$ | 2317.8 | 879.4 | 1726329 | 50.4 | 0 |
| PEMFC $LH_2$ | 2360.4 | 885.1 | 2093670 | 50 | 0 |
| SOFC LNG | 3732.6 | 2506 | 969158.1 | 53 | 194.6 |
| GT | 191.7 | 49 | 24909.8 | 36.4 | 375.4 |

*Table 17 - Results for Pax & car ferry, 48h (top) and 72h (bottom) autonomy*

| Technology | Total volume [m3] | Total weight [tonnes] | Total cost [kUSD] | Eff. [%] | $CO_2$ emission [kg/h] |
|---|---|---|---|---|---|
| ICE MDO | 23.4 | 14.2 | 14087 | 39.3 | 343.2 |
| | 28.4 | 18.2 | 14088 | | |
| PEMFC $CGH_2$ | 87.5 | 21.2 | 35593 | 52 | 0 |
| | 127.8 | 30.9 | 35831 | | |
| PEMFC $LH_2$ | 91.5 | 21.7 | 43607 | 40 | 0 |
| | 133.8 | 31.7 | 44119 | | |
| PEMFC MH | 87.3 | 176.6 | 45927 | 50 | 0 |
| | 127.7 | 264.1 | 51332 | | |
| SOFC LNG | 60.7 | 35.1 | 17950 | 53 | 190.6 |
| | 67.7 | 40.2 | 18098 | | |
| GT | 86.8 | 17.3 | 44603 | 23 | 600.5 |
| | 129.1 | 27.3 | 44575 | | |

The findings of this case demonstrate that the utilisation of hydrogen PEMFC for hotelling on an inland ferry is a viable option. Conversely, propulsion and full-load coverage remain optimised through the use of conventional fuels. Besides, a total system efficiency of 40% is considered as a more realistic value for a $LH_2$ fuel system smaller than the one for the case study 2 (Table 16), where the tank is larger and therefore expectedly less affected from percentage boil-off losses.

Methanol emerges as the most closely aligned solution in terms of weight and volumes, and LNG as the most adequate also considering carbon intensity. However, none of them is capable of ensuring a zero-emission sail. Finally, it is shown that hydrogen feedstock cost is the real paramount parameter to decrease in order to guarantee a truly viable zero-emission alternative in the mid-close future.

## 3.6 Case studies and results

In this section, the results of HELM software are reported for three case studies. These are the hotel load of a large cruise ship (>150,000 GT), the navigation load of a medium sized cruise ship (50,000-70,000 GT), and the navigation load of a Pax & car ferry (10,000-15,000 GT). Table 18 reports the main characteristics of the three ships considered as case studies.

*Table 18 – Overview of the main features of the case study ships*

| | Cruise ship – hotel load | Cruise ship – navigation | Pax & Car ferry |
|---|---|---|---|
| **Length [m]** | 325 | 248 | 55 |
| **Breadth [m]** | 42 | 32 | 10.8 |
| **Max. Power [kW]** | 7000 | 45000 | 6000 |
| **Operational hours [h]** | Variable | Variable | Variable |
| **Navigation type** | National | National | Inland |

In this analysis, liquefied, compressed at 350 bar and metal hydrides hydrogen storage forms are considered. Besides, into the HELM data repository there is no information on hydrogen power units other than fuel cells. The inclusion of different hydrogen-ready systems is forecast as future activity on the tool.

### 3.6.1 Hydrogen fuel for cruise ship – Hotel load

Hotel load is required to supply essential services on board, such as lighting and HVAC, in circumstances where the main engines are not operational and the vessel is at berth, thereby functioning as a proper "hotel". Large cruise ships often require substantial amount of power while at berth, and zero-emission hotelling could be a valuable alternative to shore-to-ship power.

Figure 22 reports the weight results for the first case study. While it is immediately clear that metal hydrides (MH) hydrogen storage cannot be competitive form this perspective, there is very little discrepancy among the baseline (ICE MDO) and the most technologically ready alternative solutions (ICE MeOH, and ICE LNG). In fact, all these solutions have a reciprocating engine as power unit, and the fuel density in storage conditions is not so different. Regarding PEMFCs, the weights of compressed and liquefied hydrogen power systems are almost equal to each other, but also consistently higher than the ICE-based. This is primarily due to both the higher volume of fuel required for the range.

However, the crucial downfall of PEMFC-based hydrogen power system is on a volume occupancy basis, as depicted in Figure 23. The tiny storage density of hydrogen in any form ($LH_2$, $CH_2$ and MH) and the low power density of fuel cells as compared to thermal generators makes the comparison with current and state-of-the-art technology ruthless. The comparison is even harsher when considering long operating mission: the volume required for powering the hotel load of a ~4000 pax cruise ship for 5 hours with hydrogen PEMFC is comparable to the one needed to cover the same demand with MDO and combustion engines for 20 hours. This result is a quantitative evidence as to hydrogen powered transportation falls irreparably behind other alternative solutions. Nevertheless, another interesting outcome (also sustained by extensive literature) is that for short mission requirements hydrogen PEMFC do not really have a real downside compared to MDO or LNG, being just slightly less performant. This can be seen as a confirmation that hydrogen for vessels is ready only for small size short mission ferries, at least from a payload capacity perspective.

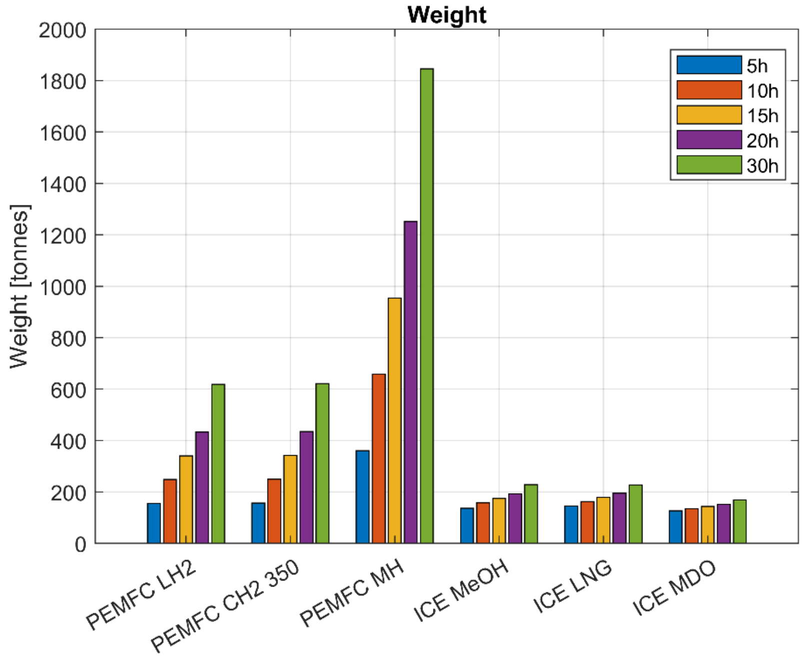


*Figure 22 – Weight comparison along different mission duration, cruise ship hotelling*

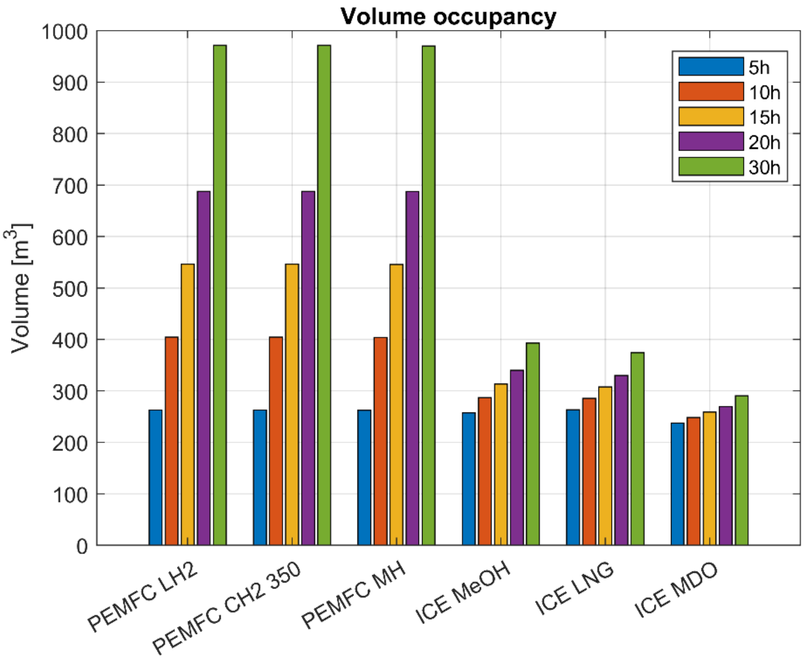


*Figure 23 – Volume comparison along different mission duration, cruise ship hotelling*

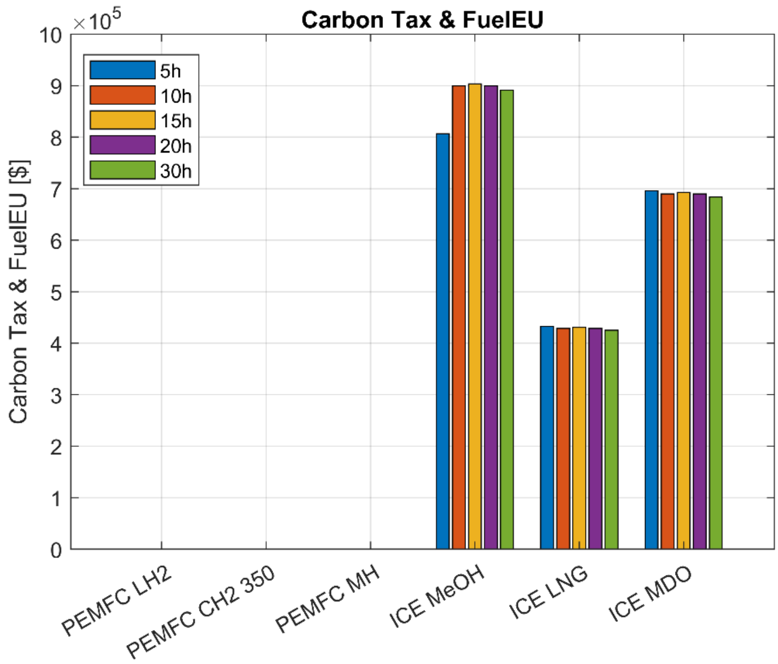


*Figure 24 – EU-ETS and FuelEU penalties along different mission duration, cruise ship hotelling*

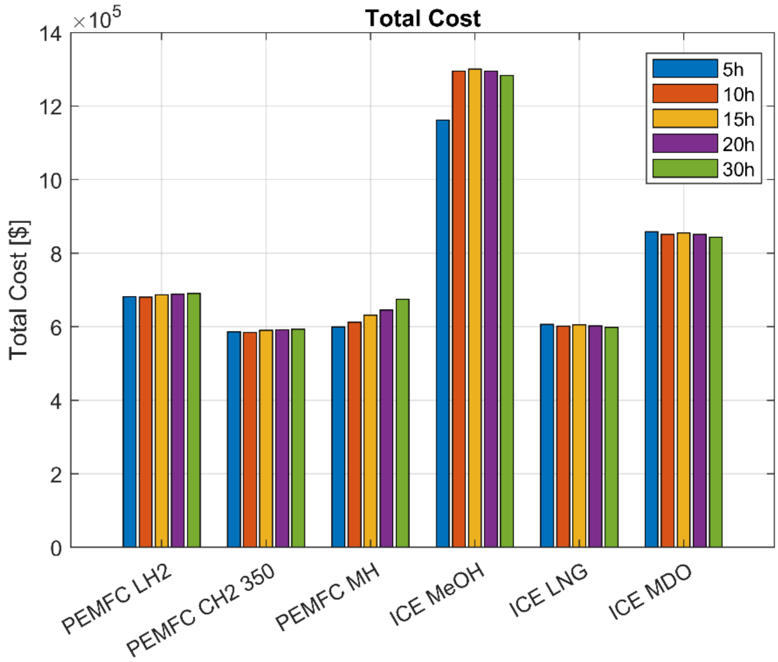


*Figure 25 – Total cost comparison along different mission duration, cruise ship hotelling*

From a cost perspective, Figure 25 reports the total cost of ownership of the hotel load powertrain along the whole ship life, which is assumed to be 30 years. Total cost include power unit and storage CAPEXs, fuel cost, O&M cost, and both EU-ETS and FuelEU taxes. Methanol is the worst scoring alternative due to the very high levies (Figure 24): this is primarily linked to its low energy content that leads to higher fuel consumptions and higher carbon emissions as a consequence. On the other hand, hydrogen PEMFC powerplants exhibit O&M costs around 5-6 times higher than more traditional solutions, with hydrides being again the costliest alternative. Regarding hydrogen PEMFC, total lifetime cost is comparable to that of ICE powered by LNG thanks to the absence of levies on GHG emission, which have a considerable share as shown in Figure 24.

### 3.6.2 Hydrogen fuel for cruise ship – Navigation load

It is clear from previous discussion and from literature that the cruise ship of the near future (10-20 years) will not sail under hydrogen power only. The reason for that is multi-fold, and includes technological challenges, market unreadiness, and lack of prescriptive regulations. To assess how far is the current scenario from a viable hydrogen-only cruise ship propulsion, results have been obtained from HELM for a medium sized cruise ship considering the whole navigation load (i.e., propulsion + hotel). Weight comparison in Figure 26 shows the same trend as the case of hotel load (Figure 22): metal hydrides weigh more than three times as much as other hydrogen systems, while methanol, LNG, and MDO all score similar values. In this case the longest mission duration is 100 hours, which is representative of an ocean voyage lasting several days.

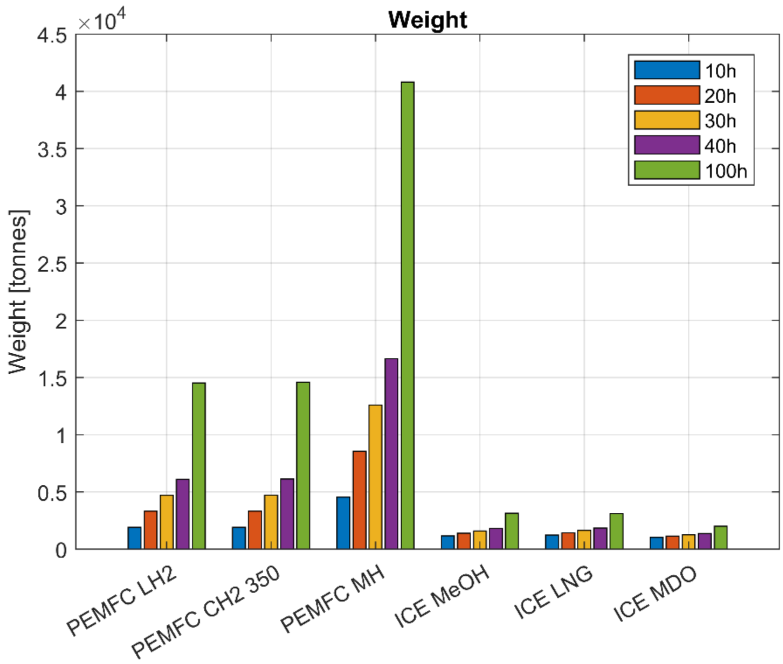


*Figure 26 - Weight comparison along different mission duration, cruise ship navigation*

Figure 27 shows once again that from a volume perspective, hydrogen represents a critical alternative. Moreover, the comparability between 10 hours autonomy of autonomy with PEMFC and 40 hours autonomy with MDO is replicated for the purpose of navigation. This demonstrates that the factor of 4 between hydrogen and traditional fuel is effectively accurate also on large power installed.

The only technologies affected by the 100 hours scenario are hydrogen and LNG, which are those whose storage and power system are most critical and require dedicated maintenance. With regard to the EU-ETS and FuelEU, there is minimal to no discrepancy in mission duration for a given technology because it is assumed that a ship is at sea for an average number of days as per IMO research [141], hence the product of number of missions and mission duration (or, in other terms, the total energy consumed) is constant.

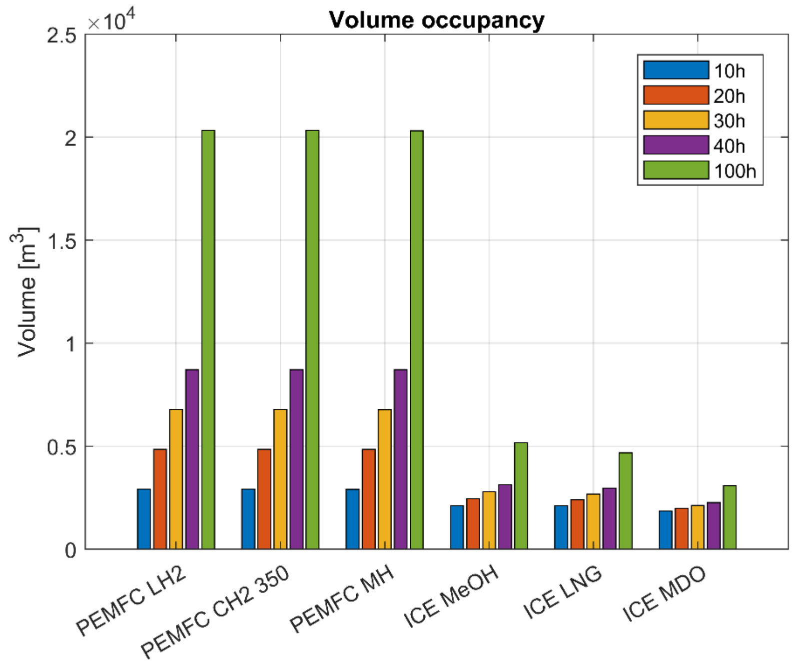


*Figure 27 – Volume comparison along different mission duration, cruise ship navigation*

The only technologies affected by the 100 hours scenario are hydrogen and LNG, which are those whose storage and power system are most critical and require dedicated maintenance. With regard to the EU-ETS and FuelEU, there is minimal to no discrepancy in mission duration for a given technology because it is assumed that a ship is at sea for an average number of days as per IMO research [141], hence the product of number of missions and mission duration (or, in other terms, the total energy consumed) is constant. Besides, methanol is the worst performing, with a total carbon penalty which sets twice as high as LNG and more than 1.5 times as MDO, again due mainly to the higher consumption associated to it. This result is shown onto Figure 28 for different mission duration.

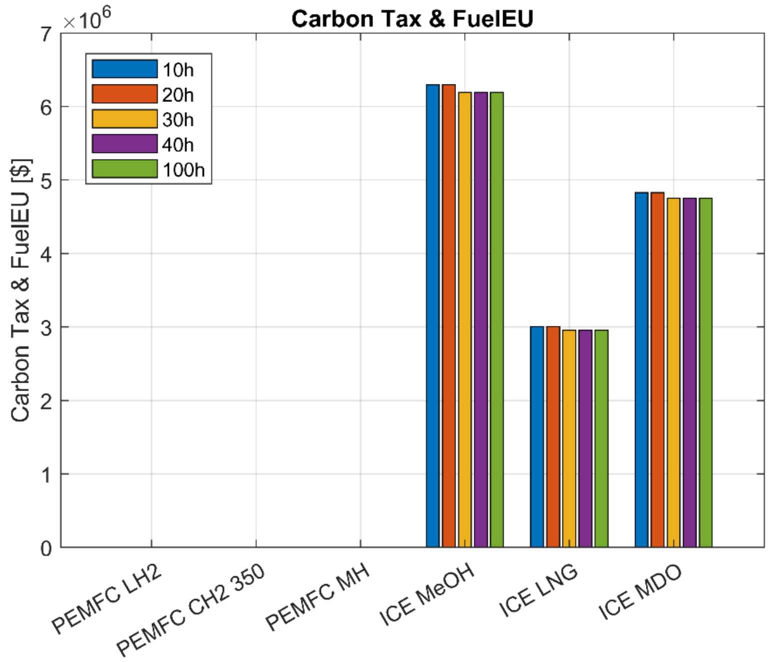


*Figure 28 – EU-ETS and FuelEU penalties along different mission duration, cruise ship navigation*

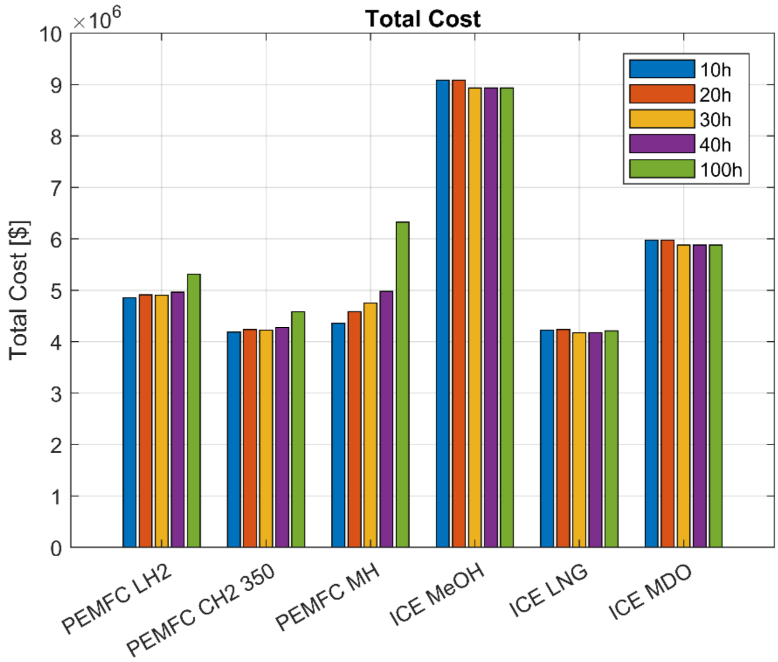


*Figure 29 – Total cost comparison along different mission duration, cruise ship navigation*

Analysing total lifetime cost for the case of cruise navigation in Figure 29, it is evident that there exists a general independence of the cost figure on the required ship autonomy, and therefore on the amount of fuel stored. This is particularly true for MDO and alternative fuels other than hydrogen. As visible by comparing Figure 28 and Figure 29, the largest part of total cost is made of carbon penalties. The overall result is that compressed hydrogen storage has a lifetime total cost which is comparable to that of LNG, while $LH_2$ and metal hydrides are more costly. Nevertheless, the immediate uptake of hydrogen for complete propulsion of dozen of MW worth of power is still far from being viable.

Well to Wake (WtW) $CO_{2,eq}$ emissions are reported in Figure 30. The differences among MDO, LNG and methanol stem mainly from the fuel consumption (Tank to Wake, TtW) rather than its production. On the other hand, since green hydrogen has been considered in this analysis, the emission associated to it are only for its production, and specifically to the carbon intensity of the energy mix utilised for the electrolysis process.

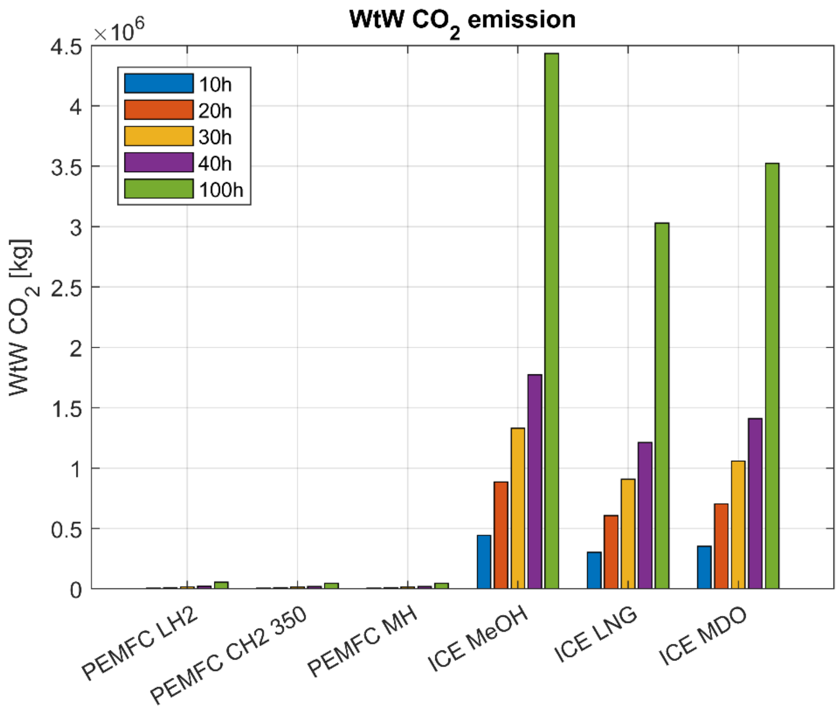


*Figure 30 - WtW emission along different mission duration, cruise ship navigation*

### 3.6.3 Hydrogen fuel for pax & car ferry - Navigation load

Cruise ships require substantial energy amount to be stored onboard. The low volumetric energy density of hydrogen is a significant hinder to its uptake onboard. Therefore, the analysis has been extended to a smaller pax & car ferry to assess whether the different ship and mission profile can lead to a different, possibly more promising result. Figure 31 and Figure 32 show weight and volume results for different alternative propulsion solutions. The tendency of MH to be the worst solution is replicated from a weight perspective, while all hydrogen powerplants seem to perform the same irrespective of the storage technology.

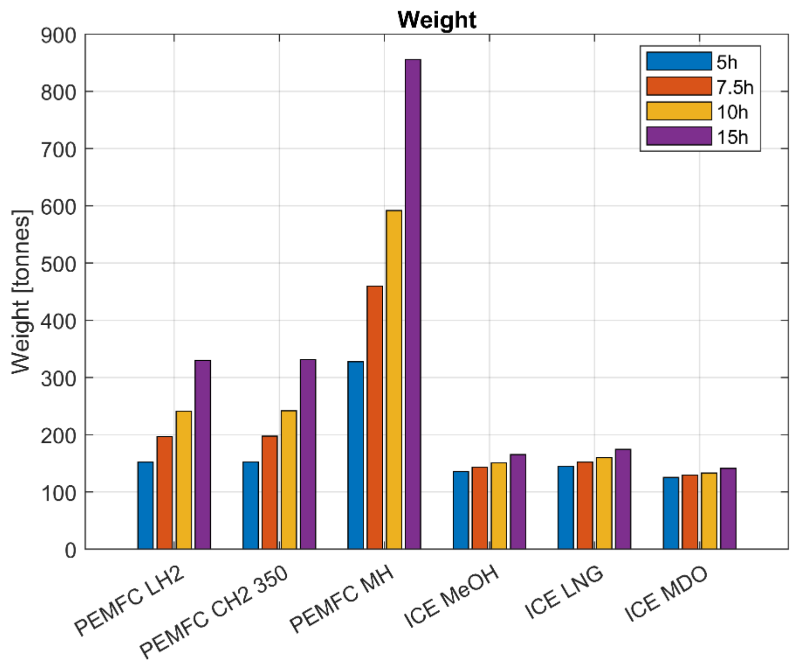


*Figure 31 - Weight comparison along different mission duration, ferry navigation*

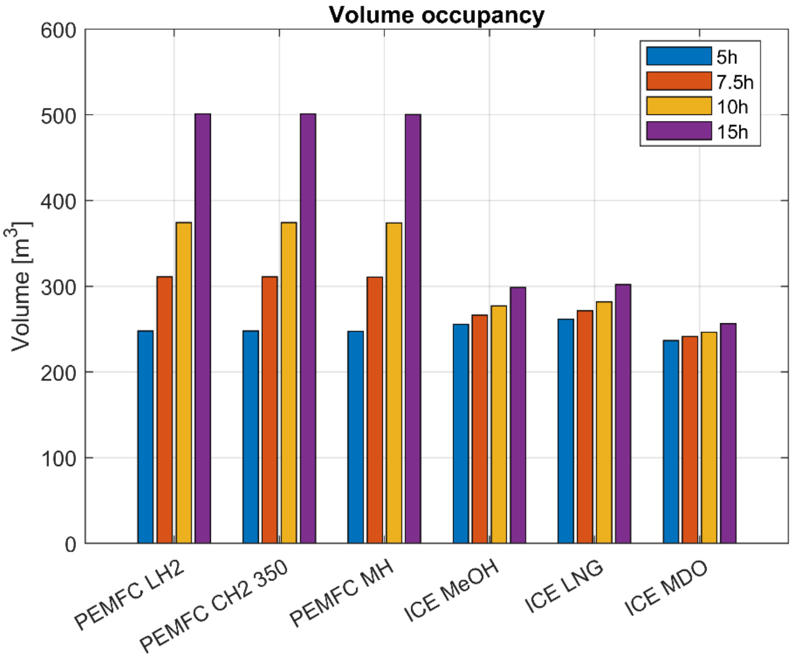


*Figure 32 - – Volume comparison along different mission duration, ferry navigation*

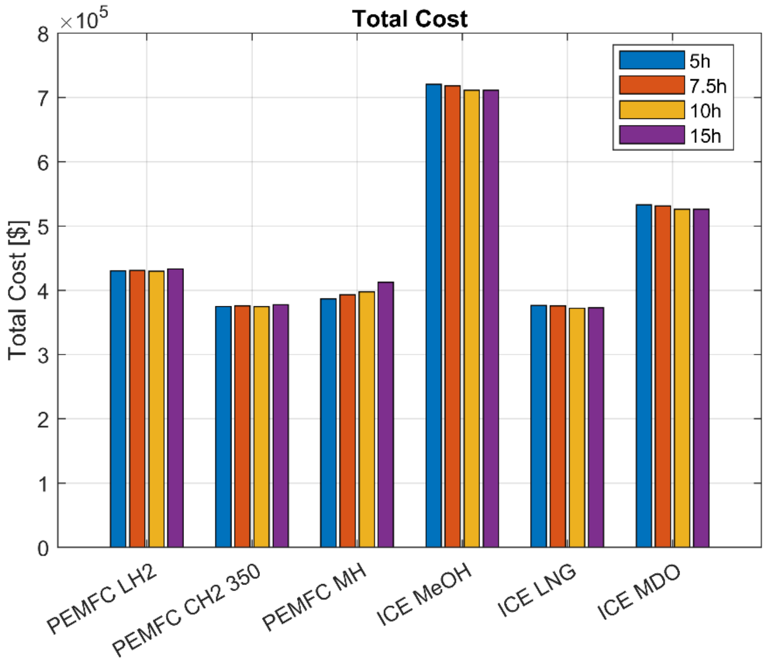


*Figure 33 – Total cost comparison along different mission duration, ferry navigation*

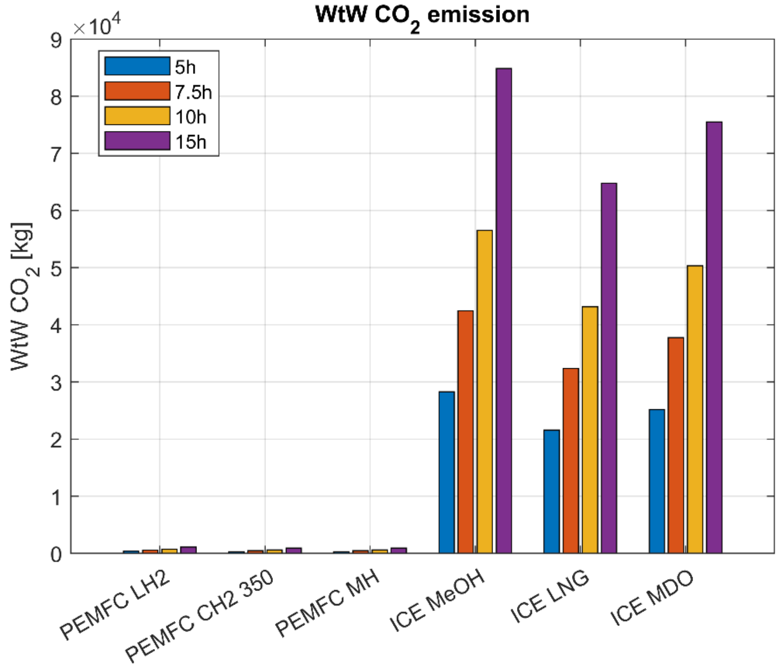


*Figure 34 – WtW emission along different mission duration, ferry navigation*

The cost of alternative hydrogen-based solutions is still higher than both conventional MDO and LNG. Figure 33 report the total cost of each solution. The trend over the different solutions replicates the ones already seen for cruise ships, but an interesting result regarding the different mission type can be seen by comparing the total cost of hotelling for cruises (Figure 25) and the navigation for pax & car ferries (Figure 33). In fact, despite having the same maximum power requirement, the ferry total cost is 37% less when powered by MDO and around 43% less when powered by hydrogen PEMFC. This is attributable to the fact that ferries usually have a lower number of average days at sea [141], hence a lower number of yearly missions for the same mission duration. This is a partial yet reliable confirmation that small ships with short and frequent voyages are the most easily convertible to hydrogen in the nearest future.

# 4 Hybrid fuel system design

In the present chapter, the plant design and performance analysis of two hybrid hydrogen-methane fuel system architectures for cruise ship applications are described. Except for the system size, which is linked to their target application, the two are almost coincident from every point of view, and the few differences are thoroughly reported in this section. The component selection was performed based on results outlined with AVEVA Pro/II process simulation software, and relevant KPIs have been chosen to evaluate the system efficiency and reliability.

## 4.1 Background

At present, almost the totality of cruise ships is powered by reciprocating internal combustion engines. The reason is many-folds and has also historical grounds. Firstly, they can run on heavy fuel oil or other low-cost marine fuels, while most marine gas turbines require cleaner, more expensive distillate fuels like marine gas oil. Other than that, ICEs guarantee better efficiency and higher torque delivery at part-loads as compared to simple cycle gas turbines, while retaining worse but still decent power density. These characteristics are crucial in case of a direct drive of the propeller, which is especially applicable to low speed ICEs mainly found on cargo ships and tankers, but lose some relevance for modern passenger ships where the propulsion is usually electrically driven and the combustion engine functions as a power generator. However, there are some relevant examples of passenger ships that are powered by gas turbines: with the exception of naval vessels, a number of fast ferries make use of gas turbine generators coupled with hydrojets. In general, wherever high navigation speed is a requirement, turbomachinery is the preferred choice. To better outline the differences, a comparison between the main parameters of internal combustion engines and simple cycle gas turbines for maritime application is outlined in Table 19. Generally, ICEs favour propulsion efficiency both at part loads and design conditions, while GTs are more fuel flexible and have a higher cogeneration/waste heat recovery potential. These aspects are also inferred from Figure 35, where the evidence of a much more wasteful use of fuel energy is depicted by comparing a widely used maritime engine (blue curve) and a two-spool industrial gas turbine (orange curve) of similar power.

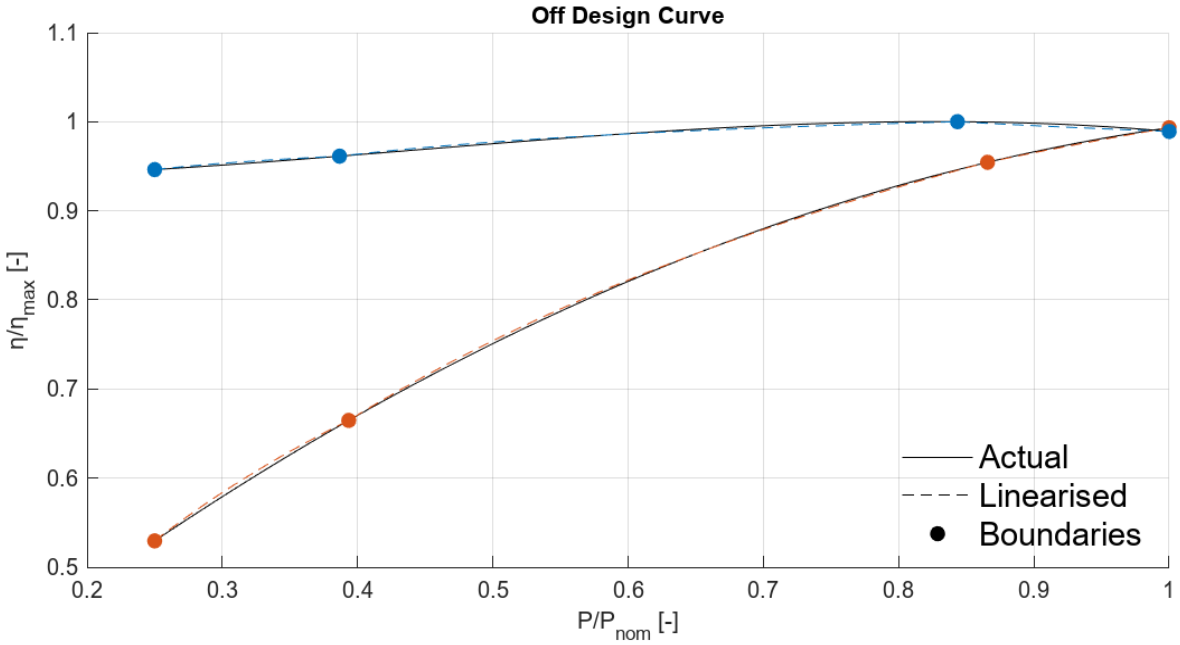


*Figure 35 – Comparison between ICE (blue) and GT (orange) off design efficiency*

It has already been pointed out that LNG constitutes the state of the art for maritime propulsion, with numerous dual fuel alternatives in the typical range for large passenger ships. However, when hydrogen is concerned, there is scarcity of alternatives in multi-MW size, while larger engines from major OEMs are only able to accept limited percentages of $H_2$, usually less than 25% in volume (4% in mass) [142,143].

Gas turbine OEMs are on a similar page. In some limited cases, industrial GTs have been proven to be 100% hydrogen ready [21,136], but in general blends with 30-50% hydrogen in volume are widely accepted. Multi-fuel marine concepts emphasize fuel flexibility: the same turbine core is designed to accept hydrogen, ammonia, or synthetic methane with minimal hardware changes, using adapted injectors, materials resistant to high flame temperature and $H_2$ embrittlement, and upgraded control systems for varying Wobbe index.

The MARPOWER project [144] is developing intercooled, recuperated marine gas turbine systems able to run flexibly on various alternative fuels, targeting about 50–55% electrical efficiency and up to 73–76% CHP efficiency for shipboard power. In light of this, the choice of a CCGT for hydrogen propulsion onboard passenger ships seems the only option to combine state-of-the-art efficiency with hydrogen capabilities.

The choice of a GT over a ICE is mainly dictated by the better hydrogen readiness, the better power density and fuel flexibility, and the highest efficiencies achievable in CCGT configuration among all large size powertrains. Besides, CCGT is the only powertrain option in order to achieve efficiencies comparable to those of the current internal combustion engines systems. From this standpoint, gas turbines have the potential to attract interest once again in the field of maritime propulsion. However, this interest would now not lie in their capacity to ensure high speeds but rather in their ability to deliver high efficiency when employed in a combined cycle configuration.

*Table 19 – Summary of comparison between reciprocating engines and gas turbines*

| Parameter | Reciprocating ICEs | Gas turbines | Comment |
|---|---|---|---|
| **Simple cycle efficiency** | ✓ | ✗ | |
| **Part-load efficiency** | ✓ | ✗ | Aerodynamic efficiency destroys off-design performance |
| **Emissions** | ✗ | ✓ | Progressive and leaner combustion |
| **Fuel flexibility** | ✗ | ✓ | Continuous VS intermittent fuel delivery |
| **Cogeneration potential** | ✓ | ✓ | Depends on exhaust temperatures |
| **WHR potential** | ✗ | ✓ | High exhaust massflow and temperature |

The systems described in this chapter is devised to be fully LNG-$LH_2$ flexible, meaning that it should be able to run on any blend composition, including pure fuels, at any time. This suggests that, in comparison to conventional dual fuel engines, a second degree of freedom is implemented in the control logic, specifically the blend composition. Indeed, any LHV-based energy supply variation to the combustor is achieved through either the augmentation of the total blend MFR or the modification of the blend composition to one containing a greater percentage of energy-dense fuel. The selection of the primary or secondary strategy remains undetermined within the present study. The determination will be primarily contingent upon practical considerations, including the mission profile of each distinct vessel, the availability of hydrogen at bunkering stations in port facilities, and the inherent capacity of the prime mover to accommodate blends of continuously variable composition.

In the following, the hydrogen fuel line and the LNG fuel line are described in details. The characteristic values resulting from the design conducted here are potentially subject to modifications following technical feasibility check, the Risk Assessment outcomes, the availability of products, especially in case of largely non-conventional components and ultimately the Class and Flag approval.

*Table 20 – Design parameters of CCGT powertrains*

| **Parameter** | **FS1** | **FS2** |
|---|---|---|
| CCGT architecture (GT + ST) | 1+1 | 2+1 |
| Target operation | Hotel load | Navigation load |

### 4.1.1 Laboratory-scale Fuel system (LFS)

A laboratory-scale $LH_2$ fuel delivery system was designed to feed a 100 kW micro gas turbine in order to evaluate dynamic behaviour of the real system under certain load profiles and validate dynamic models previously developed [145]. An existing test rig was modified to accommodate gaseous hydrogen sourced from a $LH_2$ storage tank instead of a rack of compressed hydrogen vessels. Vaporisation is achieved through a water/glycol (WG) heating loop, which delivers a significantly higher mass flow rate than the hydrogen flow, a strategy employed to mitigate the risk of freezing to a considerable extent. In this way, the lowest temperature is just 3 °C lower than the WG temperature setpoint.

### 4.1.2 Hybrid Ship Fuel System 1 (SFS 1)

The first hybrid fuel system (SFS 1) is a 1+1 CCGT devised for covering the hotel loads of the ship. The target CCGT power is in line with the typical hotelling requirements of a large cruise ship (>150000 GT). In practice, it consists of an auxiliary power system which can provide zero-emission power when required. Since the system is targeted to be installed onboard a newbuild, the fuel line has been engineered to supply fuel to both the auxiliary "green" CCGT and the main DF generators of the ship. It is evident that these will be powered exclusively by LNG gas, while the gas turbine has the potential to accommodate any blend of fuels.

### 4.1.3 Hybrid Ship Fuel System 2 (SFS 2)

The second fuel system (SFS 2) is a 2+1 CCGT devised for the whole shipboard load during both stay at berth and during navigation. The target installation is a medium-large cruise ship, a large cruise ferry or a fast ferry (50000-70000 GT). Also in this case the system is targeted to be installed onboard a newbuild, but here the CCGT consists of the whole installed power of the ship. Hence, gas turbines would be potentially able to accept any NG-$H_2$ blend and zero-emission navigation could be possible at times.

## 4.2 $LH_2$ - General description of the fuel system

The system under consideration is fairly conventional, comprising a cryogenic pump that supplies high-pressure liquefied hydrogen to a main evaporator (EVA). The evaporator actually functions also as a superheater, thereby raising the delivery temperature to a level approximately equivalent to ambient. After that, high-pressure hydrogen is temporarily collected in a buffer tank (BT) and subsequently directed to the turbine fuel inlet. In parallel, hydrogen BOG is collected, pre-heated to nearly ambient conditions in a dedicated heater (BOG HEX) and compressed to the turbine feed pressure. After compression, hydrogen is cooled down in an aftercooler (BOG AC) and finally fed into the buffer tank and fed to the GT injectors. This layout needs no pressure regulation downstream the evaporator since outlet pressure level is adjusted by regulating the pump operating point via a variable frequency drive. Instead, after the buffer tank a pressure regulating valve is installed and controlled to meet the exact pressure requirements of the gas turbine.

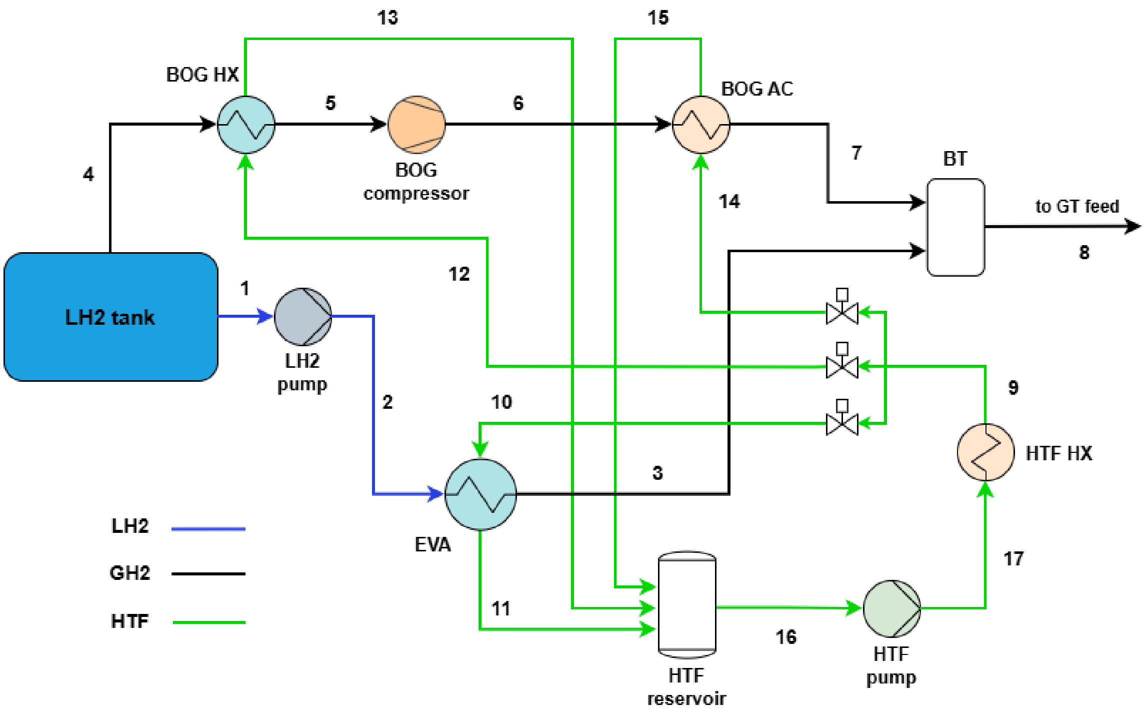


*Figure 36 – PFD schematic of $LH_2$ fuel system architecture, SFS 1 and SFS 2*

The complete hydrogen fuel system process flow diagram arrangement is visible in Figure 36. The PBU is not shown in the figure because it usually makes part of the whole tank assembly. A PBU utilising the same heat transfer fluid as the main heat exchangers is also possible in the final design but is outside the scope of this thesis. Besides, there is no precise information about operating conditions of PBUs deriving from manufacturers.

The BOG line operating principle is such that it functions as a fuel tank pressure regulator. In practice, there exists an operating pressure range of the tank which triggers the line activation when overshooting the higher boundary, and stops when reaching the lower limit. Meanwhile, the pressure inside the tank is controlled by its own pressure buildup unit, which makes up for the depressurisation resulting from the withdrawal of liquid across the main line.

Each combined cycle is considered to be installed in a single engine room. In any case, the $LH_2$ handling system for SFS1 and SFS2 has been designed by providing the necessary interfaces to connect it with a possible second identical $LH_2$ fuel system that would power a second engine room, equipped with prime movers requiring the same fuel demand, i.e., two specular power systems as shown in Figure 37. In this manner, one $LH_2$ fuel system is capable of supplying power to each of the two distinct machinery rooms, independently, with each fuel line being capable of functioning using components from either one of these. This aspect is particularly important to satisfy the Safe Return to Port (SRtP) requirements in a medium-long term time horizon, when the installed power on board capable of operating with $LH_2$ will be high and minimal reliance on LNG will be necessary to guarantee essential services and return to port under own power.

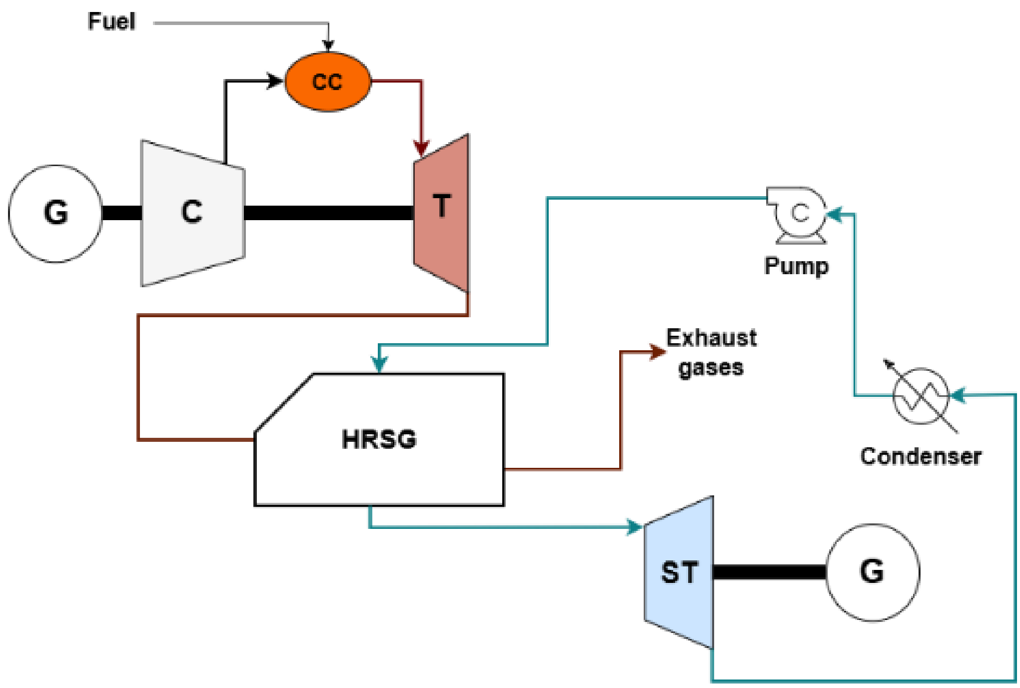


*Figure 37 – Architecture of the considered CCGT power plant for both SFS1 and SFS2*

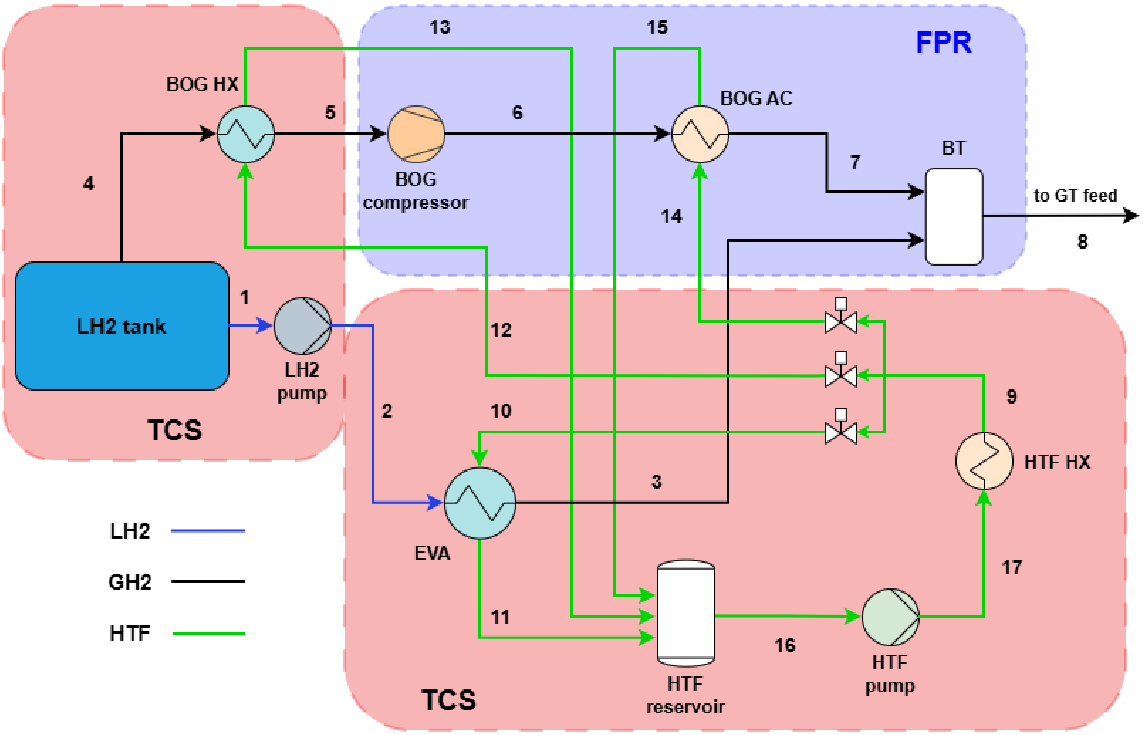


*Figure 38 – PFD schematic with details on zones subdivision as per IGF code*

All necessary peculiarities are introduced to comply with marine regulations not only from IGF and IGC codes, but also IMO CCC11 resolution. In particular, design choices such as subdivision between tank connection space (TCS) and fuel preparation room (FPR), the gas valve unit (GVU) arrangement, the ubication of the mixing skid etc. have been made employing existing LNG fuel systems as a baseline reference, considered that in any case the design is subject to the risk assessment pertaining to the alternative design procedure. In Figure 38 a detailed representation of the fuel system subdivision is presented.

### 4.2.1 Heating fluid loop

The heat source for the vaporisation is supplied by a heat transfer fluid (HTF) circuit. The HTF architecture is shown in Figure 36 together with the main fuel line. A pump in the common branch collects the heating fluid from a common reservoir and sends it to an electric heater (HTF HEX), then to three parallel branches. The massflow rate of each branch is regulated by a control valve calibrated to feed forward a nominal value. Besides, to prevent freezing even during deep transients, the temperature of the coldest point in the whole fuel system (i.e. the EVA HTF outlet, point 11 in Figure 36) is set to a minimum value, and the line and component sizing is performed accordingly. This represents a large safety margin with respect to usual freezing points of fluids used as HTFs for vaporisation of cryogens, despite negatively impacting the performance in terms of increased HTF flowrate and the energy consumption as a consequence. Besides, it is known that this fluid will not be a conventional water/ethylene glycol mixture, but rather an advanced thermal fluid with adequate low temperature properties such as the one reported in Table 21. The composition of the HTF fluid that will be used on board remains to be defined, but it is based on a organic salt solution which leads to increased density as compared to conventional water/ethylene glycol mixture.

*Table 21 – Comparison of heat transfer fluid properties at -10°C*

| **Heating Fluid Properties** | | | |
|---|---|---|---|
| HTF | Freezing temperatures [°C] | Heat capacity [kJ/kg ·K] | Density [kg/m$^3$] |
| WG 50/50 | -35 | 2.57 | 1108 |
| *HTF #1* | -50 | 2.8 | ~1300 |
| *HTF #2* | -60 | 2.6 | 1360 |

### 4.2.2 Assumptions, performance parameters and limitations

The component sizing and design performance of the two fuel systems are reported in this paragraph. Table 22 highlights all assumptions made and constraints set during the simulations. Machinery efficiency is kept constant in off-design simulation due to the lack of reliable off-design curves. The HTF feed temperature is set as per system design at 45°C for each branch, to guarantee sufficient heat input for hydrogen vaporisation and superheating. On the other hand, since HTF is actually a cooling medium in the AC branch, the hydrogen outlet temperature is chosen by design to be 50°C to avoid excessive temperatures of the hydrogen fed to the GT engines. Finally, the mixing process was modelled with a mass-enthalpy balance to mimic accurately the accumulation of heating fluid into the buffer reservoir.

Performance parameter includes, but are not limited to, the specific energy consumption (SEC) as defined in equation (1), the general stability of the system to provide the required mass flow rate, and the regarding temperature fluctuations, which are particularly critical when dealing with highly cryogenic fluids. Concerning the delivery stability, it is not easy to find a metric that evaluates this aspect without a proper transient analysis of the system. Hence this aspect needs to be further investigated to ensure reliability and actual stability of operation.

$$SEC = \frac{P_{el,TOT}}{3600 \cdot \dot{m}_{fuel}} \left[\frac{kWh}{kg}\right] \qquad (1)$$

*Table 22 – List of the assumptions and design parameters of SFS1 and SFS2.*

| Parameter | Value |
|---|---|
| Evaporator $H_2$ $T_{out}$ [°C] | 20 |
| Evaporator HTF $T_{out}$ [°C] | 30 |
| BOG aftercooler $H_2$ $T_{out}$ [°C] | 50 |
| HTF heater $T_{out}$ [°C] | 45 |
| Evaporator pressure loss [%] | 3 |
| BOG HEX pressure loss [%] | 3 |
| BOG AC pressure loss [%] | 2 |
| $LH_2$ pump isentropic efficiency [-] | 0.75 |
| BOG compressor isentropic efficiency [-] | 0.7 |
| Electrical efficiency [-] | 0.9 |
| Mechanical efficiency [-] | 0.9 |
| $LH_2$ tank BOR [%mass/day] | <1 |

The following set of design choices have been made for the design point. These hold valid for both SFS 1 and SFS 2.

- The outlet temperature at evaporator on $H_2$ side is set to 20°C. This is made to comply with the requirement as per manufacturer's specification. However, the actual temperature entering the GT combustion chamber is slightly higher, due to the mixing process with the much hotter BOG inside the buffer tank which leads to a temperature increase. Nevertheless, since BOG is a small fraction of the main liquid flow rate, the heating is always contained within 1°C for $LH_2$ and 3°C for LNG.
- The outlet temperature at evaporator on HTF side is set to 30°C. As explained in paragraph 4.2.1, it represents a conservative choice that was made to maintain normal steady-state operation sufficiently far from the freezing point of the thermal fluid. Comparing this value with those of Table 21 it is evident that even under deep transient operation, the chance of reaching freezing conditions is low.
- The working temperature of the HTF is set to 45°C. This is in fact the setpoint of the HTF electric heater, and each branch is fed with heating fluid at this very temperature.
- The outlet temperature at BOG aftercooler is set to 50°C. This setpoint is implemented because aftercooling is performed through HTF, which now serves as cooling medium rather than heating. Therefore, this value limits the heating of the HTF to 5°C above the inlet temperature, to avoid a very hot hydrogen stream into the buffer tank.
- The $LH_2$ pump and BOG compressor isentropic efficiencies have been estimated to be 0.75 and 0.7, respectively. This is due to the lack of actual characteristic curves of real components, but these values are in line with previous research [146,147]. Besides, further specifications on the machinery are not available from the manufacturers or they are covered by non-disclosure agreement.

Besides, the off-design analysis of the fuel system is performed with the assumption that the fuel consumption is exactly proportional to the gas turbine load. In reality gas turbines are regulated by mixture quality, that is with variations of air/fuel ratios that can be sometimes very large, in order to address issues related to the completion of combustion reaction or the $NO_X$ abatement.

However, at a system level the assumption of constant mixture composition all over the off-design operation is acceptable, even more so that very little information is available from the manufacturer about this parameter.

Boil-off rate is assumed to be natural only. This means that the "artificial" BOG created by the PBU in order to maintain pressure within the tank during the process of liquid depletion is being neglected. Besides, there is little knowledge on the share of the total BOG that is generated naturally or by the pressure regulation via the PBU. This aspect, combined with the fact that there is little knowledge on the PBU working conditions since most products are commercial, leads to the quite strong assumption that the line be sized for the natural BOG only, plus a 20% oversize as already considered for the main line.

The system performance is simulated through AVEVA Pro/II™. This software is devised to perform rigorous heat and material balance calculations for chemical processes; it offers the possibility to model virtually any thermodynamic process with variable degree of accuracy. Further details on the simulation tool are reported in Appendix A.

## 4.3 $LH_2$ – Components

The present section comprises the specification of all functional components (machinery and heat exchangers), which are introduced and described herein. All of the aforementioned components have been designated as 'best choice' components. This is indicative of the fact that a significant part of them require performance that is quite non-standard. It is therefore not yet possible to ensure whether the numbers reported here are those which will ultimately enable the system to operate, or whether they will be modified according to the manufacturer's requirements and planning.

### 4.3.1 Fuel tank

The fuel is stored in a conventional horizontal Type C tank. The liquid capacity is expected to be in the range 200-250m$^3$ and the normal working pressure between 1 and 10 barg. The bunkering is performed via a dedicated skid having a similar architecture to that employed by LNG refuelling. The main known characteristics of the fuel tank are reported in Table 23. In case multiple tanks should be necessary, e.g. for SFS 2 where the system will be allegedly duplicated, they will be equal to each other as per Table 23.

*Table 23 – $LH_2$ fuel tank main characteristics*

| | |
|---|---|
| **Type** | Horizontal Type C |
| **Capacity [$m^3$]** | 200-250 |
| **Normal operating pressure range [barg]** | 1-10 |
| **Insulation** | Vacuum + MLI |
| **Material** | Cryogenic grade stainless steel (e.g. AISI 304L/AISI 316L) |

The tank should be equipped with two bunkering interfaces (one top spray interface for cooldown and one bulk liquid interface at the bottom), main evaporator feed interface, BOG interface, nitrogen purge interface, and vent interface. The fuel tanks will be equipped with a pressure relief valve (PRV), which will be isolated from the vent system of the pipeline assembly.

A recirculation line will be implemented to account for reduced fuel demand. Since it is unacceptable to feed high pressure $LH_2$ back to the tank, the recirculation line will be equipped with a pressure and massflow control assembly (pressure reduction valve + massflow controller).

The tank is going to be ATEX Zone 0 and compliant with IGF code as far as filling limit and holding time requirements are concerned. Besides, in case of leak either from piping in the clearance between inner and outer vessels or from inner vessel, the outer jacket and vessel shall perform as secondary barrier, as prescribed by IMO CCC9 Guidelines and IGF code (i.e., same resistance of primary barrier).

### 4.3.2 $LH_2$ pumps

The cryogenic pumps shall be designed to work submerged in a cryosump or inside in-tank deep wells. Irrespective of their configuration, all $LH_2$ fuel pumps integrated into a tank will discharge into a common feed manifold, where each branch is intercepted through a shut-off ESD valve and a check valve. To avoid overpressure at the discharge section of the pump as well as in any other relevant sections (e.g., downstream single stage for multistage pumps), the $LH_2$ pump are equipped with pressure relief devices with proper set pressure. The pump will be powered via VFD through the shipboard electric grid. Two pumps in parallel are devised for both SFS1 and SFS2.

*Table 24 – $LH_2$ pump main characteristics*

| | SFS 1 | SFS 2 |
|---|---|---|
| **Type** | Multistage centrifugal | |
| **Inlet pressure [barg]** | 1-11 | |
| **Delivery pressure [barg]** | 20-60 | |

### 4.3.3 $LH_2$ BOG compressor

BOG compressor is a reciprocating piston machinery with specifications as reported in Table 25. BOG massflow rate has been estimated after the fuel tank characteristics, which is assumed to be 1%/day on mass basis with respect to the total fuel mass. This is a conservative estimate, considering that the manufacturer declares less than 1% of the stored mass per day.

*Table 25 – $LH_2$ BOG compressor main characteristics*

| | |
|---|---|
| **Type** | Multistage reciprocating |
| **Inlet pressure [barg]** | 1-11 |
| **Delivery pressure [barg]** | 20-60 |

### 4.3.4 Heat exchangers

The fuel system contains three main heat exchangers: the evaporator, the BOG heater and the BOG aftercooler. Their characteristics are reported in the following tables.

A plate vaporizer is preferred, thanks to its small size and because it should be placed in the TCS, which is usually quite compact to minimize heat ingress. Indeed, this is the solution most widely adopted in already existing LNG fuel systems for maritime. Besides, in the case of complete TCS inertisation with nitrogen atmosphere, no nitrogen condensation should occur in normal operating conditions (Table 26).

*Table 26 – $LH_2$ Evaporator main characteristics*

| | |
|---|---|
| **Type** | Plate/Shell and tube |
| **Cold side fluid** | $LH_2$/cold $GH_2$ |
| **Hot side fluid** | HTF |
| **Normal operating pressure [barg]** | 20 to 50 |
| **Normal cold exit temperature [°C]** | 20 |
| **Normal hot exit temperature [°C]** | 30 |

*Table 27 – $LH_2$ BOG heater and BOG aftercooler main characteristics*

| | |
|---|---|
| **Type** | Plate/Shell and tube |
| **Cold side fluid** | $LH_2$/cold $GH_2$ |
| **Hot side fluid** | HTF |
| **Normal operating pressure [barg]** | 5 to 11 |
| **Normal cold exit temperature [°C]** | -10 to 20 |
| **Normal hot exit temperature [°C]** | 30 to 40 |
| **Cold side nominal MFR [g/s]** | 1 to 3 |

*Table 28 – $LH_2$ BOG aftercooler main characteristics*

| | |
|---|---|
| **Type** | Plate/Shell and tube |
| **Cold side fluid** | $LH_2$/cold $GH_2$ |
| **Hot side fluid** | HTF |
| **Normal operating pressure [barg]** | 30 to 50 |
| **Normal cold exit temperature [°C]** | 50 |
| **Normal hot exit temperature [°C]** | 30 to 50 |

The desired characteristics of BOG heater and BOG aftercooler are reported in Table 27 and

Table 28. The first operates at low fuel storage pressure, while the second has to withstand fuel delivery pressure. Apart from that, the two items are fairly similar.

## 4.4 $LH_2$ - System performance

### 4.4.1 $LH_2$ SFS 1 – Design performance and components sizing

SFS1 is the smaller of the two systems, targeted to cover the hotel loads onboard a large cruise ship for zero carbon power generation while at port. The thermodynamic conditions of each point of SFS1 fuel system are reported in For confidentiality reasons, it is not possible to disclose the exact values of massflow at each thermodynamic point, hence values are normalised. The design MFR that normalizes the values is the one of hydrogen for points 1 to 8, while that of HTF for points 9 to 17. The pressure values are reported as ranges, because the exact values are covered by non disclosure agreements. Anyhow, these are representative of typical fuel feed pressures for power generation gas turbines.

Table 29. Hydrogen thermodynamic points are 1 to 8, while HTF are points 9 to 17 (see Figure 36 for reference). Design hydrogen mass flow rate has been oversized by 20% with respect to the nominal mass flow rate, defined by means of equation (2) and (3). The powers of each component are a result of the simulation, and appear in

Table 30. It is immediately evident that the HTF heater and the hydrogen evaporator share the most of the heat load, being in fact the main thermal source and sink of the fuel system.

$$P_{el} = \dot{m_{fuel}} \cdot LHV \cdot \eta_{el,des} \tag{2}$$

$$\dot{m}_{des} = 1.2 \cdot \dot{m}_{fuel} \tag{3}$$

For confidentiality reasons, it is not possible to disclose the exact values of massflow at each thermodynamic point, hence values are normalised. The design MFR that normalizes the values is the one of hydrogen for points 1 to 8, while that of HTF for points 9 to 17. The pressure values are reported as ranges, because the exact values are covered by non disclosure agreements. Anyhow, these are representative of typical fuel feed pressures for power generation gas turbines.

*Table 29 – On-design performance of SFS1 system, hydrogen line.*

| Point | Pressure [barg] | Temperature [°C] | $MFR/MFR_{design}$ |
|---|---|---|---|
| 1 | 1-11 | -241 | 1 |
| 2 | 20-60 | -235.5 | 1 |
| 3 | 20-60 | 20 | 1 |
| 4 | 1-11 | -241 | 0.021 |
| 5 | 1-11 | 20 | 0.021 |
| 6 | 20-60 | 235 | 0.021 |
| 7 | 20-60 | 50 | 0.021 |
| 8 | 20-60 | 20.6 | 1.02 |
| 9 | 3.5 | 45 | 1 |
| 10 | 3.5 | 45 | 0.735 |
| 11 | 3.4 | 30 | 0.736 |
| 12 | 3.5 | 45 | 0.145 |
| 13 | 3.4 | 43.6 | 0.145 |
| 14 | 3.5 | 45 | 0.12 |
| 15 | 3.4 | 46.2 | 0.12 |
| 16 | 3.4 | 33.9 | 1 |
| 17 | 3.5 | 34 | 1 |

*Table 30 – Results of components sizing in terms of heat or power duty, SFS1 $LH_2$*

| Component | Design power [kW] |
|---|---|
| $LH_2$ pump | 12.3 |
| Evaporator | 759 |
| BOG compressor | 11 |
| BOG aftercooler | 9.4 |
| BOG heater | 14.2 |
| HTF heater | 763 |
| HTF circulation pump | 0.2 |

### 4.4.2 $LH_2$ SFS 1 – Off-design performance

Figure 39 shows the share of total HTF massflow for each branch of SFS1 architecture. It is clearly visible that the BOG contribution is very small, as predictable from the tables of steady state design operation.

Figure 40 reports, as already mentioned, that the largest share of heat transfer is given by the evaporator and the HTF heater, while the BOG aftercooler and BOG heater are a mere 12% and 15% of the total installed heat exchanger power. This result is obtained with the strong assumption that the fuel massflow rate variation (i.e., the fuel consumption) is linearly proportional to the actual gas turbine load.

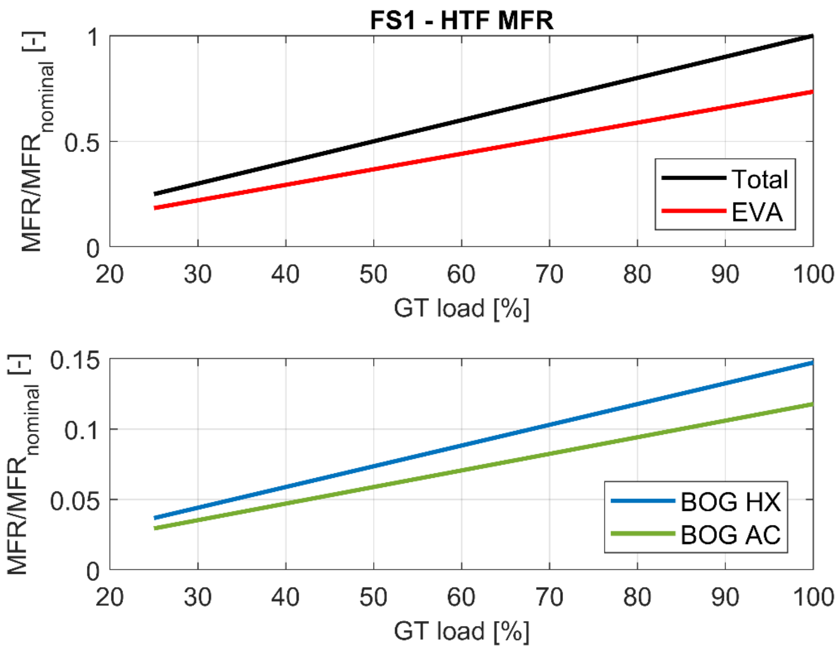


*Figure 39 – Off-design of HTF massflow rate, SFS1 $LH_2$*

The duty breakup and the outlet temperature at BOG heat exchangers (BOG HEX and BOG AC) are reported in Figure 40 and Figure 41, respectively. As mentioned, the evaporator covers almost 50% of the installed heat exchange power, while the size of BOG heat exchangers is very small, as a consequence of the very low natural boil-off rate assumed.

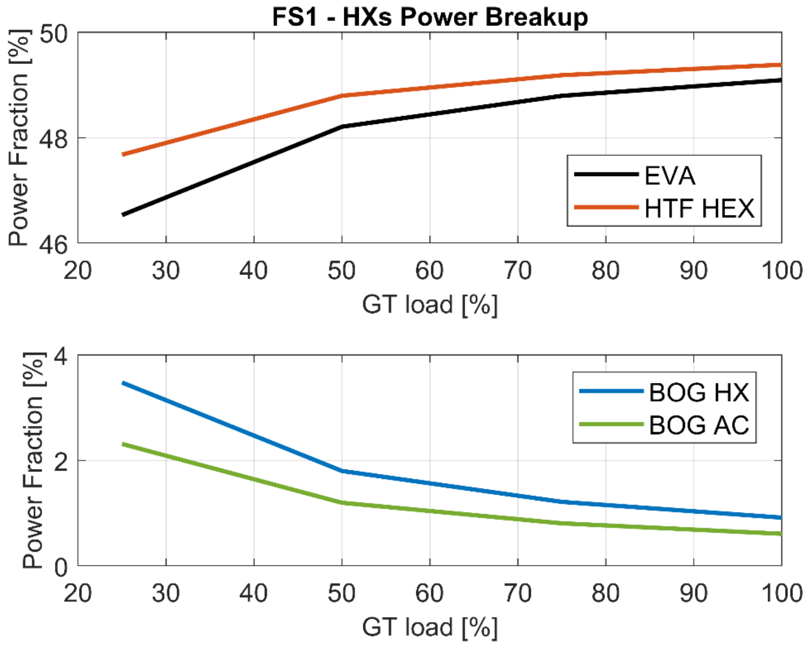


*Figure 40 – Heat exchanger duty breakup in off-design operation, SFS1 $LH_2$*

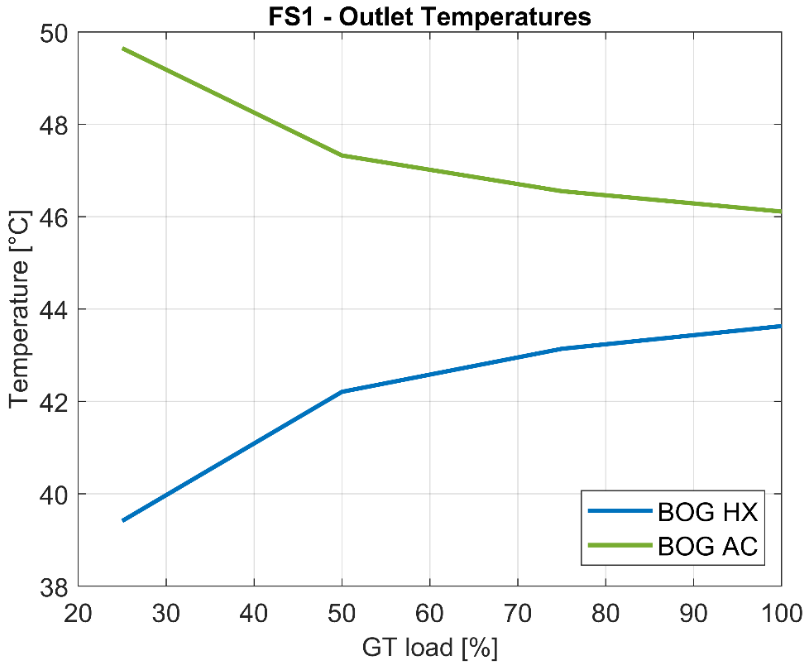


*Figure 41 – Outlet temperatures at BOG heater and BOG aftercooler, SFS1 $LH_2$*

### 4.4.3 $LH_2$ SFS 2 – Design performance and components sizing

SFS 2 is designed to cover the full navigation load of a medium-large cruise ship. The design thermodynamics of each point of the hydrogen side of SFS2 fuel system are reported in Table 31. As before, thermodynamic points correspond to those shown in Figure 36. The corresponding duties of the components are shown in Table 32. Again, design hydrogen mass flow rate has been imposed as 20% over the necessary value as per equation (1). Again, equation (2) and (3) still apply for SFS 2. The design MFR that normalizes the values is the one of hydrogen for points 1 to 8, while that of HTF for points 9 to 17.

*Table 31 - On-design performance of SFS2 system, hydrogen line.*

| Point | Pressure [barg] | Temperature [°C] | $MFR/MFR_{design}$ |
|---|---|---|---|
| 1 | 1-11 | -241 | 1 |
| 2 | 20-60 | -235.5 | 1 |
| 3 | 20-60 | 20 | 1 |
| 4 | 1-11 | -241 | 0.01 |
| 5 | 1-11 | 20 | 0.01 |
| 6 | 20-60 | 235 | 0.01 |
| 7 | 20-60 | 50 | 0.01 |
| 8 | 20-60 | 20.2 | 1.01 |
| 9 | 3.5 | 45 | 1 |
| 10 | 3.5 | 45 | 0.93 |
| 11 | 3.4 | 30 | 0.93 |
| 12 | 3.5 | 45 | 0.03 |
| 13 | 3.4 | 42.7 | 0.03 |
| 14 | 3.5 | 45 | 0.042 |
| 15 | 3.4 | 46.1 | 0.042 |
| 16 | 3.4 | 31.1 | 1 |
| 17 | 3.5 | 31.2 | 1 |

*Table 32 – Results of components sizing in terms of heat or power duty, SFS2 $LH_2$.*

| Component | Design power [kW] |
|---|---|
| $LH_2$ pump | 46.6 |
| Evaporator | 2876 |
| BOG compressor | 11 |
| BOG aftercooler | 9.4 |
| BOG heater | 14.2 |
| HTF heater | 2880 |
| HTF circulation pump | 0.8 |

### 4.4.4 $LH_2$ SFS 2 – Off-design performance

Results of SFS2 are reported in Figure 41, Figure 42 and Figure 43 for HTF massflow rate, power duty breakup and BOG heat exchangers outlet temperature, respectively. Here, the share of MFR is around 4% for BOG AC and 3% for BOG HEX, which is around 4 times less than SFS1. The same trend is present in Figure 42 as regards the heat exchangers duty.

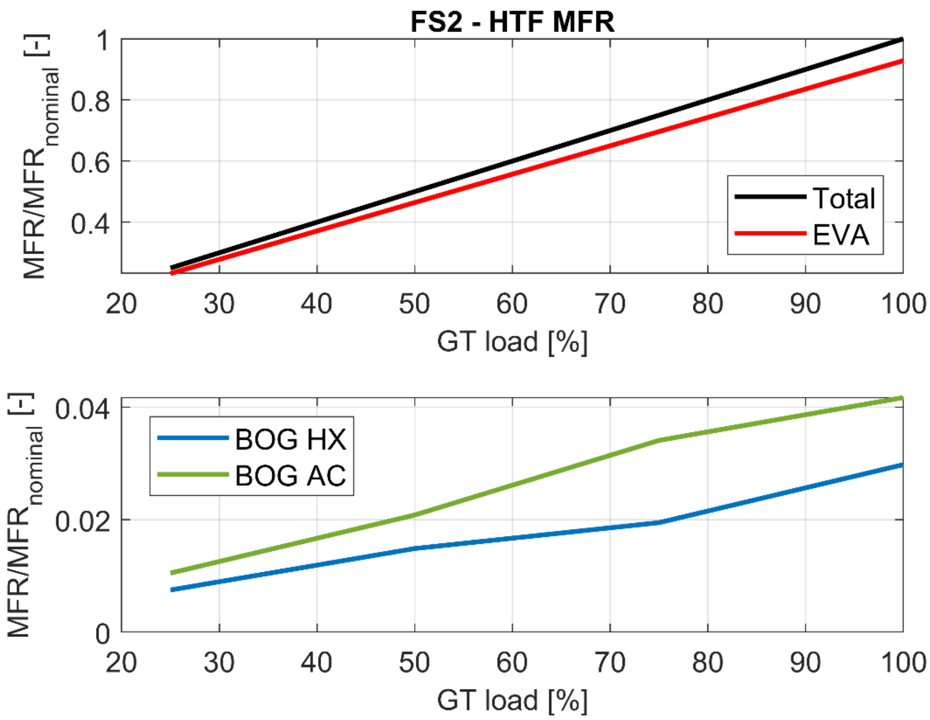

*Figure 42 – Off-design of HTF massflow rate, SFS2 $LH_2$*

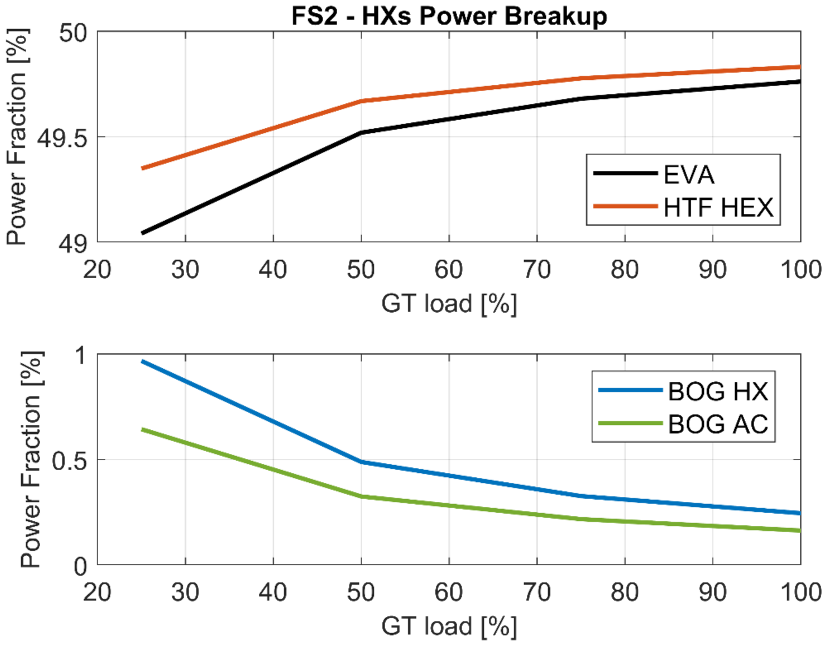


*Figure 43 – Heat exchanger duty breakup in off-design operation, SFS2 $LH_2$*

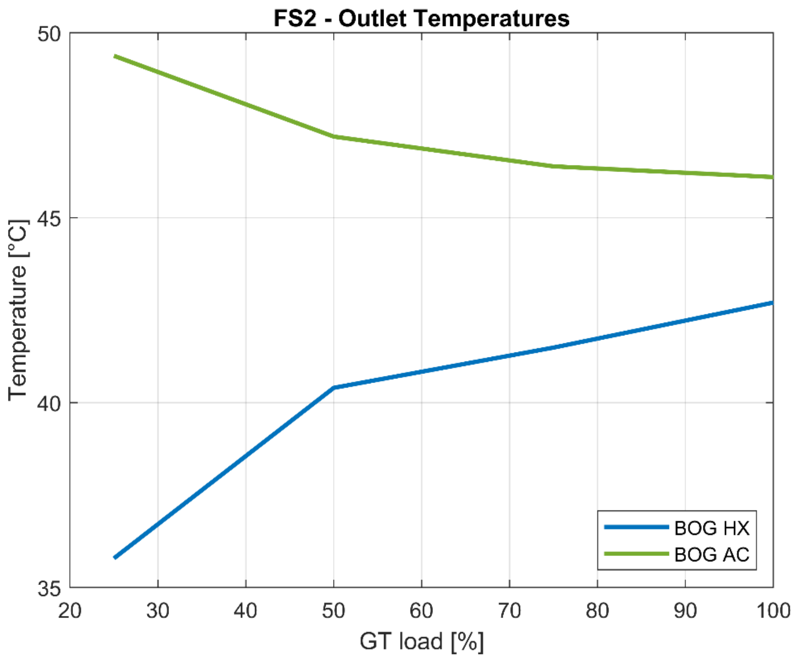


*Figure 44 - Outlet temperatures at BOG heater and BOG aftercooler, SFS2 $LH_2$*

Finally, BOG outlet temperatures show that off-design temperature variation are quite limited between minimum load and full load, setting at 4 K and 6 K for BOG AC and BOG HEX, respectively as reported in Figure 42.

## 4.5 LNG – General description of the fuel system

This paragraph contains the design specifications and the system performance of the LNG part of the hybrid fuel system described before. SFS1 and SFS2 will be eventually coupled to create a fully flexible hydrogen-natural gas system for passenger ship application.

With regard to the LNG lines, it is important to note that SFS1 differs from SFS2 in a different way from hydrogen SFS1 and SFS2. In fact, as described in paragraph 4.1.2, the whole SFS1 must be able to feed not only the CCGT with hydrogen-methane blends, but also the entire power generation system of the ship with methane only. Since SFS1 is devised for large cruise ships, this means that such configuration must be able to cover up to 70-80 MW power. Therefore, SFS1 has higher design massflow rates as compared to SFS2 where the CCGT is the only powertrain installed aboard. The main power generators of SFS1 are outside the scope of the thesis.

The arrangement of LNG fuel system is reported in Figure 45. It is rather conventional and has no major differences compared to the $LH_2$. It features high pressure delivery system to comply with the gas turbine requirements, but also a pressure reduction skid to be able to feed reciprocating engines at a much lower pressure. Since LNG is a mixture of different hydrocarbons and the composition may vary considerably depending on the source, a reference composition is assumed to be as reported in Table 33.

*Table 33 – Composition and properties of natural gas assumed in this work*

| | |
|---|---|
| **Methane (C1)** | 85.5% |
| **Ethane (C2)** | 11.7% |
| **Propane (C3)** | 2.0% |
| **Butane (C4+)** | 0.5% |
| **Nitrogen ($N_2$)** | 0.3% |
| **LHV [MJ/kg]** | 49.2 |

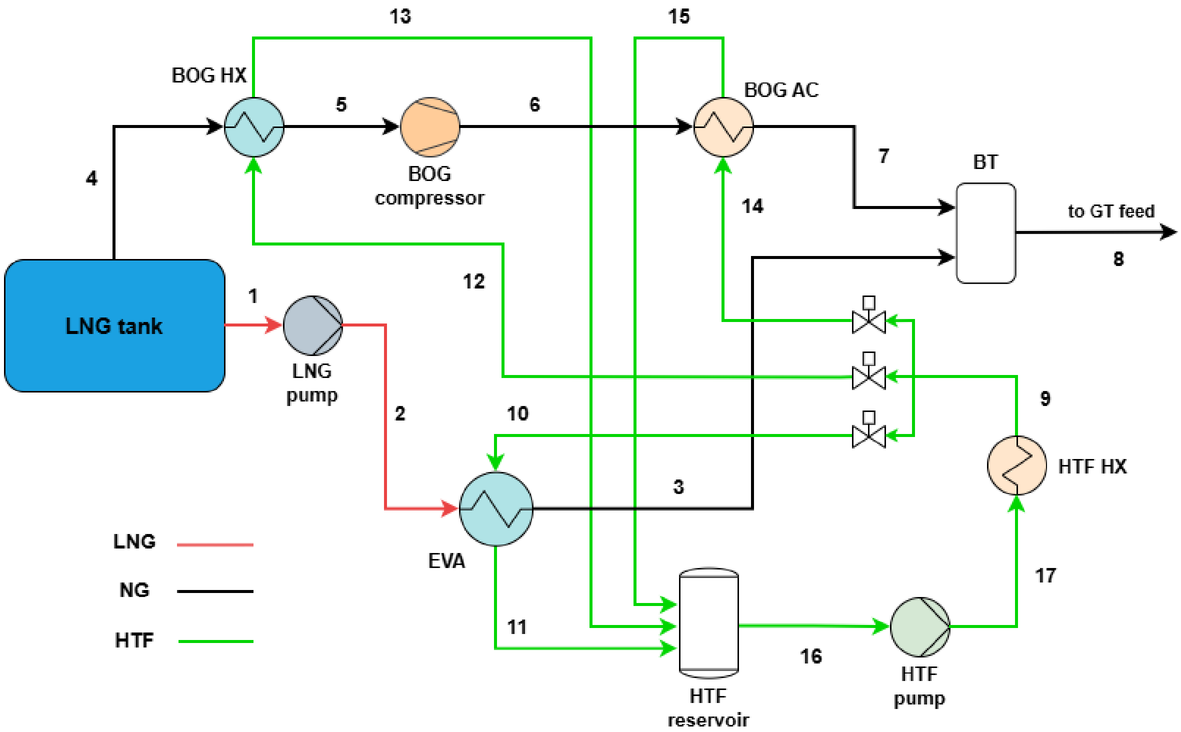


*Figure 45 - PFD schematic of LNG fuel system architecture, SFS 1 and SFS 2*

## 4.6 LNG – Components

### 4.6.1 Fuel tank

The fuel is stored in a conventional horizontal single shell bi-lobed Type C tank. The liquid capacity is expected to be in the range 2000 m$^3$ and the normal working pressure between 0.4 and 1 barg. Submerged pumps for LNG are the state of the art, therefore the tank will contain those in a deep well. The tank will be made of X7Ni9 stainless steel, a consolidated choice for LNG reservoirs. To comply with the SRtP prescriptions, two LNG tanks will be present onboard since this fuel consists of the main power source. In this case, the bunkering and vapour return lines of the two tanks (port and starboard) shall be interconnected to complete refilling using either bunkering station. Filling limits are defined as per IGF code, in the same way as for hydrogen. The tank is going to be ATEX Zone 0 and compliant with IGF code as far as filling limit and holding time requirements are concerned.

*Table 34 – LNG fuel tank main characteristics*

| | |
|---|---|
| **Type** | Horizontal bi-lobed Type C |
| **Capacity [m$^3$]** | 2000 |
| **Normal operating pressure range [barg]** | 0.4-1 |
| **Insulation** | Polyurethane foam |
| **Material** | Cryogenic grade stainless steel (e.g. X7Ni9) |

### 4.6.2 LNG pumps

LNG pumps draw natural gas in liquefied phase from the bottom of the bi-lobed storage tanks and feed the main lines. They shall have a configuration such that the LNG that cannot be drawn from the tank is minimised. The available Net Positive Suction Head ($NPSH_a$) can be derived through the following equation (4):

$$NPSH = \frac{p_{tank} - p_{vap}}{\rho_{LNG} \cdot g} + h_{static} \ \ [m] \qquad (4)$$

where g = 9.81 m/s$^2$. This value depends on the liquid height $h_{static}$ (hence on the tank size and filling limit), and on storage pressure $p_{tank}$. Usually, LNG pumps require a minimum NPSH of 2-3 m to minimize unused fuel [57].

Both the LNG fuel pumps integrated into a tank shall discharge into a common feed manifold through a shut-off ESD valve and check valve. The pumps speed is regulated via a VFD powered by the shipboard electric grid.

*Table 35 – LNG pumps main characteristics*

| | **SFS 1** | **SFS 2** |
|---|---|---|
| **Type** | Multistage centrifugal, submerged | |
| **Inlet pressure [barg]** | 0.4-1 | |
| **Delivery pressure [barg]** | 20-60 | |

As for the hydrogen SFSs, the excess of LNG is recirculated back to the LNG storage tank through a dedicated line in case the fuel required by the end user is below the minimum flow of the LNG pump. In this way, the LNG pump is kept running at minimum flow to avoid cavitation. Recirculation line could also serve during start-up, before fuel demand arises, and to keep the tank cooled down at sea while the liquid volume is low.

### 4.6.3 LNG BOG compressor

The BOG compressor for LNG is dimensioned for processing the boil off rate generated in the tank per day, for all the suction conditions required. The main characteristics that are required to this component are reported in Table 36. In the same way as the hydrogen system, the BOG line is utilised to regulate the LNG tank pressure within its pressure limits, hence activating the line when the upper threshold is reached and stopping it when the lower threshold is achieved. The BOG compressor shall be designed as much compact as possible and shall be able to be placed in the TCS, which is classified ATEX Zone 1.

*Table 36 – LNG BOG compressor main characteristics*

| | |
|---|---|
| **Type** | Multistage reciprocating |
| **Inlet pressure [barg]** | 0.4-1 |
| **Delivery pressure [barg]** | 20-60 |

### 4.6.4 LNG heat exchangers

As regards heat exchangers, a plate vaporizer is preferred because it should be placed in the TCS (Figure 38), which is usually quite compact to minimize ambient heat ingress. The BOG HEXs (BOG heater and BOG aftercooler) are much smaller components and are possibly very similar, as it is the case for hydrogen. LNG vaporizer, whose specifications are reported in Table 37, is to be installed inside the TCS, then must be classified ATEX Zone 1.

*Table 37 – LNG vaporizer characteristics*

| | |
|---|---|
| **Type** | Plate/Shell and tube |
| **Cold side fluid** | LNG/Cold NG |
| **Hot side fluid** | HTF |
| **Normal operating pressure [barg]** | 20 to 60 |
| **Normal cold exit temperature [°C]** | 25 to 40 |
| **Normal hot exit temperature [°C]** | 30 |

*Table 38 – LNG BOG heater and BOG aftercooler characteristics*

| | |
|---|---|
| **Type** | Plate/Shell and tube |
| **Cold side fluid** | LNG/cold NG |
| **Hot side fluid** | HTF |
| **Normal operating pressure [barg]** | 30 to 50 |
| **Normal cold exit temperature [°C]** | -25 to 30 |
| **Normal hot exit temperature [°C]** | 0 to 20 |

## 4.7 LNG – System performance

### 4.7.1 LNG SFS 1 – Design performance and components sizing

SFS1 is the smaller of the two systems, targeted to cover the hotel loads onboard a large cruise ship for zero carbon power generation while at port. For more information on the SFS1 characteristics, the reader is referred to sections 4.1.2 and 4.4.1.

*Table 39 - On-design performance of SFS1 system, LNG line.*

| Point | Pressure [barg] | Temperature [°C] | $MFR/MFR_{design}$ |
|---|---|---|---|
| 1 | 0.4-1 | -162 | 1 |
| 2 | 20-60 | -160.8 | 1 |
| 3 | 20-60 | 20 | 1 |
| 4 | 0.4-1 | -162 | 0.04 |
| 5 | 0.4-1 | 20 | 0.04 |
| 6 | 20-60 | 379 | 0.04 |
| 7 | 20-60 | 50 | 0.04 |
| 8 | 20-60 | 23.1 | 1.04 |
| 9 | 3.5 | 45 | 1 |
| 10 | 3.5 | 45 | 0.84 |
| 11 | 3 | 30 | 0.84 |
| 12 | 3.5 | 45 | 0.05 |
| 13 | 3 | 36.7 | 0.05 |
| 14 | 3.5 | 45 | 0.11 |
| 15 | 3.3 | 48.8 | 0.11 |
| 16 | 3 | 32.3 | 1 |
| 17 | 3.5 | 32.4 | 1 |

The design thermodynamics of each point of the hydrogen side of SFS2 fuel system are reported in Table 39. The corresponding duties of the components are shown in Table 40. Again, design hydrogen mass flow rate has been imposed as 20% over the necessary value as per equation (1). Points 1 to 8 refer to natural gas, points 9 to 17 to HTF (Figure 36). The pressure values are reported as ranges, because the exact values are covered by non disclosure agreements. Anyhow, these are representative of typical fuel feed pressures for power generation gas turbines.

*Table 40 - Results of components sizing in terms of heat or power duty, SFS1 LNG*

| Component | Design power [kW] |
|---|---|
| $LH_2$ pump | 25.5 |
| Evaporator | 1871 |
| BOG compressor | 79.1 |
| BOG aftercooler | 77.6 |
| BOG heater | 72.5 |
| HTF heater | 1863 |
| HTF circulation pump | 2.6 |

### 4.7.2 LNG SFS 1 – Off-design performance

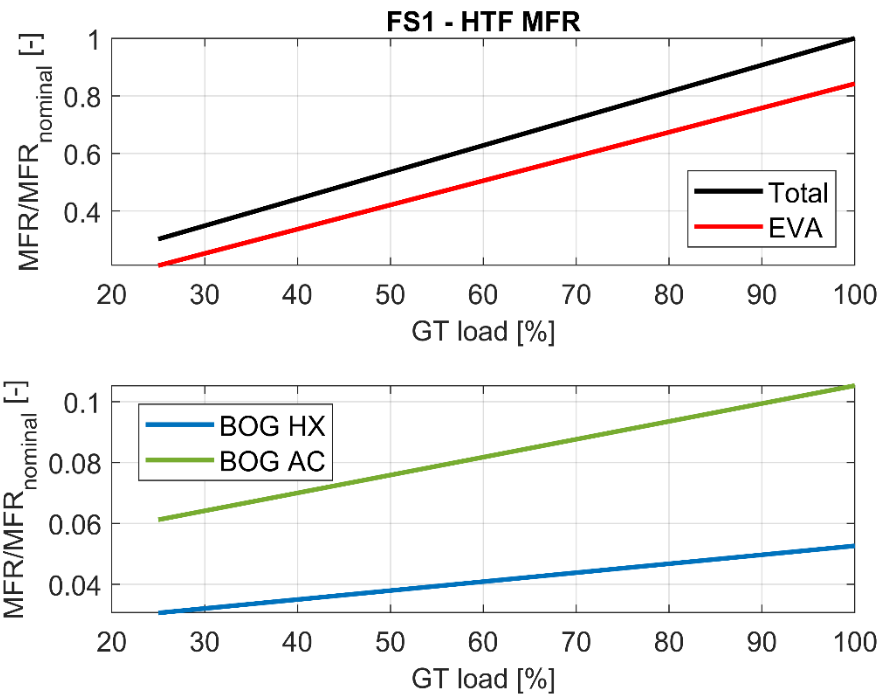


*Figure 46 - Off-design of HTF massflow rate, SFS1 LNG*

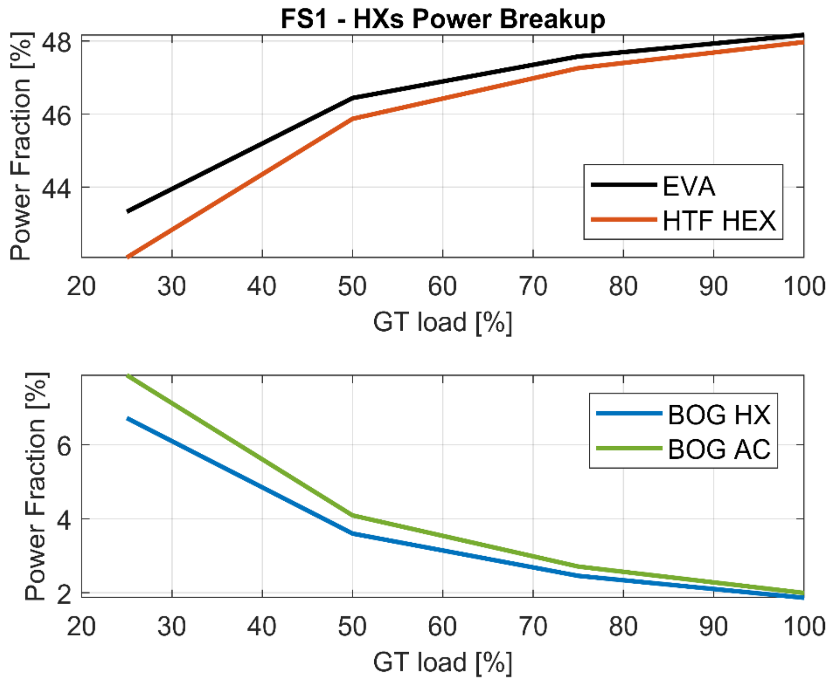


*Figure 47 - Heat exchanger duty breakup in off-design operation, SFS1 LNG*

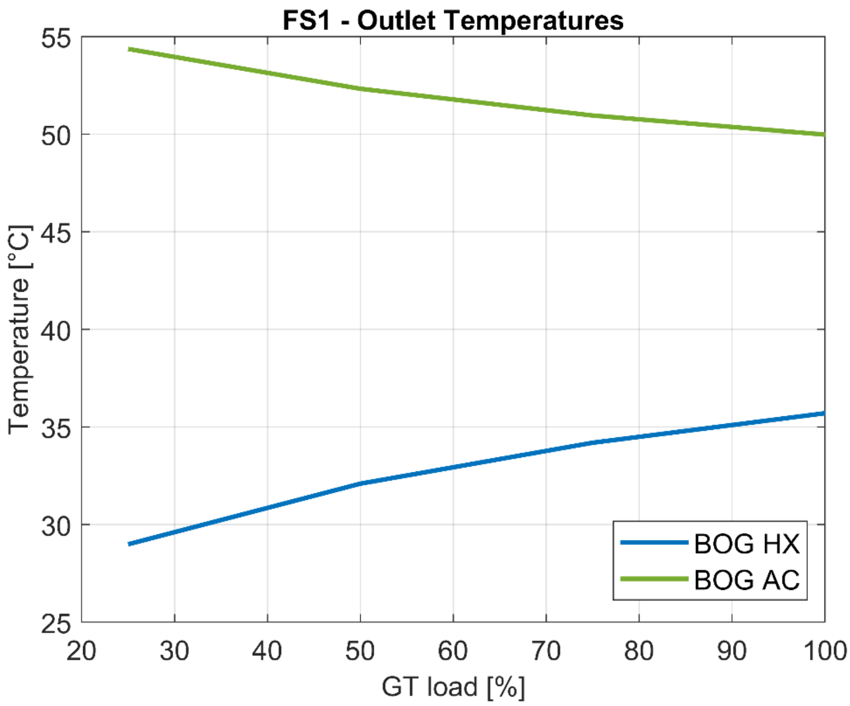


*Figure 48 - Outlet temperatures at BOG heater and BOG aftercooler, SFS1 LNG*

Off-design performance of the LNG SFS1 fuel system is reported in this paragraph. In this instance, the BOG AC is responsible for 10% of the total heat exchange, while the BOG heater accounts for 5% of the total heat duty.

Figure 47 and Figure 48 report the heat duty breakup and the off-design temperature for SFS1. The temperature difference in deep off-design is much higher due to the increased LNG massflow rate with respect to $LH_2$, but the system is designed to be resilient enough to sustain lower off-design temperatures.

### 4.7.3 LNG SFS 2 – Design performance and components sizing

*Table 41 - On-design performance of SFS2 system, LNG line.*

| Point | Pressure [barg] | Temperature [°C] | $MFR/MFR_{design}$ |
|---|---|---|---|
| 1 | 0.4-1 | -162 | 1 |
| 2 | 20-60 | -160.8 | 1 |
| 3 | 20-60 | 20 | 1 |
| 4 | 0.4-1 | -162 | 0.05 |
| 5 | 0.4-1 | 20 | 0.05 |
| 6 | 20-60 | 379 | 0.05 |
| 7 | 20-60 | 50 | 0.05 |
| 8 | 20-60 | 20.8 | 1.05 |
| 9 | 3.5 | 45 | 1 |
| 10 | 3.5 | 45 | 0.82 |
| 11 | 3 | 30 | 0.82 |
| 12 | 3.5 | 45 | 0.06 |
| 13 | 3 | 34.1 | 0.06 |
| 14 | 3.5 | 45 | 0.12 |
| 15 | 3.3 | 50.8 | 0.12 |
| 16 | 3 | 32.7 | 1 |
| 17 | 3.5 | 32.7 | 1 |

The design thermodynamics of each point of the hydrogen side of SFS2 fuel system are reported in Table 41, while the corresponding duties of the components are shown in Table 42. Again, design hydrogen mass flow rate has been imposed 20% over the necessary value as per equation (1). Again, points 1 to 8 refer to natural gas, points 9 to 17 to HTF. For confidentiality reasons, it is not possible to disclose the absolute values of massflow at each thermodynamic point, hence values are normalised.

*Table 42 - Results of components sizing in terms of heat or power duty, SFS2 LNG*

| **Component** | **Design power [kW]** |
|---|---|
| $LH_2$ pump | 19.2 |
| Evaporator | 1407 |
| BOG compressor | 79.1 |
| BOG aftercooler | 77.6 |
| BOG heater | 72.5 |
| HTF heater | 1400 |
| HTF circulation pump | 2.0 |

Results of SFS2 off-design performance in terms of HTF mass flow, heat duty split, and outlet BOG temperatures are reported in Figure 49, Figure 50, and Figure 51 respectively. Given no major differences with SFS1, in the mentioned charts the same trends are replicated. However, as opposed to $LH_2$ fuel line, BOG AC is larger on percentual basis in SFS2 than it is in SFS1. This is due to the aforementioned fact that the LNG section of SFS1 has to cover the whole power load (CCGT + power engines and generator) of a large cruise ship, while SFS2 has a target installation of a smaller ship with a smaller total fuel mass flow.

### 4.7.4 LNG SFS 2– Off-design performance

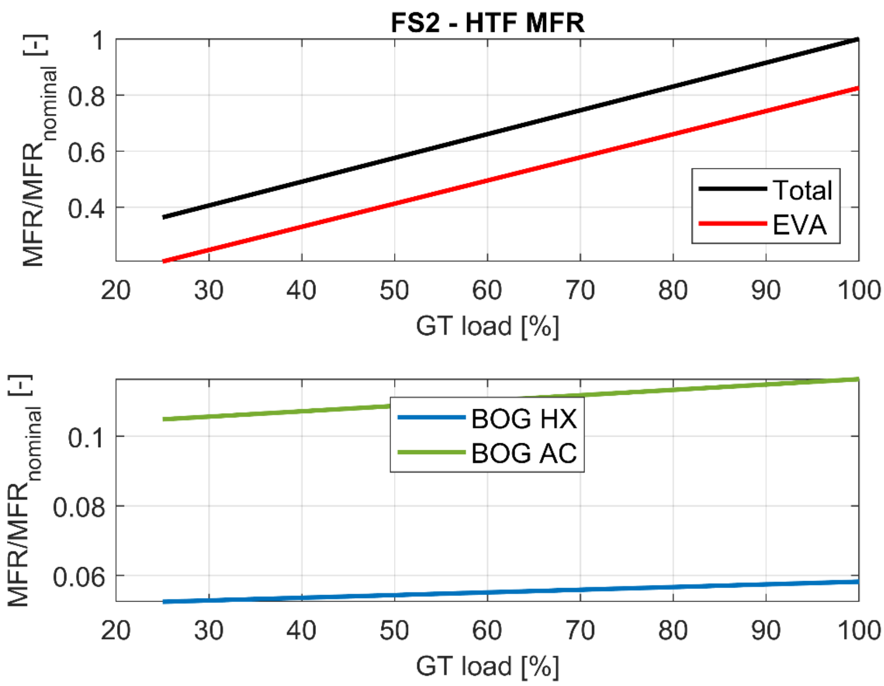


*Figure 49 - Off-design of HTF massflow rate, SFS2 LNG*

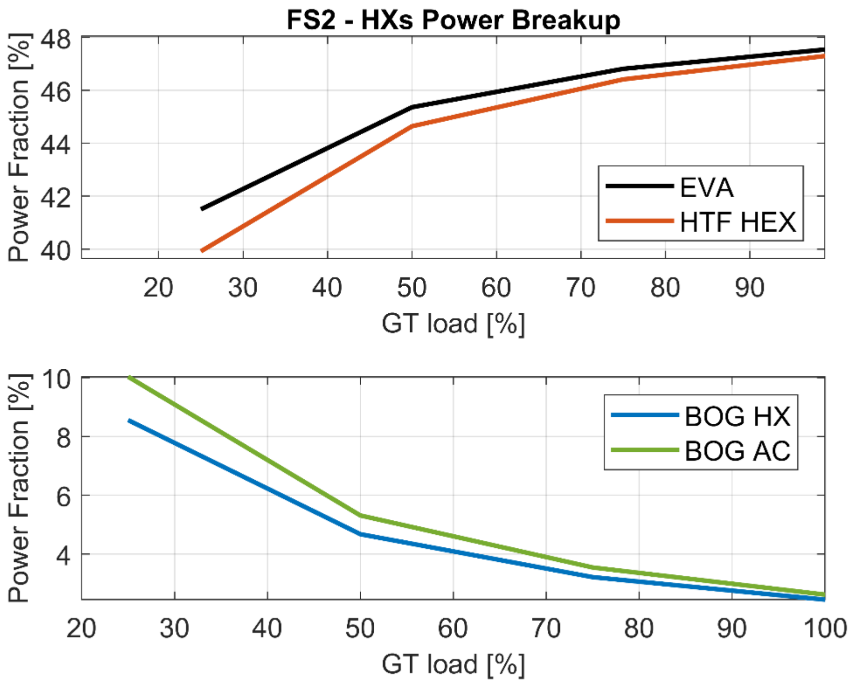


*Figure 50 - Heat exchanger duty breakup in off-design operation, SFS2 LNG*

As regards BOG outlet temperatures (Figure 51), they show a more linear trend possibly due to the different HTF massflow split.

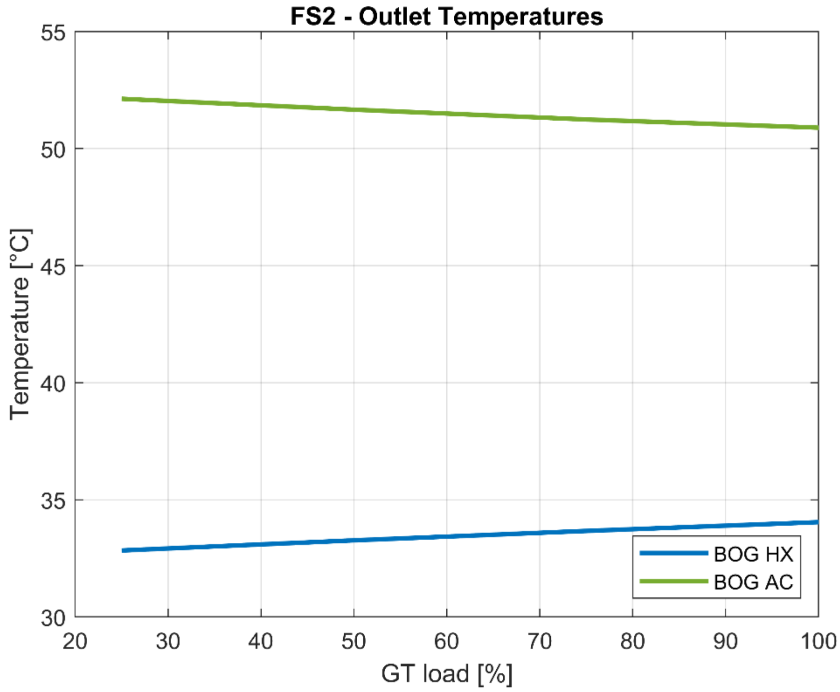


*Figure 51 - Outlet temperatures at BOG heater and BOG aftercooler, SFS2 LNG*

## 4.8 Hydrogen-Natural gas blending

Hydrogen and natural gas have quite different properties. However, the blending of it with natural gas has been identified as a mean to promote hydrogen uptake in thermal processes.

As described, the CCGTs power systems are designed to run on virtually any composition of hydrogen-natural gas blend. Any variation in the LHV-based energy supplied to the combustor is realised through one of two mechanisms: either by increasing the total mass flow rate of the fuel blend delivered to the combustor, or by altering the blend composition in order to vary its energy density. In practice, precise operating strategies will be put in place according to the navigation route, evaluating the presence of ECAs, the distance from the closest port and the availability of fuels, especially hydrogen, at said ports. For this reason, in the scope of the design of the complete system, the preliminary map correlating the actual fuel blend massflow rate to the load of the prime mover and the current or required blend composition is built.

A comparison between thermodynamic properties of hydrogen and natural gas (or sometimes referred to as pure methane) is described in paragraphs 1.2.1, 1.2.2, 2.1, 2.2, and safety-related indices are reported in Table 7. Nonetheless, when energy content is concerned, a comparison between mass densities and energy densities is necessary. Figure 52 depicts the different densities of the two as a function of temperature and storage pressure.

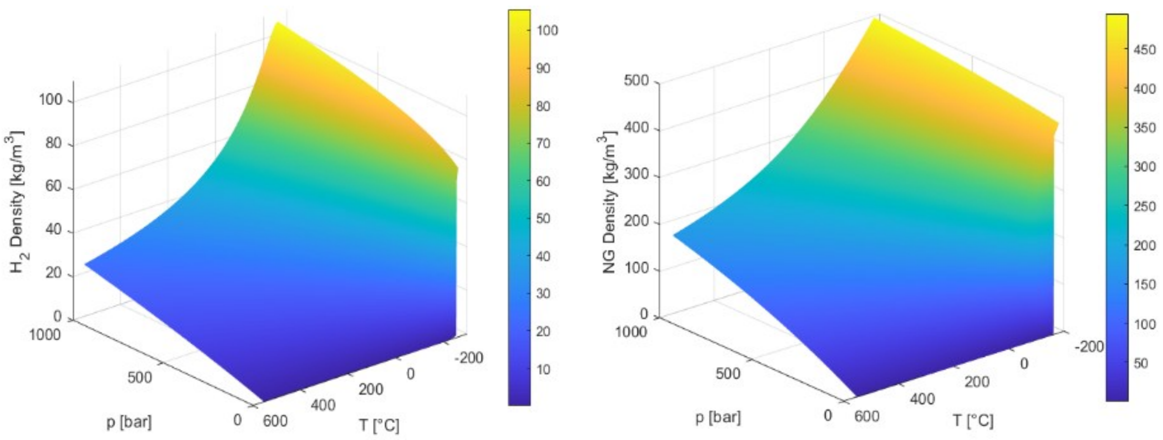


a) b)

*Figure 52 – Hydrogen (left) and methane (right) densities as a function of pressure and temperature.*

### 4.8.1 Blend composition control

The most relevant challenge when propulsion systems are concerned is the need for a precise energy delivery to the prime mover. When dealing with fuel mixtures, this implies that a new variable is added to the control logic. In fact, one can regulate the thermal engine power output not only by adjusting the mass flow rate, as in a conventional single fuel or dual fuel system, but also varying the blend composition, thereby introducing a new degree of freedom. However, the control logic of gas turbines is generally such that the Turbine Inlet Temperature (TIT) is maintained constant, in order to comply with structural requirements and reduce the time between inspections. Hence, given the required power from the onboard grid, this is met by ensuring a constant LHV. This can be met with a blend whose composition is, in theory, free to vary. However, the amount of hydrogen to be added to the natural gas is virtually decided upon three main aspects:

- The need for compliance with the IMO emission regulations, which are both set on a single ship and on the entire fleet of a ship's cruise line.
- The geographical emission limits set in the Emission Control Areas (ECAs), such as the Baltic Sea.
- The need for compliance with the SRtP requirements.

There are several examples of companies who have run tests with natural gas and hydrogen blends on existing GT engines, with promising results. Tests on a MHI MG501 heavy duty engine with blends up to 20.9% vol. hydrogen showed that turndown capabilities are enhanced and operation is overall safe [148]. The event of a rapid shutoff of the hydrogen supply was also explored. In fact, in blend operation, the lower overall energy content requires the gas valve to be wider open; the control logic was then modified so that, in case of hydrogen shutoff, the abrupt methane mass flow increase required to match the energy input would not cause over-firing. Siemens have run tests on a SGT6-600G engine, rated at 25 MW in simple cycle configuration, with blends ranging from 0% to 38% $H_2$ [149]. The simple control of the hydrogen valve opening paired with a Coriolis flow meter was adopted as a measure of hydrogen concentration in the blend. The exact blend composition was confirmed by gas-chromatograph samples [149].

From a methodological perspective, two possibilities exist: blending in a batch volume downstream the piping merge or blending by simple merging two pipes with an adequate geometry. The first, which is employed in the MHI tests [148], a better mixing is achieved to the expenses of the presence of an additional buffer reservoir that adds space occupancy and fluidic inertia. The second instead, as shown in [149], is much simpler and guarantees good performance provided that the piping downstream is sufficiently tortuous as to obtain the adequate mixing. In a pipe with bends, the mixing efficiency is enhanced by 12%

as compared to a straight pipe. The authors define the mixing efficiency $\eta_{mixing}$ as a “coefficient of variation” expressed by the ratio between the mean and the standard deviation of the hydrogen concentration at a given coordinate along the piping, as per eq. (5).

$$\eta_{mixng} = \frac{\sigma_{y,H2}}{\bar{y}_{H2}} \tag{5}$$

For the case of the CCGT in this work, the map correlating the $H_2$-NG blend mass flow rate was built taking into account the blend LHV, the molar composition of the blend and the gas turbine thermal efficiency, according to eqs. (6) to (10).

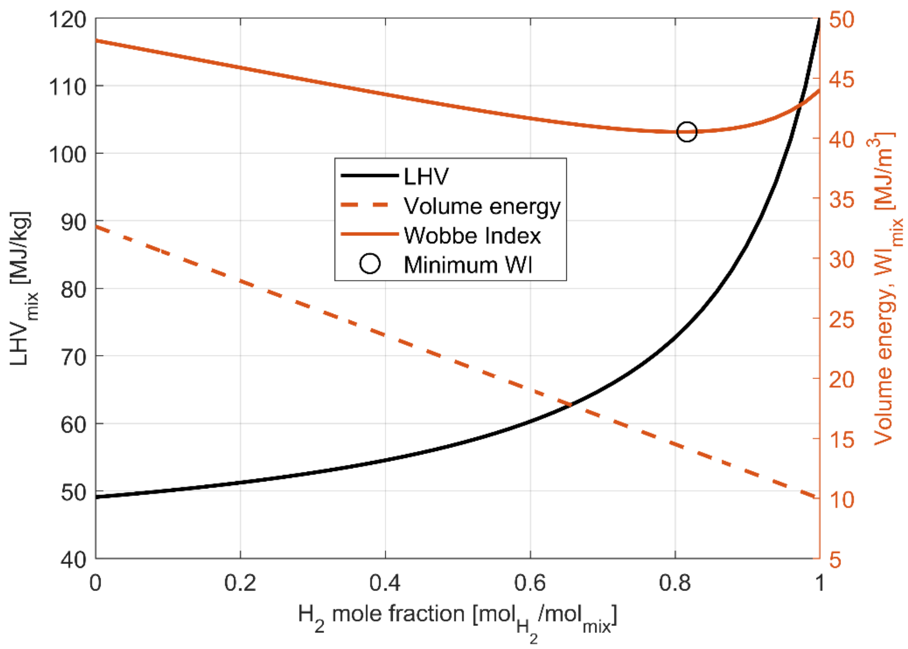


*Figure 53 – LHV and Wobbe index of hydrogen-natural gas blends*

$$P_{th} = \dot{m}_{fuel} \cdot LHV = {}^{P_{el}}/_{\eta} \tag{6}$$

$$m_{MOL,blend} = m_{MOL,H2} + m_{MOL,NG} = [y \cdot MM_{H2}] + [(1-y) \cdot MM_{NG}] \quad \left[\frac{kg}{mol}\right] \tag{7}$$

$$E_{mol,blend} = (m_{MOL,H2} \cdot LHV_{H2}) + (m_{MOL,NG} \cdot LHV_{NG}) \quad \left[\frac{MJ}{mol}\right] \tag{8}$$

$$LHV_{blend} = {}^{E_{mol.blend}}\!/\!_{m_{mol,blend}} \quad \left[\frac{MJ}{kg}\right] \tag{9}$$

$$\dot{m}_{blend} = \frac{P_{th} \cdot LHV_{blend}}{1000} \quad \left[\frac{kg}{s}\right] \tag{10}$$

Hydrogen-methane blends have a strong variation in energy content for hydrogen rich blends, where the higher LHV compensates for their reduced density. This trend is depicted in Figure 53 alongside with Wobbe index, showing a minimum for a 80%-20% hydrogen-methane. The definition of Wobbe index is reported in eq. (9), where HHV is the higher heating value, i.e. the gross energy content not accounting for heat absorbed from water evaporation.

$$WI = \frac{HHV}{\sqrt{{}^{\rho_{fuel}}\!/\!_{\rho_{air}}}} \quad \left[\frac{MJ}{m^3}\right] \tag{11}$$

The trend is partially attributable to the graphical representation of composition variation in volumetric terms and energy density in specific mass terms. However, the blend composition is generally reported on volume or molar basis, while it is ultimately the energy per unit mass that is of significance in the calculation of blend massflow rate.

Figure 54 reports the fuel massflow map with varying GT load and varying blend composition. The first represents the overall LHV energy required by the combustor, while the second how much of the LHV energy is generated through blend total flowrate variation or change in blend composition. The colourmap on the chart represents the gas turbine efficiency as per eq. (4), assumed to be almost linear with load as sourced from the manufacturer. To improve visualisation, a contour plot is also generated and reported as Figure 55. The result shows a first quite expected outcome, that is the decrease in fuel massflow rate with increase in hydrogen concentration. Besides this, the contour lines flatten out as the load is increased and the hydrogen content is reduced. This is again a result of the presence of a minimum in Wobbe index. Finally, Figure 55 shows the gas turbine power achievable with a given fuel blend massflow rate and composition. As a quantitative measure, running on pure hydrogen gives a SFC which is about 40% that of pure natural gas.

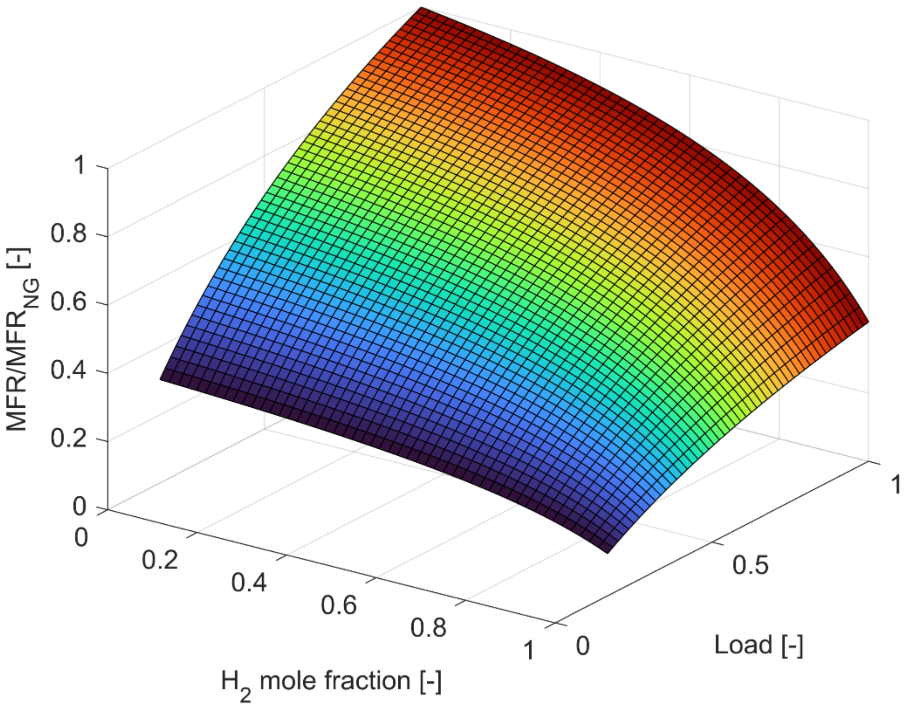


*Figure 54 – Nondimensional fuel map of $H_2$-NG blends*

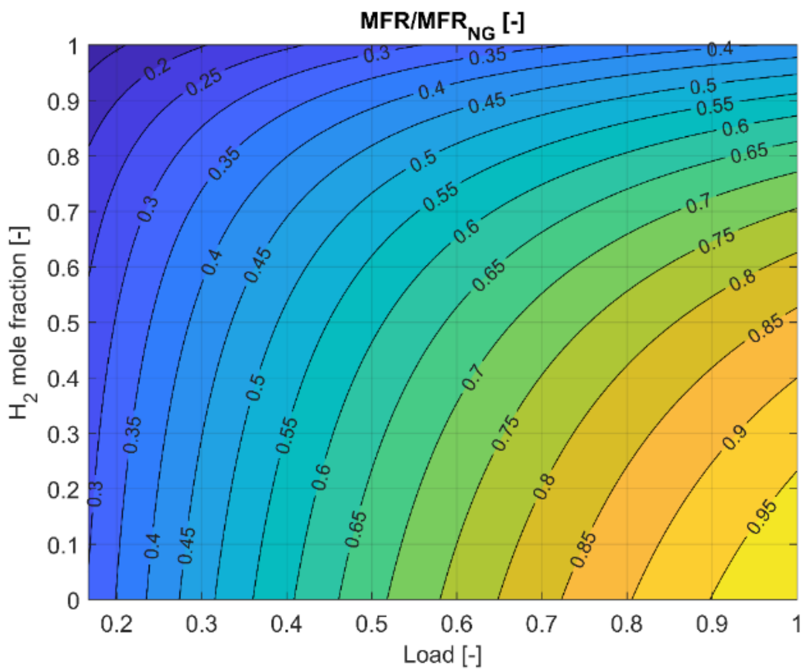


*Figure 55 – Contour plot of blend MFR*

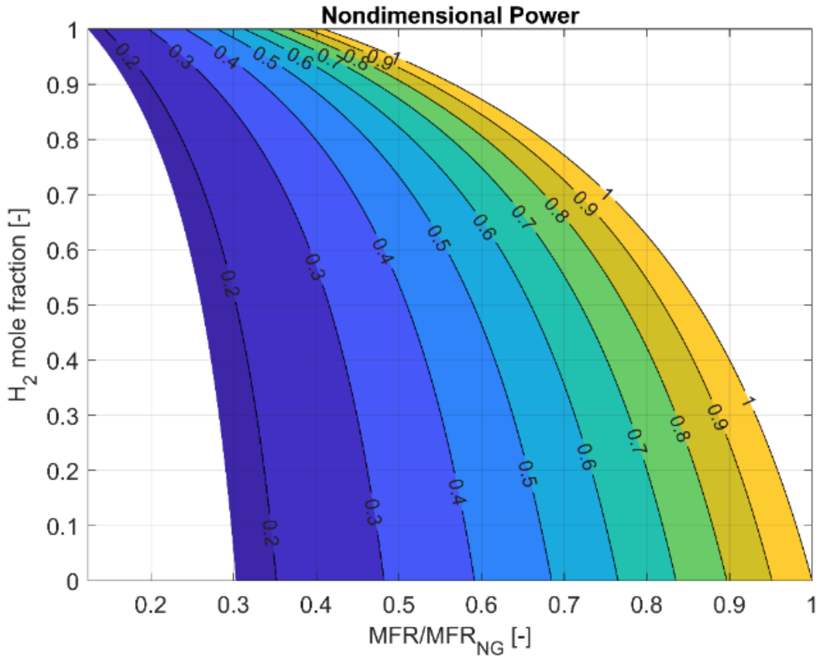

*Figure 56 – Nondimensional gas turbine power as a function of total blend massflow rate and blend composition*

### 4.8.2 Early transient dynamics of blending

Hydrogen and natural gas blending takes place in a dedicated section of the plant, namely a mixing station that will be either a pair of merging pipelines or, less likely, a dedicated buffer volume. To better understand the dynamics of the process, the fuel map generated as described in the previous paragraph was exploited as a lookup table to generate a massflow signal to be input to a simplified mixer where the mass and energy balance is computed in response to a required composition setpoint in terms of hydrogen molar concentration. A step response analysis was conducted to determine the characteristic time of the blending process and, in particular, the time needed to reach the required fuel mix composition.

Figure 57 contains the result for the SFS1 system, but since the only variable that changes is the volume of the pipeline, the same outcome is expected for SFS2 also. In this case, the volume was assumed to be 0.02 m$^3$, as representative of around 5-7 m pipe length, with diameter reasonably being DN60 or DN80, from the mixing point to the fuel injection. It is evident that following the downward step change at t = 60, the system reaches 95% of the steady-state value in approximately 10 s from the setpoint variation, corresponding to an estimated time constant about 3-4 seconds. A similar dynamic behaviour is observed following the upward step change at t = 120 seconds, where the hydrogen mole fraction reaches the new steady state within the same time as the downward step, indicating a characteristic time scale of a few seconds. These preliminary results show that the system generally exhibits fast and stable tracking performance. The system response time is significantly shorter than the duration between setpoint changes, and the characteristic time of the mixing is very close to the filling characteristic time.

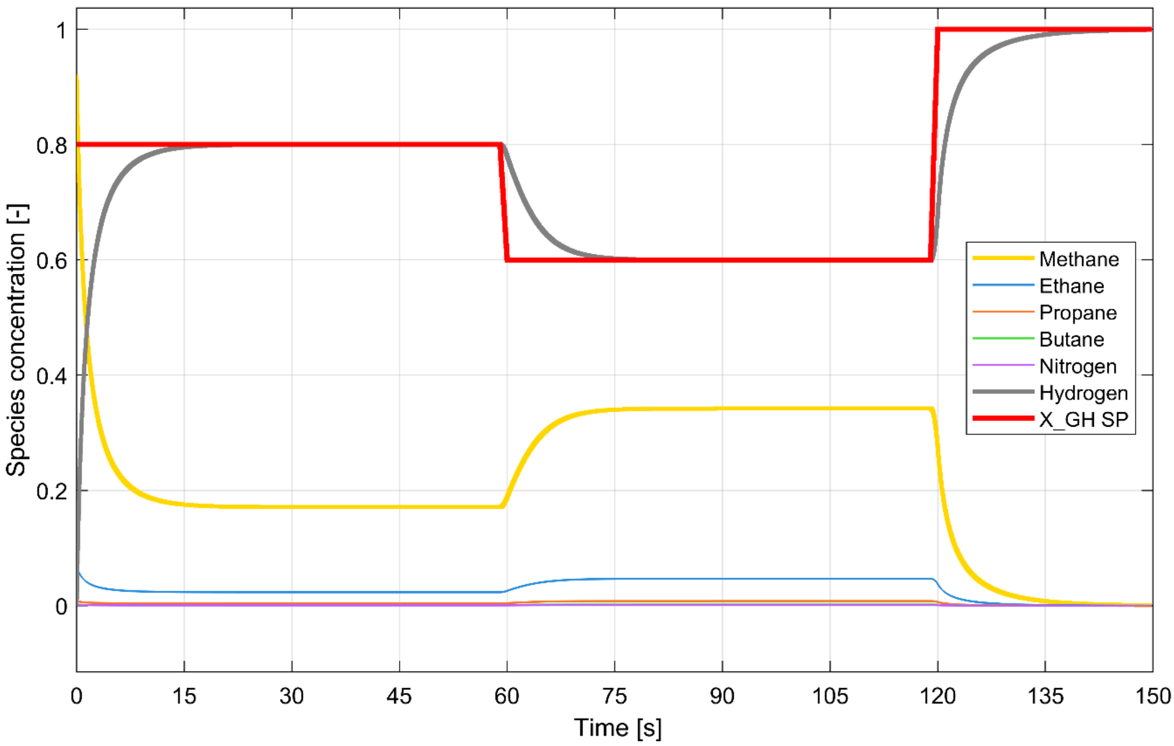


*Figure 57 – System response to a composition step variation*

It is not defined if blending will take place in a pipe merge section or within a dedicated mixing volume. In the technologically simpler first case, a convection-dominated mixing is likely to take place, hence the characteristic mixing time could be expressed as shown in eq. (12). On the other hand, the filling time is reported in eq.(13). It is immediately visible that the piping volume $V$ is pretty much coincident with the amount $A \cdot L_{mix}$ needed for mixing.

$$\tau_{mixing} = \frac{\rho \cdot A \cdot L_{mix}}{\dot{m}_{fuel}} \quad [s] \tag{12}$$

$$\tau_{filling} = \frac{\rho \cdot V}{\dot{m}_{fuel}} \quad [s] \tag{13}$$

## 4.9 Combined Cycle simulated performance

In order to have a complete understanding on how the CCGTs behave under different conditions, a map-based approach similar to that of the $H_2$-NG blend was chosen. With this method, it is possible to have a wide range of outputs for different inputs, and it is particularly useful for off-design conditions: the map based approach allows to know how the variation of all the independent variables affects the outputs.

The CCGT components (gas turbine, HRSG, and steam turbine) have been modelled in a simplified way to obtain the performance of the complete system. The GTs have been modelled in Matlab, though data were limited to a few off-design points, in which only one dependent variable was changed at a time. With regard to the bottoming steam turbine (ST) cycle, the model was constructed in EBSILON® under two distinct operational scenarios, namely a full power output mode and a full cogeneration mode. Results are presented as regressions in nondimensional form, owing to confidentiality agreements with the components manufacturers.

### 4.9.1 Gas Turbine

SFS1 and SFS2 gas turbines are foreseen to be different in architecture. Electric power maps are presented here for both architectures in Figure 58 and Figure 59. As often expected, the electric power increases with the load in a linear way being a percentage of the nominal power output. Moreover, the electric power produced increases with the percentage of $H_2$ in the fuel blend in a linear way, proving the higher heating value of hydrogen compared to natural gas. Besides, it is possible to see the comparison between known data points and interpolated ones. The known data points are represented by black squares, while the interpolated ones are represented by red ones. The perfect overlapping of the two sets of points is another proof of the accuracy of the maps created.

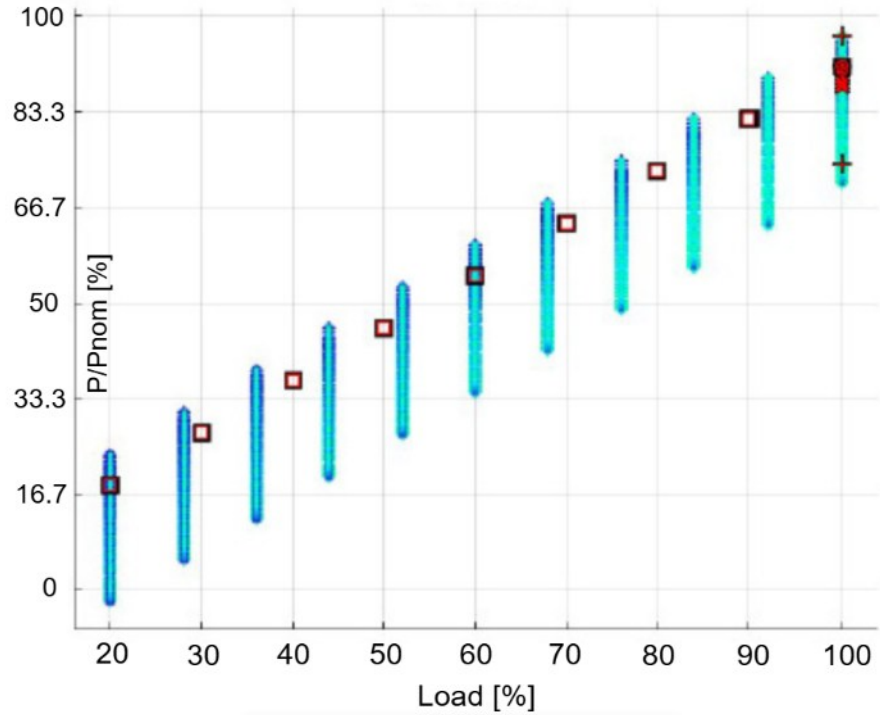


*Figure 58 – Power VS Load map, SFS1*

Efficiency maps are reported in Figure 60 and Figure 61 respectively for SFS1 and SFS2. The graphs show an expected non linear behavior of the efficiency with respect to the load. This is due to the fact that at low loads, the losses in the gas turbine are more relevant compared to the useful power output, hence the efficiency is lower. As the load increases, the losses become less relevant and, usually, the highest efficiency is reached at nominal load.

As predicted, their behavior is non linear, with a peak at nominal load. Moreover, the efficiency increases with the percentage of $H_2$ in the fuel blend, due to the better combustion properties of hydrogen compared to natural gas. Again, there is good superposition of the known data over the interpolated ones, with a $R^2$ equal to 0.9995 and 0.9988 for SFS1 and SFS2, respectively.

It is evident that the blend composition is very affective of the turbine performance, therefore it is confirmed that it represents a crucial parameter when control system is to be designed.

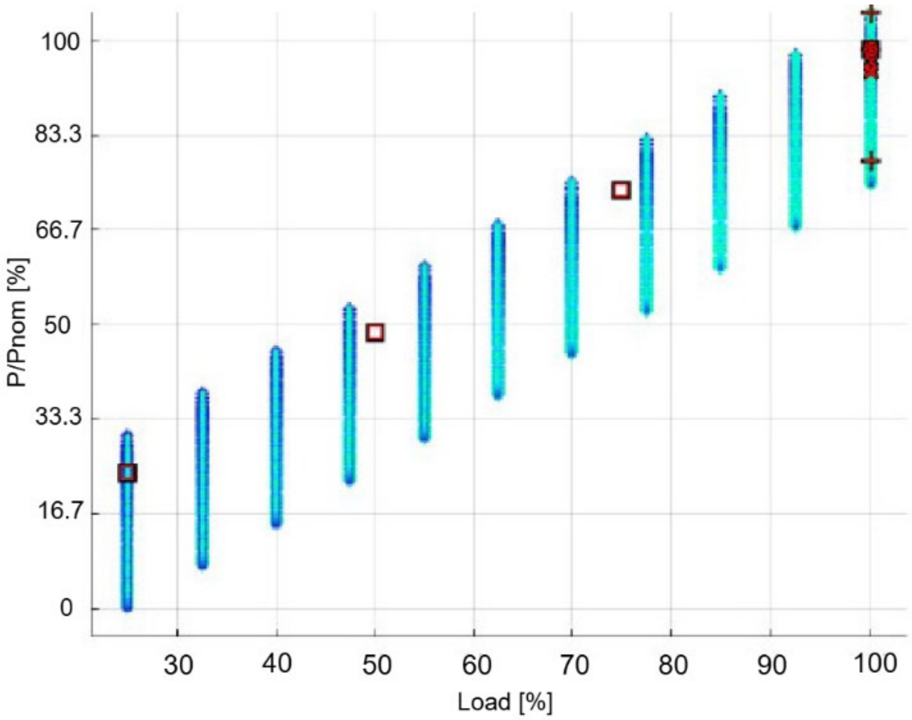


*Figure 59 - Power VS Load map, SFS2*

When determining the amount of thermal energy available for the HRSG, the exhaust mass flow rate and the exhaust temperature are the main affecting actors of the overall system performance and the amount of thermal energy available for the HRSG. As commented for GTs, the different machinery architecture leads to very different off design behaviours of SFS1 and SFS2.

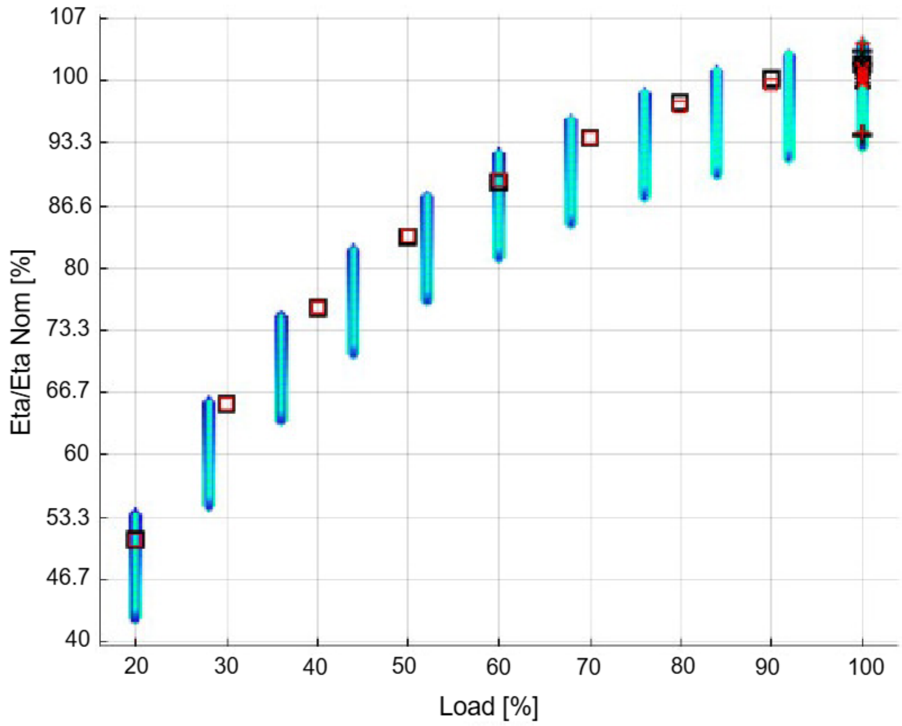


*Figure 60 – Efficiency VS Load map SFS1*

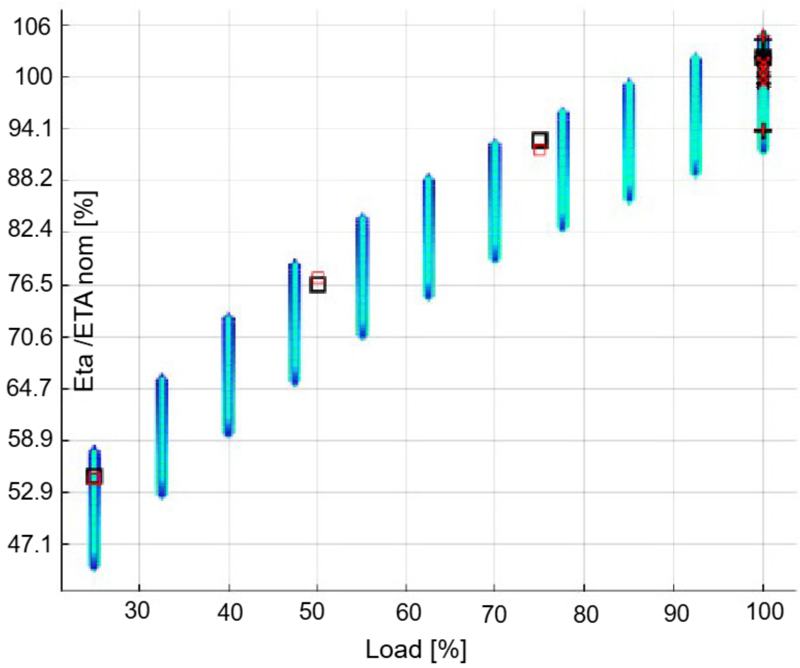


*Figure 61 – Efficiency VS Load map, SFS2*

With regard to the SFS1, the exhaust MFR remains constant along the off-design conditions, varying between 90% and 105% of the nominal value. This is due to varying fuel composition, with the higher being 100% $H_2$ and the lower being 100% NG. On the other hand, exhaust temperature of SFS1 registers an averagely increasing exhaust MFR as a function of the load, with variations less than 50 °C when shifting from pure hydrogen to pure natural gas. The $R^2$ regression coefficient remains higher than 0.98 for both correlations.

SFS2 exhaust mass flow rate shows an increasing trend with GT load, and the maximum variation between 100% hydrogen and 100% NG is 12% of the average value. Exhaust temperature averagely decreases with increasing load, showing a maximum deviation of less than 35 °C switching from one fuel to the other. Besides, $R^2$ coefficient for the temperature is as low as 0.7, probably due to the fact that the available data for the second platform either are limited in number or show an unexpected maximum trend, especially with high $H_2$ content in the fuel.

### 4.9.2 Heat Recovery Steam Generator

The results obtained from the EBSILON Professional simulations were carried out for both SFS1 and SFS2 and directly post-processed into Excel sheets. In order to have a complete overview of the CCGT performance, the chosen parameters had to be shown as functions of load percentage, as already extensively done in this thesis due to confidentiality issues. The blends containing 0% vol., 50% vol. and 100% vol. $H_2$ were considered, while the ambient temperature was fixed at 15.5 °C for all the simulations. Since temperature and pressure of the exhaust do influence heat exchange, in this calculation the reduced mass flowrate was considered, as expressed by eq. (14).

$$\dot{m}_{red} = \left(\dot{m} \cdot \sqrt{T}/p\right) \cdot \frac{p_{ref}}{\sqrt{T_{ref}}} \quad \left[\frac{kg}{s}\right] \tag{14}$$

Where $T_{ref}$ and $p_{ref}$ are the reference temperature and pressure respectively, which are equal to 288 K and 1 bar.

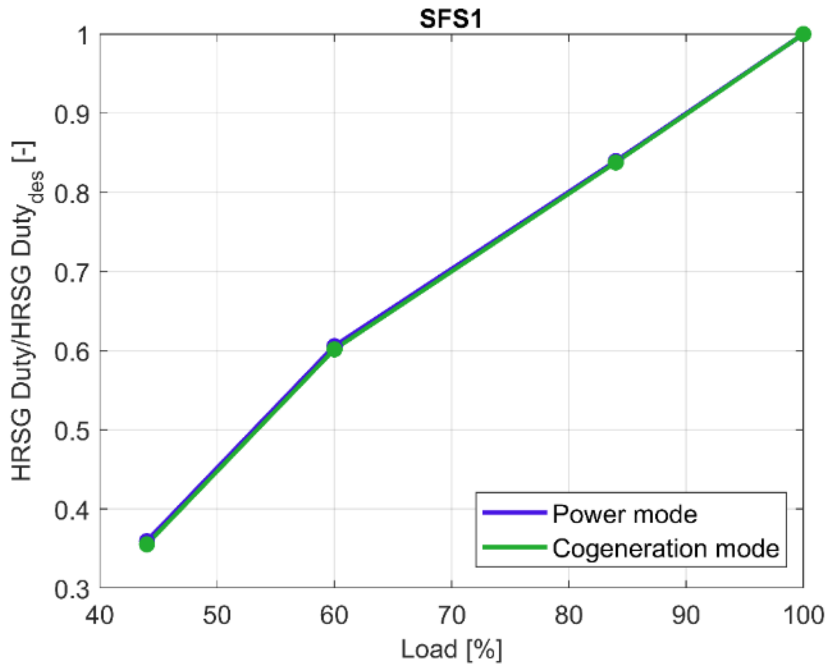


*Figure 62 – Nondimensional HRSG duties, SFS1*

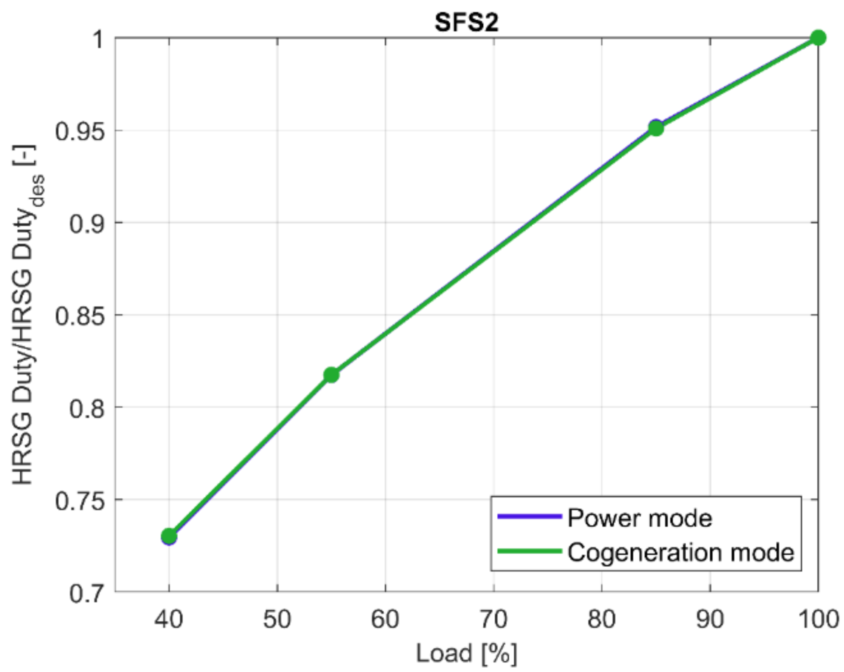


*Figure 63 - Nondimensional HRSG duties, SFS2*

Figure 62 Figure 63 report the HRSG duties in both full power and full cogeneration operating modes. The parameters and the underlying logic of each mode is covered by non disclosure agreement and cannot be described hereby.

Despite this hinders somehow the meaningfulness of the result, it can be derived that no major difference arises in HRSG heat load when functioning in either mode. However, SFS2 off-design is not as deep as SFS1, the reason being once again the different architecture between them.

### 4.9.3 Steam Turbine

One of the most important parameters to evaluate the performance of the CCGT is the overall bottoming steam turbine (ST) cycle efficiency. Higher cycle efficiencies indicate better performance and possibly higher operative range for the ship. However, the steam turbine performance curves were not available, hence their isentropic efficiency was assumed constant in off-design.

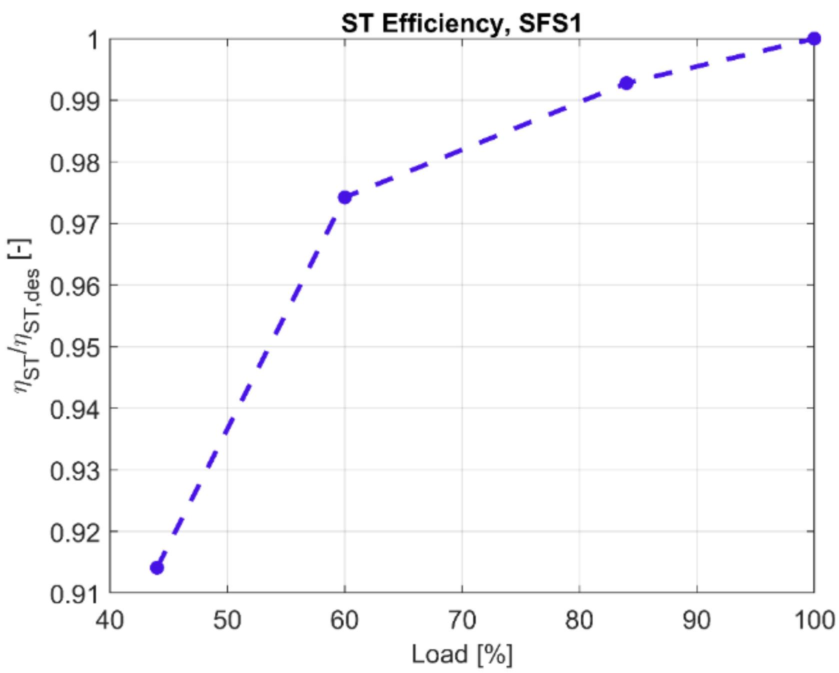


*Figure 64 – Steam bottoming cycle off-design thermal efficiency, SFS1*

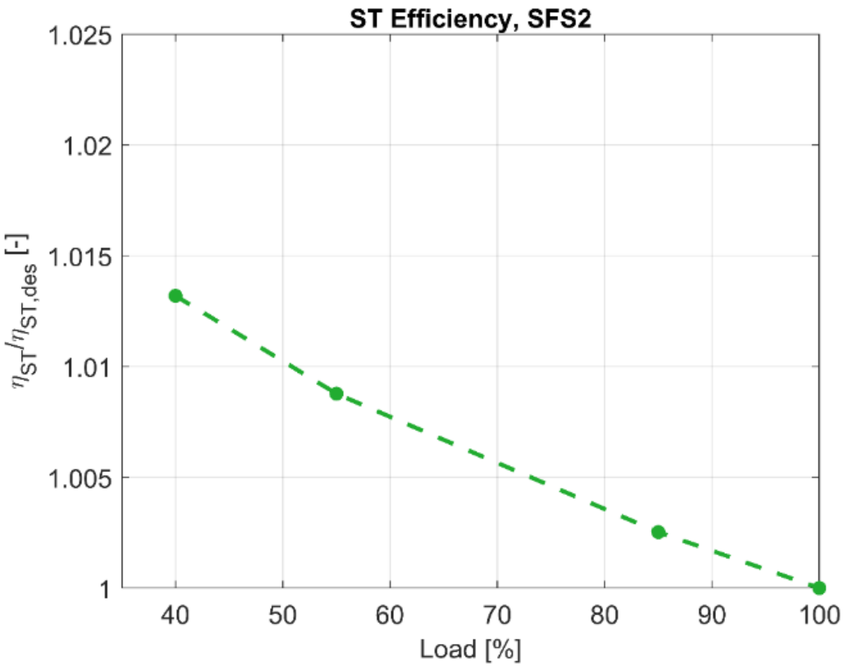


*Figure 65 - Steam bottoming cycle off-design thermal efficiency, SFS2*

It is clearly visible that the two systems have been conceived for very different operating conditions. In fact, combining the gas turbine and the steam turbine efficiencies, it can be concluded that SFS1 CCGT functions at maximum efficiency when operating at full load, while SFS2 CCGT demonstrates a flatter curve across the off-design range.

## 4.10 Novel concept for $LH_2$ vaporisation

Pumping large quantities of hydrogen and pressurizing it from storage conditions (< 12 barg) to the GT feed conditions (up to 50-60 barg) requires substantial energy input to the machinery. This might prove critical from an energy consumption point of view, especially in a very resource-constrained circumstances like a passenger ship. In such an environment, it is essential that the grid load is met, in addition to the Balance of Plant (BoP) of the shipboard being supported by the onboard generation system. Besides, hydrogen compression in gaseous form poses significant challenges from a techno-economic point of view.

Conversely, hydrogen exhibits a substantial volumetric ratio between gaseous and liquid phases, with an expansion of up to 840+ times during phase transition. Consequently, in the event of liquefied hydrogen being vaporised within a confined volume, it would concomitantly be pressurised, thereby resulting in a configuration analogous to a "pressure cooker" that would reduce the energy requirements for pumping to the evaporator. In this instance, the necessity for a high-pressure pump delivering hydrogen at the GT feed pressure would be avoided, and a simpler, potentially more economical transfer pump could be employed instead. Table 43 reports the pumping power required in the case of a transfer pump and in the case of a high pressure pump, both regarding 1 kg/s $LH_2$ elaborated. It is evident that the power required in the second case is around 40 times higher than the first, thereby justifying the exploration of such concept.

*Table 43 – Pumping power requirements for different configurations*

| Pump type | Pressure increase ($\Delta p$) | Required pumping power [kW] |
|---|---|---|
| Transfer $LH_2$ pump | 1 bar | 2.7 |
| High pressure $LH_2$ pump | Storage pressure to GT pressure (PR~10) | 73.9 |

The process would occur as described hereby. The transfer pumps feed the evaporator at a pressure which is just above the liquid storage pressure (charge phase); the evaporator is closed by means of a set of valves, and the heating fluid is supplied. The hydrogen mass evaporates and pressurizes in a isochoric process, and as soon as a pressure setpoint (which is higher than the supply pressure) is reached, the evaporator supply valves would be opened, thereby depleting the volume and feeding gaseous hydrogen to the downstream portion of the fuel system (discharge phase).

However, the discharge phase would be driven only by the pressure difference between the heat exchanger and the downstream part and, as soon as the pressure reaches an equilibrium value, the feed would be interrupted when a certain amount of hydrogen is still inside the vaporizer. Therefore, a recirculation process from the evaporator to the storage tank is needed in order not to loose that amount of fuel.

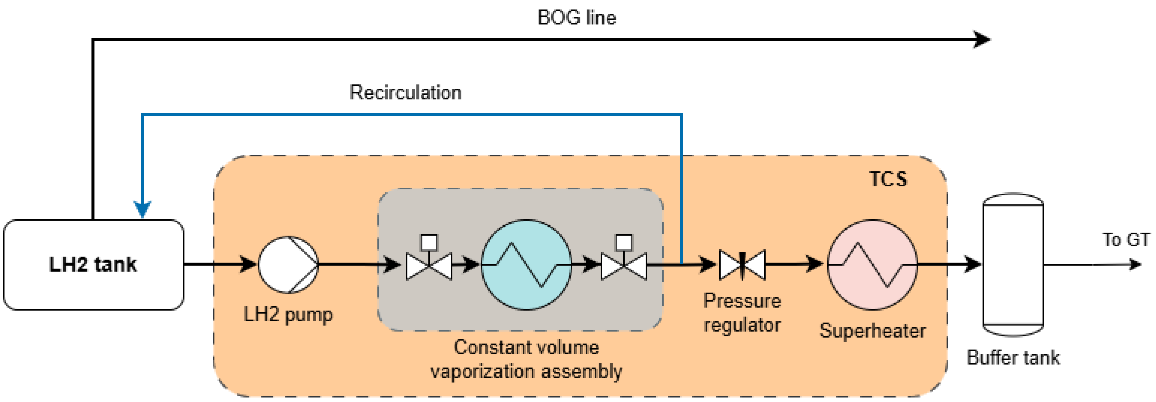


*Figure 66 – Conceptual layout of novel combined vaporisation and compression process*

### 4.10.1 Simulation results

This concept was explored conceptually, and its inherently discontinuous operation was simulated by means of a dynamic model developed by TPG. Initial conditions are 6 barg $LH_2$ storage, while buffer tank pressure is the same as the GT feed pressure. The system is controlled to maintain a buffer tank (TABUF) pressure between ±3 barg with respect to the storage pressure.

Figure 67 and Figure 68 report the results of pressure and temperature variations along eight complete cycles of the novel system, which have been simulated on the SFS1 and SFS2 hydrogen demands. The pressurizing evaporator (HTRPE) has the widest pressure, temperature, and mass fluctuation, in accordance with the discontinuous operation of the plant. Such component is required to cycle between the $LH_2$ tank pressure and its setpoint pressure, as well as between the $LH_2$ tank temperature (~28 K) and the HTRPE max temperature after recirculation (~100 K for SFS1, ~120 K for SFS2).

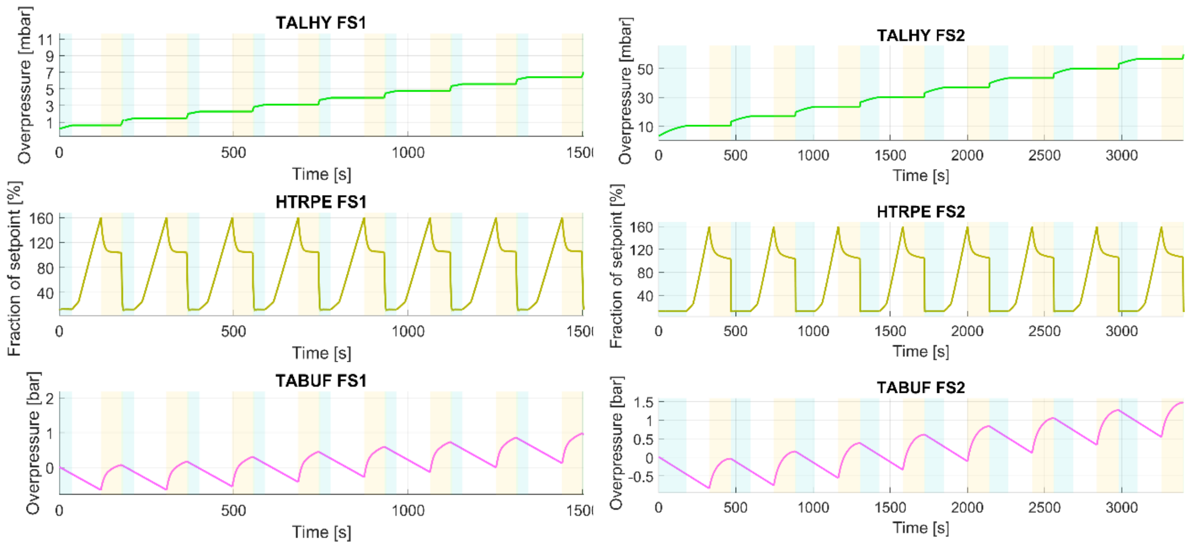


a) b)

*Figure 67 – $LH_2$ tank (TALHY), pressurizing evaporator (HTRPE), and buffer tank (TABUF) pressure variation within eight cycles of a) SFS1 and b) SFS2 operation*

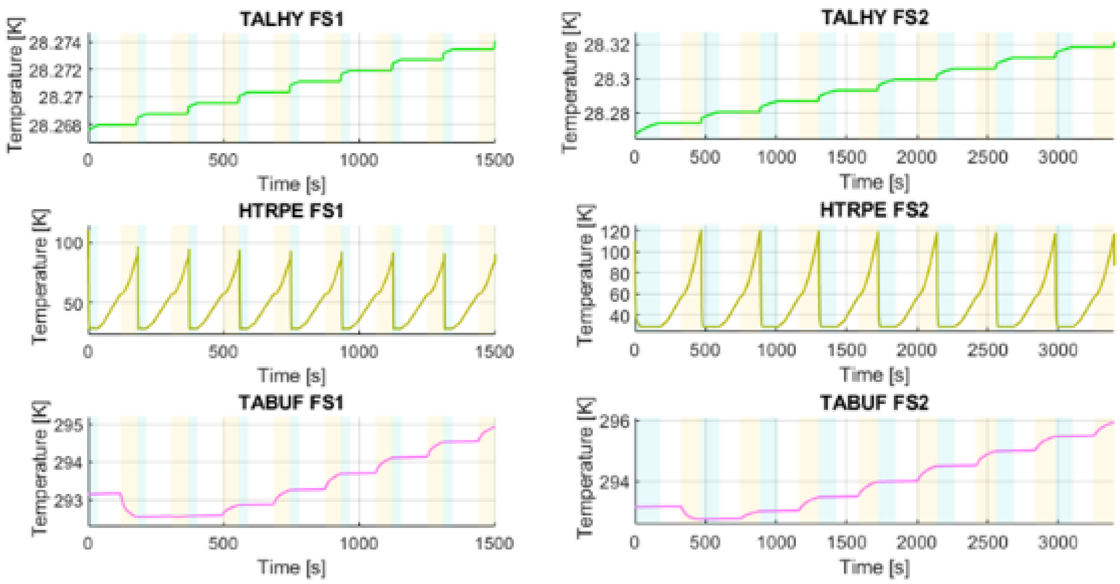


a) b)

*Figure 68 - $LH_2$ tank (TALHY), pressurizing evaporator (HTRPE), and buffer tank (TABUF) temperature variation within eight cycles of a) SFS1 and b) SFS2 operation*

System components procurement and experimental tests are hindered by their highly non-standard nature. In the future, it is not excluded that experimental tests could be conducted with appropriate stakeholders capable of handling this type of technological novelty.

Finally, given the novelty of the system and the potential interest into different industrial scenarios, a patent containing this idea was issued. The specifications are reported in Italian hereby:

*Domanda di brevetto n. 102025000024511 depositata a nome FINCANTIERI S.p.A. avente per titolo "IMPIANTO E METODO PER LA COMPRESSIONE E VAPORIZZAZIONE DI UN FLUIDO CRIOGENICO ALLO STATO LIQUIDO, IN PARTICOLARE IDROGENO LIQUIDO".*

# 5 Hydrogen onboard utilisation: Experiments on a turbocharged PEMFC emulator

The primary challenge to the utilisation of hydrogen on board vessels pertains to its availability. The employment of such molecule is restricted to chemical synthesis (ammonia, methanol, etc.), the food industry, and metallurgy. Utilising this substance as a fuel requires a substantial increase in production rate, a task that is rather challenging to accomplish in a limited time and necessitates inputs that are not really technological, but rather socio-economic. Consequently, when hydrogen is available, it is imperative to optimise its utilisation. Although the primary focus of this thesis concerns thermo-mechanical hydrogen conversion systems, namely combined cycle gas turbines, hydrogen-based power generation is not limited to combustion processes. In fact, the use of hydrogen for large power installations, propulsion, and significant hotel loads necessitates the consideration of high-power-density systems, such as thermal engines or combined cycle plants, which were analysed in the previous chapters for cruise ship application. Nevertheless, in situations where auxiliary power units (APU) are required, as is the case with passenger ships, the utilisation of PEMFC is a promising solution due to their enhanced efficiency compared to thermal engines of comparable size. In particular, PEMFC can be the technology of choice for power size of up to 1MWe, after which more conventional solutions remain attractive, also considering the weight and volume constraints of on-board installations. It is evident that the prospect of utilising electrochemical converters that exploit zero-carbon fuels to cover the hotelling power load during port visits is a subject of considerable interest and relevance.

In this chapter, an experimental activity involving a cyber-physical PEMFC emulator is described. The cathode air loop is real and consists of a bladeless compressor supplying air to a saturation column, where air humidification is reproduced. Conversely, the anode loop consists of a detailed Simulink model, as further described in the text. The activity described in this section does not aim to provide a detailed electrochemical investigation, but rather to establish performance benchmarks, evaluate dynamic response characteristics, and pave the way towards better control logics of PEM fuel cells air supply system or hybrid configurations including combustion and electrochemical systems.

Performance and compactness of PEMFCs can be further enhanced by pressurizing the stack, which increases the partial pressures of reagents in the fuel cell, driving up both efficiency and power density [150]. This can be done with a blower or a turbocharger. Even if the adoption of a blower is simpler, the turbocharger recovers part of the energy in the PEMFC off-gases, reducing the net power required for the pressurisation [151]. However, as opposed to traditional turbocharger applications such as internal combustion engines (ICE), the temperature of a PEMFC exhaust gas typically remains below 370 K [152]. Hence, it is paramount to assess to what extent such devices are applicable to other power plants which operate at lower temperature. In this scope, the utilisation of a turbocharger with variable geometry turbine (VGT) might help improve the electrical power output and the system efficiency by adjusting the flow velocity, thereby reducing the compressor parasitic losses up to 15% when the fuel cell operates at high current density [153].

As described in previous sections, hydrogen is more conveniently used for power generation in fuel cells rather than in combustion engines or turbines, thanks to their higher electrical efficiency, compactness and fast response. Although fuel cell technology is improving significantly, such devices can sometimes be cumbersome to operate in research environments. In fact, operating a full PEMFC system requires a hydrogen supply, whose presence in a laboratory is often challenging due to severe regulations and inherent safety concerns. Therefore, numerical simulation of fuel cell systems is the preferred method to evaluate the performance of the system [154,155]. Sometimes, in order to retain the purely experimental characteristics of a real system, a system emulator is designed to serve as a compromise between the ease of retrieval of simpler components into a real laboratory environment while still dealing with a real system facing real operating challenges. Most of the research in this sense focuses on cyber-physical emulators, where only a part of the system is made by physical components and the remaining components are simulated through modelling. Due to a lack of research on cyberphysical PEMFC emulators focusing on the working conditions of turbomachinery and the thermochemical aspects of the stack rather than to the power electronics and the chemical features of the system, the final activity of this PhD thesis focused on such an innovative test rig, with an experimental demonstration character.

## 5.1 The TC-PEMFC emulator plant

The plant was designed to condition the air flow provided by the compressor in the same way as it would be conditioned by the PEMFC system object of this study.

The plant is composed by two circuits – one for the air and one for the water – which converge into the saturator. In Figure 69 a simplified scheme of the layout is shown, where the air flows are represented in green lines, water flows by blue lines, signals received from the model by dashed pink lines, signals sent to the model by dashed violet lines. The operative points (1-9) are represented in red colour. Part of the air entering the recuperator (REC) can be bypassed through a 3-way valve (3-MV_1), which is useful during the warmup of the system. Inside the saturator, the air flows bottom-top direction lapping the water stream counterflow. Outside the saturator (SAT, point 4), the air reaches a 3-way valve (4-CV_0), which controls the bypass rate of the second branch of the REC. By adjusting the bypass rate, it is possible to control the temperature at point 3. After the REC (point 5), the air expands through the Tesla turbine and then is released to the ambient (point 6). The integration vessel is equipped with a level sensor that automatically feeds water into the system. A solenoid on-off valve (9-XV_0) has been incorporated to ensure proper water integration. This valve opens when the level falls below a predefined low threshold and closes once the high-level threshold is reached in the integration vessel. The circulation of water is facilitated by the pump, which is positioned between the integration vessel (IV, point 9) and the heater (7-XR_0, point 7). The water is heated to the required temperature by the heater and can be laminated, if necessary, prior to being injected into the saturator. In the event of partial boiling, this occurs just after the lamination valve and not in the saturator, thus avoiding any augmentation of water droplet entrainment by the air flow. Air can be discharged by means of 3-CV_0 to simulate the air flow reduction due to the oxygen depletion caused by the chemical reaction into the stack. On the other hand, water discharge has no operational purpose and is only performed manually via 8-MV_0 when needed.

At the current state, the communication between the physical plant and the model embedded in MATLAB Simulink is not in place yet, while it will be subject of future activities alongside the PID controllers tuning on the basis of the results of the plant step response included in this section.

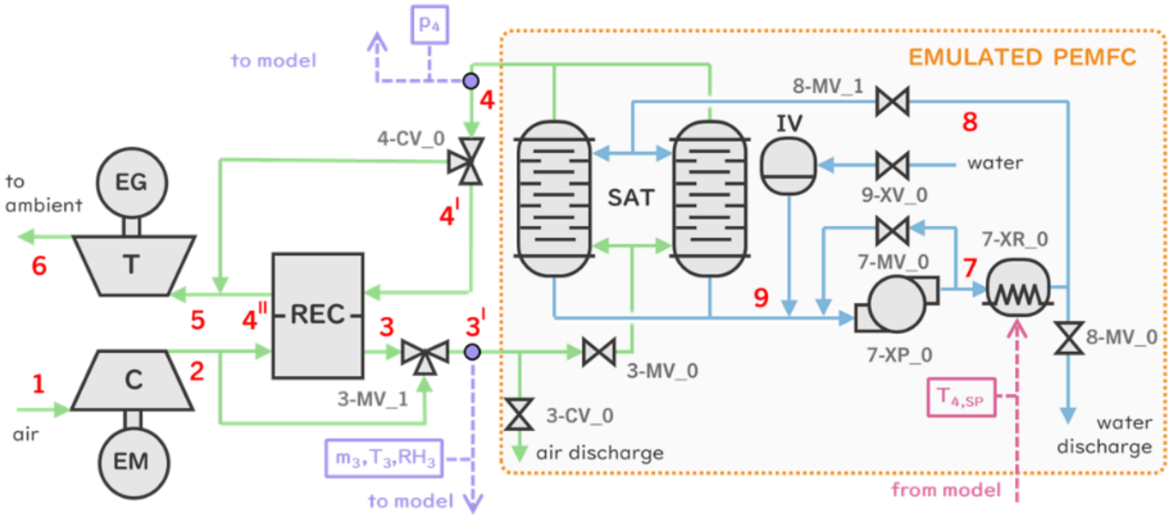


*Figure 69 - Cyberphysical setup of the PEMFC emulator plant*

## 5.2 Physical system design

The system is designed to accommodate air mass flow rates up to 12 g/s, corresponding to an electric power around 15 kW. The saturator mimics the conditions usually obtained at the PEMFC cathode outlet, i.e. a mixture of dry air and saturated water vapour. Immediately after the injection, the water pressure is the same as that of the air exiting the saturator, while at the bottom, it equals the inlet air pressure. The inlet water temperature T8, controlled by the heater, was assumed to be 110 °C for the preliminary thermodynamic evaluation, with the heater supplying 4.3 kW of thermal power.

*Table 44 – Plant thermodynamic properties at design conditions*

| Point | Fluid | T [°C] | p [bara] | $\dot{m}$ [g/s] | RH [%] |
|---|---|---|---|---|---|
| 1 | Ambient air | 25 | 1.01 | 12 | Ambient (60) |
| 2 | Ambient air | 80 | 1.24 | 12 | 4.9 |
| 3 | Ambient air | 67.3 | 1.20 | 12 | 8.1 |
| 4 | Saturated air | 64.1 | 1.17 | 13.8 | 100 |
| 5 | Humid air | 74.1 | 1.14 | 13.8 | 62.9 |
| 6 | Humid air | | | | |
| 7 | Water | 38.9 | 2 | 14.4 | - |
| 8 | Water | 110 | 2 | 14.4 | - |
| 9 | Water | 38.9 | 1.2 | 12.6 | - |

### 5.2.1 Plant components

As described, the main components are a bladeless blower, a bladeless expander, a water saturator, a recuperator and a water circuit. Both machines were manufactured by SIT Technologies, and innovative start-up of the University of Genoa.

Thanks to the reversibility of bladeless Tesla machinery, the blower and the expander are twins except for the braking resistor installed onto the turbine motor. The rotor consists of 20 discs, each one having a thickness of 0.1 mm, spaced 0.3 mm between each other. The machine is designed for a mechanical speed of 22 krpm, delivers a maximum power of 654W to the air flow at a maximum massflow rate of 13.4 g/s and a compression ratio of 1.23. The rotor is driven by a three-phase induction motor with a rated rotational speed of 24 krpm. More details on the turbomachine design and characterisation are reported in [156].

The recuperator is an air-air heat exchanger used to condition the air temperature before the saturator. The REC heat exchanger is a plate type, with dimension height x length x depth = 750mm x 200mm x 100 mm, 16 plates, wetted area of 1.34 m$^2$ and a heat transfer capacity of 2.6 kW.

The saturator is specifically designed for this emulator. It is composed of two columns where the packed bed is located and where the air (bottom-top direction) laps the water (top-down direction). Each saturation column is composed by two modules of packed bed having 75 mm diameter and 160 mm length, which ensures a sufficient wetted area able to properly humidify the air and containing as much as possible the pressure drops of the air stream.

*Figure 70 – Overview of the emulator plant in its final configuration.*

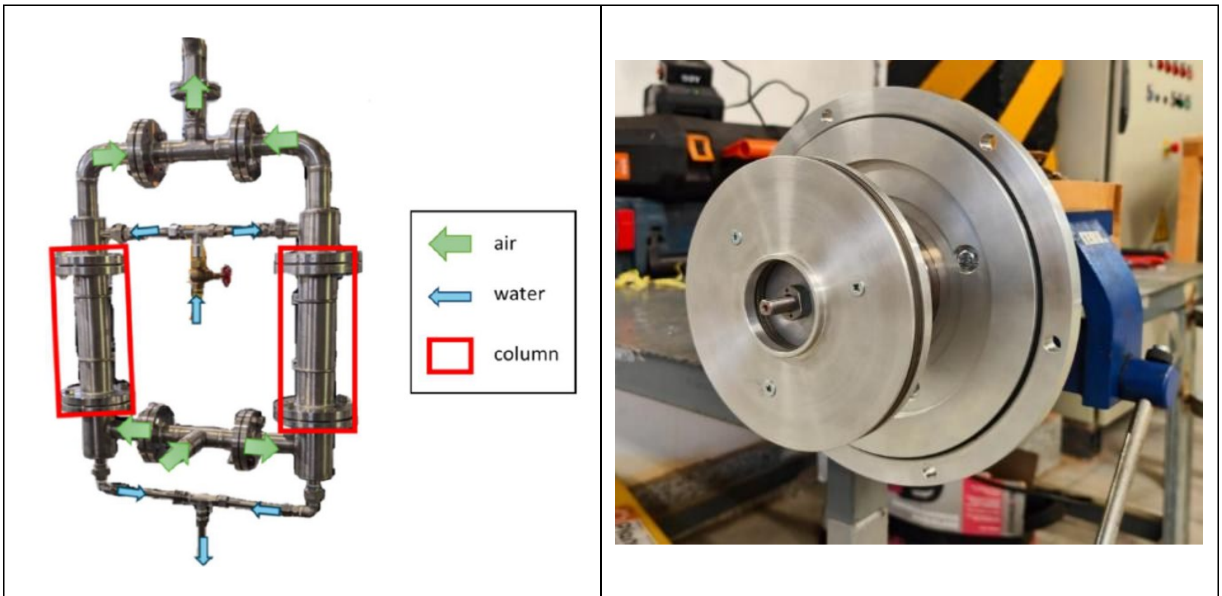


| a) | b) |
|---|---|

*Figure 71 – Detail of the air and water paths (left) and of the bladeless turbomachinery (right)*

*Table 45 – Main design parameters of the emulator test rig components*

| Component | Power [kW] | Dimension |
|---|---|---|
| **Bladeless impeller (fluid/motor)** | 0.66/2.2 | Ø160mm |
| **Saturator column (single)** | - | Ø75mm x L160mm |
| **REC heat exchanger** | 2.6 | 750 x 200 x 100mm (H x L x D) |
| **Water pump** | 0.15 | Impeller Ø60mm |
| **Water heater** | 5 | - |

The water loop circulates water to the nominal rate of 1 l/min, with a manual valve in parallel to ensure the correct water flow rate reaching the saturation column. The water heater inside the reservoir has a nominal power of 5 kW and is regulated via a PWM in duty cycle.

### 5.2.2 Cyberphysical integration

Simulink simulation model and Labview interface must exchange information in real time to ensure proper emulation of the PEMFC system and replicate the performance parameters reported in Table 46, which are typical of a 5 kW PEMFC. Data reported differ from those in Table 44 mainly for the air mass flow, which is approximately 2.5 times lower than the design value: in fact, system maximum capacitances are those illustrated in Table 44, while the plant has the possibility to operate to any intermediate load, by adjusting turbomachinery speed and/or air line pressure drops. In this case, pressure drop is achieved by manual throttling to ensure the correct air flow to the cell.

At each acquisition timestep (0.1 s), the emulator plant sends to the model:

- the MFR, the temperature and RH of the saturator air inlet (point $3^{I}$), corresponding to the cathode inlet of the PEMFC.
- the pressure at the saturator air outlet (point 4), corresponding to the cathodic outlet of the FC.

The plant instead receives from the model to the LabVIEW interface:

- The cathode outlet temperature, used as setpoint of the air saturator outlet temperature $T_{4,SP}$ through the control of 7-XR_0 electric heater.
- Pressure loss on the cathode side, used as reference to manually adjust the pressure drop via the valve 3-MV_0.
- Mass flow difference between cathode inlet and outlet. In the future this value could be used to regulate the flow through the air discharge line at the saturator inlet to simulate the oxygen depletion due to electrochemical reactions.

*Table 46 – Emulated TC-PEMFC system design performance*

| Parameter | Value |
|---|---|
| **Air stack inlet pressure [barg]** | 0.24 |
| **PEMFC output power [kW]** | 5.36 |
| **Consumed $H_2$ LHV power [kW]** | 9.07 |
| **Conversion efficiency (includes 5% AC/DC conv.) [%]** | 52 |
| **Compressor rotational speed [krpm]** | 17.7 |

## 5.3 Experimental campaign

To characterize the performance of the physical system, data have been acquired from the DAQ system and subsequently analysed. From a stand still, stable operation of the whole system is reached in about 30 minutes. Although it seems like a long start-up time for a small test rig, it has to be considered that some components of the physical system, especially the REC, are oversized with respect to the current operating parameters, and also in comparison to a real PEM stack of similar power. Therefore, the thermal transient is negatively affected in terms of time response.

To speed up startup, the procedure was revised so the water loop is activated first and stabilised before air is allowed to circulate through the loop and saturation column. This preheats the air quicker, as it immediately encounters water already at the required temperature. In addition, the REC bypass on the compressor side remains open, so the REC is not used, and its cold metal mass does not cool down the air flow. Regarding the turbomachinery, turbine speed cannot be measured because the tachometer optical sensor malfunctions when hit by water vapor and potential condensation with fog formation. Hence, only the synchronous frequency of the turbine motor is monitored, while the actual mechanical speed will be slightly lower due to rotor slip. On the other hand, compressor mechanical speed is accurately measured.

### 5.3.1 Design point operation

The first run was acquired for a total sampled period of 150 s. The synchronous frequency of the compressor and turbine inverter were set to 300 Hz and 160 Hz, respectively, corresponding to just below 17.7 and 9.6 krpm. As shown in Figure 72, the system runs smoothly and fluctuations are within the measurement error. The design air massflow rate is set at 4.5 g/s, and pressure drop is around 12 mbar.

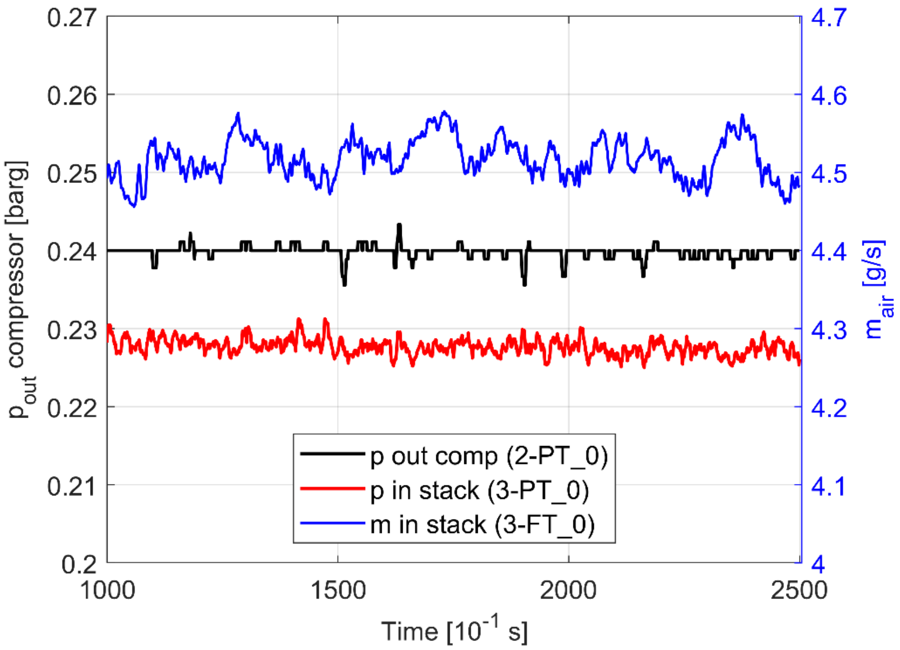


*Figure 72 – Pressure and massflow rate at steady on-design operation*

### 5.3.2 Early transient operation

In order to characterise the system dynamic behaviour, a series of step response tests have been performed. Table 47 summarizes the conditions of the conducted tests. Only the results relating to the most significant tests are shown below. These are the ones involving responses to broader steps, which are generally more demanding on the system.

T3 involved a pronounced step decrease in turbine speed. As demonstrated in Figure 73, the compressor outlet pressure is slightly reduced, while compressor mechanical speed measurement is not affected and is equal to 17.7 krpm for the whole test, giving a rotor slip factor of 1.67%. The stack inlet and outlet pressures evolve as shown in Figure 74. Slowing down the turbine has the effect of reducing the backpressure of the system, with the result that a greater mass flow is allowed through the saturator and the downstream portion of the plant. The reduction of stack inlet pressure is more pronounced than the one at compressor outlet because of an increase of pressure losses due to the higher mass flow rate.

*Table 47 – Overview of step response tests*

| **Varied parameter** | **Initial value** | **Final value** | **Test tag** |
|---|---|---|---|
| Turbine speed (comp. 300 Hz) | 130 Hz | 170 Hz | T1 |
| Turbine speed (comp. 300 Hz) | 130 Hz | 250 Hz | T2 |
| Turbine speed (comp. 300 Hz) | 130 Hz<br>40 Hz | 40 Hz<br>130 Hz | T3 |
| Compressor speed (turb. 130 Hz) | 300 Hz<br>310 Hz | 310 Hz<br>300 Hz | T4 |
| Compressor speed (turb. 130 Hz) | 310 Hz | 200 Hz | T5 |
| RES load (comp. 300Hz, turb. 130 Hz) | 25% | 40% | T6 |

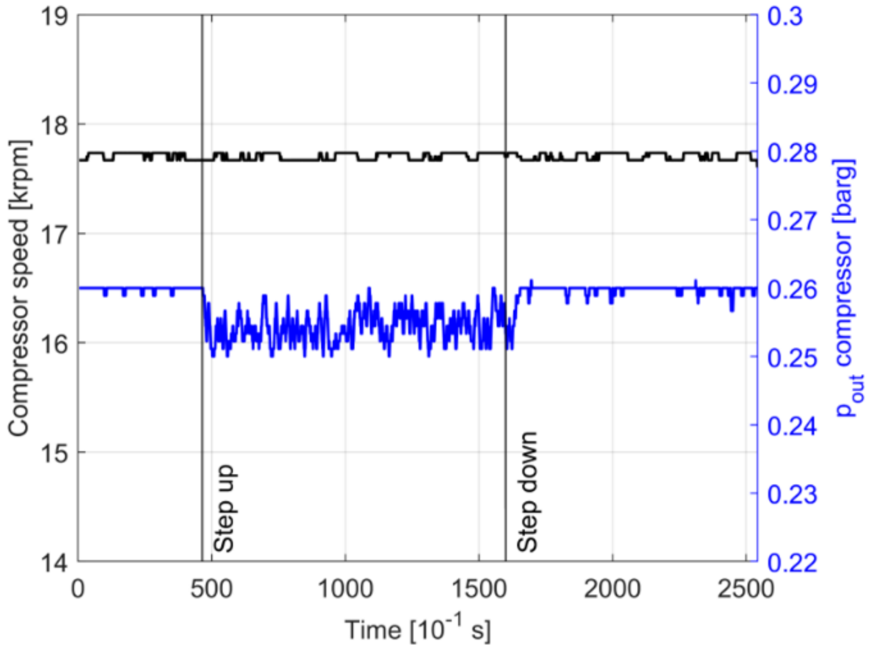


*Figure 73 – Compressor speed and outlet pressure, test T3*

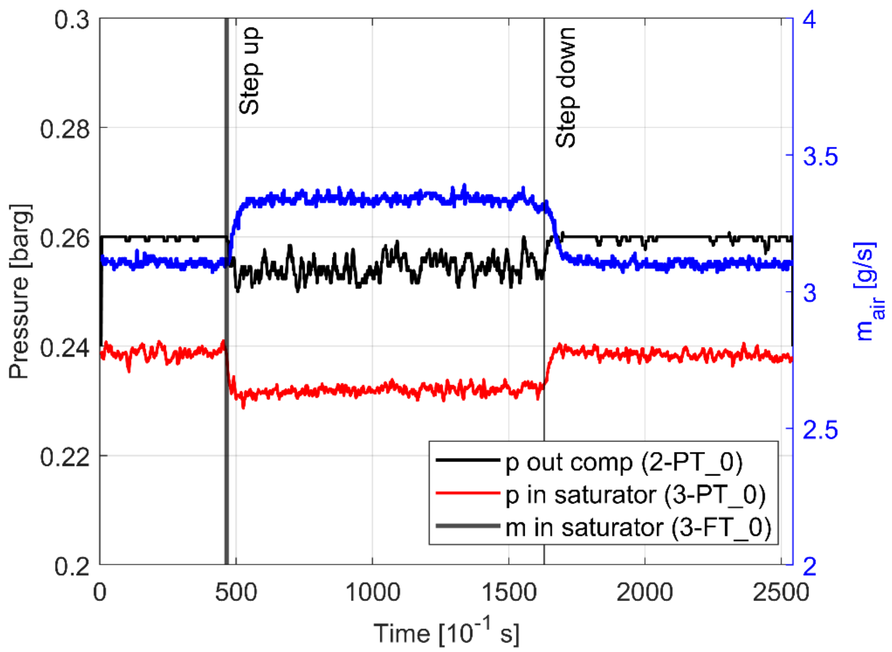


*Figure 74 – Pressures and air massflow rate at compressor outlet and saturator inlet, test T3.*

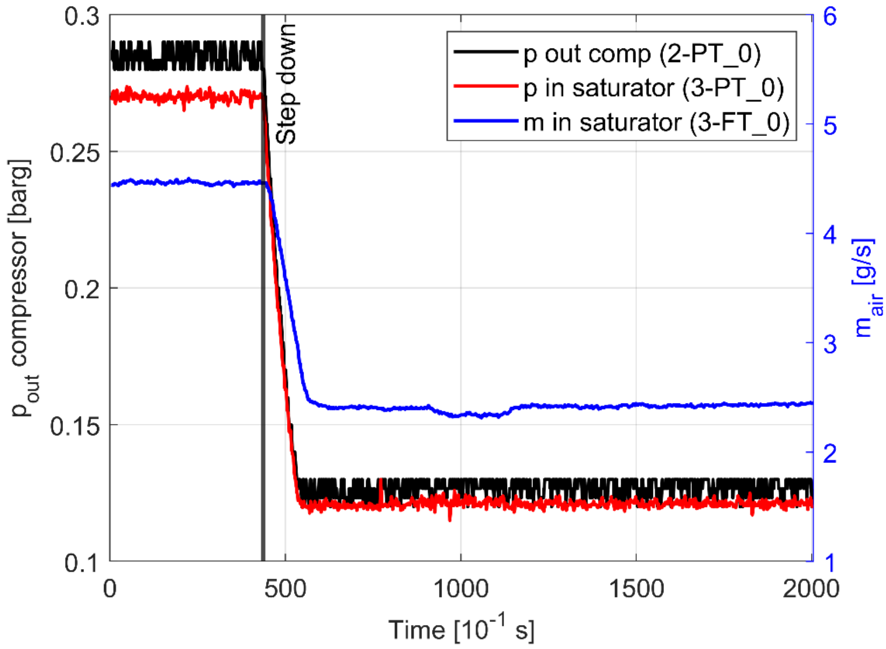


*Figure 75 - Pressures and air mass flow rate at compressor outlet and saturator inlet, detail of test T5.*

Test T5 is performed by reducing compressor synchronous frequency to 200 Hz (just short of 12 krpm), which causes a steep decrease in pressure levels and in air mass flow rate supplied to the stack (Figure 75). It is interesting to observe that the temperature change at the saturator outlet is much more limited (~1.5 K) than the one at its inlet (~9.0 K). Since the water temperature is kept approximatively constant, this can be explained considering that the air outlet temperature depends mostly on the water conditions and the capacity of the air flow to absorb water. In fact, when the air temperature decreases, the amount of water that is transferred to reach saturation is reduced, and so is the latent heat required for its evaporation, mitigating the impact on the outlet temperature.

Regarding the system dynamics, the responses in terms of mass flow rate and pressure are fairly fast, requiring 5 to 10 s to reach a new steady pressure level and mass flow rate after a perturbation of compressor speed (Figure 74 and Figure 75). Conversely, the variations of temperature at compressor outlet and saturator inlet are much slower (Figure 76) due to the high thermal capacity of the Tesla compressor with respect to the air mass flow rate. This mismatch is probably the most evident limitation of emulating the performance of a fast-responding PEMFC system with a thermally inert saturator/recuperator assembly.

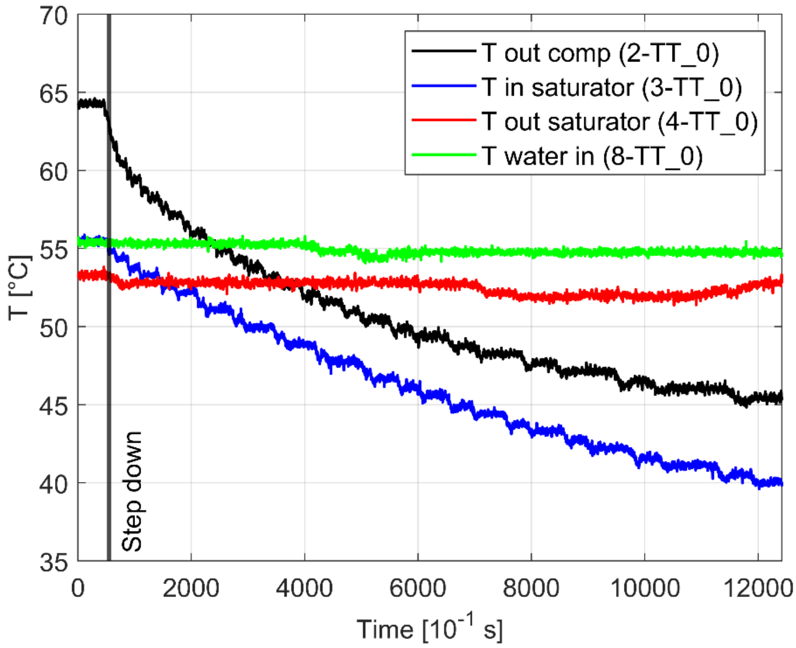


*Figure 76 – Temperatures at saturator inlet, outlet, and water inlet, test T5*

Besides, compressor performance has considerably improved as compared to previous versions of the same design, which is shown in Figure 77. Indeed, the bladeless Tesla compressor can generate a pressure ratio (PR) of 1.28 at 310 Hz synchronous frequency (i.e., ~18 krpm, slip included) and 4.5 g/s massflow rate, which is better than the CFD predictions of previous models calculated at the rated rotor mechanical speed of 22 krpm. This results are achieved thanks to a novel PTFE-based seal that drastically reduces the majority of recirculation, which is, in fact, a known affection to this category of machines. This also expectedly improves efficiency as a consequence, despite the exact value is not computed but will be subject of future investigation.

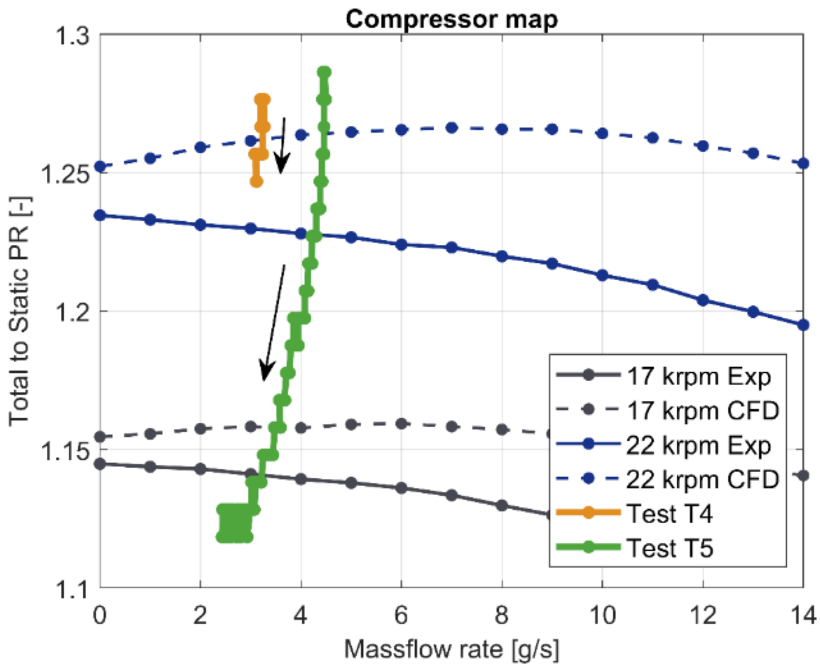


*Figure 77 – Evolution of operating point on the machine map, tests T4 and T5*

Finally, the test T6 in Figure 78 highlights the extremely slow pace at which an increase in RES load impacts the system, with the temperatures still growing after more than 900 s. The direct effect is a higher water temperature at saturator inlet, followed consistently by the humid air outlet temperature. This result can be considered as a quantitative representation of the large thermal capacity of the whole system.

This last aspect represents the most significant deviation from the dynamic behaviour of an actual fuel cell stack. Specifically, the saturation column introduces a substantial contribution to the overall thermal capacitance, which is not exactly characteristic of a real PEMFC module. Moreover, the low pressure ratio imposed by the compressor, in addition to the significantly larger metal mass that constitutes it, results in the enhancement of the slow thermal transient of the physical system. As a result, although the dynamic phenomena associated with mass transport occur on time scales comparable to those of a real system, the evolution of heat transfer is markedly different and follows a noticeably slower and less representative dynamic response.

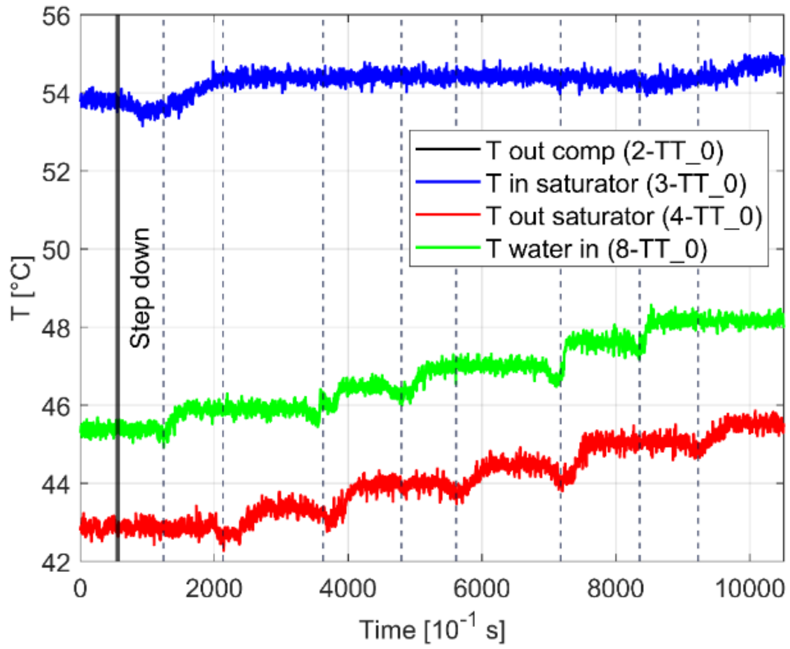


*Figure 78 – Temperatures at saturator inlet, outlet, and water inlet, test T6*

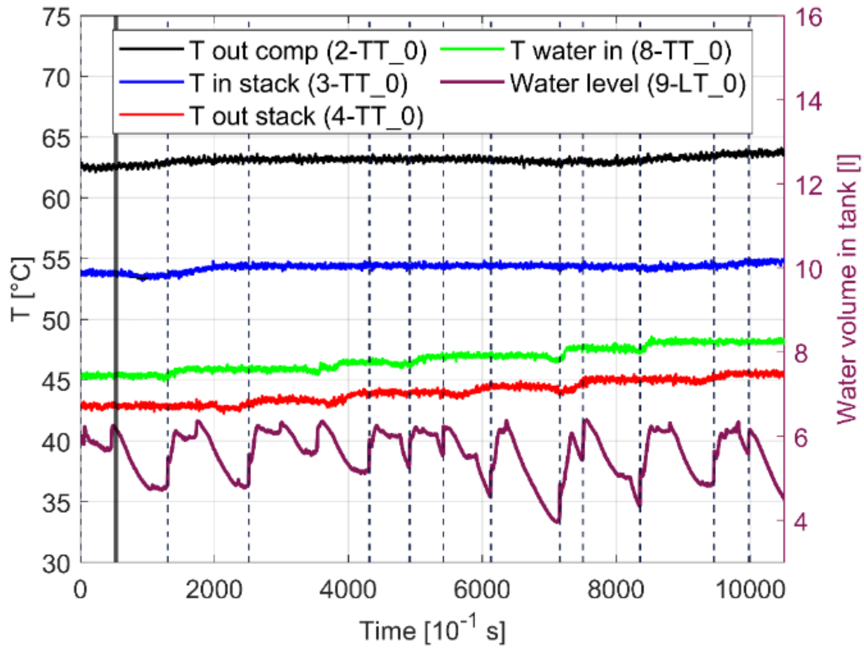


*Figure 79 - Temperatures at saturator inlet, outlet and water inlet with details on the water level into the integration reservoir, test T6*

As a final consideration, from Figure 76 and Figure 78, a peculiar "stick-slip" stepwise trend read by the temperature sensors downstream the saturator (4-TT_0 and 8-TT_0) is observed. This phenomenon is still of uncertain attribution, but it is likely to be consequence, at least partially, of a piston effect of the intermediate reservoir IV (see Figure 69). This effect is clearly visible in Figure 79, where water level into the buffer reservoir seems to correlate strongly with the abrupt temperature steps, especially when the increase in level is rapid. This is in fact reasonable since the buffer vessel is pneumatically linked with the upper part of the saturation column. The water volume in the buffer vessel is relatively small in relation to the total water volume within the loop, thereby creating a stiff dampening that causes the temperature to evolve in such specific manner. Nevertheless, this relation is still to be studied adequately and the causality to be unquestionably demonstrated.

# 6 Combined hydrogen and freshwater production for isolated scenarios

Notwithstanding the principal objective of this thesis, it has been demonstrated that the establishment of a hydrogen economy remains a protracted process. Therefore, in order to facilitate hydrogen penetration as a commonly employed energy carrier, it is also interesting to investigate possible synergies with other critical feedstocks, such as freshwater. Islands and maritime vessels can both be regarded as semi- or fully autonomous energy systems. In many cases, these environments are defined by limited—or even entirely absent—connections to centralised electricity grids, a condition that often parallels the restricted availability of freshwater resources. Under such circumstances, integrated approaches that combine hydrogen production with freshwater generation, alongside high-efficiency energy conversion technologies, become especially valuable. This is particularly true in contexts where primary energy resources are constrained and the demand for both electricity and potable water is highly variable, as exemplified by passenger cruise ships. The deployment of a reversible solid oxide cell (rSOC) represents a promising pathway to achieve this objective. This technology can operate flexibly in dual modes: as a fuel cell to generate electricity while simultaneously producing freshwater, and as an electrolyser to produce hydrogen when surplus energy is available. Although the rSOC system analysed in this study is conceptually tailored for island applications, its relevance naturally extends to maritime energy systems. In fact, both domains share key characteristics of isolation, resource scarcity, and fluctuating demand profiles, making them well-suited to benefit from integrated hydrogen–water–energy solutions devised to achieve lower emissions while ensuring that compliance to resources demand.

The simulated system combines hydrogen production via solid oxide electrolysis (SOEC) with freshwater (FW) generation through integrated desalination, using seawater as the primary feedstock. High-temperature operation enables internal heat recovery, improving overall system efficiency. In reversible solid oxide fuel cell (SOFC) mode, stored hydrogen can be reconverted to electricity, enhancing system flexibility under fluctuating demand profiles typical of isolated grids. For islands, this configuration supports local energy autonomy and reduces dependence on imported fossil fuels. From a maritime perspective, similar integrated hydrogen–water systems may be relevant in two respects: (i) ships themselves function as off-grid microgrids with comparable efficiency and redundancy requirements, and (ii) island-based hydrogen production could provide localised refueling infrastructure for ferries and short-sea vessels. Consequently, the island case study offers insights into the integration challenges, and performance limits of reversible solid oxide cell (rSOC) based hydrogen systems that are transferable to maritime applications.

In this chapter, a Mixed Integer-Linear Programming (MILP) based techno-economic optimisation is carried out in order to evaluate the best operation profile of the aforementioned integrated system for a touristic island, exploring the benefit of off-peak freshwater and hydrogen production in a demand-driven logic. Seasonal variation in energy and freshwater demand are also accounted for, as well as discrepancies between resident population and tourists' needs throughout the whole year.

## 6.1 System description

The system is principally designed around the utilisation of renewable sources (RES) to produce electricity, which is then used for two key purposes. Firstly, it helps meet the local electricity demand, and secondly, it provides the necessary electricity to operate desalination plants, which are responsible for producing potable water. These facilities employ two well-established desalination techniques: Reverse Osmosis (RO) and Multi-Stage Flash (MSF) distillation. The MSF distillation process necessitates a substantial amount of thermal energy. To enhance energy autonomy, the system integrates waste heat recovery from conventional ICE generators, which are an integral component of the island's power infrastructure alongside the RES plant to enhance grid stability. The system configuration is reported in Figure 80.

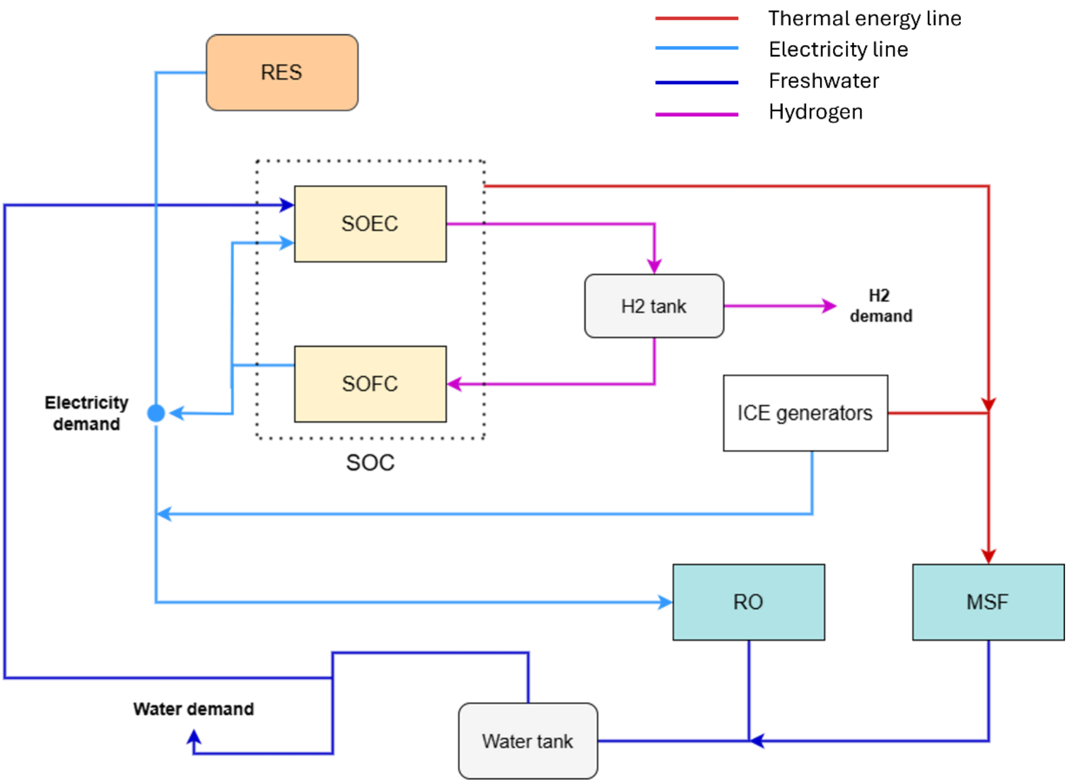


*Figure 80 – Layout of the integrated water/hydrogen production system*

The FW yielded by this process serves numerous critical functions. A substantial part of this water is allocated to meet the daily water consumption needs of the local and tourist population, ensuring a consistent and sufficient supply. Furthermore, this purified water facilitates the operation of a reversible rSOC which, in electrolyser mode, relies on a consistent supply of water for the production of green hydrogen. As shown, also the reversible SOC in FC mode can supply heat energy for the MSF demand in form of water vapour.

## 6.2 MILP modelling approach

The MEDO software was developed as a scheduler able to run optimisation of multi-energy systems both in a demand-driven logic, hence with a minimisation of relevant objective functions such as operating cost or $CO_2$ emission, or in a market-driven logic, where the net revenue is maximised. It employs a MILP approach, utilising a combination of linear and integer variables to identify the minimum of a specified objective function accounting for some relevant constraint, e.g. minimum and maximum power for each generator, and impossible simultaneous operation in SOEC and SOFC mode of a rSOC, which are set by the user. This approach is coupled with a piecewise-linearisation of the components' operating curves, which are typically non-linear as a function of the normalised load. This approach has been used in previous works [155,157]. Eqs. (15) through (19) describe the steps of the approach followed for the rSOC efficiency curve in fuel cell mode. However, the same logic is retained for the rSOC in electrolyser mode and also all power systems included in the configuration. Here, φ is a integer variable whose value is 1 or 0 depending on whether the rSOC is operative or not at that particular hour. The indices refer to $i$ for the specific component, $j$ for the linearised segment, and $t$ for the optimised time step. To manage the yearly variability, the authors have decided to simplify the yearly profile with 12 typical days, one for each month.

$$P_{SOC,min}(i,j) \cdot \varphi_{SOC}(i,j,t) \leq P_{SOC}(i,j,t) \leq P_{SOC,max}(i,j) \cdot \varphi_{SOC}(i,j,t) \tag{15}$$

$$\alpha(i,j) = \frac{\dot{m}_{fuel,max}(i,j) - \dot{m}_{fuel,mix}(i,j)}{P_{max}(i,j) - P_{min}(i,j)} \tag{16}$$

$$\beta(i,j) = \dot{m}_{fuel,max} - \alpha(i,j) \cdot P_{max}(i,j) \tag{17}$$

$$\dot{m}_{fuel}(i,j,t) = \alpha(i,j) \cdot P_{SOC}(i,j) + \beta(i,j) \cdot \varphi_{SOC}(i,j,t) \tag{18}$$

$$\eta_{SOC}(i,j) = \frac{P_{SOC}(i,j)}{\dot{m}_{fuel} \cdot LHV} = \frac{P_{SOC}(i,j)}{[\alpha(i,j) \cdot P_{SOC}(i,j) + \beta(i,j)] \cdot LHV} \tag{19}$$

The outcome of such process for the reversible SOC in both SOEC and SOFC modes is reported in Figure 81, assuming the mass and energy rate are always positive. In both cases the x-axis reports the nondimensional load in terms of electricity, which is the energy input and output in the two cases. It is to point out that the perfect linearity of the fuel mass flow curves is an assumption, but the expected error is minimal as demonstrated in [155].

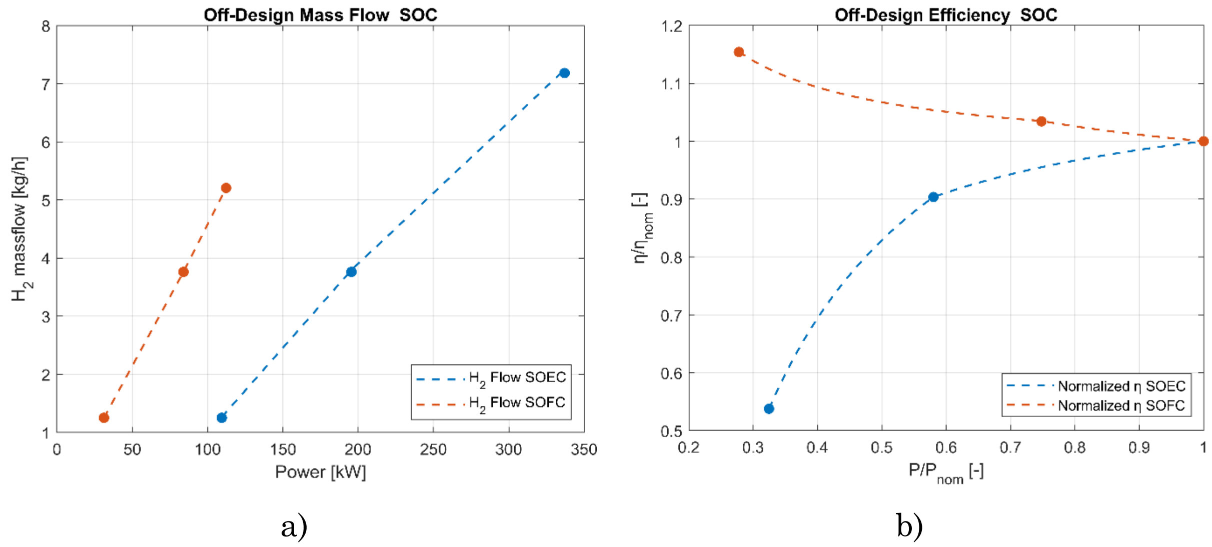


*Figure 81 – a) fuel massflow and b) efficiency of rSOC as a result of piecewise linearisation of fuel consumption*

## 6.3 Case study and investigated scenarios

In this work, the case study of a mediterranean Greek island was chosen. The main simulation parameters of the islands, population data [158] and freshwater demand per capita [159] are reported in Table 48. Besides, Figure 82a and Figure 82b report the seasonal population variation and the hourly freshwater demand for a typical winter and a typical summer day, respectively. The typical months were chosen considering the highest difference in population, hence January and August. As shown, the number of inhabitants shows a sharp peak during summer with a more that two-fold increase. Moreover, the resident population was assumed constant over the year.

To date, the island has an installed power of 17 MW, of which 15.6 MW are Diesel generators, 0.9 MW are wind turbines, and 0.4 MW are PV panels . In this work, the potential of an increased RES penetration on the island is presented alongside the installation of rSOC for hydrogen and freshwater production. To put this into context, it may be noted that these installed power ratings align closely with those typically observed on smaller cruise ships, cruise ferries, or Pax & Car ferries.

*Table 48 – Main features of the case study island*

| Resident population (2021) | Climate type (Koppen zone) | Installed desalination capacity [m³/day] | Winter FW consumption [l/day pc] | Summer FW consumption [l/day pc] |
|---|---|---|---|---|
| 8845 | Temperate (Csa) | 500 (RO) | 150 | 250 |

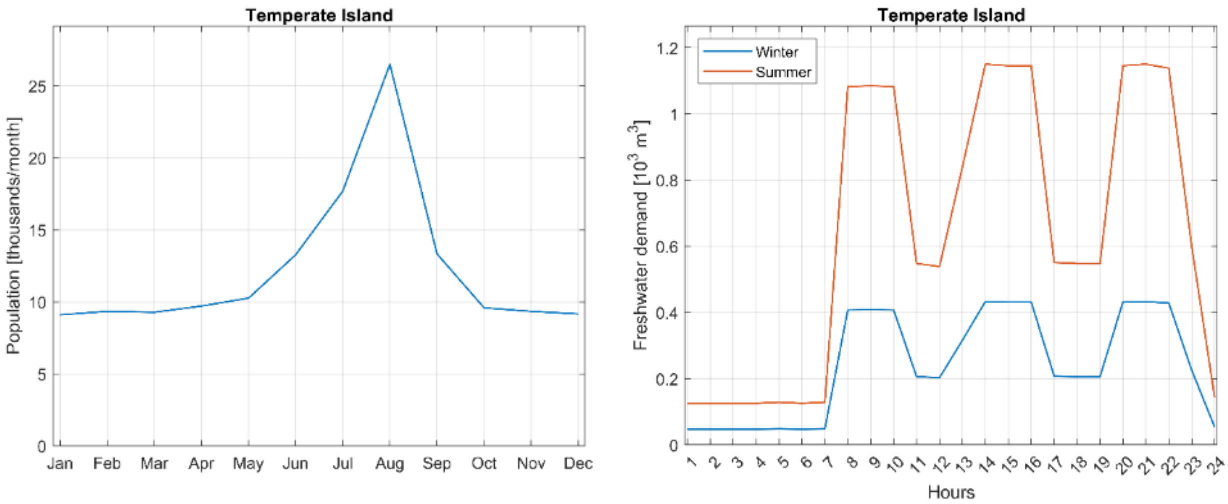


a) b)

*Figure 82 - Monthly variation of population (a) and hourly freshwater consumption (b) on the case study island*

To explore the advantages of coupling an integrated RO/rSOC system to a photovoltaic panel renewable power system, three cases were considered. The baseline (BL) case is the one where ICE are already present to produce electricity, thus the CAPEX of those components is not accounted, and the desalinated water is obtained only via MSF fed by ICE waste heat recovery. The Scenario 1 includes the addition of membrane-based RO desalination and photovoltaic (PV) for power production (PV/RO), while Scenario 2 is expanded with the inclusion of the reversible cell rSOC, which will be named "RC" in the future equations (PV/RO/RC). A sensitivity analysis has been performed depending on the relevant parameters, such as installed PV power, RO installed capacity, and rSOC installed power in electrolyser mode. The results are compared in terms of techno-economic metrics, including Levelised cost of electricity (LCOE), Levelised cost of water (LCOW), RES share, and Specific Carbon Intensity (SCI).

The levelised costs are defined as per Eqs. (20) through (24), differentiated by the absence or presence of the RC, while the specific CAPEX values used to compute the economic figures are reported in Table 49. The interest rate *i* is set equal to 5% and the useful life *n* is assumed as 30 years for each technology. On the other hand, $P_{RO,PAY}$ is the fraction of power supplied by the RO which does not derive from curtailed PV power, thus representing an active cost item in the LCOW definition.

*Table 49 - Simulation cases and economic parameters for each technology*

| Technology | Present in scenario "#" | Specific CAPEX |
|---|---|---|
| **ICE** | BL,1,2 | 350 €/kW |
| **MSF** | BL,1,2 | $2567 \cdot \dot{V}^{0.988}$ €/m³ day |
| **RES (PV)** | 1,2 | 530 €/kW |
| **RO** | 1,2 | 1910 €/ m³ day |
| **rSOC** | 2 | 1000 €/$kW_{EC}$ |

$$LCOE_{w/o\ RC}\left[\frac{€}{MWh}\right] = \frac{CAPEX_{PV} + OPEX_{ICE} + CO_{2,ICE}}{Demand_{el} + P_{RO}} \tag{20}$$

$$LCOW_{w/o\ RC}\left[\frac{€}{MWh}\right] = \frac{CAPEX_{RO} + CAPEX_{MSF} + LCOE \cdot P_{RO,PAY}}{Prod_{RO} + Prod_{MSF}} \tag{21}$$

$$LCOE_{RC}\left[\frac{€}{MWh}\right] = \frac{CAPEX_{PV} + CAPEX_{RC} + OPEX_{ICE} + CO_{2,ICE}}{Demand_{el} + P_{RO}} \tag{22}$$

$$LCOW_{RC}\left[\frac{€}{MWh}\right] = \frac{CAPEX_{RO} + CAPEX_{MSF} + LCOE \cdot P_{RO,PAY}}{Prod_{RO} + Prod_{MSF} + Prod_{RC}} \tag{23}$$

$$CRF_j = \frac{i \cdot (1+i)^n}{(1+i)^n - 1} \tag{24}$$

## 6.4 Results

Firstly, the levelised costs of the main products of the combined generation system are evaluated for different RO installed capacities and different levels of PV power. Next, also RES share, Specific Carbon Intensity (SCI), and water production via MSF and RO are also evaluated as a function of the same parameters.

### 6.4.1 Scenario 1: Baseline + PV/RO

Figure 83 presents the LCOE (a) and LCOW (b) for the Scenario 1, also reporting the RES curtailment levels as red contour lines as percentage of RES potential. From Figure 83a it is evident how PV installation initially lowers LCOE by replacing ICE generation, with no influence from RO capacity up to about 4 MW of installed PV, where LCOE reaches 120–125 €/MWh. In this zero-curtailment range, LCOE depends only slightly on RO size, as a significant share of electricity is still generated by higher-cost ICE units. Beyond this PV capacity, an optimal trend appears: RES curtailment becomes linked to RO capacity, which can absorb excess generation to produce water at zero cost, effectively acting as energy storage and leading to the lowest electricity costs when both PV and RO capacities are large. In Figure 83, a boundary of LCOW dependence on photovoltaic capacity is shown to be around 2 MW. Below this value, the freshwater cost is mainly driven by the cost of electricity used by RO plant and remunerated at LCOE cost. For larger values, the energy absorbed by RO is just provided by PV overgeneration, so it becomes irrelevant how much RES potential is installed.

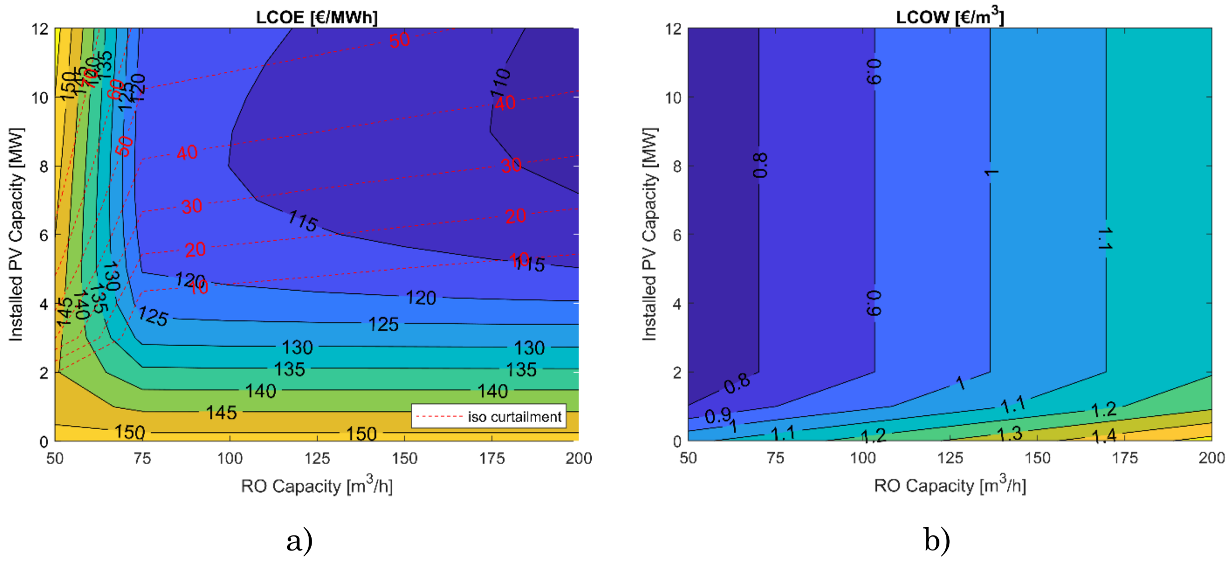


*Figure 83 – a) LCOE and b) LCOW for different RO capacities and PV installed power*

It can be noticed that the impact of RO adoption on LCOE and LCOW is opposite: moving from MSF to RO production the LCOE reduced from 115 to 110 €/MWh (-4.5%) since less electricity is produced by ICE, while the water production cost increase from 0.9 to 1.1 €/m³ (+22%).

Figure 84a confirms that 4 MW marks the boundary beyond which RES share becomes influenced by RO capacity. Interestingly, PV electricity remains below 35% even at high PV and RO capacities. This is because MSF operates simultaneously to produce freshwater, and the thermal energy supplied by ICEs does not increase electricity production costs. As a result, the optimizer consistently favours the cheaper water from MSF, even when renewable potential is high. The SCI (total specific carbon emissions) in Figure 84b follows a trend opposite to RES share, supporting this interpretation.

It can be noticed from Figure 85 the different behaviour below 2 MW of PV capacity is mainly driven by the quantity of RO input electricity that is not part of the overgeneration. Besides, it seems clear that despite having a consistent potential, the share of water production via RO/RES is limited to just over 60%. This can be explained again as consequence of MSF exploitation being still more convenient, even when ICE operates at lower loads.

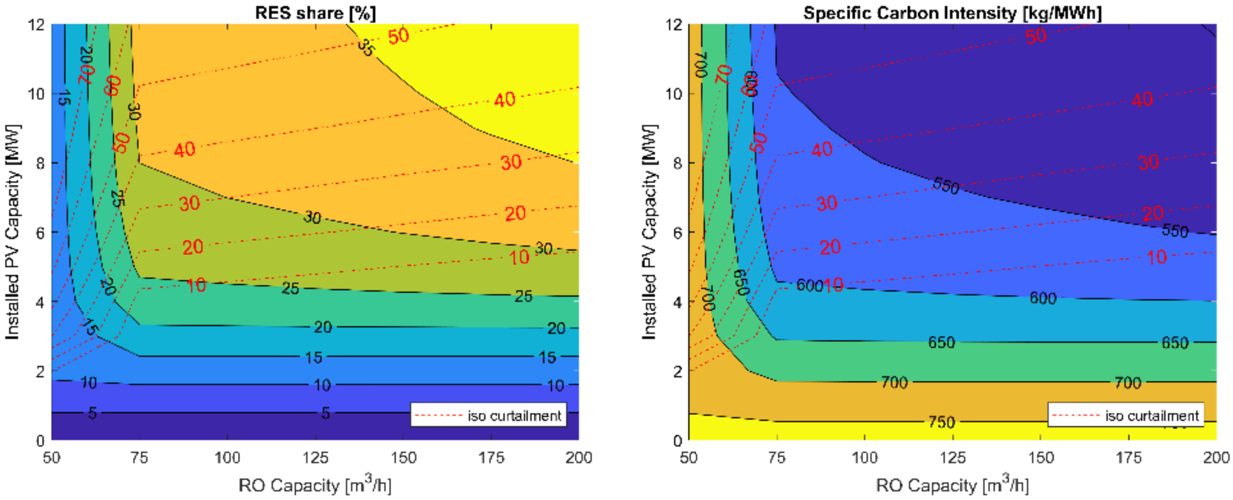


a) b)

*Figure 84 – RES share and SCI for different RO capacities and PV installed power*

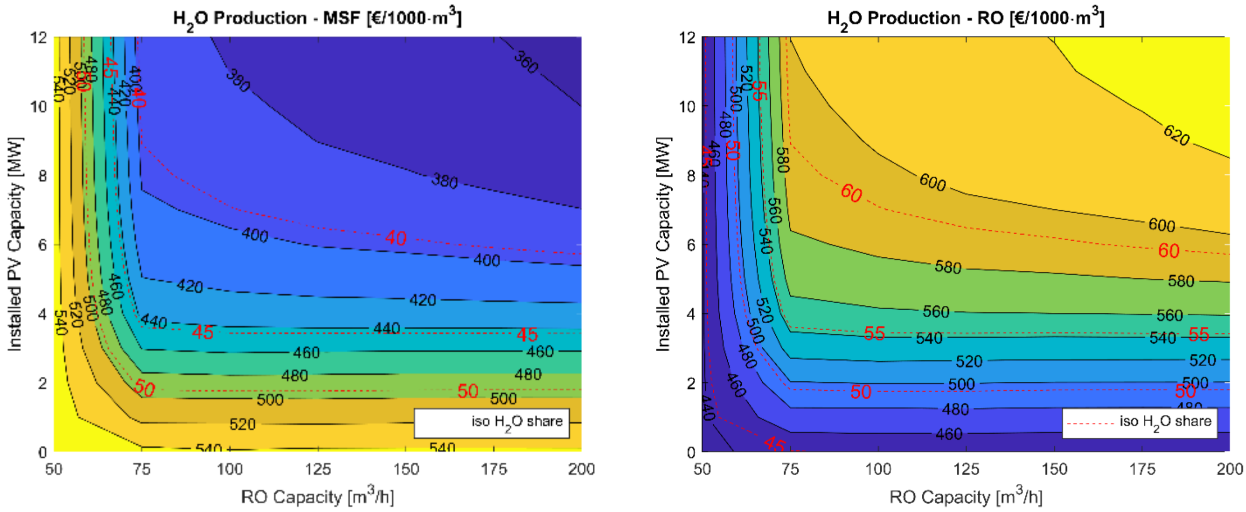


a) b)

*Figure 85 – Water production via a) MSF and b) RO for different RO and PV capacities*

### 6.4.2 Scenario 2: Baseline + PV/RO/rSOC

In the Scenario 2 the sensitivity analysis is carried on with the rSOC installed power in electrolyser cell (EC) mode, based on the 100 m$^3$/h conditions (i.e a minimum of 115 €/MWh reached for 8 MW of installed PV Capacity for LCOE and 0.9 €/m$^3$ for LCOW not influenced by RES production). The SOEC installed capacity on the x-axis was considered as the aggregate of multiple units of the same type, hence the unusual scale on horizontal axis. In this analysis, no hydrogen demand was considered due to the lack of a reliable one, and the only use of produced hydrogen is its use as fuel when the rSOC operates in FC mode as a storage.

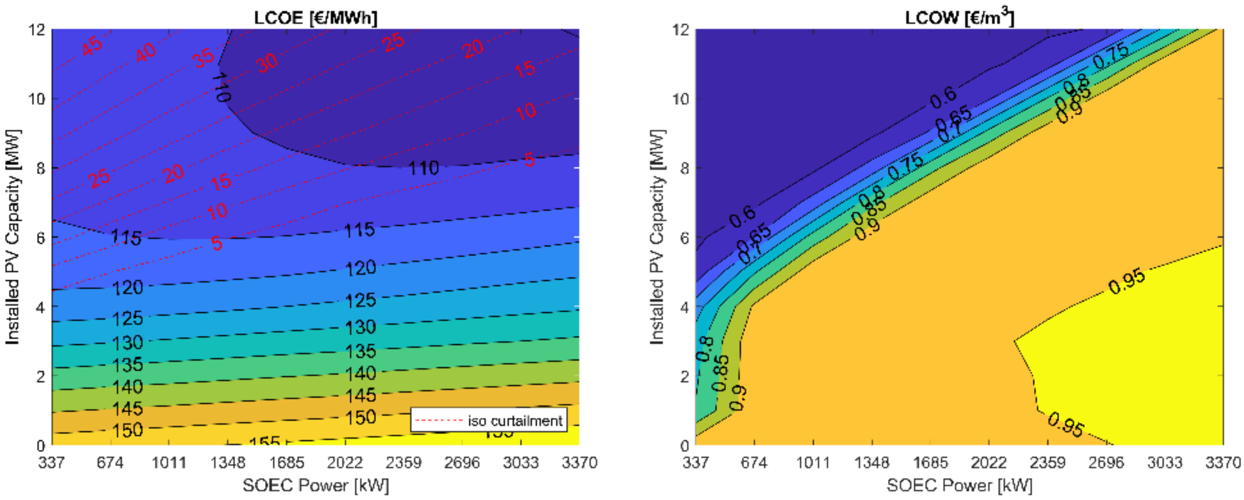


a) b)

*Figure 86 - LCOE and LCOW for different SOEC capacities and PV installed power*

Figure 86 shows the Levelised Cost results. Without using rSOC as storage, proportional to water production, SOEC capacity negatively affects LCOE due to increased CAPEX (Eq. 8). Above 4 MW of PV, rSOC operation increases, reducing RES curtailment compared to Scenario 1 (Figure 83). This is due to the larger rSOC/RO capacity, which enhances its role as storage by producing water and hydrogen. At 6 MW of PV, the minimum LCOE of Scenario 1 (115 €/MWh) is achieved with 1.3 MW of SOEC and only 5% curtailment, compared to 38% RES rejection in Scenario 1. At 8 MW of PV, LCOE further decreases to about 110 €/MWh with 2.5 MW of SOEC, while keeping curtailment below 10%.

On the other hand, LCOW retains the dependence on both SOEC CAPEX and correlated LCOE variation. As opposed to Scenario 1, there exists a broad area of low water costs for high PV capacity and low size of the electrolyzer. In addition, the LCOW trend differs significantly from that of Scenario 1, indicating that the amount of installed PV has a substantial impact on the cost of water.

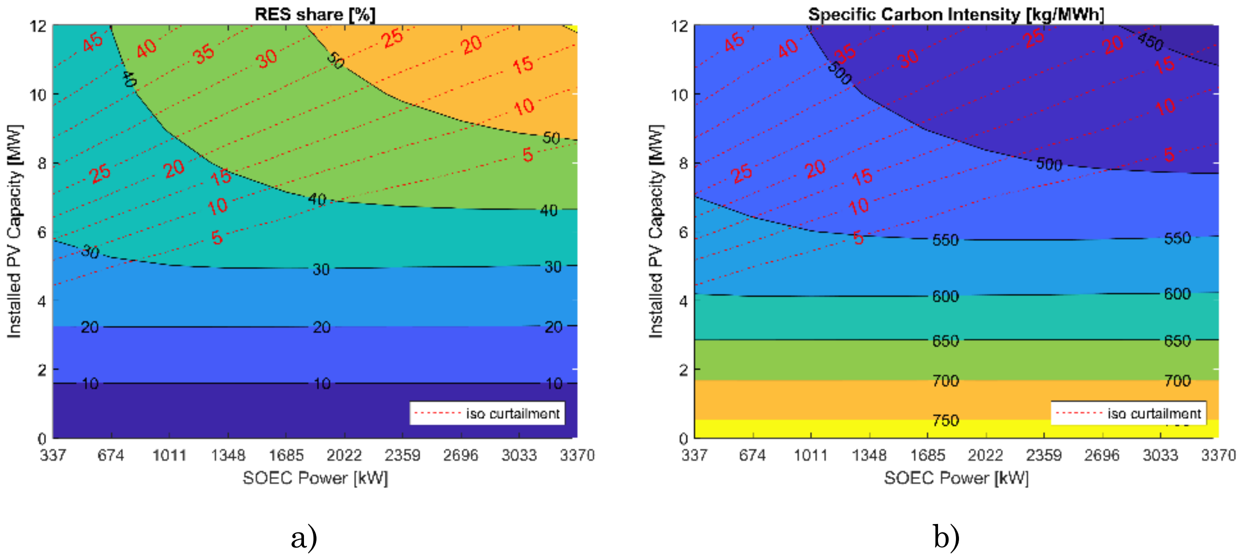


*Figure 87 - RES share and SCI for different SOEC capacities and PV installed power*

As far as RES Share for Scenario 2 is concerned (Figure 87), there is no substantial difference with Scenario 1 (Figure 84) in terms of trend, while the absolute value is consistently higher, thanks to the larger capacity of surplus energy uptake given by both RO and rSOC. The contour plot of curtailed RES energy also confirm this tendency. The SCI highlighted in Figure 87 also mirrors the same trend. It is interesting to note that the absolute value of the carbon emission per MWh produced is not significantly lower in Scenario 2 than it is in Scenario 1. This may be due to the fact that ICE generators still produce a significant amount of electricity and water through the MSF process.

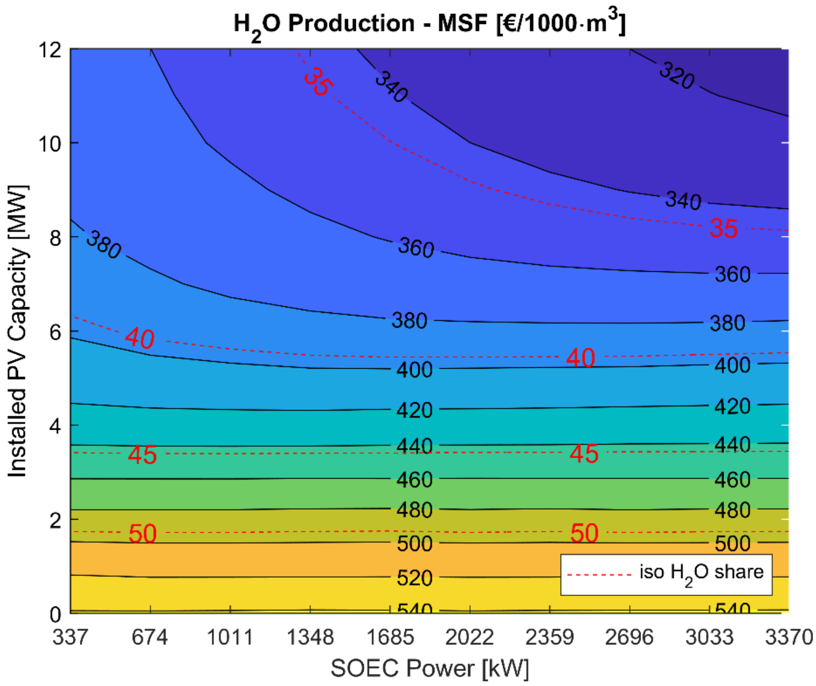


*Figure 88 – Water production via MSF for different SOEC capacities and PV installed power*

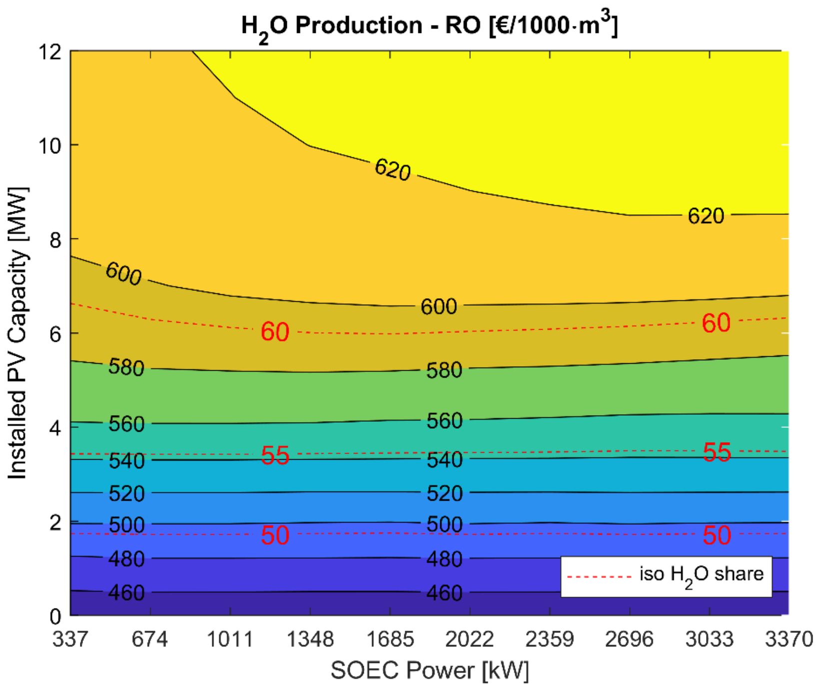


*Figure 89 – Water production via RO for different SOEC capacities and PV installed power*

Finally, in confirmation of this observation, Figure 88 to Figure 90 show that freshwater production is divided almost equally between RO and MFS, even with the largest PV capacities and installed SOEC power. In essence, no more than 3.5% of the total freshwater supply is generated via the rSOC, either in EC or FC modes, and only with considerable amount of RES powering a large rSOC system. This is partially due to the fact that the solid oxide cell performance are sourced from a commercial product whose size is limited, and so is its water production potential. Onboard a passenger ship, where the demand is possibly lower, this could prove more valuable.

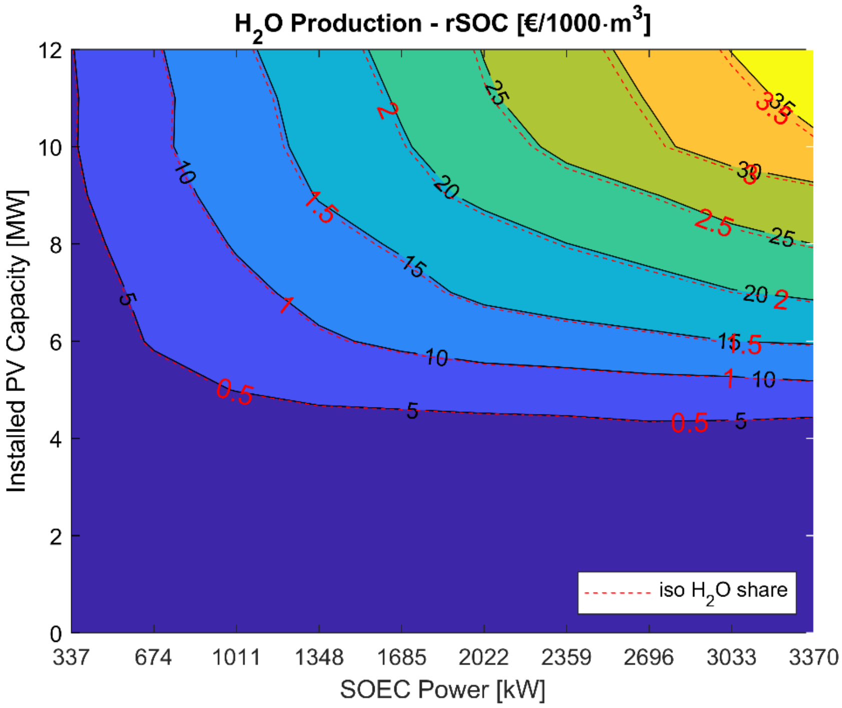


*Figure 90 - Water production via rSOC for different SOEC capacities and PV installed power*

# 7 Conclusion

In order to encourage the decarbonisation of maritime transport and meet the objectives set by the relevant institutions, the transition to alternative fuels is both a promising and necessary option. It is evident that reliance on efficiency improvements alone is inadequate for achieving net zero emissions. The adoption of alternative zero-carbon fuels is associated with a number of challenges, including technological, regulatory and safety issues. Moreover, in the absence of a substantial increase in market penetration, it is improbable that they will experience development comparable to their fossil fuel counterparts. Integrating hydrogen into mobile power systems requires developing robust and energy-efficient storage and supply solutions. Where high-density storage is a must, $LH_2$ storage systems are increasingly seen as a viable option. However, this value is still as low as ~40% of the volumetric energy density of its readiest alternative, namely LNG. However, the extensive experience gained with LNG can effectively promote the hydrogen uptake in liquefied form, in order to guarantee a sufficient zero-emission range to passenger ships. In this dissertation, the feasibility of having liquefied hydrogen onboard form a techno-economic perspective is evaluated, ad the expected result that hydrogen PEMFC cannot perform as the current state of the art power generation technology is obtained.

With these premises, and given that large passenger ships need either energy dense storage and power dense generators to be operated in an economically realistic manner, the component sizing, design and off-design performance analysis of a $LH_2$ fuel system for maritime gas turbine application is carried out. Two configurations of powertrain in different size and intended use are explored, both based on CCGT architecture for its unmatched conversion efficiency and potential hydrogen readiness. The component sizing was made on the basis of the required fuel massflow at the powertrain, and their off-design performance are also assessed. The duty breakup of the heat exchangers has been computed, showing that the main heat source of the system is the HTF heater and the main sink is represented by the main evaporator. The $LH_2$ pumping power was evaluated in order to provide insight on the actual electrical requirement, which must be provided by the shipboard grid. Reliable operational conditions are indicated by the measured values of temperature, size, and SEC, thereby ensuring the absence of freezing of the heat transfer fluid even during deep off-design operation. Finally, a fuel massflow rate map of a $H_2$-NG blend is built taking into account the varying energy content with composition and the gas turbine off-design operation. This might be regarded as a basic requirement towards the development of fuel flexible gas turbines for maritime propulsion.

Within the hydrogen transportation economy, additionally to the main focus on the $LH_2$ powered combined cycles for large ship propulsions, two additional investigations have been performed, as potential auxiliaries to the sustainable navigation and/or on-shore small-size supplies: pressurised PEMFC systems for <1MW power production, and freshwater production through reversible high temperature fuel cells. PEMFC still represent a good option for high efficiency energy conversion whenever hydrogen is present on board.

A cyber-physical emulator of a turbocharged PEMFC is developed and evaluated through experimental testing in conjunction with bladeless turbomachinery to assess control strategies for air supply to the cathode of the FC stack. The cathode side is reproduced by means of a saturation column that humidifies air. Early experiments demonstrated reliable operation, to be further studied testing advanced control solutions to enhance system responsiveness to external loads and mitigating the impact of the stack thermal capacitance.

In the broader context of maritime hydrogen production and consumption in combination with other feedstocks, a MILP optimisation software is developed and exploited to assess the potential of combined freshwater and hydrogen production through a reversible solid oxide cell in a isolated context. Despite the analysis is conducted with an island as case study, the same paradigm can be applicable to a passenger ship. Results show that reverse osmosis starts performing as a storage by reducing RES curtailment only for large RES capacity, but even with high RES and RO capacities, electricity share stays below 35% due to MSF prioritisation, as it remains the cheapest option thanks to the waste heat utilisation from the ICE flue gases. However, with lower installed capacity, rSOC has a minor role in freshwater production.

Future development of this research could possibly include the techno-economic analysis of the real, ship-ready system in a demand-driven optimization with actual demand profiles and definite routes, exploring the trade-off between cost and emission minimization according to the evolving EU-ETS and FuelEU mechanisms. Furthermore, a comprehensive safety assessment of the machinery spaces could be undertaken, evaluating several risk instances and their potential outcome in order to increase awareness and knowledge on real world safety engineering applied to novel technologies.

# Appendix A – AVEVA PRO/II™ Software

AVEVA PRO/II™ process simulation software performs rigorous steady state mass and energy balance calculations for processes ranging from oil and gas separation to reactive distillation. Although being originally devised to chemical processes, it offers the possibility to model virtually any thermodynamic process with various degree of accuracy, from a single component to a complete and complex layout.

The tool contains a library of default components, both general (compressors, heat exchangers, valves) and more chemical engineering devoted (reactors, separators, distillers, adsorbers etc.), and counts on a comprehensive library of species properties. The user can choose to use existing components and tweak them to its convenience or to design new or tailored components by specifying completely their characteristics. Besides, the thermodynamic method can be either equations of state (EoS), SIMSCI libraries or dedicated tables, e.g. for steam.

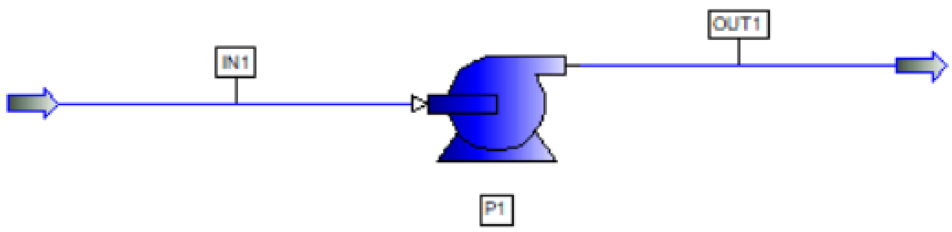


*Figure A1 – User interface representation of a pump in AVEVA PRO-II™*

Figure A1 reports the user interface outlay of a pump as shown in the software, while Figure A2 represents an example for a hydrogen-water heat exchanger with extended information on the basic stream properties, in particular molar flow rate, pressure and temperature. To obtain the mass flow rate, one can simply multiply the value by the molar mass of the species pertaining to that stream. The output results are created in a .txt file as shown in Figure A4 for the same heat exchanger example.

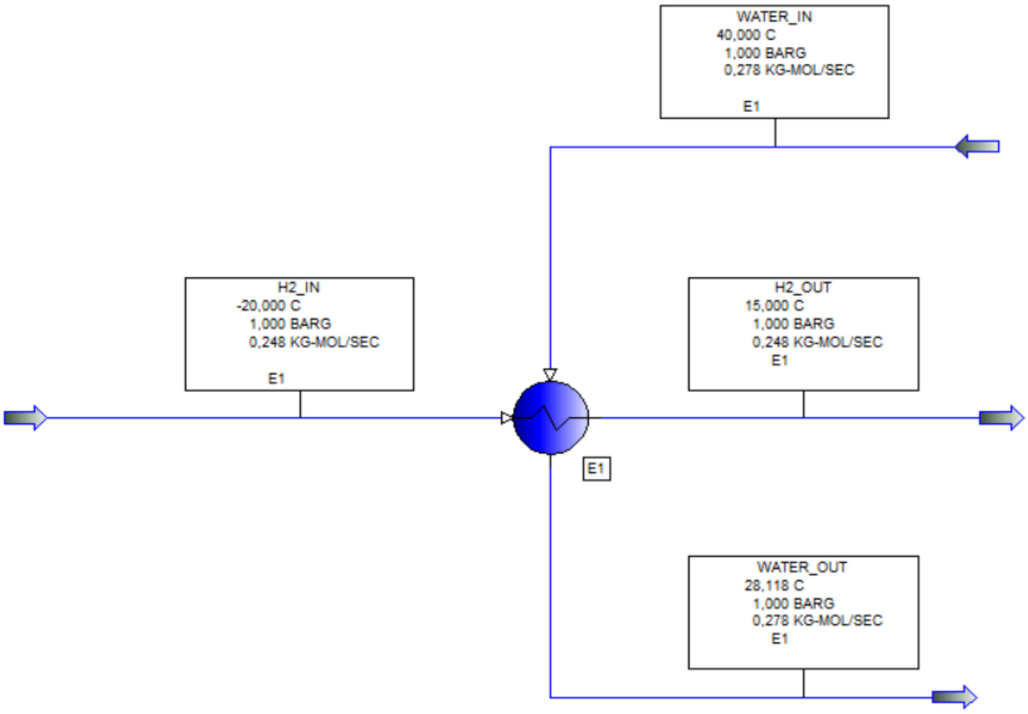


*Figure A2 - User interface representation of a heat exchanger in AVEVA PRO-II™ with details on the inlet and outlet streams*

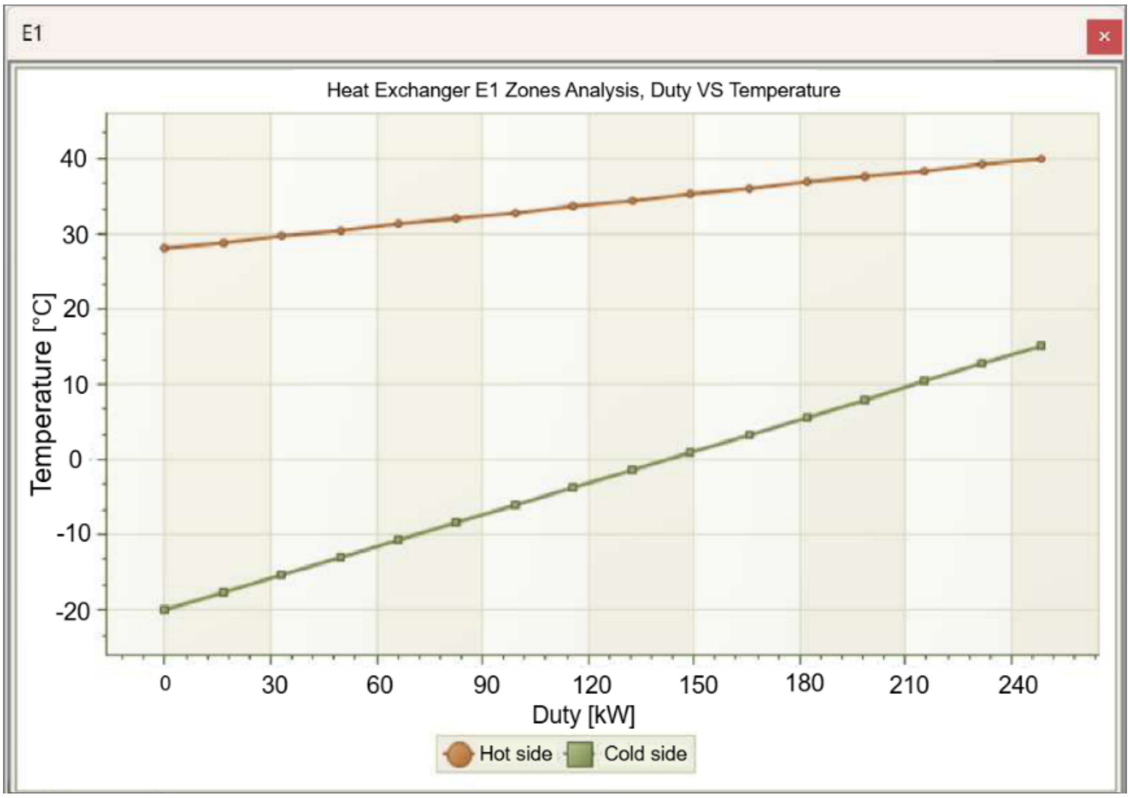


*Figure A3 – T-Q chart of the $H_2$-water heat exchanger (adapted)*

```
OPERATING CONDITIONS                              OVERALL    FROM ZONES
                                               -----------  -----------
     DUTY, KJ/SEC                                 248.273
     LMTD, C                                       35.306       35.281
     F FACTOR (FT)                                  0.940        0.940
     MTD, C                                        33.198       33.174
     U*A, KCAL/HR-C                              6430.304     6435.023

HOT SIDE CONDITIONS                                 INLET       OUTLET
                                               -----------  -----------
     FEED                                        WATER_IN
     WATER PRODUCT                                           WATER_OUT
      WATER, KG-MOL/SEC                             0.278        0.278
             K*KG/SEC                           5.000E-03    5.000E-03
         CP, KJ/KG-C                                4.178        4.180
      TOTAL, KG-MOL/SEC                             0.278        0.278
             K*KG/SEC                           5.000E-03    5.000E-03
     CONDENSATION, KG-MOL/SEC                                    0.000
      TEMPERATURE, C                               40.000       28.118
      PRESSURE, BAR(GA)                             1.000        1.000

COLD SIDE CONDITIONS                                INLET       OUTLET
                                               -----------  -----------
     FEED                                           H2_IN
     VAPOR PRODUCT                                              H2_OUT
      VAPOR, KG-MOL/SEC                             0.248        0.248
             K*KG/SEC                           5.000E-04    5.000E-04
         CP, KJ/KG-C                               14.123       14.248
      TOTAL, KG-MOL/SEC                             0.248        0.248
             K*KG/SEC                           5.000E-04    5.000E-04
     CONDENSATION, KG-MOL/SEC                                    0.000
      TEMPERATURE, C                              -20.000       15.000
      PRESSURE, BAR(GA)                             1.000        1.000
```

*Figure A4 – Output results of heat exchanger example*

Although the software has a inherent 0-D black box logic, it features the possibility to perform more accurate discretisation. For instance, a 1-D analysis of the heat exchangers by specifying the number of discretisation points is possible. In Figure A3 the temperature-heat duty chart for the same $H_2$-water heat exchanger example is reported. Unfortunately, there is no possibility to modify the plots generated by the software, which are usually quite low quality. Finally, also simple targeted simulations as well as sensitivity analysis can be performed by means of a "calculator" block and a "case study" tool, respectively.

# Publications


1. C. Nevoloso, M. Caruso, G. Schettino, R. Miceli, M. Passalacqua, L. Mantelli, A. Traverso, “Techno-Economic Investigation of Power Systems for a Decarbonised Naval Sector”, International Conference on Electrical Systems for Aircraft, Railway, Ship Propulsion and Road Vehicles and International Transportation Electrification Conference (ESARS-ITEC), 2024.
2. G.N. Montagna, S. Piccardo, M. Passalacqua, D. Bellotti, L. Mantelli, M. Rivarolo, “The Energy Systems Analysis with a Multi-Criteria Design Tool to Decarbonize Maritime Transport”, 37th International Conference on Efficiency, Cost, Optimisation, Simulation and Environmental Impact of Energy Systems (ECOS), 2024
3. A. Vasylyev, M. Passalacqua, L. Mantelli, M. Rivarolo, A. Sorce, “Piecewise-linear MILP optimisation for energy system design onboard hybrid ships”, Journal of Physics Conference Series, 2893(1), 2024.
4. S. Tucker, M. Passalacqua, A. Dotto, A. Traverso, G. Schiaffino, “Liquid hydrogen storage system for micro gas turbines: Dynamic modelling and performance with variable demand profile”, Proceedings of the ASME Turbo Expo 2025, GT2025-152917.
5. M. Passalacqua, A. Traverso, “From $LH_2$ to LNG in Maritime Transport: A Review of Technology, Materials, and Safety Challenges”, Journal of Maritime Science and Engineering, 13(9), 1748, 2025.
6. A. Vasylyev, M. Bozzolo, M. Passalacqua, K. Machaj, A.M. de Càssia Crispim, C. Anfosso, D. Bellotti, A. Baldinelli, F. Pineider, A. Sorce, “Strategies for Solar-Driven Freshwater and Hydrogen Production in Island Scenarios”, 38th International Conference on Efficiency, Cost, Optimisation, Simulation and Environmental Impact of Energy Systems (ECOS), 2025.
7. M. Passalacqua, S. Tucker, A. Dotto, A. Traverso, G. Schiaffino, “Design and Off-Design Performance Analysis of a Liquefied Hydrogen Fuel System for Maritime Gas Turbines”, ASME Turbo Expo 2026, GT2026-176518 (*Accepted for conference*).
8. S. Crosa, L. Mantelli, F. Reggio, A. Patti, M. Passalacqua, T. Reboli, A. Traverso, “Design and Characterisation of a Cyberphysical Turbocharged PEMFC Emulator Plant”, ASME Turbo Expo 2026, GT2026-178754 (*Accepted for conference*).

# Bibliography


[1] IEA, 2025, *World Energy Outlook 2025*. [Online]. Available: www.iea.org/terms.

[2] Urban, F., Nurdiawati, A., Harahap, F., and Morozovska, K., 2024, “Decarbonizing Maritime Shipping and Aviation: Disruption, Regime Resistance and Breaking through Carbon Lock-in and Path Dependency in Hard-to-Abate Transport Sectors,” Environ. Innov. Soc. Transit., **52**. https://doi.org/10.1016/j.eist.2024.100854.

[3] IMO, 1974, “Safety Of Life At Sea (SOLAS).” [Online]. Available: https://www.imo.org/en/about/conventions/pages/international-convention-for-the-safety-of-life-at-sea-(solas),-1974.aspx. [Accessed: 04-Dec-2025].

[4] European Union, 2021, “Fit for 55.” [Online]. Available: https://www.consilium.europa.eu/en/policies/fit-for-55/. [Accessed: 04-Dec-2025].

[5] 2025, “EU ETS - EU Emission Trading System.”

[6] Office of the EU, 2023, *REGULATION 2023/1805 - Use of Renewable and Low-Carbon Fuels in Maritime Transport, and Amending Directive 2009/16/EC*. https://doi.org/10.2771/793264.

[7] DNV, 2023, *MARITIME FORECAST TO 2050*.

[8] Anders, J., 2019, *Comparison of Alternative Marine Fuels*. [Online]. Available: www.dnvgl.com.

[9] Jain, M., Muthalathu, R., and Wu, X. Y., 2022, “Electrified Ammonia Production as a Commodity and Energy Storage Medium to Connect the Food, Energy, and Trade Sectors,” iScience, **25**(8). https://doi.org/10.1016/j.isci.2022.104724.

[10] IGU, 2022, *2022 WORLD LNG REPORT*. [Online]. Available: https://maritimecyprus.com/wp-content/uploads/2022/08/World-LNG-Report2022.pdf. [Accessed: 14-Jul-2023].

[11] Milojević, S., Stopka, O., Orynycz, O., Tucki, K., Šarkan, B., and Savić, S., 2025, “Exploitation and Maintenance of Biomethane-Powered Truck and Bus Fleets to Assure Safety and Mitigation of Greenhouse Gas Emissions,” Energies (Basel)., **18**(9). https://doi.org/10.3390/en18092218.

[12] Kochunni, S. K., and Chowdhury, K., 2022, “Concept and Evaluation of Energy-Efficient Boil-off Gas Reliquefiers in LNG Carrier Ships Propelled by Dual-Fuel Engines,” Cryogenics (Guildf)., **123**. https://doi.org/10.1016/j.cryogenics.2022.103453.

[13] Duan, Z., Xue, H., Gong, X., and Tang, W., 2021, “A Thermal Non-Equilibrium Model for Predicting LNG Boil-off in Storage Tanks Incorporating the Natural Convection Effect,” Energy, **233**. https://doi.org/10.1016/j.energy.2021.121162.

[14] Kanbur, B. B., Xiang, L., Dubey, S., Choo, F. H., and Duan, F., 2017, “Cold Utilization Systems of LNG: A Review,” Renewable and Sustainable Energy Reviews, **79**, pp. 1171–1188. https://doi.org/10.1016/j.rser.2017.05.161.

[15] Cao, X., Yang, J., Zhang, Y., Gao, S., and Bian, J., 2022, “Process Optimization, Exergy and Economic Analysis of Boil-off Gas Re-Liquefaction Processes for LNG Carriers,” Energy, **242**. https://doi.org/10.1016/j.energy.2021.122947.

[16] Kwak, D. H., Heo, J. H., Park, S. H., Seo, S. J., and Kim, J. K., 2018, “Energy-Efficient Design and Optimization of Boil-off Gas (BOG) Re-Liquefaction Process for Liquefied Natural Gas (LNG)-Fuelled Ship,” Energy, **148**, pp. 915–929. https://doi.org/10.1016/j.energy.2018.01.154.

[17] Lemmon E W, Bell I H, Huber M L, and McLinden M O, 2018, “NIST Standard Reference Database 23:Reference Fluid Thermodynamic and Transport Properties - REFPROP, Version 10.0, National Institute of Standards and Technology,” NIST. [Online]. Available: https://www.nist.gov/srd/refprop. [Accessed: 18-Jan-2024].

[18] Passalacqua, M., and Traverso, A., 2025, “From LNG to LH2 in Maritime Transport: A Review of Technology, Materials, and Safety Challenges,” J. Mar. Sci. Eng., **13**(9). https://doi.org/10.3390/jmse13091748.

[19] 2025, “BeHydro.” [Online]. Available: https://www.behydro.com/. [Accessed: 11-Dec-2025].

[20] 2023, “Siemens Energy - Gas Turbines.” [Online]. Available: https://www.siemens-energy.com/global/en/offerings/power-generation/gas-turbines.html. [Accessed: 01-Aug-2023].

[21] Harper, J., Gibeaut, D., Lozier, M., Sake, R., Wolf, T., and Noble, D. R., 2025, “Hydrogen Cofiring Demonstration at Constellation Hillabee Siemens Energy SGT6-6000G Power Plant,” J. Eng. Gas Turbine. Power, **147**(5). https://doi.org/10.1115/1.4067181.

[22] Ustolin, F., Campari, A., and Taccani, R., 2022, “An Extensive Review of Liquid Hydrogen in Transportation with Focus on the Maritime Sector,” J. Mar. Sci. Eng., **10**(9). https://doi.org/10.3390/jmse10091222.

[23] Niccolò Montagna, G., Piccardo, S., Passalacqua, M., Bellotti, D., Mantelli, L., and Rivarolo, M., 2024, “The Energy System Analysis with a Multi-Criteria Design Tool To Decarbonize Maritime Transport,” *International Conference on Efficiency, Cost, Optimization, Simulation and Environmental Impact of Energy Systems (ECOS)*, Paris.

[24] Rivarolo, M., Piccardo, S., Montagna, G. N., and Bellotti, D., 2023, “A Multi-Criteria Approach for Comparing Alternative Fuels and Energy Systems Onboard Ships,” Energy Conversion and Management: X, **20**. https://doi.org/10.1016/j.ecmx.2023.100460.

[25] Morales-Ospino, R., Celzard, A., and Fierro, V., 2023, “Strategies to Recover and Minimize Boil-off Losses during Liquid Hydrogen Storage,” Renewable and Sustainable Energy Reviews, **182**. https://doi.org/10.1016/j.rser.2023.113360.

[26] Al-Breiki, M., and Bicer, Y., 2020, “Investigating the Technical Feasibility of Various Energy Carriers for Alternative and Sustainable Overseas Energy Transport Scenarios,” Energy Convers. Manag., **209**. https://doi.org/10.1016/j.enconman.2020.112652.

[27] Song, Q., Tinoco, R. R., Yang, H., Yang, Q., Jiang, H., Chen, Y., and Chen, H., 2022, “A Comparative Study on Energy Efficiency of the Maritime Supply Chains for Liquefied Hydrogen, Ammonia, Methanol and Natural Gas,” Carbon Capture Science and Technology, **4**. https://doi.org/10.1016/j.ccst.2022.100056.

[28] Noh, H., Kang, K., and Seo, Y., 2023, “Environmental and Energy Efficiency Assessments of Offshore Hydrogen Supply Chains Utilizing Compressed Gaseous Hydrogen, Liquefied Hydrogen, Liquid Organic Hydrogen Carriers and Ammonia,” Int. J. Hydrogen Energy, **48**(20), pp. 7515–7532. https://doi.org/10.1016/j.ijhydene.2022.11.085.

[29] Ahn, J., You, H., Ryu, J., and Chang, D., 2017, “Strategy for Selecting an Optimal Propulsion System of a Liquefied Hydrogen Tanker,” Int. J. Hydrogen Energy, **42**(8), pp. 5366–5380. https://doi.org/10.1016/j.ijhydene.2017.01.037.

[30] 2022, “HESC - The Suiso Frontier.” [Online]. Available: https://www.hydrogenenergysupplychain.com/about-the-pilot/supply-chain/the-suiso-frontier/. [Accessed: 22-Nov-2023].

[31] Valera-Medina, A., and Banares-Alcantara, R., 2020, *Techno-Economic Challenges of Green Ammonia as an Energy Vector*.

[32] Serpell, O., Hsain, Z., Chu, A., and Johnsen, W., 2023, *Ammonia’s Role in a Net-Zero Hydrogen Economy*.

[33] Aziz, M., 2021, “Liquid Hydrogen: A Review on Liquefaction, Storage, Transportation, and Safety,” Energies (Basel)., **14**(18). https://doi.org/10.3390/en14185917.

[34] Valera-Medina, A., Xiao, H., Owen-Jones, M., David, W. I. F., and Bowen, P. J., 2018, “Ammonia for Power,” Prog. Energy Combust. Sci., **69**, pp. 63–102. https://doi.org/10.1016/j.pecs.2018.07.001.

[35] Alnajideen, M., Shi, H., Northrop, W., Emberson, D., Kane, S., Czyzewski, P., Alnaeli, M., Mashruk, S., Rouwenhorst, K., Yu, C., Eckart, S., and Valera-Medina, A., 2024,

"Ammonia Combustion and Emissions in Practical Applications: A Review," Carbon Neutrality, **3**(1). https://doi.org/10.1007/s43979-024-00088-6.

[36] Marine, W., *Wärtsilä 25 Brochure*. [Online]. Available: www.wartsila.com.

[37] MAN Energy Solutions, 2023, "MAN ES." [Online]. Available: https://www.man-es.com/. [Accessed: 01-Aug-2023].

[38] Kosmajac, S., and Offshore Energy, 2025, "Green Methanol-Fueled Disney Adventure Makes First Foray Into the World." [Online]. Available: https://www.offshore-energy.biz/green-methanol-fueled-disney-adventure-makes-first-foray-into-the-world/. [Accessed: 08-Jan-2026].

[39] Sonthalia, A., and Kumar, N., 2019, "Hydroprocessed Vegetable Oil as a Fuel for Transportation Sector: A Review," Journal of the Energy Institute, **92**(1), pp. 1–17. https://doi.org/10.1016/j.joei.2017.10.008.

[40] Bohl, T., Smallbone, A., Tian, G., and Roskilly, A. P., 2018, "Particulate Number and NOx Trade-off Comparisons between HVO and Mineral Diesel in HD Applications," Fuel, **215**, pp. 90–101. https://doi.org/10.1016/j.fuel.2017.11.023.

[41] Hunicz, J., Krzaczek, P., Gęca, M., Rybak, A., and Mikulski, M., 2021, "Comparative Study of Combustion and Emissions of Diesel Engine Fuelled with FAME and HVO," Combustion Engines, **184**(1), pp. 72–78. https://doi.org/10.19206/ce-135066.

[42] Chiong, M. C., Chong, C. T., Ng, J. H., Lam, S. S., Tran, M. V., Chong, W. W. F., Mohd Jaafar, M. N., and Valera-Medina, A., 2018, "Liquid Biofuels Production and Emissions Performance in Gas Turbines: A Review," Energy Convers. Manag., **173**, pp. 640–658. https://doi.org/10.1016/j.enconman.2018.07.082.

[43] 2001, "Engineering Toolbox." [Online]. Available: https://www.engineeringtoolbox.com/. [Accessed: 06-Jan-2026].

[44] Pechan, E. H., and Gagnon, A. C., 1993, *EMISSION FACTOR DOCUMENTATION FOR AP-42 - LIQUEFIED PETROLEUM GAS COMBUSTION EPA*.

[45] de Jong, P., Andrade Torres, E., Beisl Vieira de Melo, S. A., Mendes-Santana, D., and Valverde Pontes, K., 2023, "Socio-Economic and Environmental Aspects of Bio-LPG and Bio-Dimethyl Ether (Bio-DME) Production and Usage in Developing Countries: The Case of Brazil," Cleaner and Circular Bioeconomy, **6**. https://doi.org/10.1016/j.clcb.2023.100055.

[46] Batthar, P., and Wartsila, 2020, "Retrofit Highlights - Use of LPG as a Marine Fuel." [Online]. Available: https://www.wartsila.com/insights/article/retrofit-highlights-use-of-lpg-as-a-marine-fuel. [Accessed: 06-Jan-2026].

[47] 2026, "BW LPG." [Online]. Available: https://www.bwlpg.com/vlgc_fleet/lpg-propulsion/. [Accessed: 07-Jan-2026].

[48] US DOE, 2022, *U.S. Ethane: Market Issues and Opportunities*.

[49] Gassner, G., and Wartsila, 2016, "Ethane-Powered Marine Vessel." [Online]. Available: https://www.wartsila.com/insights/article/worlds-first-ethane-powered-marine-vessels. [Accessed: 07-Jan-2026].

[50] Tien, W. K., Yeh, R. H., and Hong, J. M., 2007, "Theoretical Analysis of Cogeneration System for Ships," Energy Convers. Manag., **48**(7), pp. 1965–1974. https://doi.org/10.1016/j.enconman.2007.01.032.

[51] Mondejar, M. E., Andreasen, J. G., Pierobon, L., Larsen, U., Thern, M., and Haglind, F., 2018, "A Review of the Use of Organic Rankine Cycle Power Systems for Maritime Applications," Renewable and Sustainable Energy Reviews, **91**, pp. 126–151. https://doi.org/10.1016/j.rser.2018.03.074.

[52] Baldasso, E., Mondejar, M. E., Andreasen, J. G., Rønnenfelt, K. A. T., Nielsen, B. Ø., and Haglind, F., 2020, "Design of Organic Rankine Cycle Power Systems for Maritime Applications Accounting for Engine Backpressure Effects," Appl. Therm. Eng., **178**. https://doi.org/10.1016/j.applthermaleng.2020.115527.

[53] Barsi, D., Costa, C., Satta, F., Zunino, P., Busi, A., Ghio, R., Raffaeli, C., and Sabattini, A., 2020, "Design of a Mini Combined Heat and Power Cycle for Naval Applications," Journal of Sustainable Development of Energy, Water and Environment Systems, **8**(2), pp. 281–292. https://doi.org/10.13044/j.sdewes.d7.0309.

[54] Larsen, U., Sigthorsson, O., and Haglind, F., 2014, "A Comparison of Advanced Heat Recovery Power Cycles in a Combined Cycle for Large Ships," Energy, **74**(C), pp. 260–268. https://doi.org/10.1016/j.energy.2014.06.096.

[55] Andreasen, J. G., Meroni, A., and Haglind, F., 2017, "A Comparison of Organic and Steam Rankine Cycle Power Systems for Waste Heat Recovery on Large Ships," Energies (Basel)., **10**(4). https://doi.org/10.3390/en10040547.

[56] Agazzani, A., Massardo, A. F., and Asme, M., 1999, "An Assessment of the Performance of Closed Cycles With and Without Heat Rejection at Cryogenic Temperatures," *Proceedings of ASME Turbo Expo GT1999*. [Online]. Available: http://asmedigitalcollection.asme.org/gasturbinespower/article-pdf/121/3/458/5889603/458_1.pdf.

[57] Zhang, J., Meerman, H., Benders, R., and Faaij, A., 2020, "Comprehensive Review of Current Natural Gas Liquefaction Processes on Technical and Economic Performance," Appl. Therm. Eng., **166**. https://doi.org/10.1016/j.applthermaleng.2019.114736.

[58] Zhao, L., Dong, H., Tang, J., and Cai, J., 2016, "Cold Energy Utilization of Liquefied Natural Gas for Capturing Carbon Dioxide in the Flue Gas from the Magnesite Processing Industry," Energy, **105**, pp. 45–56. https://doi.org/10.1016/j.energy.2015.08.110.

[59] Kim, Y., Lee, J., An, N., and Kim, J., 2023, "Advanced Natural Gas Liquefaction and Regasification Processes: Liquefied Natural Gas Supply Chain with Cryogenic Carbon Capture and Storage," Energy Convers. Manag., **292**. https://doi.org/10.1016/j.enconman.2023.117349.

[60] Si, H., Chen, S., Xie, R. Y., Zeng, W. Q., Zhang, X. J., and Jiang, L., 2024, "Techno-Economic Analysis on a Hybrid System with Carbon Capture and Energy Storage for Liquefied Natural Gas Cold Energy Utilization," Energy, **308**. https://doi.org/10.1016/j.energy.2024.132958.

[61] Zanobetti, F., Pio, G., Bucelli, M., Miani, L., Jafarzadeh, S., and Cozzani, V., 2024, "Onboard Carbon Capture and Storage (OCCS) for Fossil Fuel-Based Shipping: A Sustainability Assessment," J. Clean. Prod., **470**. https://doi.org/10.1016/j.jclepro.2024.143343.

[62] Ballout, J., Al-Rawashdeh, M., Al-Mohannadi, D., Rousseau, J., Burton, G., and Linke, P., 2024, "Assessment of CO2 Capture and Storage Onboard LNG Vessels Driven by Energy Recovery from Engine Exhaust," Clean. Eng. Technol., **22**. https://doi.org/10.1016/j.clet.2024.100802.

[63] Restelli, F., Spatolisano, E., Pellegrini, L. A., Cattaneo, S., de Angelis, A. R., Lainati, A., and Roccaro, E., 2024, "Liquefied Hydrogen Value Chain: A Detailed Techno-Economic Evaluation for Its Application in the Industrial and Mobility Sectors," Int. J. Hydrogen Energy, **52**, pp. 454–466. https://doi.org/10.1016/j.ijhydene.2023.10.107.

[64] Zhang, T., Uratani, J., Huang, Y., Xu, L., Griffiths, S., and Ding, Y., 2023, "Hydrogen Liquefaction and Storage: Recent Progress and Perspectives," Renewable and Sustainable Energy Reviews, **176**. https://doi.org/10.1016/j.rser.2023.113204.

[65] Colozza, A. J., 2002, *Hydrogen Storage for Aircraft Applications Overview*, Brook Park, OH. [Online]. Available: http://www.sti.nasa.gov.

[66] Krainz G, Bartlok G, Bodner P, Casapicola P, Doeller C, Hofmeister F, Neubacher E, and Zieger A, 2004, "Development of Automotive Liquid Hydrogen Storage System," Advances in Cryogenic Engineering: Transactions of the Cryogenic Engineering Conference, **49**, pp. 35–40.

[67] Qiu, Y., Yang, H., Tong, L., and Wang, L., 2021, "Research Progress of Cryogenic Materials for Storage and Transportation of Liquid Hydrogen," Metals (Basel)., **11**(7). https://doi.org/10.3390/met11071101.

[68] Ahluwalia, R. K., Roh, H. S., Peng, J. K., Papadias, D., Baird, A. R., Hecht, E. S., Ehrhart, B. D., Muna, A., Ronevich, J. A., Houchins, C., Killingsworth, N. J., and Aceves, S. M., 2023, "Liquid Hydrogen Storage System for Heavy Duty Trucks: Configuration, Performance, Cost, and Safety," Int. J. Hydrogen Energy, **48**(35), pp. 13308–13323. https://doi.org/10.1016/j.ijhydene.2022.12.152.

[69] Kang, D., Yun, S., and Kim, B. K., 2022, "Review of the Liquid Hydrogen Storage Tank and Insulation System for the High-Power Locomotive," Energies (Basel)., **15**(12). https://doi.org/10.3390/en15124357.

[70] Elkafas, A. G., Rivarolo, M., Gadducci, E., Magistri, L., and Massardo, A. F., 2023, "Fuel Cell Systems for Maritime: A Review of Research Development, Commercial Products, Applications, and Perspectives," Processes, **11**(1). https://doi.org/10.3390/pr11010097.

[71] Di Micco, S., Mastropasqua, L., Cigolotti, V., Minutillo, M., and Brouwer, J., 2022, "A Framework for the Replacement Analysis of a Hydrogen-Based Polymer Electrolyte Membrane Fuel Cell Technology on Board Ships: A Step towards Decarbonization in the Maritime Sector," Energy Convers. Manag., **267**. https://doi.org/10.1016/j.enconman.2022.115893.

[72] Nerheim, A. R., Æsøy, V., and Holmeset, F. T., 2021, "Hydrogen as a Maritime Fuel–Can Experiences with LNG Be Transferred to Hydrogen Systems?," J. Mar. Sci. Eng., **9**(7). https://doi.org/10.3390/jmse9070743.

[73] International Maritime Organization (IMO), 2015, *RESOLUTION MSC.370(93) - AMENDMENTS TO THE INTERNATIONAL CODE FOR THE CONSTRUCTION AND EQUIPMENT OF SHIPS CARRYING LIQUEFIED GASES IN BULK*.

[74] Kim, T. W., Kim, S. K., Park, S. B., and Lee, J. M., 2018, "Design of Independent Type-B LNG Fuel Tank: Comparative Study between Finite Element Analysis and International Guidance," Advances in Materials Science and Engineering, **2018**. https://doi.org/10.1155/2018/5734172.

[75] LNT Marine, 2024, *Independent Prismatic Tank Type A and Type B for LNG and Ammonia-Differences, Experience, Constructability and Suitability*.

[76] DNV, 2019, "LNG Containment Systems: Finding the Way for Type A." [Online]. Available: https://www.dnv.com/expert-story/maritime-impact/LNG-containment-systems-finding-the-way-for-Type-A.html. [Accessed: 17-Jul-2023].

[77] Wartsila, 2024, "Ammonia Fuel Supply System." [Online]. Available: https://www.wartsila.com/marine/products/gas-solutions/ammonia-supply-systems/afss. [Accessed: 07-Jan-2026].

[78] International Maritime Organization, 2016, *RESOLUTION MSC.420(97) - INTERIM RECOMMENDATIONS FOR CARRIAGE OF LIQUEFIED HYDROGEN IN BULK*. [Online]. Available: https://edocs.imo.org/Final.

[79] Wartsila, 2017, *LNG as a Marine Fuel Boosts Profitability While Ensuring Compliance*.

[80] Marine Solutions, W., *LNG Shipping Solutions 2 Gas: A Green Solution*.

[81] 2023, "Wartsila Engines & Gensets." [Online]. Available: https://www.wartsila.com/marine/products/engines-and-generating-sets. [Accessed: 01-Aug-2023].

[82] MAN ES, *MAN Cryo Cryogenic Solutions for Onshore and Offshore Applications*. [Online]. Available: https://www.man-es.com/docs/default-source/document-sync-archive/man-cryo-eng.pdf?sfvrsn=f1030ce2_3. [Accessed: 08-Nov-2023].

[83] Wartsila Marine Power, 2023, "New Balearia Innovative Fast Ferry Features Wartsila Propulsion Solution." [Online]. Available: https://www.wartsila.com/media/news/06-02-2023-new-bale%C3%A0ria-innovative-fast-ferry-will-feature-wartsila-propulsion-solutions-3221398. [Accessed: 20-Jan-2026].

[84] Ebrahimi, A., Rolt, A., Jafari, S., and Anton, J. H., 2024, "A Review on Liquid Hydrogen Fuel Systems in Aircraft Applications for Gas Turbine Engines," Int. J. Hydrogen Energy, **91**, pp. 88–105. https://doi.org/10.1016/j.ijhydene.2024.10.121.

[85] Lamprakis, D., Rajendran, D. J., Santhanakrishnan, M., Coskun, S., Roumeliotis, I., Pachidis, V., and Yates, M., 2025, "On Leakage Flows in a Liquid Hydrogen Multistage Pump for Aircraft Engine Applications," J. Eng. Gas Turbine. Power, **147**(5). https://doi.org/10.1115/1.4066827.

[86] Patrao, A. C., Jonsson, I., Xisto, C., Lundbladh, A., and Grönstedt, T., 2024, "Compact Heat Exchangers for Hydrogen-Fueled Aero Engine Intercooling and Recuperation," Appl. Therm. Eng., **243**. https://doi.org/10.1016/j.applthermaleng.2024.122538.

[87] Koudounas, G., Renuke, A., Bermperis, D., Chen, H., Claesson, J., Västerås, M., and Konstantinos Kyprianidis, S., 2025, "Thermal Management System Modelling for Liquid Hydrogen-Fueled Hybrid Eletric Aircraft," *Proceedings of ASME Turbo Expo*.

[88] Rompokos, P., Kang, S., and Roumeliotis, I., 2025, "Integrated Design and Operation Assessment of a Preheating System for Liquid Hydrogen Fuelled Engines," *Proceedings of ASME Turbo Expo, GT2025-154015.*

[89] Kim, B. Il, Kim, K. T., and Islam, M. S., 2024, "Development of Strength Evaluation Methodology for Independent IMO TYPE C Tank with LH2 Carriers," Journal of Ocean Engineering and Technology, **38**(3), pp. 87–102. https://doi.org/10.26748/KSOE.2024.047.

[90] MAN Energy Solutions, 2019, *MAN LH2 Marine Power Pack*. [Online]. Available: https://www.man-es.com/campaigns/download-Q4-2023/Download/man-lh-sub-2-sub-marine-power-pack/5123cf76-6869-4326-aa69-0bb2ba15a6e2/MAN-LH2-Power-Pack. [Accessed: 08-Nov-2023].

[91] 2023, "SHyPS: Sustainable Hydrogen Powered Shipping." [Online]. Available: https://www.shyps.eu/. [Accessed: 08-Jan-2026].

[92] Fincantieri, 2025, "Fincantieri and Viking Announce the World's First Hydrogen-Powered Cruise Ship." [Online]. Available: https://www.fincantieri.com/globalassets/press-releases/price-sensitive/2025/fincantieri-and-viking-announce-the-worlds-first-hydrogen-powered-cruise-ship-and-sign-contracts-for-two-new-units.pdf?_gl=1*a8hxrb*_up*MQ..*_ga*NTYwNzQ5NTcwLjE3NjM0NTYwMTU.*_ga_NM23K8YMS4*czE3NjM0NTYwMTUkbzEkZzAkdDE3NjM0NTYwMTUkajYwJGwwJGgw. [Accessed: 18-Nov-2025].

[93] Østvik, I., and Norled, 2021, *MF Hydra - World's First LH2 Driven Ship and the Challenges Ahead Towards Zero-Emission Shipping*.

[94] Balestra, L., and Schjølberg, I., 2021, "Modelling and Simulation of a Zero-Emission Hybrid Power Plant for a Domestic Ferry," Int. J. Hydrogen Energy, **46**(18), pp. 10924–10938. https://doi.org/10.1016/j.ijhydene.2020.12.187.

[95] Balestra, L., and Schjølberg, I., 2021, "Energy Management Strategies for a Zero-Emission Hybrid Domestic Ferry," Int. J. Hydrogen Energy, **46**(77), pp. 38490–38503. https://doi.org/10.1016/j.ijhydene.2021.09.091.

[96] Duthil, P., 2015, *Material Properties at Low Temperature*.

[97] ASM International., 2002, *Atlas of Stress-Strain Curves.*, ASM International.

[98] Park J, Chun K, Lee T, Kim Y, and Kim J, *Guidelines for Selection of Metallic Materials of Containment System for Alternative Fuels for Ships*.

[99] Muragishi O, Inatsu S, Uraguchi R, Yamashiro K, Imai T, Ohashi T, Shimogaki T, Yoshida T, and Koumoto T, 2021, *Hydrogen Transportation-Development of Liquefied Hydrogen Carrier*.

[100] Schutz, J. B., 1998, "Properties of Composite Materials for Cryogenic Applications," Cryogenics (Guildf)., **38**, pp. 3–12.

[101] Lee, J. A., 2016, *Hydrogen Embrittlement*, Huntsville, AL. [Online]. Available: http://www.sti.nasa.gov.

[102] Chun, K. W., 2022, "Technical Guide for Materials of Containment System for Hydrogen Fuels for Ships," Journal of Advanced Marine Engineering and Technology, **46**(5), pp. 212–217. https://doi.org/10.5916/jamet.2022.46.5.212.

[103] Gregory, F. D., 1997, *Safety Standards for Hydrogen and Hydrogen Systems*.

[104] Yatsenko, E. A., Goltsman, B. M., Novikov, Y. V., Izvarin, A. I., and Rusakevich, I. V., 2022, "Review on Modern Ways of Insulation of Reservoirs for Liquid Hydrogen Storage," Int. J. Hydrogen Energy, **47**(97), pp. 41046–41054. https://doi.org/10.1016/j.ijhydene.2022.09.211.

[105] Scholtens, B. E., Fesmire, J. E., Sass, J. P., Augustynowicz, S. D., and Heckle, K. W., 2008, "Cryogenic Thermal Performance Testing of Bulk-Fill and Aerogel Insulation Materials," *AIP Conference Proceedings*, pp. 152–159. https://doi.org/10.1063/1.2908517.

[106] Leng, Y., Zhang, S., Wang, X., Pu, L., and Xu, P., 2024, "Comparative Study on Thermodynamic Performance of Liquid Hydrogen Storage Insulation System Incorporating Vapor-Cooled Shield with Para–Ortho Hydrogen Conversion by One-Dimensional and Quasi-Two-Dimensional Model," Energy Convers. Manag., **321**. https://doi.org/10.1016/j.enconman.2024.119068.

[107] Jiang, W. B., Zuo, Z. Q., Huang, Y. H., Wang, B., Sun, P. J., and Li, P., 2018, "Coupling Optimization of Composite Insulation and Vapor-Cooled Shield for on-Orbit Cryogenic Storage Tank," Cryogenics (Guildf)., **96**, pp. 90–98. https://doi.org/10.1016/j.cryogenics.2018.10.008.

[108] Chan, C. K., and Mem ASME, P., 1973, *Conductance of Packed Spheres in Vacuum*. [Online]. Available: http://asmedigitalcollection.asme.org/heattransfer/article-pdf/95/3/302/5663791/302_1.pdf.

[109] Linde AG, *Datenblatt LITS F2 D*.

[110] Wang, P., Liao, B., An, Z., Yan, K., and Zhang, J., 2019, "Measurement and Calculation of Cryogenic Thermal Conductivity of HGMs," Int. J. Heat Mass Transf., **129**, pp. 591–598. https://doi.org/10.1016/j.ijheatmasstransfer.2018.09.113.

[111] Schiaroli, A., Claussner, L., Campari, A., Cirrone, D., Linseisen, B., Friedrich, A., Torres de Ritter, E. L., Kuznetsov, M., and Ustolin, F., 2025, "A Comprehensive Review on Liquid Hydrogen Transfer Operations and Safety Considerations for Mobile Applications," Int. J. Hydrogen Energy, **107**, pp. 164–182. https://doi.org/10.1016/j.ijhydene.2024.12.266.

[112] International Maritime Organization, 2024, *RESOLUTION MSC.565(108) - REVISED INTERIM RECOMMENDATIONS FOR CARRIAGE OF LIQUEFIED HYDROGEN IN BULK*.

[113] DNV, 2025, *IMO CCC 11: INTERIM GUIDELINES FOR HYDROGEN AS FUEL COMPLETED*.

[114] DNV, 2021, *HANDBOOK FOR HYDROGEN-FUELLED VESSELS*.

[115] Verfondern, K., Cirrone, H. D., Molkov, V., Makarov, D., Coldrick, U. S., Ren, Z., Wen, J., Proust, C., Friedrich, A., and Jordan, P. T., 2020, *Pre-Normative REsearch for Safe Use of Liquid Hydrogen (PRESLHY) Handbook of Hydrogen Safety: Chapter on LH2 Safety*.

[116] Calabrese, M., Portarapillo, M., Di Nardo, A., Venezia, V., Turco, M., Luciani, G., and Di Benedetto, A., 2024, "Hydrogen Safety Challenges: A Comprehensive Review on Production, Storage, Transport, Utilization, and CFD-Based Consequence and Risk Assessment," Energies (Basel)., **17**(6). https://doi.org/10.3390/en17061350.

[117] Dwyer, J., Hansel, J. G., and Philips, T., 2003, *Temperature Influence on the Flammability Limits of Heat Treating Atmospheres*.

[118] Pio, G., and Salzano, E., 2019, "Flammability Limits of Methane (LNG) and Hydrogen (LH2) at Extreme Conditions," Chem. Eng. Trans., **77**, pp. 601–606. https://doi.org/10.3303/CET1977101.

[119] Panda, P. P., and Hecht, E. S., 2017, "Ignition and Flame Characteristics of Cryogenic Hydrogen Releases," Int. J. Hydrogen Energy, **42**(1), pp. 775–785. https://doi.org/10.1016/j.ijhydene.2016.08.051.

[120] Cirrone, D., Makarov, D., Proust, C., and Molkov, V., 2024, “Numerical Study of the Spark Ignition of Hydrogen-Air Mixtures at Ambient and Cryogenic Temperature,” Int. J. Hydrogen Energy, **79**, pp. 353–363. https://doi.org/10.1016/j.ijhydene.2024.06.362.

[121] Kojima, Y., 2024, “Safety of Ammonia as a Hydrogen Energy Carrier,” Int. J. Hydrogen Energy, **50**, pp. 732–739. https://doi.org/10.1016/j.ijhydene.2023.06.213.

[122] Li Y, Bi M, Gan B, Yan C, Ren J, and Gao W, 2019, “Inhibition of Confined Hydrogen Explosion by Inert Gases,” *International Conference on Hydrogen Safety*, Seoul.

[123] Li, Y., Bi, M., Huang, L., Liu, Q., Li, B., Ma, D., and Gao, W., 2018, “Hydrogen Cloud Explosion Evaluation under Inert Gas Atmosphere,” Fuel Processing Technology, **180**, pp. 96–104. https://doi.org/10.1016/j.fuproc.2018.08.015.

[124] Aarskog, F. G., Hansen, O. R., Strømgren, T., and Ulleberg, Ø., 2020, “Concept Risk Assessment of a Hydrogen Driven High Speed Passenger Ferry,” Int. J. Hydrogen Energy, **45**(2), pp. 1359–1372. https://doi.org/10.1016/j.ijhydene.2019.05.128.

[125] Willoughby, D., and Royle, M., 2014, *Releases of Unignited Liquid Hydrogen*.

[126] Lach, A. W., and Gaathaug, A. V., 2021, “Large Scale Experiments and Model Validation of Pressure Peaking Phenomena-Ignited Hydrogen Releases,” Int. J. Hydrogen Energy, **46**(11), pp. 8317–8328. https://doi.org/10.1016/j.ijhydene.2020.12.015.

[127] van Wingerden, K., Kluge, M., Habib, A. K., Skarsvåg, H. L., Ustolin, F., Paltrinieri, N., and Odsæter, L. H., 2022, “Experimental Investigation into the Consequences of Release of Liquified Hydrogen onto and under Water,” Chem. Eng. Trans., **90**, pp. 541–546. https://doi.org/10.3303/CET2290091.

[128] Georgopoulou, C., Di Maria, C., Di Ilio, G., Cigolotti, V., Minutillo, M., Rossi, M., Sullivan, B. P., Bionda, A., Rautanen, M., Ponzini, R., Salvadore, F., Alvarez-Cardozo, M., Douska, P., Koukoulopoulos, L., Psaraftis, G., Dimopoulos, G., Wannemacher, T., Baumann, N., Mahos, K., Tome, M., Torres, O. N., Oikonomou, F., Hamalainen, A., Chillè, F., Papagiannopoulos, Y., Sakellaridis, N., and Boonen, E. J., 2025, “On the Identification of Regulatory Gaps for Hydrogen as Maritime Fuel,” Sustainable Energy Technologies and Assessments, **75**. https://doi.org/10.1016/j.seta.2025.104224.

[129] European Maritime Safety Agency, 2025, *Study Investigating the Safety of Hydrogen as Fuel on Ships*, Lisbon. [Online]. Available: www.emsa.europa.eu.

[130] Compressed Gas Association, 2021, *CGA G-5-5 - Standard for Hydrogen Vent Systems*.

[131] ANSI/AIAA, 2017, *Guide to Safety of Hydrogen and Hydrogen Systems (G-095A-2017)*.

[132] Piccardo, S., 2025, “Innovative Technologies and Low-Impact Alternative Fuels for Maritime Sector Decarbonisation: Applicability, Integration, Techno-Economic Assessment, and Operational Simulations,” PhD Thesis.

[133] Shin, H., Jang, D., Lee, S., Cho, H. S., Kim, K. H., and Kang, S., 2023, “Techno-Economic Evaluation of Green Hydrogen Production with Low-Temperature Water Electrolysis Technologies Directly Coupled with Renewable Power Sources,” Energy Convers. Manag., **286**. https://doi.org/10.1016/j.enconman.2023.117083.

[134] Rivarolo, M., Rattazzi, D., Lamberti, T., and Magistri, L., 2020, “Clean Energy Production by PEM Fuel Cells on Tourist Ships: A Time-Dependent Analysis,” Int. J. Hydrogen Energy, **45**(47), pp. 25747–25757. https://doi.org/10.1016/j.ijhydene.2019.12.086.

[135] Rivarolo, M., Rattazzi, D., Magistri, L., and Massardo, A. F., 2021, “Multi-Criteria Comparison of Power Generation and Fuel Storage Solutions for Maritime Application,” Energy Convers. Manag., **244**. https://doi.org/10.1016/j.enconman.2021.114506.

[136] 2023, “Siemens SGT-A35.” [Online]. Available: https://www.siemens-energy.com/global/en/offerings/power-generation/gas-turbines/sgt-a30-a35-rb.html. [Accessed: 21-Jul-2023].

[137] 2023, “Solar Turbines.” [Online]. Available: https://www.solarturbines.com/en_US.html. [Accessed: 01-Aug-2023].

[138] Abedin, T., Pasupuleti, J., Paw, J. K. S., Tak, Y. C., Mahmud, M., Abdullah, M. P., and Nur-E-Alam, M., 2025, “Proton Exchange Membrane Fuel Cells in Electric Vehicles:

Innovations, Challenges, and Pathways to Sustainability," J. Power Sources, **640**. https://doi.org/10.1016/j.jpowsour.2025.236769.

[139] Crespi, E., Guandalini, G., Gößling, S., and Campanari, S., 2021, "Modelling and Optimization of a Flexible Hydrogen-Fueled Pressurized PEMFC Power Plant for Grid Balancing Purposes," Int. J. Hydrogen Energy, **46**(24), pp. 13190–13205. https://doi.org/10.1016/j.ijhydene.2021.01.085.

[140] Rivarolo, M., Rattazzi, D., and Magistri, L., 2018, "Best Operative Strategy for Energy Management of a Cruise Ship Employing Different Distributed Generation Technologies," Int. J. Hydrogen Energy, **43**(52), pp. 23500–23510. https://doi.org/10.1016/j.ijhydene.2018.10.217.

[141] IMO, 2020, *Fourth IMO GHG Study 2020 Full Report*.

[142] MTU, 2021, "Rolls Royce Launches Mtu Hydrogen Solutions for Power Generation."

[143] MAN Energy Solutions, 2021, "H2-Ready: MAN Gas Engines Enable Hydrogen Use in Power Plants."

[144] 2025, "MARPOWER ."

[145] Tucker, S., Passalacqua, M., Dotto, A., Traverso, A., and Schiaffino, G., 2025, "Liquid Hydrogen Storage System for Micro Gas Turbines: Dynamic Modelling and Performance with Variable Demand Profile," *Proceedings of ASME Turbo Expo 2025 (GT2025)*.

[146] Lee, E., Kim, J., Jung, W., Lee, J., and Chang, D., 2025, "Design and Modeling of Liquid Hydrogen Cargo Transfer System with Make-up Boil-off Gas Compression," Int. J. Hydrogen Energy, **179**. https://doi.org/10.1016/j.ijhydene.2025.151675.

[147] Molkov, V., Ebne-Abbasi, H., and Makarov, D., 2024, "Liquid Hydrogen Refuelling at HRS: Description of SLH2 Concept, Modelling Approach and Results of Numerical Simulations," Int. J. Hydrogen Energy, **93**, pp. 285–296. https://doi.org/10.1016/j.ijhydene.2024.10.392.

[148] Harper, J., Cloyd, S., Pigon, T., Thomas, B., Wilson, J., Johnson, E., and Noble, D. R., 2023, "Hydrogen Co-Firing Demonstration at Georgia Power Plant McDonough: M501G Gas Turbine," *Proceedings of ASME Turbo Expo*. [Online]. Available: http://asmedigitalcollection.asme.org/GT/proceedings-pdf/GT2023/86991/V006T08A007/7044334/v006t08a007-gt2023-102660.pdf.

[149] Harper, J., Gibeaut, D., Lozier, M., Sake, R., Wolf, T., and Noble, D. R., 2025, "Hydrogen Cofiring Demonstration at Constellation Hillabee Siemens Energy SGT6-6000G Power Plant," J. Eng. Gas Turbine. Power, **147**(5). https://doi.org/10.1115/1.4067181.

[150] Kim, D. K., Seo, J. H., Kim, S., Lee, M. K., Nam, K. Y., Song, H. H., and Kim, M. S., 2014, "Efficiency Improvement of a PEMFC System by Applying a Turbocharger," Int. J. Hydrogen Energy, **39**(35), pp. 20139–20150. https://doi.org/10.1016/j.ijhydene.2014.09.152.

[151] Iester, F., Mantelli, L., Bozzolo, M., Magistri, L., and Massardo, A. F., 2023, "Performance Assessment of an Innovative Turbocharged Proton-Exchagne Membrane Fuel Cell System," *Proceedings of ASME Turbo Expo*.

[152] García, A., Monsalve-Serrano, J., Martinez-Boggio, S., and Gaillard, P., 2021, "Emissions Reduction by Using E-Components in 48 V Mild Hybrid Trucks under Dual-Mode Dual-Fuel Combustion," Appl. Energy, **299**. https://doi.org/10.1016/j.apenergy.2021.117305.

[153] Ma, T., Li, C., Xu, Z., Liu, W., and Lin, W., 2024, "Modeling and Simulation of the PEMFC System Equipped with a Variable Geometry Turbocharger," Int. J. Hydrogen Energy, **77**, pp. 1327–1338. https://doi.org/10.1016/j.ijhydene.2024.06.283.

[154] Gadducci, E., Lamberti, T., Bellotti, D., Magistri, L., and Massardo, A. F., 2021, "BoP Incidence on a 240 KW PEMFC System in a Ship-like Environment, Employing a Dedicated Fuel Cell Stack Model," Int. J. Hydrogen Energy, **46**(47), pp. 24305–24317. https://doi.org/10.1016/j.ijhydene.2021.04.192.

[155] Vasylyev, A., Passalacqua, M., Mantelli, L., Rivarolo, M., and Sorce, A., 2024, "Piecewise-Linear MILP Optimization for Energy System Design Onboard Hybrid Ships," *Journal*

*of Physics: Conference Series*, Institute of Physics. https://doi.org/10.1088/1742-6596/2893/1/012040.

[156] Tiwari, R. N., Reggio, F., Ferrari, M. L., De Paepe, W., and Traverso, A., 2025, "Experimental Characterization of a Bladeless Air Compressor," J. Eng. Gas Turbine. Power, **147**(4). https://doi.org/10.1115/1.4066732.

[157] Saadeldin, M., Vasylyev, A., Rivarolo, M., and Sorce, A., 2026, "Feasibility Analysis of Hydrogen Fuel Cell-Powered Passenger Vessels: A Multi-Criteria and MILP-Based Analysis for Sustainable Inland Navigation," Ocean Engineering, **349**. https://doi.org/10.1016/j.oceaneng.2026.124186.

[158] "City Population," 2024. [Online]. Available: https://www.citypopulation.de/. [Accessed: 10-Mar-2025].

[159] Spyrou, I. D., and Anagnostopoulos, J. S., 2010, "Design Study of a Stand-Alone Desalination System Powered by Renewable Energy Sources and a Pumped Storage Unit," Desalination, **257**(1–3), pp. 137–149. https://doi.org/10.1016/j.desal.2010.02.033.